



**Scuola Internazionale Superiore di Studi Avanzati - Trieste**

DOCTORAL THESIS

---

A journey in dark matter  
models with  
non-standard features

---

CANDIDATE : Alessandro Davoli  
SUPERVISOR : Prof. Andrea De Simone

ACADEMIC YEAR 2018 – 2019

**SISSA - Via Bonomea 265 - 34136 TRIESTE - ITALY**



*Ai miei nonni*



# Abstract

In this thesis, we investigate some non-standard aspects of dark matter in the context of weakly-interacting massive particles.

We first study the impact of searches for long-lived particles on dark matter models with two concrete realizations: a simplified model which delivers displaced vertices and an effective one which predicts the existence of bound states similar to  $R$ -hadrons. In both cases, we find that non-standard signatures are essential in order to fully exploit the potential of LHC for dark matter searches.

We then focus our attention on a non-minimal composite Higgs model which can account for dark matter; the greater complexity of the model with respect to the simplest case allows for thermal production of dark matter with a fine tuning which is significantly lower than in other models. In addition, we find that also non-thermal production is possible.



# List of publications

This thesis is based on the following publications, listed in chronological order:

- A. Davoli, A. De Simone, T. Jacques and V. Sanz, *Displaced Vertices from Pseudo-Dirac Dark Matter*, *JHEP* **11** (2017) 025, [1706.08985].
- A. Davoli, A. De Simone, T. Jacques and A. Morandini, *LHC Phenomenology of Dark Matter with a Color-Octet Partner*, *JHEP* **07** (2018) 054, [1803.02861].
- A. Davoli, A. De Simone, D. Marzocca and A. Morandini, *Composite 2HDM with singlets: a viable dark matter scenario*, 1905.13244.

The research performed by the author during his PhD studies has also led to the publication:

- J. Alimena et al., *Searching for Long-Lived Particles beyond the Standard Model at the Large Hadron Collider*, 1903.04497.





# Acknowledgements

First of all, I want to thank Andrea for being an excellent supervisor; he always encouraged and guided me for these three years of research, and he transmitted his enthusiasm for the subject to me. In addition, I could always rely on him for advice and suggestions, and not only related to physics.

Thanks to Thomas and David, for their patience and continuous availability for answering to my many (and sometimes rather stupid) questions; it was a pleasure to work with them, and I learnt many things from them.

I must then thank Alessandro; the discussions we had have probably been the most fruitful and efficient way in which I learnt things during these years.

I enjoyed life in SISSA also thanks to the people I met there; I then express my gratitude to J and Mihael for being great office mates, and to Hrach, Paolo, Elena, Riccardo and Marco for all the time we spent together.

I then thank my family for allowing me to get to this point and for always supporting my choices unconditionally; although indirectly, it is certainly thanks to them as well if I reached this goal.

Finally, I want to thank Ilaria for always being on my side and for always encouraging me; she also had an important role in this path, even if she does not admit it.



# Contents

<b>Abstract</b>	<b>i</b>
<b>List of publications</b>	<b>iii</b>
<b>Acknowledgements</b>	<b>v</b>
<b>Preface</b>	<b>1</b>
<b>1 The Standard Model of particle physics</b>	<b>3</b>
1.1 Standard Model Lagrangian . . . . .	3
1.1.1 Gauge contribution . . . . .	4
1.1.2 Flavour contribution . . . . .	5
1.1.3 EWSB contribution . . . . .	5
1.1.4 More about the Higgs . . . . .	6
1.2 Global symmetries of the Standard Model . . . . .	9
1.2.1 Number conservations and flavour symmetry . . . . .	10
1.2.2 Custodial symmetry . . . . .	13
1.3 Electroweak precision tests . . . . .	14
1.4 Hierarchy problem . . . . .	16
1.4.1 Unnaturalness of the Higgs mass . . . . .	17
1.4.2 Possible solutions . . . . .	18
<b>2 Dark matter</b>	<b>19</b>
2.1 History and evidences . . . . .	19
2.2 Main dark matter candidates . . . . .	24
2.2.1 WIMP candidates . . . . .	24
2.2.2 Non-WIMP candidates . . . . .	24
2.3 Freeze-out production of WIMP dark matter . . . . .	26
2.3.1 Standard freeze-out . . . . .	26
2.3.2 Exceptions to the standard paradigm . . . . .	29
2.4 Experimental searches . . . . .	33
2.4.1 Direct detection . . . . .	33
2.4.2 Indirect detection . . . . .	37
2.4.3 LHC searches . . . . .	37
<b>3 LHC interplay between dark matter and long-lived particles</b>	<b>41</b>
3.1 Pseudo-Dirac dark matter . . . . .	42
3.1.1 Model Lagrangian . . . . .	43
3.1.2 Constraints on the parameter space . . . . .	46

3.1.3	Results . . . . .	48
3.2	Chromo-electric dark matter . . . . .	53
3.2.1	Model Lagrangian . . . . .	53
3.2.2	LHC analysis . . . . .	57
3.A	Appendices for the pDDM model . . . . .	63
3.A.1	Mass eigenstates . . . . .	63
3.A.2	Full expressions for decay widths and thermally-averaged cross sections . . . . .	64
3.A.3	Details about the analysis . . . . .	65
3.B	Appendices for the chromo-electric DM model . . . . .	66
3.B.1	Full expressions for the thermally-averaged cross sections . . . . .	66
3.B.2	Sommerfeld enhancement . . . . .	68
<b>4</b>	<b>Dark matter within a composite 2HDM with extra singlets</b>	<b>71</b>
4.1	Vacuum misalignment . . . . .	72
4.2	Construction of the model . . . . .	74
4.2.1	Goldstone embedding . . . . .	75
4.2.2	Partial compositeness . . . . .	78
4.2.3	Potential for the pNGBs . . . . .	81
4.3	pNGBs dynamics . . . . .	84
4.3.1	Structure of the vacuum . . . . .	84
4.3.2	Spectrum of the pNGBs . . . . .	85
4.3.3	Interactions among the pNGBs . . . . .	86
4.4	Thermal dark matter scenario . . . . .	88
4.4.1	Relic Density . . . . .	88
4.4.2	LHC searches . . . . .	91
4.4.3	Direct detection . . . . .	92
4.4.4	Indirect detection . . . . .	93
4.4.5	Discussion . . . . .	93
4.5	Non-thermal dark matter scenario . . . . .	96
4.A	Identification of the physical fields . . . . .	98
4.B	Bounds from EWPTs and Higgs couplings fit . . . . .	99
4.B.1	Higgs couplings fit . . . . .	99
4.B.2	EWPTs . . . . .	101
4.B.3	Combined results . . . . .	103
4.C	Expressions of the effective couplings . . . . .	103
4.C.1	Interactions between NGBs and gauge bosons . . . . .	104
4.C.2	Interactions between NGBs and fermions . . . . .	105
4.C.3	Interactions among pNGBs . . . . .	105
<b>5</b>	<b>Summary and conclusions</b>	<b>109</b>
<b>A</b>	<b>CCWZ formalism</b>	<b>111</b>
A.1	Geometrical interpretation . . . . .	111
A.2	General construction . . . . .	112
A.2.1	$d$ and $e$ symbols . . . . .	115
A.2.2	Local invariance . . . . .	116
<b>B</b>	<b>Effective field theories</b>	<b>117</b>





# Preface

In the present thesis, we investigate the properties of dark matter (DM) from the point of view of particle physics; in particular, we focus our attention on the category of weakly-interacting massive particles (WIMPs), which represents the most widely studied class of DM candidates. The interest in WIMPs lies in the fact that their annihilation cross section naturally points to the weak scale, making it possible to look for them with different experimental techniques.

The original part of the present work is ideally divided in two parts: the first one is dedicated to the study of the interplay between standard monojet searches and strategies involving long-lived particles (LLPs), while in the second one we consider dark matter in association with the hierarchy problem of the Standard Model (SM).

In chapter 1, we review the concepts of the SM which we will refer to in the following; in particular, after a brief recap about the SM Lagrangian, we discuss in detail its global symmetries, we outline the main aspects of electroweak precision tests and we present the hierarchy problem, in particular related to the Higgs mass.

In chapter 2, we review some aspects of the DM problem; after discussing the main experimental evidences which led physicists to believe that a large amount of invisible matter exists in the universe, we focus our attention on the case of WIMPs, discussing some of their properties, together with the experimental searches they can be looked for with.

In chapter 3, which is based on refs. [1, 2], we focus on DM searches at the Large Hadron Collider, studying the importance of those involving LLPs. We first study a model which predicts the existence of displaced vertices, where an unstable dark particle travels a macroscopic distance before decaying; the second model we consider, instead, is characterized by a coloured particle belonging to the dark sector which can form bound states with SM particles, similarly to what happens in supersymmetry. In both cases, we show that experimental searches involving LLPs are essential in order to correctly explore the parameter space of the models.

In chapter 4, which is based on ref. [3], we consider a possibility to address both the DM and the hierarchy problems at once, in the context of composite Higgs (CH) models; in particular, by considering a scenario which is beyond the minimal one, it is possible to find interesting features which would be otherwise absent: this is precisely what happens in the model we consider, where the DM can be produced via non-thermal effects. In addition, we also find that the level of fine tuning which is required in order to correctly reproduce the DM relic abundance and evade experimental constraints is significantly lower than that of other non-minimal CH models which aim to address the DM problem.

Finally, we summarize the results and conclude in chapter 5.





# Chapter 1

## The Standard Model of particle physics

*Elementary particle physics is the quadrant of nature whose laws can be written in a few lines with absolute precision and the greatest empirical adequacy.*

Riccardo Barbieri

The Standard Model of particle physics constitutes the theoretical tool at our disposal to understand and explain how nature behaves at the shortest distances we can probe; developed since the 60's by some of the most brilliant scientists of the last century (like in the seminal papers [4–6], just to cite a few), it received many experimental confirmations, culminated in 2012 with the discovery of the Higgs bosons at the Large Hadron Collider (LHC) by the experiments ATLAS and CMS [7, 8].

Despite its incredible success, we know that the SM cannot be the definitive answer to the question “how does nature behaves at the shortest scales?”; in fact, there are several arguments which do not find an answer in this framework: they are both theoretical (quantum gravity, hierarchy problem, strong  $CP$  problem, cosmological constant problem, etc.) and experimental (dark matter, neutrino masses, baryon asymmetry, etc.). This led physicists to develop many beyond the Standard Model (BSM) theories.

Nevertheless, SM remains an extraordinary tool to study particle physics, and it must be our guidance for the search of new physics (NP); for this reason, it is worth spending some words on it before proceeding. In section 1.1, we recall the SM Lagrangian and some of its features; in section 1.2, we discuss the global symmetries of the SM, while in section 1.3 we briefly review the main aspects of precision measurements; finally, section 1.4 is dedicated to the hierarchy problem.

### 1.1 Standard Model Lagrangian

The Standard Model is a gauge theory based on the group:

$$\mathcal{G}_{\text{SM}} = \text{SU}(3)_c \times \text{SU}(2)_L \times \text{U}(1)_Y, \quad (1.1.1)$$

broken to  $\text{SU}(3)_c \times \text{U}(1)_{\text{em}}$  after electroweak symmetry breaking (EWSB).

	$SU(3)_c$	$SU(2)_L$	$U(1)_Y$
$q_L = \begin{pmatrix} u_L \\ d_L \end{pmatrix}$	<b>3</b>	<b>2</b>	1/6
$u_R$	<b>3</b>	<b>1</b>	2/3
$d_R$	<b>3</b>	<b>1</b>	-1/3
$\ell_L = \begin{pmatrix} \nu_L \\ e_L \end{pmatrix}$	<b>1</b>	<b>2</b>	-1/2
$e_R$	<b>1</b>	<b>1</b>	-1
$H$	<b>1</b>	<b>2</b>	1/2

Table 1.1: Field content of the SM (except for the gauge bosons): in the first two columns, we indicate the representations under  $SU(3)_c$  and  $SU(2)_L$ , while in the last one we show the value of the hypercharge. The generation index for the fermions is understood.

To recall the interactions dictated by the SM Lagrangian, it is convenient to consider it as the sum of three contributions:

$$\mathcal{L}_{\text{SM}} = \mathcal{L}_{\text{SM}}^{\text{gauge}} + \mathcal{L}_{\text{SM}}^{\text{flavour}} + \mathcal{L}_{\text{SM}}^{\text{EWSB}}, \quad (1.1.2)$$

where the first one describes the interactions between the fermions and the gauge bosons, the second one the interactions between fermions and the Higgs, and the last one is responsible for EWSB.

In the following, we consider these three contributions separately. The field content is summarized in table 1.1, where we show the representations under  $SU(3)_c$  and  $SU(2)_L$ , while for  $U(1)_Y$  we indicate the value of the hypercharge; for clarity, we omit the generation index. We then denote the Higgs doublet by  $H$  and the gauge fields as  $G_\mu^A$ ,  $W_\mu^a$  and  $B_\mu$ , where  $A = 1, \dots, 8$  and  $a = 1, \dots, 3$  are  $SU(3)_c$  and  $SU(2)_L$  indices, respectively.

### 1.1.1 Gauge contribution

The first contribution is represented by the covariant kinetic terms for the fermions and the field strengths:

$$\mathcal{L}_{\text{SM}}^{\text{gauge}} = \sum_{\psi} i\bar{\psi}\gamma^\mu D_\mu\psi - \frac{1}{4} \sum_V V_{\mu\nu}^i V_i^{\mu\nu}, \quad (1.1.3)$$

where  $\psi$  and  $V$  stand in general for fermions and gauge fields, respectively. In our convention, the covariant derivative and the field strength are:

$$D_\mu = \partial_\mu - ig_S G_\mu^A T_A^{(3)} - ig W_\mu^a T_a^{(2)} - ig' B_\mu Y \quad (1.1.4a)$$

$$V_{\mu\nu}^i = \partial_\mu V_\nu^i - \partial_\nu V_\mu^i + g_{(V)} f^{ijk} V_\mu^j V_\nu^k, \quad (1.1.4b)$$

where  $T_A^{(3)}$ ,  $T_a^{(2)}$  and  $Y$  are the generators of  $SU(3)_c$ ,  $SU(2)_L$  and  $U(1)_Y$  in the appropriate representation (the first two are  $\lambda^A/2$  and  $\sigma^a/2$  in the fundamental representation, with  $\lambda^A$  and  $\sigma^a$  being the Gell-Mann and Pauli matrices, respectively).

### 1.1.2 Flavour contribution

The second contribution is represented by the interactions between fermions and the Higgs field. By restoring the flavour indices, we have:

$$\mathcal{L}_{\text{SM}}^{\text{flavour}} = -y_{ij}^{(u)} \bar{q}_{L,i} u_{R,j} H^c - y_{ij}^{(d)} \bar{q}_{L,i} d_{R,j} H - y_{ij}^{(e)} \bar{\ell}_{L,i} e_{R,j} H + \text{h.c.}, \quad (1.1.5)$$

with  $H^c \equiv i\sigma_2 H^*$  and  $i, j$  being family indices.

As it is well-known, it is possible to diagonalize  $y^{(e)}$  and either  $y^{(u)}$  or  $y^{(d)}$  with unitary transformations.

After EWSB, eq. (1.1.5) is responsible for the generation of masses in the fermion sector, giving rise to:

$$\mathcal{L}_{\text{SM}}^{\text{mass}} = -m_{ij}^{(u)} \bar{u}_{L,i} u_{R,j} - m_{ij}^{(d)} \bar{d}_{L,i} d_{R,j} - m_{ij}^{(e)} \bar{e}_{L,i} e_{R,j} + \text{h.c.}, \quad (1.1.6)$$

where  $m^{(f)} = y^{(f)} v / \sqrt{2}$ . Diagonalization of the mass matrices by means of bi-unitary transformations then leads to the appearance of the Cabibbo-Kobayashi-Maskawa (CKM) matrix  $V$  in the charged current.

The interactions between the fermionic mass eigenstates and the physical Higgs are given by:

$$\mathcal{L}_{\text{SM}}^{f-h} = -\frac{m^{(u)}}{v} \bar{u} u h - \frac{m^{(d)}}{v} \bar{d} d h - \frac{m^{(e)}}{v} \bar{e} e h. \quad (1.1.7)$$

### 1.1.3 EWSB contribution

The last contribution is represented by the Higgs Lagrangian:

$$\mathcal{L}_{\text{SM}}^{\text{EWSB}} = |D_\mu H|^2 - (\mu^2 |H|^2 + \lambda |H|^4). \quad (1.1.8)$$

We use the convention in which the Higgs vacuum expectation value (VEV) is normalized such that, in the unitary gauge:

$$\langle H \rangle = \frac{1}{\sqrt{2}} \begin{pmatrix} 0 \\ v \end{pmatrix}, \quad (1.1.9)$$

and  $v \equiv (-\mu^2/\lambda)^{1/2} \approx 246 \text{ GeV}$ . After EWSB, the potential for the physical Higgs becomes:

$$V(h) = \frac{m_h^2}{2} h^2 + \frac{m_h^2}{2v} h^3 + \frac{m_h^2}{8v^2} h^4, \quad (1.1.10)$$

with  $m_h^2 \equiv -2\mu^2 \approx 125 \text{ GeV}$ .

EWSB is responsible for the generation of masses for the  $W$  and  $Z$  bosons, given by:

$$m_W^2 = \frac{v^2 g^2}{4}, \quad m_Z^2 = \frac{v^2 (g^2 + g'^2)}{4}. \quad (1.1.11)$$

The interactions between the gauge bosons and the physical Higgs are:

$$\mathcal{L}_{\text{SM}}^{W,Z-h} = \left( m_W^2 W_\mu^+ W_\mu^- + \frac{m_Z^2}{2} Z_\mu Z^\mu \right) \left( 2\frac{h}{v} + \frac{h^2}{v^2} \right). \quad (1.1.12)$$

In terms of the weak angle,  $\theta_w \equiv \arctan g'/g$ , the SM then predicts:

$$\rho \equiv \frac{m_W^2}{m_Z^2 \cos^2 \theta_w} = 1. \quad (1.1.13)$$

This value is in excellent agreement with experiments but, as we will see, can change significantly in SM extensions.

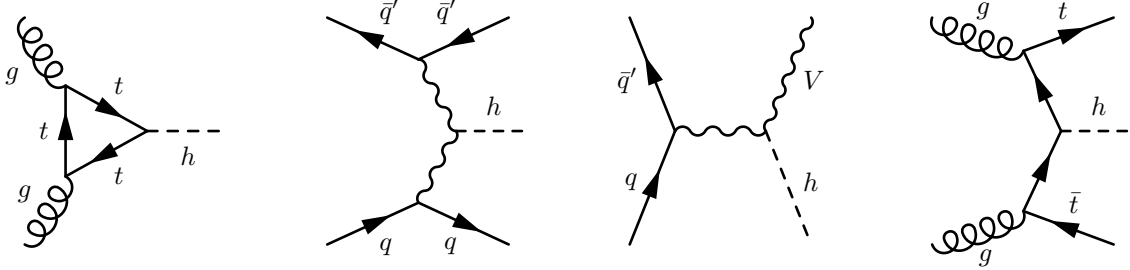


Figure 1.1: Main channels for Higgs production at LHC.

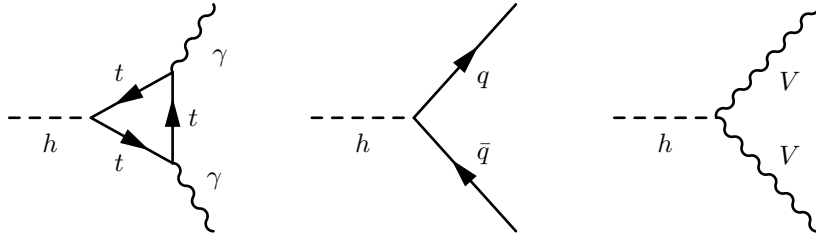


Figure 1.2: Main channels for Higgs decay at LHC.

### 1.1.4 More about the Higgs

The discovery of the Higgs in 2012 was one of the greatest achievements of modern physics, closing the circle around the success of the SM. On the other hand, however, there is a very challenging issue (i.e., the hierarchy problem) which characterizes this particle, as we will discuss later; for this reason, the Higgs sector constitutes the starting point for important extensions of the SM. It is then useful to recall some aspects about Higgs physics before going on.

The main channels for Higgs production at LHC are shown in fig. 1.1. The first one (called gluon fusion) is the main contribution, but also the other ones are relevant because of their signatures, and are called vector boson fusion (VBF), Higgs strahlung and associated production, respectively. On the other hand, also the Higgs decay channels are important signatures for LHC physics: the main ones are shown in fig. 1.2; of course, given the measured mass of the Higgs,  $m_h \approx 125$  GeV, the decay into two on-shell massive gauge bosons is not allowed. The Higgs branching ratios (*BRs*), as functions of the Higgs mass, are showed in fig. 1.3.

However, one could ask: “is the Higgs really a fundamental ingredient of the SM?”; after all, it is the only elementary scalar, and it was initially introduced just to generate a mass term for the gauge bosons and the fermions. A good approach to address this question is represented by the Callan-Coleman-Wess-Zumino (CCWZ) formalism, developed in the seminal papers [10, 11]; we review it in appendix A.

In order to apply the CCWZ prescription to the SM, we consider the breaking pattern  $\mathcal{G} \rightarrow \mathcal{H}$ , with  $\mathcal{G} = \text{SU}(2)_L \times \text{U}(1)_Y$  and  $\mathcal{H} = \text{U}(1)_{\text{em}} \text{ (SU}(3)_c \text{ does not play any role for this discussion)}$ ; we can then parametrize the standard coordinates, i.e. the would-be Nambu-Goldstone bosons (NGBs)  $\chi^a$ , as:

$$\Sigma = e^{i\frac{2}{v}\chi^a \hat{T}_a}, \quad (1.1.14)$$

where  $\hat{T}_a = \sigma^a/2$  are the broken generators. It is easy to show that  $\Sigma$  transforms

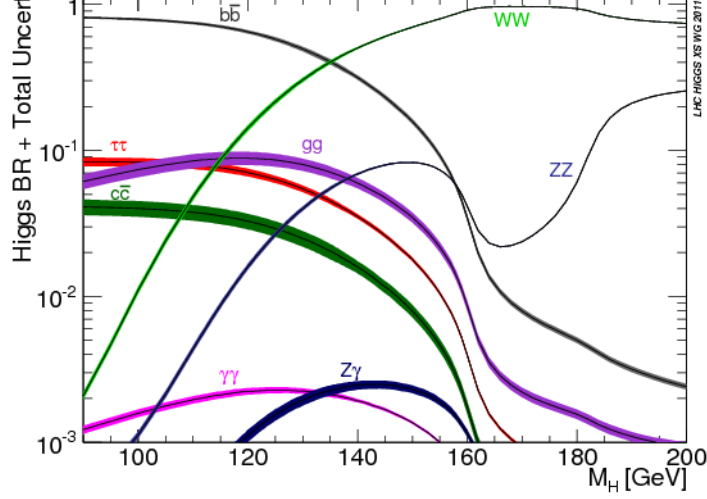


Figure 1.3: Higgs branching ratios as functions of the Higgs mass. Figure taken from ref. [9].

precisely as required by CCWZ, i.e. eq. (A.2.7): in particular, under a transformation  $g = \exp\{i\alpha_L^a \sigma^a / 2\} \exp\{i\alpha_Y Y\} \equiv U_L U_Y \in \mathcal{G}$ , we have:

$$\Sigma \rightarrow U_L \Sigma e^{-i\alpha_Y \frac{\sigma^3}{2}} \quad (1.1.15)$$

In order to have local invariance under  $\mathcal{G}$ , we introduce a covariant derivative for  $\Sigma$ , defined as:

$$D_\mu \Sigma \equiv \partial_\mu \Sigma - ig W_\mu \Sigma + ig' B_\mu \Sigma \frac{\sigma^3}{2}, \quad (1.1.16)$$

where  $W_\mu \equiv W_\mu^a \sigma^a / 2$  and  $g, g'$  are the coupling constants; this definition is consistent with eq. (1.1.15). The Lagrangian constructed out of  $\Sigma$  which induces EWSB is:

$$\mathcal{L}_\Sigma^{(2)} = \frac{v^2}{4} \text{Tr}[(D_\mu \Sigma)^\dagger (D^\mu \Sigma)], \quad (1.1.17)$$

which is easily shown to be invariant under  $\mathcal{G}$ . To show that this Lagrangian correctly encodes the mechanism of EWSB, we first notice that we can rewrite it as:

$$\mathcal{L}_\Sigma^{(2)} = \frac{v^2}{4} \text{Tr}[(\Sigma^\dagger D_\mu \Sigma)^\dagger (\Sigma^\dagger D^\mu \Sigma)]. \quad (1.1.18)$$

It is then useful to introduce the field:

$$\tilde{W}_\mu \equiv \Sigma^\dagger W_\mu \Sigma + \frac{i}{g} \Sigma^\dagger \partial_\mu \Sigma, \quad (1.1.19)$$

which is nothing but the gauge-transformation of  $\Sigma$  (with transformation matrix given by  $\Sigma^\dagger$ ). In this way,  $\Sigma^\dagger D_\mu \Sigma = -ig \tilde{W}_\mu + ig' B_\mu \sigma^3 / 2$ ; with the definition of the gauge boson masses in eq. (1.1.11), we obtain:

$$\mathcal{L}_\Sigma^{(2)} \supset m_W^2 \tilde{W}_\mu^+ \tilde{W}_\mu^- + \frac{1}{2} m_Z^2 \tilde{Z}_\mu \tilde{Z}^\mu, \quad (1.1.20)$$

where we defined:

$$\tilde{W}_\mu^\pm \equiv \frac{\tilde{W}_\mu^1 \mp i \tilde{W}_\mu^2}{\sqrt{2}}, \quad \tilde{Z}_\mu \equiv \frac{g \tilde{W}_\mu^3 - g' B_\mu}{\sqrt{g^2 + g'^2}}. \quad (1.1.21)$$

We then see that eq. (1.1.20) reproduces both the gauge bosons masses and an infinite series of interactions between them and the NGBs; in fact, if we expand  $\Sigma^\dagger D_\mu \Sigma$ , we find:

$$\tilde{W}_\mu^\pm = W_\mu^\pm - \frac{1}{m_W} \partial_\mu \chi^\pm + \dots, \quad \tilde{Z}_\mu = Z_\mu - \frac{1}{m_Z} \partial_\mu \chi^3 + \dots, \quad (1.1.22)$$

with  $\chi^\pm$  being defined analogously to  $W_\mu^\pm$ . This analysis also shows that the mass eigenstates  $\tilde{W}_\mu^\pm, \tilde{Z}_\mu$  are the result of the gauge bosons eating the NGBs.

With the analysis presented so far, it seems that the answer to the question “is the Higgs really a fundamental ingredient of the SM?” is “no”; eq. (1.1.20), in fact, clearly shows that a mass for the gauge bosons can be generated without any scalar boson in the theory: what is really necessary is the set of NGBs  $\chi$ 's, originated by the spontaneous breaking  $SU(2)_L \times U(1)_Y \rightarrow U(1)_{em}$ . In particular, eq. (1.1.22) shows that the NGBs are eaten by the gauge bosons, becoming the corresponding longitudinal components.

Similar considerations can be repeated for the fermions, for which the Lagrangian is:

$$\mathcal{L}_\Sigma^{(f)} = -\frac{v}{\sqrt{2}} \bar{q}_{L,i} \Sigma \begin{pmatrix} y_{ij}^{(u)} u_{R,j} \\ y_{ij}^{(d)} d_{R,j} \end{pmatrix} - \frac{v}{\sqrt{2}} \bar{\ell}_{L,i} \Sigma \begin{pmatrix} 0 \\ y_{ij}^{(e)} e_{R,j} \end{pmatrix} + \text{h.c.}, \quad (1.1.23)$$

which can be easily shown to be invariant under  $\mathcal{G}$ . Both eqs. (1.1.17) and (1.1.23) reduce to the SM predictions in the unitary gauge, where the NGBs are set to zero and  $\langle \Sigma \rangle = \mathbf{1}$ .

In the following, we only focus on quarks, the analysis for leptons being analogous.

Actually, it turns out that a theory like the one outlined so far suffers the violation of perturbative unitarity in high energy interactions involving longitudinally-polarized gauge bosons (see, e.g., ref. [12] for a nice review), such as in  $W^+W^-$  scattering; this issue can be cured in at least two ways, which we are now going to review:

- i) a first possibility is to introduce a new scalar boson  $h$  in the theory which is a singlet under  $\mathcal{G}$ , resulting in the Lagrangian [13]:

$$\begin{aligned} \mathcal{L}_{\Sigma-h} &= \frac{1}{2} \partial_\mu h \partial^\mu h + \frac{v^2}{4} \text{Tr}[(D_\mu \Sigma)^\dagger (D^\mu \Sigma)] \left( 1 + 2a \frac{h}{v} + b \frac{h^2}{v^2} + \dots \right) - V(h) \\ &\quad - \frac{v}{\sqrt{2}} \bar{q}_{L,i} \Sigma \begin{pmatrix} y_{ij}^{(u)} u_{R,j} \\ y_{ij}^{(d)} d_{R,j} \end{pmatrix} \left( 1 + c \frac{h}{v} + \dots \right) + \text{h.c.}, \end{aligned} \quad (1.1.24)$$

where  $V(h)$  is some potential for  $h$ .

The three parameters  $a, b$  and  $c$  can then be tuned in such a way that perturbative unitarity is recovered. The field  $h$ , in fact, enters in the scattering of gauge bosons as well;  $W^+W^-$  scattering, for example, is unitarized for  $a = 1$ . On the other hand, however, one has to make sure that also new processes involving  $h$  preserve perturbative unitarity; it is possible to show that this is the case if  $b = a^2$  and  $ac = 1$ . The combination of these three conditions leads to  $a = b = c = 1$ .

It is easy to realize that this choice for  $a, b$  and  $c$  is nothing but the SM (when the higher-order interactions of  $h$  are neglected); in fact, if we introduce the doublet:

$$H_\Sigma \equiv \frac{1}{\sqrt{2}} \Sigma \begin{pmatrix} 0 \\ h + v \end{pmatrix}, \quad (1.1.25)$$

the standard interactions between the gauge bosons and the physical Higgs are reproduced by the standard covariant kinetic Lagrangian for  $H_\Sigma$  where  $D_\mu H_\Sigma \equiv \partial_\mu H_\Sigma - ig/2 W_\mu^a \sigma^a H_\Sigma - ig'/2 B_\mu H_\Sigma$ .

We can also notice that perturbative unitarity is intimately linked to renormalizability: in fact, it is straightforward to show that the Lagrangian written in terms of  $H_\Sigma$ , introduced to unitarize gauge bosons scattering, is renormalizable. In general, the lack of perturbative unitarity can be traced in the lack of renormalizability.

As a final comment, if we take  $a < 1$ , we have violation of perturbative unitarity in  $W^+W^-$  scattering at energies of the order of  $4\pi v/\sqrt{1-a^2}$ . Similar considerations apply also to the other channels;

- ii) another example in which perturbative unitarity is recovered, although in a completely different way, is in quantum chromodynamics- (QCD-)like theories. In QCD, for example, pions exhibit the same feature we discussed above for  $W^+W^-$  scattering; here, however, no scalar particle enters the scene to cure the lack of perturbative unitarity, but what happens is that a full tower of resonances (like the  $\rho$ ) also participate to scattering processes, compensating for the exchange of pions. Notice also that QCD can be described with the formalism just introduced, with  $v$  substituted by  $f_\pi \sim \mathcal{O}(90 \text{ MeV})$ , the pion decay constant.

We can imagine QCD as a theory with an  $SU(2)_L \times SU(2)_R$  invariance (ignoring the third family of quarks), spontaneously broken by the quark condensate to  $SU(2)_V$ , thus delivering 3 NGBs (the pions). We can then introduce a set of gauge fields by gauging a subgroup  $SU(2)_L \times U(1)_Y$ ; this implies the NGBs having non-vanishing couplings to the currents which couple to the gauge bosons [14], leading to the generation of a mass term for the gauge fields.

While this mechanism in real QCD would give a mass to the  $W$  boson more than three orders of magnitude smaller than the observed one, we could imagine to introduce new interactions, associated to a so-called *technicolour gauge group* and with a decay constant  $f \sim v$ . This idea is exactly the one behind the technicolour proposal by Susskind [15].

While this discussion pointed out that in principle the Higgs boson is not a fundamental ingredient of the SM, it is undoubtedly true that the discovery of a particle with the same characteristics in 2012 ruled out technicolour-like models; nevertheless, the idea that EWSB could be associated to a strong dynamics, still remains an intriguing possibility for SM extensions.

## 1.2 Global symmetries of the Standard Model

Symmetries are a crucial aspect of modern physics; in a quantum field theory (QFT), they dictate which operators can be present, what are the conserved quantities, and so on. Also the SM exhibits symmetries, both local (gauge) and global; the global ones, however, are peculiar, and we spend some words about them in this subsections.

As we will now discuss, SM global symmetries are special because they manifest as *accidental symmetries*, i.e. symmetries which are such only at the renormalizable level. We could expect these accidental symmetries to be the correct paradigm to describe nature: after all, we have been used to deal with renormalizable theories for a long time,

especially after it was shown that the SM itself can be renormalized [16, 17]. From a modern point of view, however, renormalizability is not a fundamental requirement for a QFT anymore [18]: what really matters are locality and symmetries (in particular, Lorentz and gauge invariance); in this perspective, the general idea is that a Lagrangian contains all the local operators which are compatible with the symmetries, independently of their canonical dimension.

If we follow this recipe for the SM, it is clear that  $\mathcal{L}_{\text{SM}}$  does not exhaust all the possible interactions between the fields; in particular, it is only the renormalizable contribution to an effective field theory (EFT) of the Standard Model, where infinitely other interactions appear. We review some concepts of EFTs in appendix B. If we denote now as  $\mathcal{L}_{\text{SM}}^{\text{ren}}$  the Lagrangian in eq. (1.1.2), we could write the effective SM Lagrangian as:

$$\mathcal{L}_{\text{SM}}^{\text{eff}} = \mathcal{L}_{\text{SM}}^{\text{ren}} + \mathcal{L}_{\text{SM}}^{\text{NR}}, \quad (1.2.1)$$

where NR stands for “non-renormalizable”.

Accidental symmetries, then, are nothing but symmetries of  $\mathcal{L}_{\text{SM}}^{\text{ren}}$  which are not respected by the full Lagrangian  $\mathcal{L}_{\text{SM}}^{\text{eff}}$ ; surprisingly enough, nature obeys these symmetries to a great extent. In addition, accidental symmetries are relevant because operators which violate them can only be generated by  $\mathcal{L}_{\text{SM}}^{\text{NR}}$ , and as such their effects are more likely to be observable, with respect to higher-order corrections to  $\mathcal{L}_{\text{SM}}^{\text{ren}}$ .

### 1.2.1 Number conservations and flavour symmetry

If Yukawa interactions were not there, the renormalizable SM Lagrangian would be invariant under the group:

$$\mathcal{G}_{\text{acc}} = \text{U}(3)^5 \times \text{U}(1), \quad (1.2.2)$$

under which each fermion  $\psi$  transforms as  $\psi \rightarrow U_\psi \psi$ ,  $U_\psi \in \text{U}(3)$ , and the Higgs as  $H \rightarrow e^{i\alpha_H} H$ ,  $\alpha_H \in \mathbb{R}$ . Clearly, Yukawa interactions are present, but we are going to see that we can think in terms of accidental and approximate symmetries in order to explain many observational evidences.

#### Lepton and baryon number conservation

The flavour contribution  $\mathcal{L}_{\text{SM}}^{\text{flavour}}$ , given in eq. (1.1.5), would be invariant under the group defined in eq. (1.2.2) if the Yukawa couplings behaved like fields, called *spurions*, transforming as:

$$U_{qL}^\dagger y^{(u)} U_{dR} e^{-i\alpha_H} = y^{(u)} \quad , \quad U_{qL}^\dagger y^{(d)} U_{dR} e^{i\alpha_H} = y^{(d)}, \quad (1.2.3)$$

and similarly for the leptons. In general, these relations are not satisfied; however, if there were a subgroup of  $\mathcal{G}_{\text{acc}}$  under which  $\mathcal{L}_{\text{SM}}^{\text{flavour}}$  is invariant, this would be a symmetry group for all the renormalizable SM Lagrangian, describing then an accidental symmetry. In order to look for this subgroup, it is convenient to go to a basis where the Yukawa matrices are in the “most diagonal” form: since the latter can be diagonalized with bi-unitary matrices, it is easy to show  $\mathcal{G}_{\text{acc}}$  transformations can be employed to obtain:

$$y^{(u)} \rightarrow y_{\text{diag}}^{(u)} \quad , \quad y^{(d)} \rightarrow V y_{\text{diag}}^{(d)} \quad , \quad y^{(e)} \rightarrow y_{\text{diag}}^{(e)}, \quad (1.2.4)$$

where  $V$  is the CKM matrix, and the diagonal Yukawa eigenvalues are positive. By applying eq. (1.2.3) to this basis, it turns out that  $U_{uR}$ ,  $U_{qL}$ ,  $U_{eR}$ ,  $U_{lL}$  have to be diagonal with complex exponentials as matrix elements; on the other hand, the same condition



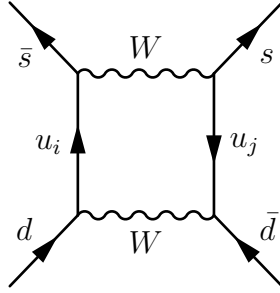


Figure 1.4: Parton-level contribution to  $K_0$ - $\bar{K}_0$  oscillations.

applied to  $y^{(d)}$  implies that  $U_{qL} = e^{i\alpha_q}\mathbf{1}$ , which in turn requires also  $U_{uR}$  and  $U_{dR}$  to be proportional to the identity. Altogether, we obtain from eq. (1.2.3) the following relations for the phases:

$$\begin{aligned}
 \alpha_{uR} - \alpha_{qL} - \alpha_H &= 0 \\
 \alpha_{dR} - \alpha_{qL} + \alpha_H &= 0 \\
 \alpha_{i,eR} - \alpha_{i,\ell L} + \alpha_H &= 0 \quad , \quad i = 1, 2, 3
 \end{aligned}
 \tag{1.2.5}$$

We therefore have 5 equations for 10 variables, meaning that 5 phases remain free: this implies that a subgroup  $U(1)^5 \subset \mathcal{G}_{\text{acc}}$  is a group of symmetry transformations for all the renormalizable SM Lagrangian.

A convenient basis for this  $U(1)^5$  leads to the conservation of total baryon number ( $B$ ), individual lepton number ( $L_i$ ) and hypercharge; while the first two are accidental symmetries, the hypercharge is not (it is a gauge symmetry the SM is constructed on). Non-renormalizable operators which violate these accidental symmetry can lead to features absent in the SM, such as neutrino masses, proton decay, etc..

## Flavour symmetry

Flavour-changing neutral currents (FCNCs) represent processes in which either up- or down-type (neutrino- or charged lepton-) flavours are involved, and where initial and final states have different flavour number; this kind of processes is of great importance because FCNCs are strongly suppressed in the SM, as we will briefly discuss: for this reason, BSM effects have better prospects to be detectable. The prototypical example of FCNC is represented by  $K_0 - \bar{K}_0$  oscillations, whose parton-level contribution is shown in fig. 1.4; in the SM, such a process is heavily suppressed for three different reasons:

### i) Loop suppression

FCNC processes arise at loop level in the SM. As far as the couplings between fermions and both photon and gluon are concerned, they are *flavour universal*, i.e. they are proportional to the unit matrix in flavour space; this is indeed guaranteed by gauge invariance. Therefore, they are not responsible for the mixing between fermions of different flavour.

As far as the couplings with the  $Z$  are concerned, they are also flavour universal, but for a different reason: it is so because all mass eigenstates in a given representation of  $SU(3)_c \times U(1)_{\text{em}}$  come from interaction eigenstates in the same representation of  $\mathcal{G}_{\text{SM}}$ . If this were not the case, non-universal couplings with the  $Z$  boson could be

generated.

Finally, the Yukawa interactions with the Higgs are *flavour diagonal*, again not mixing fermions with different flavours; this is once again a special feature of the SM, due to the fact that all fermions are chiral (so that no bare mass term can be present) and there is only one Higgs doublet. This latter aspect has the consequence that the Yukawa and mass matrices can be simultaneously diagonalized.

We then conclude that FCNC processes cannot be generated at tree level, leading to a first suppression due to loop factors.

ii) CKM suppression

A second reason why FCNC processes are suppressed has to be looked for in the CKM matrix; clearly, flavour-changing processes are accompanied by non-diagonal entries of the CKM matrices, which in the Wolfenstein parametrization [19] can be schematically written as  $V_{us}, V_{cd} \propto \lambda$ ,  $V_{cb}, V_{ts} \propto \lambda^2$ ,  $V_{ub}, V_{td} \propto \lambda^3$ , and  $\lambda = 0.22465 \pm 0.00039$  [20].

iii) GIM suppression

A third source of suppression comes from the so-called Glashow-Iliopoulos-Maiani (GIM) mechanism [21], which predicts that no flavour-changing couplings with the  $W$  boson exist if all the quarks in a given sector are degenerate in mass. To understand this, let us consider the explicit example shown in fig. 1.4; the amplitude is estimated to be:

$$\mathcal{M}_{K_0-\bar{K}_0} \sim \frac{g^4}{16\pi^2} \frac{1}{m_W^2} \sum_{i,j} V_{su_i}^\dagger V_{u_i d} V_{su_j}^\dagger V_{u_j d} f\left(\frac{m_{u_i}^2}{m_W^2}, \frac{m_{u_j}^2}{m_W^2}\right), \quad (1.2.6)$$

where  $f$  is an  $\mathcal{O}(1)$  function in its arguments. First of all, we can restrict the sum over the first two generations because of the CKM suppression we discussed before; in addition, because of the unitarity of the CKM matrix, we have  $V_{su}^\dagger V_{ud} \approx -V_{sc}^\dagger V_{cd}$ , so that:

$$\begin{aligned} \sum_i V_{su_i}^\dagger V_{u_i d} f\left(\frac{m_{u_i}^2}{m_W^2}\right) &\approx V_{sc}^\dagger V_{cd} \left[ f\left(\frac{m_c^2}{m_W^2}\right) - f\left(\frac{m_u^2}{m_W^2}\right) \right] \\ &\approx V_{sc}^\dagger V_{cd} f'(0) \frac{m_c^2 - m_u^2}{m_W^2}, \end{aligned} \quad (1.2.7)$$

where in the last step we have expanded  $f$  in series. We clearly see that if the all the quarks of a given sector (recall the we are neglecting the third generation) are degenerate in mass, the amplitude vanishes. This is the essence of the GIM mechanism.

The suppression of FCNC processes can also be traced in the accidental symmetries of  $\mathcal{L}_{\text{SM}}^{\text{ren}}$ ; in fact, both the smallness of masses for the first two generations and the form of the CKM matrix comes from the fact that the Yukawa couplings can be approximated (in an appropriate basis) as:

$$y^{(u),(d),(e)} \approx y_{t,b,\tau} \begin{pmatrix} 0 & 0 & 0 \\ 0 & 0 & 0 \\ 0 & 0 & 1 \end{pmatrix} + \text{small contributions}. \quad (1.2.8)$$

In the limit where these small contributions are exactly zero, the flavour Lagrangian in eq. (1.1.5) (and then the full renormalizable SM Lagrangian) is invariant a subgroup of  $\mathcal{G}_{\text{acc}}$  (defined in eq. (1.2.2)) where the transformation matrices act only on the first two generations; this is nothing but the global group  $U(2)^5 \subset \mathcal{G}_{\text{acc}}$ . Since these small contributions are not zero, we can understand the suppression of FCNC processes in terms of an approximate, global  $U(2)^5$  symmetry.

Given that  $\mathcal{G}_{\text{acc}}$  is broken only by the Yukawa interactions, and in the very peculiar way we briefly recalled, the concept of minimal-flavour-violating (MFV) theory was introduced in the literature [22]: an effective theory constructed from SM and the spurions satisfies the MFV criterion if all non-renormalizable operators are invariant under  $\mathcal{G}_{\text{acc}}$  (and  $CP$ ).

## 1.2.2 Custodial symmetry

We discussed in section 1.1.4 how the CCWZ formalism can be employed to discuss EWSB; however, it turns out that the one in eq. (1.1.17) is not the most general term allowed by symmetries. Actually, we should have considered the Lagrangian:

$$\mathcal{L}_{\Sigma}^{(2)} = \frac{v^2}{4} \text{Tr}[(D_{\mu}\Sigma)^{\dagger} (D^{\mu}\Sigma)] + a_T \frac{v^2}{8} \text{Tr}^2[\Sigma^{\dagger} D_{\mu}\Sigma \sigma^3], \quad (1.2.9)$$

which leads to the prediction for the gauge boson masses:

$$m_W^2 = \frac{v^2 g^2}{4}, \quad m_Z^2 = \frac{v^2 g^2}{4 \cos^2 \theta_w} (1 - a_T) \quad \Rightarrow \quad \rho = \frac{1}{1 - a_T}. \quad (1.2.10)$$

The current experimental value,  $\rho = 1.00039 \pm 0.00019$  [20], requires  $a_T \sim 10^{-4}$ ; in general, we think of small values of dimensionless parameters as very much related to symmetry arguments [23]: it is then natural to ask whether the smallness of the coefficient  $a_T$  can also be explained in terms of symmetries.

The Lagrangian in eq. (1.2.9) is invariant under local  $SU(2)_L \times U(1)_Y$  transformations; however, if  $a_T = 0$ , it is invariant under a larger group, namely a global  $SU(2)_L \times SU(2)_R$  under which  $\Sigma \rightarrow U_L \Sigma U_R^{\dagger}$ ,  $U_{L,R} \in SU(2)_{L,R}$ . To be more precise,  $SU(2)_L \times SU(2)_R$  is a symmetry group for eq. (1.2.9) only if also  $g' = 0$ .

In general,  $SU(2)_L \times SU(2)_R$  is broken in the SM Lagrangian:

- explicitly by  $g'$ , since the term proportional to it in  $D_{\mu}\Sigma$  does not commute with general  $SU(2)_R$  transformations, but only with the corresponding third component;
- explicitly by Yukawa interactions, because  $y_{ij}^{(u)} \neq y_{ij}^{(d)}$ , as clear from eq. (1.1.23);
- spontaneously by the VEV of  $\Sigma$ ,  $\langle \Sigma \rangle = \mathbf{1}$ , being the latter invariant only under transformations with  $U_L = U_R$ , i.e. only under the *diagonal* subgroup  $SU(2)_V \subset SU(2)_L \times SU(2)_R$ . This residual symmetry is called *custodial symmetry* [24–26].

The relation  $\rho = 1$  remains valid at tree level, while corrections proportional to  $g'$  and  $y^{(u)} - y^{(d)}$  emerge at loop level. If the equalities  $g' = 0$  and  $y^{(u)} = y^{(d)}$  were respected, we would have  $\rho = 1$  to all orders in perturbation theory.

Actually, the custodial symmetry is not exact, since  $SU(2)_L \times SU(2)_R$  is already broken explicitly; in addition, it could be even more heavily broken by NP operators, analogously to what happened with the term proportional to  $a_T$  in eq. (1.2.9). However, the experimental fact that  $\rho \approx 1$  is an indication that both  $g'$  and  $y^{(u)} - y^{(d)}$  must be sufficiently

small, making the custodial symmetry an approximate symmetry of the theory. Not to be in contrast with experiments, then, one usually requires that also BSM extensions respect the custodial symmetry, at least approximately.

If not for the sources of explicit breaking we have just discussed, the custodial symmetry would be a symmetry of the whole SM Lagrangian after EWSB, including the Higgs potential in eq. (1.1.8). If we parametrize the Higgs doublet as:

$$H = \frac{1}{\sqrt{2}} \begin{pmatrix} h_1 + ih_2 \\ h_3 + ih_4 \end{pmatrix}, \quad (1.2.11)$$

the potential is only function of  $|H|^2 = \sum_i h_i^2$ , and so invariant under an SO(4) symmetry group; since  $\text{SO}(4) \simeq \text{SU}(2) \times \text{SU}(2)$ , we recognize the invariance of the potential under  $\text{SU}(2)_L \times \text{SU}(2)_R$ . Once the Higgs acquires a VEV,  $h_i = 0$  for  $i \neq 3$ , this symmetry is explicitly broken to  $\text{SO}(3) \simeq \text{SU}(2)$ , i.e. the custodial symmetry.

### 1.3 Electroweak precision tests

The weak sector of the Standard Model has been tested very accurately, in particular at the Large Electron-Positron Collider (LEP), in the so-called electroweak precision tests (EWPTs). The operators relevant for EWPTs do not violate any of the accidental symmetries we discussed before; their importance lies in the fact that their effects are measured with a high level of accuracy, and can therefore be sensitive also to NP originating at high scales. Examples of these observables are  $m_W$ ,  $m_Z$ ,  $WW\gamma$  and  $ZZ\gamma$  couplings, the asymmetry in left- and right-handed fermions in the final state, defined as:

$$A_{LR}^f \equiv \frac{\Gamma(Z \rightarrow f_L \bar{f}_R) - \Gamma(Z \rightarrow f_R \bar{f}_L)}{\Gamma(Z \rightarrow f_L \bar{f}_R) + \Gamma(Z \rightarrow f_R \bar{f}_L)}, \quad (1.3.1)$$

and so on.


In this kind of analysis, the parameters  $g$ ,  $g'$  and  $v$  are expressed in terms of the electromagnetic fine structure constant  $\alpha_{\text{em}}$  (determined from  $\gamma^* \rightarrow e^+e^-$  scattering), the Fermi constant  $G_F$  (determined from  $\mu$  decay) and the  $Z$  boson mass  $m_Z$ ; the reason for doing this is that the latter are measured with a high degree of accuracy. New physics can then change the relation between  $g$ ,  $g'$ ,  $v$  and  $\alpha_{\text{em}}$ ,  $G_F$ ,  $m_Z$ .

In the following, we focus on *universal theories* of EWSB, defined as those theories where the only gauge interactions of light fermions are of the type [27]:

$$\mathcal{L}_{\text{int}} = \bar{\psi} \gamma^\mu (g T^a \bar{W}_\mu^a + g' Y \bar{B}_\mu) \psi, \quad (1.3.2)$$

$T^a$  being the generators of  $\text{SU}(2)_L$  and  $Y$  the hypercharge. In general,  $\bar{W}_\mu^a$  and  $\bar{B}_\mu$  are not the usual SM gauge bosons, but are rather a mixture of them with possible heavy new gauge bosons. We consider only leptons and light quarks because these are the most relevant particles for EWPTs. The SM can be considered a universal theory in the limit in which the Yukawa couplings are set to zero.

In universal theories, important deviations from the SM reside in the *oblique parameters*, related to the vacuum polarization amplitudes of the SM gauge bosons. For this reason, we introduce a uniform notation and define the vacuum polarization amplitude for the gauge bosons  $I$  and  $J$  as:



$$\equiv i\Pi_{IJ}^{\mu\nu}(q^2) \equiv i [\Pi_{IJ}(q^2)g^{\mu\nu} - \Delta(q^2)q^\mu q^\nu] , \quad (1.3.3)$$

where  $q$  denotes the incoming momentum. The last term usually drops out of calculation once this amplitude is dotted in a fermion current, since we are considering light fermions.

With the definition above, a positive value of  $\Pi_{IJ}$  gives a positive mass shift to the gauge bosons:

$$m_V^2 \rightarrow m_V^2 + \Pi_{VV}(m_V^2) . \quad (1.3.4)$$

The masslessness of the photon requires that (see, e.g., ref. [28]<sup>1</sup>):

$$\Pi_{\gamma\gamma}(0) = 0 = \Pi_{\gamma Z}(0) . \quad (1.3.5)$$

It also useful to define:

$$\Pi'_{VV}(0) \equiv \left. \frac{d\Pi_{VV}}{dq^2} \right|_{q^2=0} . \quad (1.3.6)$$

We can relate the parameters  $g$ ,  $g'$  and  $v$  to this polarization amplitudes as [29]:

$$\frac{1}{g^2} = \Pi'_{W^+W^-}(0) \quad , \quad \frac{1}{g'^2} = \Pi'_{BB}(0) \quad , \quad v^2 = -4\Pi_{W^+W^-}(0) . \quad (1.3.7)$$

The two oblique parameters which will be most relevant for us in the following are [27]:

$$\hat{S} \equiv g^2 \Pi'_{W^3B}(0) \quad (1.3.8a)$$

$$\hat{T} \equiv \frac{4}{v^2} [\Pi_{W^3W^3}(0) - \Pi_{W^1W^1}(0)] . \quad (1.3.8b)$$

These are related to the  $S$  and  $T$  Peskin-Takeuchi parameters introduced in ref. [30] by [29]:

$$S = \frac{4 \sin^2 \theta_w}{\alpha_{\text{em}}} \hat{S} \quad , \quad T = \frac{\hat{T}}{\alpha_{\text{em}}} . \quad (1.3.9)$$

It can be shown that the parameter  $\hat{T}$  is related to  $\rho$  by the relation  $\hat{T} = \rho - 1$ .

The current combined limits on  $S$  and  $T$  from GFitter are [31]:

$$S = 0.04 \pm 0.08 \quad , \quad T = 0.08 \pm 0.07 , \quad (1.3.10)$$

where we assumed the oblique parameter  $U$  vanishing.

We conclude by recalling that other oblique parameters are defined and often used in the literature; however,  $\hat{S}$  and  $\hat{T}$  are the two that will be most relevant for our future analysis.

---

<sup>1</sup>In quantum electrodynamics (QED), it is customary to normalize  $\Pi(q^2)$  as  $\Pi(q^2) = q^2 \tilde{\Pi}(q^2)$ , with  $\tilde{\Pi}(q^2)$  regular in  $q^2 = 0$ .

## 1.4 Hierarchy problem

Although its incredible success, for sure SM is not the ultimate theory of nature, but rather an EFT; a complete description of gravity, for instance, is missing. Of course, one can treat gravity within the SM in a perturbative way, i.e. by expanding general relativity semiclassically; such a description is perfectly legitimate for energies much smaller than the Planck mass,  $M_{Pl} \equiv (8\pi G)^{-\frac{1}{2}} \approx 2.4 \times 10^{18}$  GeV.

While the perturbative description of gravity breaks down at the Planck scale, it is definitely possible (and even desired, as we are going to discuss) that some new physics emerges before reaching quantum gravity energies; for this reason, we can think the SM as an EFT of some underlying ultraviolet (UV) theory endowed with an intrinsic cutoff  $\Lambda_{SM}$ .

Independently of the specific UV theory, the considerations of section 1.2 and appendix B reveal that the SM has an intrinsic disturbing feature, called *hierarchy problem*<sup>2</sup>. Such a problem is not a peculiarity of the SM; in general, in fact, theories with scalars can suffer of the same feature. To illustrate this, let us consider theory for a real scalar field  $\phi$  (respecting a  $\mathbb{Z}_2$  symmetry, for simplicity) emerging as an EFT from some unknown theory defined above a scale  $\Lambda$ ; the most general Lagrangian is:

$$\begin{aligned} \mathcal{L}_\phi &= \frac{1}{2} \partial_\mu \phi \partial^\mu \phi + \lambda_{2,0} \phi^2 + \lambda_{4,0} \phi^4 + \lambda_{6,0} \phi^6 + \lambda_{8,0} \phi^8 + \dots \\ &+ \lambda_{2,2} \phi^2 \partial_\mu \phi \partial^\mu \phi + \lambda_{4,2} \phi^4 \partial_\mu \phi \partial^\mu \phi + \dots \\ &+ \lambda_{2,4} \phi^2 (\partial_\mu \phi \partial^\mu \phi)^2 + \lambda_{4,4} \phi^4 (\partial_\mu \phi \partial^\mu \phi)^2 + \dots \\ &+ \dots \\ &\equiv \sum_I \lambda_I \mathcal{O}_I. \end{aligned} \tag{1.4.1}$$

If we denote by  $\Delta_I$  the dimension of the operator  $\mathcal{O}_I$ , then each coefficient  $\lambda_I$  can be parametrized as:

$$\lambda_I = \frac{g_I}{\Lambda^{\Delta_I-4}}, \tag{1.4.2}$$

with being  $g_I$  dimensionless and expected to be  $\mathcal{O}(1)$  in order to be able to perform a perturbative expansion; this assumption is not a strict requirement, but turns out to be valid in all examples of strongly-interacting theories we know.

This assumption, however, poses a problem: for the mass term,  $\lambda_{2,0} = g_{2,0} \Lambda^2 \equiv m^2/2$ , we need  $g_{2,0} \ll 1$ ; if this were not the case, in fact, no quanta with energy much smaller than  $\Lambda$  would exist (since the mass represents the minimum energy a particle can have), and in turn no low-energy description would be possible; we are then forced to require  $g_{2,0} \ll 1$ , although without a real motivation. This brief discussion represents the simplest example of naturalness problem.

In general, naturalness is not a necessary condition for a theory [32], although it is very deeply connected to an idea which guided physicists for centuries: the concept of separation of scales; the idea is that processes happening at a given scale are not affected by the ones taking place at much shorter distances. In general, we can think of unnaturalness as the signal for the emergence of some new physics around the corner.

---

<sup>2</sup>In the following, with maybe an abuse of notation, we indifferently use the terms “naturalness” and “hierarchy”.

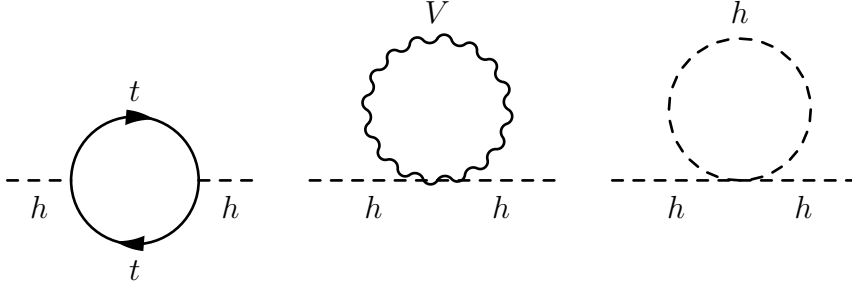


Figure 1.5: Main contributions to  $m_h^2|_{\text{SM}}$  coming from loops of  $t$ , gauge bosons and  $h$ .

If this is not the case, on the other hand, it would imply a strong correlation between infrared (IR) and UV physics, invalidating the EFT approach [33].

It is important to stress that this discussion is not a mere consequence of the considering a large cutoff  $\Lambda$  for the theory; even with other regularization schemes, such as dimensional regularization, there would be large contributions to the mass parameter of  $\phi$ , for example due to the interactions with some other scalar  $\Phi$  with mass  $M \gg m$  (see ref. [32] for a detailed discussion about this point).

### 1.4.1 Unnaturalness of the Higgs mass

Having discussed the bottom line of the naturalness problem, we can consider the case of the Standard Model. (One of) the naturalness problem(s) is related to the mass of the Higgs bosons; analogously to the previous example, we should write the mass term for the Higgs, in the formulation where the SM is treated as an effective theory, as:

$$\mathcal{L}_H \supset c \Lambda_{\text{SM}}^2 H^\dagger H. \quad (1.4.3)$$

If we take  $\Lambda_{\text{SM}} \sim \mathcal{O}(10^{15} \text{ GeV})$ , this requires  $c \lesssim 10^{-26}$  in order to be in agreement with experimental evidences.

We can discuss the problem in a more formal way with the following approach: in full generality, we can assume that the UV theory predicts a mass for the Higgs boson given by [27]:

$$m_h^2 = \int_0^\infty dE \frac{dm_h^2}{dE}, \quad (1.4.4)$$

where the integrand is a not specified function of the input parameters of the UV theory. Since the integral is performed over all the possible energies, we can consider it as the sum of two contributions:

$$m_h^2 = \int_0^{\Lambda_{\text{SM}}} dE \frac{dm_h^2}{dE} + \int_{\Lambda_{\text{SM}}}^\infty dE \frac{dm_h^2}{dE} \equiv \delta m_h^2|_{\text{SM}} + \delta m_h^2|_{\text{BSM}}, \quad (1.4.5)$$

where the first term can be fully computed within the SM, while the second one depends on the specific underlying UV theory. The main contributions to  $\delta m_h^2|_{\text{SM}}$  come from loops of the top quark, the gauge bosons, and the Higgs itself, and are shown in fig. 1.5; the result is:

$$\delta m_h^2|_{\text{SM}} \approx \frac{3\Lambda_{\text{SM}}^2}{16\pi^2 v^2} (4m_t^2 - 2m_W^2 - m_Z^2 - m_h^2). \quad (1.4.6)$$

Once again, the underlying hypothesis in eq. (1.4.5) is that contributions coming from scales which are very separated from each others do not interfere; but then, it is clear that a problem arises: since by assumption  $\Lambda_{\text{SM}} \gg v \sim m_h$ , a cancellation between  $\delta m_h^2|_{\text{SM}}$  and  $\delta m_h^2|_{\text{BSM}}$  is necessary, although being the two terms completely unrelated. In particular, we can estimate the minimum level of *fine tuning*  $\xi^{-1}$  that is needed as:

$$\xi^{-1} \gtrsim \frac{\delta m_h^2|_{\text{SM}}}{m_h^2} \sim \mathcal{O}\left(\frac{\Lambda_{\text{SM}}^2}{10^4 \text{ GeV}^2}\right). \quad (1.4.7)$$

If, for example,  $\Lambda_{\text{SM}} \sim \mathcal{O}(10^{14} \text{ GeV})$ , we obtain  $\xi^{-1} \gtrsim 10^{24}$ , meaning that at least a 24 digits cancellation between two unrelated contributions must occur; this is the essence of the hierarchy problem related to the unnaturality of the Higgs mass.

## 1.4.2 Possible solutions

During the last few decades, many solutions to the Higgs naturalness problem were proposed, relying on very different assumptions. We briefly recall here some ideas:

- a first possibility is that fields with masses much larger than the EWSB scale do not exist. Such an assumption could be motivated by the fact that many open problems of the SM require the existence of new physics at scales which are not much larger than  $v$ . On the other hand, however, this hypothesis presents some problems as well: first of all, no gauge coupling unification is possible, since grand unified theories (GUTs) are usually associated to a scale  $\Lambda_{\text{GUT}} \sim \mathcal{O}(10^{15} \text{ GeV})$ ; in addition, an even more serious problem is represented by gravity: the latter is usually associated to the Planck scale,  $M_{Pl} \sim \mathcal{O}(10^{18} \text{ GeV})$ . A solution to this second problem was presented in the context of large extra dimensions, where the real scale of gravity  $M_*$  can be much smaller, e.g.  $M_* \sim \mathcal{O}(1 \text{ TeV})$ , while the value of  $M_{Pl}$  is just the result of the compactification of extra dimensions;
- a second possibility is that there exist fields much heavier than the EWSB scale, but the Higgs is a composite, rather than fundamental, particle, made up of fermions belonging to a new, strongly-interacting, sector. This is the idea, for example, of composite Higgs [34–37]. If we denote by  $\Lambda_{\text{strong}}$  the scale at which the strong dynamics confines, we could expect corrections to the Higgs mass of the order  $\delta m_h^2 \propto \Lambda_{\text{strong}}^2$ ; for this reason,  $\Lambda_{\text{strong}} \sim \mathcal{O}(1 \text{ TeV})$  is usually required;
- a third possibility is that the mass of the Higgs, considered as an elementary particle, is kept small by symmetries. The most famous example of BSM model belonging to this category is supersymmetry (SUSY) (see, e.g., refs. [38–40]), where large corrections to the Higgs mass are avoided thanks to a cancellation between loop contributions of bosons and fermions.

Although the plethora of proposals for BSM models, it is important to stress that all of them seem to be more and more in tension with experimental results, given also that no significant departure from the SM has been found.

In future developments of particle physics, naturalness arguments may remain valid guiding principles anyway; if this is not the case, on the other hand, it would mean that a deep change in the way we look at nature on small scales is necessary.



# Chapter 2

## Dark matter

*If this would be confirmed, we would get the surprising result that dark matter is present in much greater amount than luminous matter.*

Fritz Zwicky

One very important missing piece of the SM is represented by dark matter: nowadays, we know from experiment that most of the matter in the universe (more than 80%) is not represented by ordinary baryons or leptons, but rather by a new, extra-ordinary form of matter whose existence can be inferred by many indirect effects.

In this chapter, we review the main properties of DM and discuss quite in detail the case of WIMPs, from both a theoretical and an experimental point of view.

### 2.1 History and evidences

The first mentions about a dark component of matter in the universe already appeared in the 20's [41], although we have to wait until 1933 for the first real evidence, due to the work by Zwicky [42]. We now briefly review some of the main evidences that historically brought to the awareness that most of the matter in the universe is dark:

- Zwicky studied the Coma Cluster, a group of more than 1000 galaxies, and applied the virial theorem, stating that for a system in equilibrium:

$$2\langle T \rangle + \langle V \rangle = 0, \quad (2.1.1)$$

where  $T$  and  $V$  are the kinetic and potential energies, respectively. He assumed the size of the cluster to be  $R \sim \mathcal{O}(1 \text{ Mpc})$ , and determined the mass of the galaxies from measuring the velocity dispersions. By estimating the corresponding mass-to-luminosity ratio and comparing it with the one of the close-by Kapteyn stellar system, he concluded that the amount of matter in the cluster was more than 300 times larger than expected; from this, he concluded that most of the matter had to be optically dark;

- another milestone in the history of DM is represented by the work of Rubin and Ford [43], where they considered the rotation curves of stars in galaxies; Newton's law predicts

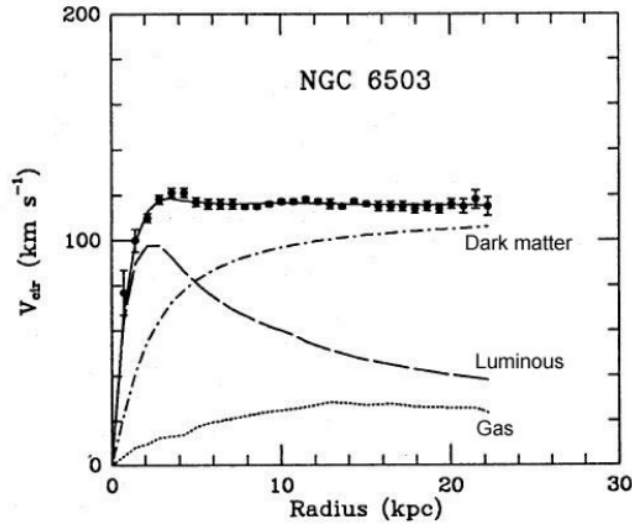


Figure 2.1: Rotation curve for the galaxy NGC 6503. Figure taken from ref. [44].

that the circular velocity  $v_c$  of a star is related to its distance  $r$  from the center of the galaxy by:

$$v_c = \sqrt{\frac{G_N M(r)}{r}}, \quad (2.1.2)$$

where  $G_N$  is the Newton constant and  $M(r)$  is the mass enclosed in a sphere or radius  $r$ :

$$M(r) = \int_{|x| \leq r} d^3x \rho(x), \quad (2.1.3)$$

with  $\rho$  being the density. By assuming that the mass of a galaxy is within the disk, eq. (2.1.2) implies that  $v_c \propto r^{-1/2}$  at large distances. However, observations suggest that the velocities tend to a constant value for large  $r$  (see fig. 2.1). These results can be explained if one assumes an additional component which behaves like ordinary matter from a gravitational point of view, but is characterized by a density scaling as  $\rho \propto r^{-2}$ ;

- another famous evidence for the existence of DM is represented by the so-called “Bullet Cluster” [45], where two clusters of galaxies collide. The image in fig. 2.2 clearly shows that the baryonic component, i.e. the intercluster gas, is strongly affected by the collision, whereas the gravitational potential, represented with the green lines, is not: this suggests that the latter is not produced by the gas, but some other, extra-ordinary, component of matter;
- according to General Relativity, gravity influences the path of light: this process is known as *gravitational lensing*; in particular, by studying how an image of distant galaxies is distorted by a foreground object (a cluster, for instance), it is possible to estimate the gravitational potential of the lens. In fig. 2.3, we show this effect due to the cluster Abell 2218. With gravitational lensing, it has been inferred that most of the matter is not visible;

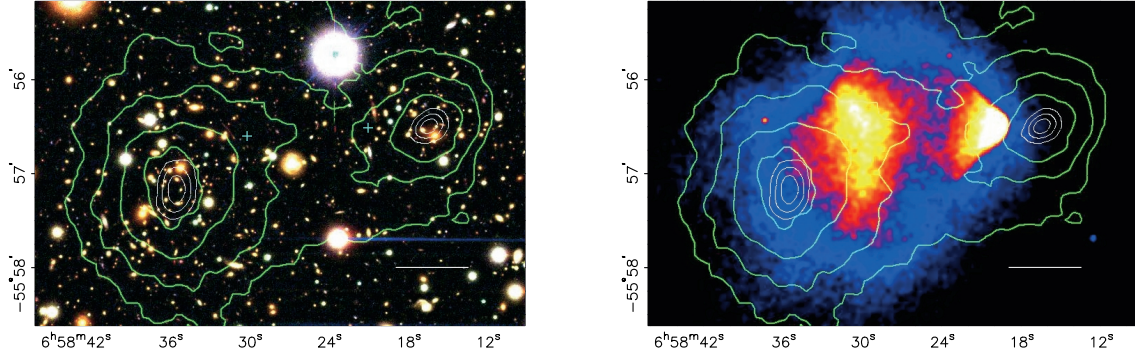


Figure 2.2: Collision of two clusters of galaxies, also known as “Bullet Cluster”. In the right panel, the event is shown in the X-ray; the green lines correspond to gravitational equipotential surfaces. Figure taken from ref. [45]

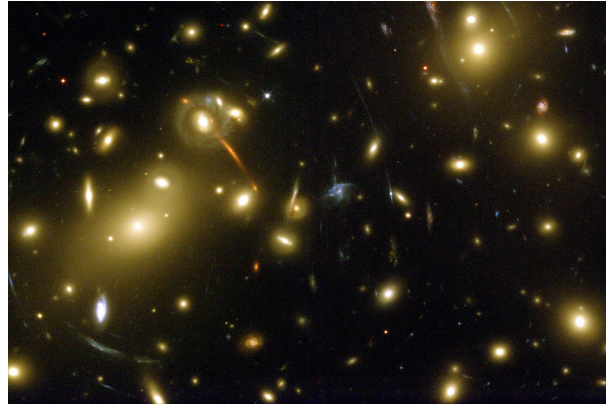


Figure 2.3: Gravitational lensing from the cluster of galaxies Abell 2218.

- one of the strongest evidences for the existence of DM is represented by cosmology, and in particular by the cosmic microwave background (CMB); the anisotropies in temperature can be expanded in spherical harmonics as:

$$\frac{\Delta T}{T}(\theta, \phi) = \sum_{\ell, m} a_{\ell m} Y_{\ell m}(\theta, \phi), \quad (2.1.4)$$

from which the power spectrum can be computed as:

$$\mathcal{D}_{\ell}^{TT} = \frac{\ell(\ell + 1)C_{\ell}}{2\pi} \quad , \quad C_{\ell} \equiv \frac{1}{2\ell + 1} \sum_m |a_{\ell m}|^2. \quad (2.1.5)$$

The CMB spectrum obtained by the Planck collaboration [46] is shown in fig. 2.4. Important properties of DM can be deduced by the peaks in the power spectrum; in fact, their angular position (measured in terms of  $\ell$ ) gives us informations about the cosmological parameters; in particular, the abundance of baryons reflects in the ratio of the amplitudes of even and odd peaks. Observations indicate that the abundance of baryons at 68% confidence level (CL) is given by [46]:

$$\Omega_b h^2 = 0.02233 \pm 0.00015, \quad (2.1.6)$$

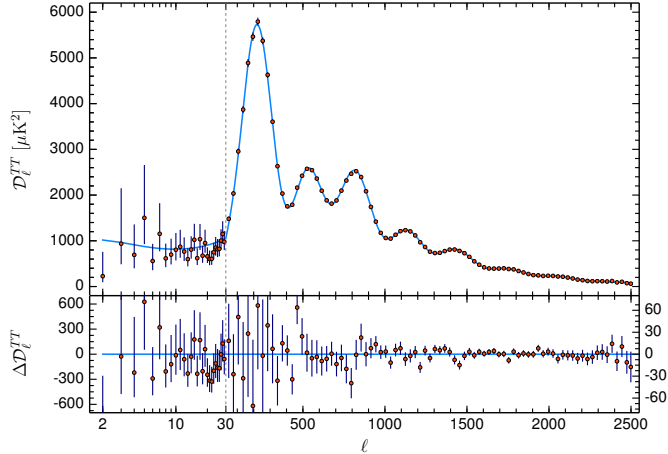


Figure 2.4: CMB temperature power spectrum from Planck 2018. Figure taken from ref. [46].

where, as we will see in section 2.3, we indicate by  $\Omega_X h^2$  the ratio between the density of a species  $X$  and the critical density of the universe.

On the other hand, the dark matter density is:

$$\Omega_c h^2 = 0.1198 \pm 0.0012. \quad (2.1.7)$$

Therefore, CMB not only tells us that a dark component of matter is present in the universe, but also that it is about 5 times more abundant than the ordinary one.

All these observations, and others, also give important insights about the properties of DM:

- i) DM is dark, meaning that its coupling to photon must be strongly suppressed. This constraint comes from the fact that DM does not contribute to the radiation background and that it cannot cool radiating photons.

In addition to the electromagnetic ones, also DM interactions with gluons have to be suppressed;

- ii) DM is collisionless, meaning that DM self-interactions are strongly suppressed; the Bullet Cluster is a clear example of this property;
- iii) DM behaves like a fluid, rather than having a granular structure; massive compact halo objects (MACHOs) are potential astrophysical bodies which behave like DM. Searches from microlensing excluded a dominant contribution to DM density from MACHOs with masses in the range  $10^{-7} M_\odot \lesssim m \lesssim 10 M_\odot$  [47];
- iv) DM behaves classically, at least on the galactic scales where it is confined. Depending on the particle nature of DM, we can infer a lower limit on its mass [48]:

- if DM is a boson, Bose-Einstein statistics allows one to have an arbitrarily large number of particles per a single cell of phase space volume; the DM then behaves

like a coherent field and, similarly to what happens for the hydrogen atom, its stability can be formulated in terms of the uncertainty principle, requiring that:

$$\Delta x \Delta p \lesssim 1, \quad (2.1.8)$$

where  $\Delta p \sim m_{\text{DM}}v$  and  $\Delta x \sim 2R_{\text{halo}}$ . The most stringent bound comes by applying this limit to dwarf galaxies, leading to:

$$m_{\text{DM}} \gtrsim 10^{-22} \text{ eV}; \quad (2.1.9)$$

- if DM is a fermion, on the other hand, the halo mass can be estimated as:

$$M_{\text{halo}} = m_{\text{DM}}V \int \frac{d^3p}{1 + e^{\beta E(p)}} \lesssim m_{\text{DM}}R_{\text{halo}}^3 (m_{\text{DM}}v)^3. \quad (2.1.10)$$

This estimate, applied to dwarf galaxies, leads to

$$m_{\text{DM}} \gtrsim 0.7 \text{ keV}; \quad (2.1.11)$$

v) DM is not hot (i.e. it is non-relativistic at matter-domination equality), since otherwise it would have erased structures; to quantify this statement more precisely, it is useful to introduce the so-called *free-streaming length*, defined as the distance a particle travels between its production and matter-radiation equality:

$$\lambda_{\text{FS}} \equiv \int_{t_0}^{t_{\text{eq}}} dt \frac{v(t)}{a(t)}. \quad (2.1.12)$$

The integral is dominated by the relativistic regime, i.e. when  $v \sim 1$  and  $t < t_{\text{nr}}$ ; if we assume radiation domination, we get [49]:

$$\lambda_{\text{FS}} \sim 2\sqrt{t_{\text{nr}}} \sim 0.4 \text{ Mpc} \frac{1 \text{ keV}}{m_{\text{DM}}}. \quad (2.1.13)$$

In general, we can classify a DM candidate according to its free-streaming length, as:

- *hot dark matter* (HDM) if  $\lambda_{\text{FS}} \gg 1 \text{ Mpc}$ ;
- *warm dark matter* (WDM) if  $\lambda_{\text{FS}} \sim 1 \text{ Mpc}$ ;
- *cold dark matter* (CDM) if  $\lambda_{\text{FS}} \ll 1 \text{ Mpc}$ .

Hot relics also lead to a top-down picture, where large structures fragment into smaller ones. On the contrary, cold relics lead to clustering of small structures into larger ones.

Observations favour cold dark matter, but some room is left also to warm candidates; interestingly enough, the latter could solve some tensions between observations and predictions on small scales (such as the missing satellite [50] and the too big to fail [51] problems);

vi) DM is stable, since we still see its effects nowadays. In principle, it is possible it is unstable but extremely long-lived: recent bounds set a lower limit of  $\tau_{\text{DM}} \gtrsim 160 \text{ Gyr}$  [52]. For our considerations, we can safely consider DM to be absolutely stable.

## 2.2 Main dark matter candidates

Historically, many models to explain the origin of DM were proposed, very different from each others; during the time, as sensitiveness of experiments became higher and higher, some of them have been completely ruled out, while for others the available parameter space has been reduced.

We briefly review here some famous ideas proposed in the last few decades, without the will of being exhaustive in any way. In general, DM candidates can be classified depending to the fact that they belong or not to the category of WIMPs. We will discuss in detail properties of WIMP candidates in the following, being the latter the core of this work.

### 2.2.1 WIMP candidates

On general ground, WIMPs can be defined as non-baryonic massive particles which interact weakly with the SM, are produced via the freeze-out mechanism and have a mass in the range  $2 \text{ GeV} \lesssim m_{\text{DM}} \lesssim 100 \text{ TeV}$  [53], where the upper limit comes from violation of unitarity in the annihilation cross section [54]. Although this vague definition, WIMPs have been by far the most widely studied candidates of DM, since they arise in some of the most well-motivated BSM proposals. In addition, they usually have interactions and rates which can be probed with current and future experiments.

Among the most famous WIMP candidates, we can recall:

- lightest supersymmetric particle (LSP): supersymmetry is in general endowed with the so-called *R-parity*, a symmetry which prevents large violations of baryon number and consequent proton decay. Supersymmetric particles are usually assigned a value  $P_R = -1$ , while SM ones have  $P_R = 1$ ; as a consequence, the lightest state of the supersymmetric spectrum is absolutely stable, leading to a possible DM candidate. Examples of LSPs which can be DM candidates are the neutralino or the sneutrino;
- Kaluza-Klein (KK) states: theories with extra dimensions (see, e.g., refs. [55–57]) predict a full tower of states for each particle; as an example, in the case of only one universal extra dimension (i.e., with all particles propagating in all the spacetime) compactified on a  $S^1/\mathbb{Z}_2$  orbifold, the KK-parity conservation can make the lightest KK particle a DM candidate [58];
- dark matter candidates in the form of WIMPs can be present in many other extensions of the SM, as we will discuss in detail in the following: in chapter 3, we consider the case in which a simple WIMP Lagrangian is added on top of the SM one, while in chapter 4 we consider the problem of DM associated to the hierarchy one.

### 2.2.2 Non-WIMP candidates

WIMPs are of course not the only possibility to account for DM. Some famous alternatives to the WIMP paradigm are:

- axions: these are hypothetical particles firstly introduced to solve the strong *CP* problem; on top of the QCD Lagrangian, we can add the term:

$$\mathcal{L}_\theta = \frac{\theta}{64\pi^2} \epsilon_{\mu\nu\rho\sigma} G_a^{\mu\nu} G_a^{\rho\sigma}, \quad (2.2.1)$$

where  $G_{\mu\nu}$  is the (non-canonically normalized) gluon field strength. Such a term violates both  $P$  and  $CP$ .

Let us now consider the effect of the redefinition of all the quark fields in the QCD Lagrangian  $q_f \rightarrow e^{i\alpha_f\gamma^5} q_f$ ; because of the chiral anomaly, this has the effect of changing the QCD Lagrangian as:

$$\mathcal{L}_{\text{QCD}} \rightarrow \mathcal{L}_{\text{QCD}} + \frac{1}{32\pi^2} \epsilon_{\mu\nu\rho\sigma} G_a^{\mu\nu} G_a^{\rho\sigma} \sum_f \alpha_f. \quad (2.2.2)$$

By comparing this with eq. (2.2.1), we see that it is equivalent to shifting  $\theta$  by  $\theta \rightarrow \theta + 2 \sum_f \alpha_f$ ; on the other hand, the field redefinition  $q_f \rightarrow e^{i\alpha_f\gamma^5} q_f$  also affects the mass term, leading to  $m_f \rightarrow e^{2i\alpha_f} m_f$ .

Given that the observables are usually computed with the path integral formalism, where the fields are integration variables, the field redefinition cannot have any physical consequence, and therefore observable quantities cannot depend separately on  $\theta$  or on the phases of the mass matrix, but only on the combination

$$e^{i\theta} \prod_f m_f. \quad (2.2.3)$$

It is then evident that if any of the quark masses vanished,  $\theta$  would not be physical (it could be set to zero by redefining the massless quark field), and no  $P$ - or  $CP$ -violation would be present in QCD. In general, it is always possible to redefine the quark fields in such a way that  $\theta = 0$ , but at the price of introducing  $P$ - or  $CP$ -violating phases in the mass parameter. If, on the other hand, we define the quark fields in such a way that all the mass parameters are real, a  $\theta \neq 0$  appears, leading to  $P$ - and  $CP$ -breaking; in particular, it causes an anomalous dipole moment for the neutron. Experimental measurements lead to a bound on  $\theta$  of  $|\theta| \lesssim 10^{-10}$ , thus posing a naturalness problem. A solution was found by Peccei and Quinn [59], who supposed the existence of a global  $U(1)_{PQ}$  spontaneously broken at a scale  $f_a \gg \Lambda_{\text{QCD}}$ ; the corresponding NGB was called *axion* [60]. According to the general discussion of appendix A, under a  $U(1)_{PQ}$  the axion field shifts: therefore, the only non-derivative term which is allowed is:

$$\mathcal{L}_a = \frac{1}{64\pi^2 f_a} a \epsilon_{\mu\nu\rho\sigma} G_a^{\mu\nu} G_a^{\rho\sigma}, \quad (2.2.4)$$

where  $a$  is the axion field and  $f_a$  is the axion decay constant. In this way, the smallness of  $\bar{\theta}$  can be seen as a dynamical problem, related to the minimum of the axion potential; it can be shown that such a minimum is for  $a = 0$ , providing an elegant solution to the strong  $CP$  problem.

Astrophysics sets a lower bound on the scale of breaking of  $U(1)_{PQ}$ , namely  $f_a \gtrsim 10^{7-9}$  GeV.

The axion can be a viable DM candidate; recent studies showed that if it constitutes the totality of dark matter, its mass is predicted to be  $m_a \sim \mathcal{O}(20 \mu\text{eV})$  [61].

- sterile neutrinos: from observations, we now know that neutrinos are massive particles. On the other hand, however, the SM predicts their mass to be zero; possible mechanisms to generate neutrino masses generally assume the existence of new heavy neutrinos, which are singlets under  $\mathcal{G}_{\text{SM}}$  [62, 63]. If, however, also sufficiently light ones exist, say with  $m_{\bar{\nu}} \sim \mathcal{O}(\text{keV})$ , they can be DM candidates [64]. It is interesting to note that sterile neutrino are usually WDM candidates;

- primordial black holes (PBHs); the possibility that DM could be constituted by black holes traces back to the 70s [65, 66]. PBHs are thought to form in the early universe by overdensities in the primordial fluid. Currently, models predicting PBHs received constraints from several searches (e.g., CMB, dwarf galaxies, lensing,  $\gamma$ -ray emission), but PBHs with masses of  $\mathcal{O}(10^{-12}M_\odot)$  can constitute the totality of dark matter [67];
- gravitino: if gravitino is the LSP, it can be a viable DM candidate. In this case, one of the most stringent constraints comes from the requirement of avoiding overclosure of the universe. While the gravitino can be a good WDM candidate for masses of  $\mathcal{O}(\text{keV})$ , if it is heavier, behaving as CDM, some mechanism is needed to dilute its density and avoid overclosure. Also constraints from Big Bang nucleosynthesis are relevant, and roughly set  $m_{3/2} \lesssim \mathcal{O}(\text{MeV})$ ;
- fuzzy dark matter (FDM): DM could be formed by ultra-light scalar particles, with masses of  $\mathcal{O}(10^{-22} \text{ eV})$  [68]; if this is the case, the associated de Broglie wavelength is  $\lambda_{\text{dB}} \sim \mathcal{O}(1 \text{ kpc})$ . Such a framework could alleviate some of the small scales problems of DM, and could be motivated by models in string theory, where light scalar fields usually appear.

## 2.3 Freeze-out production of WIMP dark matter

In this subsection, we discuss the cosmological history of WIMP dark matter in detail, since this is the main focus of the future discussion.

Before discussing the relevant physics of freeze-out quantitatively, it is useful to get a qualitative glimpse of what happens. The idea is relatively simple: to determine the abundance of DM, one has to consider the interactions which change the number of DM particles; if we assume that there exists only one dark matter particle, and denote it by  $\chi$ , the main contribution to this kind of interactions is:

$$\chi\chi \leftrightarrow \text{SM SM}, \quad (2.3.1)$$

where SM stands for a generic Standard Model particle. We are deliberately ignoring all possible indices and similar details, the general picture not being altered by them.

As long as this interaction can take place in both directions, DM is in equilibrium with the rest of the plasma, and its number density distribution  $n_\chi$  follows the laws of statistical mechanics; in particular, when the temperature drops below  $m_\chi$  and the DM becomes non-relativistic,  $n_\chi$  becomes exponentially suppressed by the Maxwell-Boltzmann factor  $e^{-m_\chi/T}$ . If, however, the rate of interactions in eq. (2.3.1) becomes sufficiently small compared to the expansion rate of the universe, DM is not able to annihilate anymore, and its number density freezes-out to the asymptotic value  $n_\chi^\infty$ . The relevant quantities to be compared are the rate of interactions  $\Gamma_\chi = n_\chi \langle \sigma v \rangle$  and the Hubble parameter  $H$ ; here  $v$  represent the relative velocity of two DM particles, and is  $v \sim \mathcal{O}(10^{-3})$ . As a rough estimate, we can consider the freeze-out to occur when:

$$\Gamma_\chi \lesssim H. \quad (2.3.2)$$

### 2.3.1 Standard freeze-out

To formalize the previous qualitative discussion, it is necessary to resort to the formalism of Boltzmann equations; in general, the Boltzmann equation for the phase space



distribution function  $f(\mathbf{p})$  can be written as [49]:

$$\hat{L}[f] = C[f], \quad (2.3.3)$$

where the first term is the Liouville operator, while the second one represents a collision term.

In the Friedman-Robertson-Walker (FRW) metric, eq. (2.3.3) for the DM number density becomes:

$$\dot{n}_\chi + 3Hn_\chi = g_\chi \int \frac{d^3p}{(2\pi)^3 2E} C[f], \quad (2.3.4)$$

where  $g_\chi$  is the number of internal degrees of freedom of  $\chi$ .

If we consider a generic process  $\chi + 1 + 2 + \dots \leftrightarrow a + b + \dots \equiv I \leftrightarrow F$ , the collision term can be written as:

$$g \int \frac{d^3p}{(2\pi)^3 E} C[f] = - \prod_{\{i \in I\}} \prod_{\{j \in F\}} \int d\Pi_i d\Pi_j (2\pi)^4 \delta(P_f - P_i) \\ \times [|\mathcal{M}|_{I \rightarrow F}^2 f_i(1 \pm f_j) - |\mathcal{M}|_{F \rightarrow I}^2 f_j(1 \pm f_i)], \quad (2.3.5)$$

where  $P_f$  and  $P_i$  are the final and initial momenta, respectively, and we defined:

$$d\Pi \equiv g \frac{d^3p}{(2\pi)^3 2E}. \quad (2.3.6)$$

Finally, the  $\pm 1$  in eq. (2.3.5) applies to bosons and fermions, respectively.

We can now specialize to a simpler case, i.e. the two-to-two interaction  $\chi + \psi \leftrightarrow a + b$ ; to simplify the analysis, we make two assumptions: first, we assume  $CP$  invariance, which implies that  $|\mathcal{M}|_{I \rightarrow F}^2 = |\mathcal{M}|_{F \rightarrow I}^2 \equiv |\mathcal{M}|^2$ ; the second assumption is the fact that we can ignore both Bose condensation and Fermi blocking, in such a way that  $1 \pm f \approx 1$  (well motivated if we consider energies smaller than  $E - \mu$ ). With these hypotheses, the Boltzmann equation becomes:

$$\dot{n}_\chi + 3Hn_\chi = - \int d\Pi_\chi d\Pi_\psi d\Pi_a d\Pi_b (2\pi)^4 \delta(P_f - P_i) |\mathcal{M}|^2 (f_\chi f_\psi - f_a f_b). \quad (2.3.7)$$

By exploiting energy conservation and introducing the equilibrium phase space distribution function, defined as  $f^{\text{eq}} \equiv e^{-E/T}$ , we can write:

$$f_\chi f_\psi - f_a f_b = e^{-\frac{E_\chi + E_\psi}{T}} \left( e^{\frac{\mu_\chi + \mu_\psi}{T}} - e^{\frac{\mu_a + \mu_b}{T}} \right) = f_\chi^{\text{eq}} f_\psi^{\text{eq}} \left( \frac{n_\chi n_\psi}{n_\chi^{\text{eq}} n_\psi^{\text{eq}}} - \frac{n_a n_b}{n_a^{\text{eq}} n_b^{\text{eq}}} \right), \quad (2.3.8)$$

where we took into account that  $e^{\mu/T} = n/n^{\text{eq}}$ . Since the term in parenthesis does not depend on the momenta, eq. (2.3.7) becomes:

$$\dot{n}_\chi + 3Hn_\chi = -\langle \sigma v \rangle \left( n_\chi n_\psi - \frac{n_a n_b}{n_a^{\text{eq}} n_b^{\text{eq}}} n_\chi^{\text{eq}} n_\psi^{\text{eq}} \right), \quad (2.3.9)$$

where we defined the thermally-averaged cross section as:

$$\langle \sigma v \rangle \equiv \frac{1}{n_\chi^{\text{eq}} n_\psi^{\text{eq}}} \int d\Pi_\chi d\Pi_\psi d\Pi_a d\Pi_b (2\pi)^4 \delta(P_f - P_i) |\mathcal{M}|^2 f_\chi^{\text{eq}} f_\psi^{\text{eq}} \quad (2.3.10)$$

At this point, it is important to distinguish two different concepts of equilibrium: in general, a particle is said to be in *kinetic equilibrium* (KE) if it follows its corresponding distribution, i.e. Bose-Einstein or Fermi-Dirac; the condition of KE is usually fulfilled if scatterings like  $\chi + \text{SM} \leftrightarrow \chi + \text{SM}$  are fast enough. A particle is instead in *chemical equilibrium* (CE) if its chemical potential is related to the ones of the other particles it interacts with, i.e.  $\mu_\chi + \mu_\psi = \mu_a + \mu_b$  for the reaction  $\chi + \psi \leftrightarrow a + b$ . If a particle is in both kinetic and chemical equilibrium, it is said to be in *local thermal equilibrium* (LTE). By taking into account that  $e^{\mu/T} = n/n^{\text{eq}}$ , it is easy to see that in the presence of chemical equilibrium the L.H.S. of eq. (2.3.9) vanishes: given that this equation can be schematically written as  $n_\chi H \sim n_\chi n_\psi \langle \sigma v \rangle \equiv n_\chi \Gamma_\psi$ , the parenthesis can become  $\mathcal{O}(1)$  if  $\Gamma_\psi \lesssim H$ , i.e. we can expect CE to break down when a species freezes-out [69].

In order to discuss DM freeze-out, we refer to eq. (2.3.9), but in a simpler framework: we study DM annihilations into light SM particles which are in equilibrium with the plasma, i.e.  $\chi\bar{\chi} \leftrightarrow \text{SM}\overline{\text{SM}}$ . This assumption allows us to consider SM states to be in LTE, so that  $n_{\text{SM}} = n_{\text{SM}}^{\text{eq}}$ . In this case, then, eq. (2.3.9) simply becomes:

$$\dot{n}_\chi + 3Hn_\chi = -\langle \sigma v \rangle (n_\chi^2 - n_\chi^{\text{eq}2}), \quad (2.3.11)$$

By defining now the quantities  $Y \equiv n_\chi/s$ ,  $x \equiv m_\chi/T$ , where  $s = 2\pi^2/45 g_{*,S} T^3$  is the entropy density, we can rewrite eq. (2.3.11) as:

$$\frac{dY}{dx} \approx -\frac{s\langle \sigma v \rangle}{xH} (Y^2 - Y_{\text{eq}}^2), \quad (2.3.12)$$

where we assumed that  $g_{*,S}$  does not depend on the temperature.

Let us now define the freeze-out temperature  $T_F$  as the one at which the rate of the interactions  $\chi\bar{\chi} \leftrightarrow \text{SM}\overline{\text{SM}}$  roughly equals the Hubble parameter; we then expect that  $Y \gg Y_{\text{eq}}$  if  $T \ll T_F$ , so that:

$$\frac{1}{Y_\infty} - \frac{1}{Y_F} \approx \int_{x_F}^{\infty} dx \frac{s\langle \sigma v \rangle}{xH}. \quad (2.3.13)$$

Since freeze-out is not an instantaneous process, it is also natural to expect that  $Y_F \gg Y_\infty$ ; therefore, if we substitute the expressions for  $s$  and  $H$ , we arrive at:

$$Y_\infty \approx \frac{\sqrt{45}}{2\sqrt{2}\pi} \frac{1}{m_\chi M_{Pl} \int_{x_F}^{\infty} dx \frac{g_{*,S}}{\sqrt{g_*}} \frac{\langle \sigma v \rangle}{x^2}}, \quad (2.3.14)$$

In order to determine the freeze-out temperature in a quantitative way, we introduce the variable  $\Delta \equiv Y - Y_{\text{eq}}$ , in terms of which eq. (2.3.12) reads:

$$\frac{d\Delta}{dx} = -\frac{dY_{\text{eq}}}{dx} - \frac{s\langle \sigma v \rangle}{xH} \Delta(2Y_{\text{eq}} + \Delta). \quad (2.3.15)$$

Since we expect that after freeze-out  $Y_{\text{eq}}$  ceases to trace the equilibrium behaviour, we define  $x_F$  by the requirement that  $\Delta(x_F) = \alpha Y_{\text{eq}}(x_F)$ , where  $\alpha$  is an  $\mathcal{O}(1)$  number. At early times,  $x \ll x_F$ , both  $\Delta$  and  $|d\Delta/dx|$  are small, and we can approximate the equation above by setting  $d\Delta/dx \approx 0$ ; this then implies:

$$\Delta|_{x \ll x_F} \approx -\frac{xH}{s\langle \sigma v \rangle} \frac{1}{2 + \frac{\Delta}{Y_{\text{eq}}}}, \quad (2.3.16)$$

where we took into account that  $1/Y_{\text{eq}} dY_{\text{eq}}/dx \approx 1$ . If we now put in this equation the constraint  $\Delta(x_F) = \alpha Y_{\text{eq}}(x_F)$ , and equal it to  $\alpha Y_{\text{eq}}(x_F)$ , we obtain:<sup>1</sup>

$$\begin{aligned} x_F &\approx \log \left[ \frac{2\sqrt{90}}{(2\pi)^{\frac{5}{2}}} \frac{g_\chi}{\sqrt{g_* x_F}} m_\chi M_{Pl} \langle \sigma v \rangle \right] \\ &\approx 25 + \log \left[ \frac{1.67 g_\chi}{\sqrt{g_* x_F}} \frac{m_\chi}{100 \text{ GeV}} \frac{\langle \sigma v \rangle}{1 \text{ pb}} \right]. \end{aligned} \quad (2.3.17)$$

In getting this equation, we chose a value of  $\alpha$  such that  $\alpha(2 + \alpha) = 1$ , i.e.  $\alpha \approx 0.4$ .

The relic density is then computed in terms of the dimensionless quantity:

$$\Omega_\chi h^2 \equiv \frac{\rho_\chi}{\rho_c} h^2 \quad , \quad \rho_c \equiv 3M_{Pl}^2 H^2. \quad (2.3.18)$$

From eq. (2.3.14), the DM abundance results in:

$$\begin{aligned} \Omega h^2 &= \frac{n_\chi m_\chi}{3M_{Pl}^2} \left( \frac{h}{H} \right)^2 = \frac{s_0 Y_\infty m_\chi}{3M_{Pl}^2} \left( \frac{1}{100 \text{ km Mpc}^{-1} \text{ s}^{-1}} \right)^2 \\ &\approx \frac{\pi}{3\sqrt{90}} g_{*,S}^{(0)} \left( \frac{T_0}{M_{Pl}} \right)^3 \int_{x_F}^{\infty} dx \frac{g_{*,S}}{\sqrt{g_*}} \frac{\langle \sigma v \rangle}{x^2} \left( \frac{1}{100 \text{ km Mpc}^{-1} \text{ s}^{-1}} \right)^2 \\ &\approx \frac{0.03}{\int_{x_F}^{\infty} dx \frac{g_{*,S}}{\sqrt{g_*}} \frac{1}{x^2} \frac{\langle \sigma v \rangle}{1 \text{ pb}}}, \end{aligned} \quad (2.3.19)$$

where subscripts or superscripts 0 refer to quantities evaluated at the present epoch, as usual. We show the behaviour of  $Y$ , as a function of  $x$ , in fig. 2.5; it is evident that larger values of  $\langle \sigma v \rangle$  (denoted by  $\langle \sigma_A | v | \rangle$  in the figure) lead to a smaller relic density today, in accordance with eq. (2.3.19).

By taking into account that  $1 \text{ pb} \approx 3 \times 10^{-26} \text{ cm}^3 \text{ s}^{-1}$ , if we assume that the integral above is dominated by the region around  $x_F \sim \mathcal{O}(25)$ , and that  $g_* \sim g_{*,S} \sim \mathcal{O}(100)$ , we obtain:

$$\frac{\Omega_\chi h^2}{0.1} \sim \frac{3 \times 10^{-26} \text{ cm}^3 \text{ s}^{-1}}{\langle \sigma v \rangle} \sim 0.2 \frac{G_F}{\sigma}, \quad (2.3.20)$$

where  $G_F$  is the Fermi constant. Since the latter can be viewed as the scale associated to the weak theory (as we discuss, e.g., in appendix B), we see that a roughly correct relic abundance corresponds to an annihilation cross section of the order of typical weak interactions; this feature represents the so-called *WIMP miracle*.

### 2.3.2 Exceptions to the standard paradigm

The one outlined above is the standard paradigm for WIMP freeze-out; however, several exceptions to this picture are possible. In the famous paper [70], three of them are discussed in detail: coannihilations, annihilations into forbidden channels and annihilations

---

<sup>1</sup>Sometimes, a different criterium to determine  $x_F$  is used:  $T_F$  is defined as the temperature at which  $n_\chi(\sigma v) = H(T_F)$ . With this other definition, the only change is that in the R.H.S. of eq. (2.3.17),  $\sqrt{x_F}$  appears in the numerator [49].

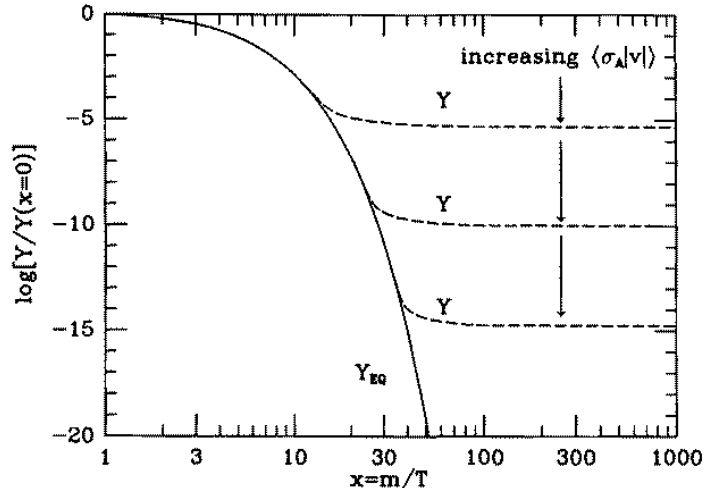


Figure 2.5: Dependence of  $Y$  as a function of  $x$ ; larger values of the annihilation cross section lead to a smaller relic abundance. Figure taken from ref. [49].

near poles. In the following, we very briefly recall the last two and discuss the first one in detail. In addition, we also study the possible departure from chemical equilibrium, since it will be relevant for our future discussion. In the literature, other exceptions to the standard freeze-out mechanism have been studied (see, e.g., ref. [71]).

### Annihilations into forbidden channels

The idea is that if a particular channel of DM annihilation is kinematically forbidden at zero temperature, thermal effects can make it become accessible. If we denote by  $\psi$  the final state of this channel, i.e.  $\chi\bar{\chi} \rightarrow \psi\bar{\psi}$ , if the two states are such that  $m_\chi \lesssim m_\psi$ , the net rate of annihilations does not vanish. Roughly, if  $(m_\psi - m_\chi)/m_\chi \lesssim 10\%$ , this effect can be appreciable.

In general, the consequence of including thermal effects is that in the plane  $m_\chi$ - $\Omega_\chi h^2$  all channels open up slightly before the mass of the products of DM annihilation.

### Annihilations near a pole

If DM annihilations take place near a pole of the cross section, there is a significant enhancement of the annihilation cross section, and consequently a dip in the relic abundance. We will encounter an example of this effect in chapter 4. Such an enhancement of the cross section usually takes place if the Higgs can mediate DM annihilations in  $s$ -channel and  $m_\chi \approx m_h/2$ .

### Coannihilations

The previous discussion implicitly assumed the existence of a single particle belonging to the dark sector; however, if more than one such states exist, the situation changes. Let us assume a set of particles  $\chi_i$ ,  $i = 1, \dots, N$  charged under a symmetry which stabilizes the lightest state (e.g., a  $\mathbb{Z}_2$  symmetry under which the dark sector is odd and the SM is even) exists, such that  $m_{\chi_i} < m_{\chi_j}$  if  $i < j$ ; if we denote two generic Standard Model

particles by SM and SM', we can have three different types of processes, namely:

$$\chi_i + \chi_j \leftrightarrow \text{SM} + \text{SM}' \quad (2.3.21a)$$

$$\chi_i + \text{SM} \leftrightarrow \chi_j + \text{SM}' \quad (2.3.21b)$$

$$\chi_j \leftrightarrow \chi_i + \text{SM} + \text{SM}', \quad (2.3.21c)$$

which represent *coannihilations*, *conversions* and decays (with also the inverse processes).

By repeating the previous analysis, we can consider the Boltzmann equation for a single species  $\chi_i$ , which can be schematically written as [70]:

$$\begin{aligned} \dot{n}_{\chi_i} + 3Hn_{\chi_i} = & - \sum_{j, \text{SM}, \text{SM}'} \left[ \langle \sigma_{ij} v \rangle \left( n_{\chi_i} n_{\chi_j} - n_{\chi_i}^{\text{eq}} n_{\chi_j}^{\text{eq}} \right) \right. \\ & + \left( \langle \sigma'_{ij} v \rangle n_{\chi_i} n_{\text{SM}} - \langle \sigma'_{ji} v \rangle n_{\chi_j} n_{\text{SM}'} \right) \\ & \left. + \Gamma_{ij} \left( n_{\chi_i} - n_{\chi_i}^{\text{eq}} \right) \right], \end{aligned} \quad (2.3.22)$$

where  $\sigma_{ij}$ ,  $\sigma'_{ij}$  are the cross sections for coannihilations and conversions, respectively, and  $\Gamma_{ij}$  is the decay width of  $\chi_i$ .

It is important to notice that the three kinds of reactions in eqs. (2.3.21a) to (2.3.21c) take place on very different time scales; for instance, if we compare the rate of conversions with the one of coannihilations, we get:

$$\frac{\langle \sigma_{ij} v \rangle n_{\chi_i} n_{\chi_j}}{\langle \sigma'_{ij} v \rangle n_{\chi_i} n_{\text{SM}}} \sim \frac{n_{\chi_j}}{n_{\text{SM}}} \sim \left( \frac{m_{\chi_j}}{T} \right)^{\frac{3}{2}} e^{-\frac{m_{\chi_j}}{T}} \approx 6 \times 10^8, \quad (2.3.23)$$

where we assumed the SM particles to be relativistic at freeze-out and took  $m_{\chi_j}/T = 25$  for the last equality. Decay and inverse decay can in general be even faster.

Given that all  $\chi_i$ 's eventually decay to  $\chi_1$ , the relevant quantity is the total number density of dark particles,  $n_\chi \equiv \sum_i n_{\chi_i}$ ; by summing over  $i$  in eq. (2.3.22), we obtain the following equation for  $n_\chi$ :

$$\dot{n}_\chi + 3Hn_\chi = - \sum_{i,j} \langle \sigma_{ij} v \rangle \left( n_{\chi_i} n_{\chi_j} - n_{\chi_i}^{\text{eq}} n_{\chi_j}^{\text{eq}} \right). \quad (2.3.24)$$

In addition, since conversions and decays are so fast, they maintain the equilibrium between the  $\chi_i$ 's, allowing us to approximate  $n_{\chi_i}/n_{\chi_i}^{\text{eq}} \approx n_\chi/n_\chi^{\text{eq}}$ , and then:

$$\dot{n}_\chi + 3Hn_\chi \approx - \langle \sigma v \rangle_{\text{eff}} \left( n_\chi^2 - n_\chi^{\text{eq}2} \right), \quad (2.3.25)$$

which is precisely of the form of eq. (2.3.11), but written in terms of the effective cross section:

$$\langle \sigma v \rangle_{\text{eff}} \equiv \sum_{i,j} \langle \sigma_{ij} v \rangle \frac{n_{\chi_i}^{\text{eq}}}{n_\chi^{\text{eq}}} \frac{n_{\chi_j}^{\text{eq}}}{n_\chi^{\text{eq}}}. \quad (2.3.26)$$

The ratio  $n_{\chi_i}^{\text{eq}}/n_\chi^{\text{eq}}$  can be simply written in terms of  $\Delta_i \equiv (m_{\chi_i} - m_{\chi_1})/m_{\chi_1}$  as:

$$\frac{n_{\chi_i}^{\text{eq}}}{n_\chi^{\text{eq}}} = \frac{g_{\chi_i} m_{\chi_i}^{3/2} e^{-m_{\chi_i}/T}}{\sum_j g_{\chi_j} m_{\chi_j}^{3/2} e^{-m_{\chi_j}/T}} = \frac{g_{\chi_i} (1 + \Delta_i)^{3/2} e^{-x\Delta_i}}{\sum_j g_{\chi_j} (1 + \Delta_j)^{3/2} e^{-x\Delta_j}}, \quad (2.3.27)$$

where  $g_{\chi_i}$  denotes the number of internal degrees of freedom of  $\chi_i$ .

Once the effective cross section is computed, the determination of the DM relic abundance reduces to the problem of standard freeze-out for the effective number density  $n_\chi$ .

## Departure from chemical equilibrium

In the previous discussion, we claimed that in eq. (2.3.22) the reactions dictated by the last two lines usually take place on much shorter time scales compared to the first one; these processes are responsible for the maintenance of chemical equilibrium, as defined in section 2.3.1, since they change the number of particles of a giving species.

Let us consider the case of only two dark particles,  $\chi$  and  $\psi$ , and two Standard Model ones, SM and SM', and let us also assume for simplicity the dark states to be scalars (the analysis for fermions follows straightforwardly, with simply the appearance of some factors of 2); if we consider the conversion process  $\chi + \text{SM} \leftrightarrow \psi + \text{SM}'$ , and assume that all the SM states are in thermal equilibrium, the condition of CE implies:

$$\frac{n_\chi}{n_\chi^{\text{eq}}} = \frac{n_\psi}{n_\psi^{\text{eq}}}. \quad (2.3.28)$$

If this condition breaks down, on the other hand, we have to resort to the full set of Boltzmann equations. To this purpose, let us first consider the decay,  $\psi \rightarrow \chi + \text{SM} + \text{SM}'$ ; in this case, the contribution to the Boltzmann equation for  $\chi$  is:

$$\begin{aligned} \dot{n}_\chi + 3Hn_\chi &\supset \int d\Pi_\chi d\Pi_\psi d\Pi_{\text{SM}} d\Pi_{\text{SM}'} (2\pi)^4 \delta(P_f - P_i) |\mathcal{M}|^2 (f_\psi - f_\chi f_{\text{SM}} f_{\text{SM}'}) \\ &= \left( \frac{n_\psi}{n_\psi^{\text{eq}}} - \frac{n_\chi}{n_\chi^{\text{eq}}} \right) \int d\Pi_\psi 2m_\psi \Gamma_\psi e^{-\frac{E_\psi}{T}} = \left( \frac{n_\psi}{n_\psi^{\text{eq}}} - \frac{n_\chi}{n_\chi^{\text{eq}}} \right) \frac{m_\psi^2 T \Gamma_\psi}{2\pi^2} K_1 \left( \frac{m_\psi}{T} \right) \\ &= \left( \frac{n_\psi}{n_\psi^{\text{eq}}} - \frac{n_\chi}{n_\chi^{\text{eq}}} \right) n_\psi^{\text{eq}} \frac{K_1(x_\psi)}{K_2(x_\psi)} \Gamma_\psi \equiv \left( n_\psi - \frac{n_\chi}{n_\chi^{\text{eq}}} n_\psi^{\text{eq}} \right) \langle \Gamma_\psi \rangle, \end{aligned}$$

where we defined  $x_\psi \equiv m_\psi/T$ , took into account that  $n^{\text{eq}} = m^2 T / (2\pi^2) K_2(m/T)$  and considered the integral representation of the modified Bessel functions:

$$K_n(x) = \frac{\sqrt{\pi}}{(n - \frac{1}{2})!} \left( \frac{x}{2} \right)^n \int_1^\infty dt (t^2 - 1)^{n-1/2} e^{-tx}. \quad (2.3.29)$$

It is now simple to write down the full Boltzmann equation for the DM particle  $\chi$ , which reads:

$$\begin{aligned} \frac{dY_\chi}{dx} &= -\frac{s}{xH} \left[ \langle \sigma_{\chi\chi} v \rangle (Y_\chi^2 - Y_\chi^{\text{eq}2}) + \langle \sigma_{\chi\psi} v \rangle (Y_\chi Y_\psi - Y_\chi^{\text{eq}} Y_\psi^{\text{eq}}) \right. \\ &\quad + \langle \sigma_{\chi\text{SM}} v \rangle Y_{\text{SM}}^{\text{eq}} \left( Y_\chi - \frac{Y_\psi}{Y_\psi^{\text{eq}}} Y_\chi^{\text{eq}} \right) - \frac{\langle \Gamma_\psi \rangle}{s} \left( Y_\psi - \frac{Y_\chi}{Y_\chi^{\text{eq}}} Y_\psi^{\text{eq}} \right) \\ &\quad \left. + \langle \sigma_{\chi\chi \rightarrow \psi\psi} v \rangle \left( Y_\chi^2 - \frac{Y_\psi^2}{Y_\psi^{\text{eq}2}} Y_\chi^{\text{eq}2} \right) \right], \end{aligned} \quad (2.3.30)$$

where the thermal cross sections are defined analogously to eq. (2.3.10). The first line concerns annihilations and coannihilations, the second one conversions and decays of  $\psi$ , and the last one annihilations within the dark sector. An analogous equation obviously holds for  $\psi$  as well.

From the discussion above, it is then clear that the last three terms are the ones responsible for maintaining chemical equilibrium. If CE breaks down, the full set of coupled equations for  $\chi$  and  $\psi$  has to be solved.

## 2.4 Experimental searches

WIMPs are by far the most widely studied candidates of dark matter: for this reason, also a very intense program of experimental searches has been developed during the decades. In this subsection, we discuss the three different strategies we can look for WIMP dark matter with: direct detection (DD), indirect detection (ID) and LHC searches.

### 2.4.1 Direct detection

The history of direct detection dates back to the 80s, when it was first proposed [72]. As we already stressed, the DM electromagnetic coupling, if any, must be very small; for this reason, DM does not interact with electrons within an atom, but is able to scatter off the nucleus. The main current DD experiments include XENON1T [73], PandaX [74] and LUX [75].

What is experimentally measured is the recoil energy  $E_r$  of the nucleus of mass  $m_T$ , which can be easily estimated; in the center of mass (CM) frame, if  $v$  is the relative velocity between the DM and the nucleus, the momentum transfer is:

$$|\mathbf{q}| \equiv |\mathbf{p}_\chi - \mathbf{p}_T| = \sqrt{2\mathbf{p}_\chi^2(1 - \cos\theta)} = \mu_{\chi T} v \sqrt{2(1 - \cos\theta)}, \quad (2.4.1)$$

with  $\theta$  and  $\mu_{\chi T}$  being the angle between  $\mathbf{p}_\chi$  and  $\mathbf{p}_T$ , and the reduced mass of the system, respectively.

The maximum recoil energy is then:

$$E_r^{\max} = \frac{2\mu_{\chi T}^2 v^2}{m_T} \quad (2.4.2)$$

Typical ranges of  $E_r^{\max}$  are  $0.1 \text{ keV} \lesssim E_r^{\max} \lesssim 100 \text{ keV}$  for DM masses in the range  $10 \text{ GeV} \lesssim m_\chi \lesssim 1 \text{ TeV}$  and  $v \sim 10^{-3}$ . In addition, DD experiments usually have a lower threshold  $E_r^{\text{thr}}$  below which events are not measured; this translates in a minimal velocity for DM, which can be easily calculated from eq. (2.4.2) as:

$$v^{\min} = \sqrt{\frac{m_T E_r^{\text{thr}}}{2\mu_{\chi T}^2}} \quad (2.4.3)$$

The rate  $R$  of interactions between  $\chi$  and the nucleus is expected to be proportional to the number of targets  $N_T = M_T/m_T$  (with  $M_T$  being the total target mass), the interaction cross section and the DM flux; the differential rate per unit detector mass is:

$$\frac{dR}{dE_r} = \frac{\rho_0}{m_\chi m_T} \int d^3v v f(v) \frac{d\sigma_T}{dE_r}, \quad (2.4.4)$$

where  $f(v)$  is the velocity distribution distribution,  $\rho_0 \approx 0.3 \text{ GeV cm}^{-3}$  is the local DM density and  $\sigma_T$  is the DM-nucleus cross section.

For our purposes, it will be important to distinguish between *spin independent* (SI) and *spin dependent* (SD) interactions. Let us recall that a Dirac spinor can be written in the Weyl representation as:

$$u_r(p) = \begin{pmatrix} \sqrt{p \cdot \sigma} \xi_r \\ \sqrt{p \cdot \bar{\sigma}} \xi_r \end{pmatrix}, \quad (2.4.5)$$

where  $\sigma^\mu \equiv (\mathbf{1}, \boldsymbol{\sigma})$ ,  $\bar{\sigma}^\mu \equiv (\mathbf{1}, -\boldsymbol{\sigma})$  and  $\xi_r$  is normalized such that  $\xi_r^\dagger \xi_s = \delta_{rs}$ . We are then interested in the non-relativistic limit, where we can approximate:

$$\sqrt{\mathbf{p} \cdot \boldsymbol{\sigma}} \approx \sqrt{m} - \frac{\mathbf{p} \cdot \boldsymbol{\sigma}}{2\sqrt{m}} \quad , \quad \sqrt{\mathbf{p} \cdot \bar{\boldsymbol{\sigma}}} \approx \sqrt{m} + \frac{\mathbf{p} \cdot \boldsymbol{\sigma}}{2\sqrt{m}}. \quad (2.4.6)$$

If we finally recall that in the Weyl basis  $\gamma^\mu = \begin{pmatrix} 0 & \sigma^\mu \\ \bar{\sigma}^\mu & 0 \end{pmatrix}$  and  $\gamma^5 = \begin{pmatrix} -1 & 0 \\ 0 & 1 \end{pmatrix}$ , it is easy to show that:

$$\bar{u}_r(\mathbf{p}) u_s(\mathbf{p}') \approx 2m \delta_{rs} \quad (2.4.7a)$$

$$\bar{u}_r(\mathbf{p}) \gamma^\mu u_s(\mathbf{p}') \approx 2m \delta_{rs} \delta^{\mu 0} \quad (2.4.7b)$$

$$\bar{u}_r(\mathbf{p}) \gamma^5 u_s(\mathbf{p}') \approx -2\delta_{rs} (\mathbf{p} - \mathbf{p}') \cdot \mathbf{s} \quad (2.4.7c)$$

$$\bar{u}_r(\mathbf{p}) \gamma^\mu \gamma^5 u_s(\mathbf{p}') \approx 4m s^i \delta_{rs} \delta^{\mu i} \quad (2.4.7d)$$

Therefore, we see that while scalar and vector interactions are SI, axial-vector ones are SD. In addition, pseudo-scalar interactions are SD and also suppressed by the small momentum transfer.

Connection with experiments can be done in a quite model-independent way [76]; first of all, as long as the mass of the particle mediating the interactions between DM and SM quarks is larger than the transfer momentum, say  $m_{\text{med}} \gtrsim \mathcal{O}(100 \text{ MeV})$ , the interaction can be parametrized via an effective theory; in general, then, we can schematically write the Lagrangian as (see appendix A of ref. [77]):

$$\mathcal{L}_{\text{eff}}^{(\text{DD})} = \mathcal{O}_{\text{DM}} \mathcal{O}_q, \quad (2.4.8)$$

The general approach is then to go from the partonic operator  $\mathcal{O}_q$  to the operators  $\mathcal{O}_{n,p}$  which describe the interactions of the DM with the nucleons; if we consider  $\mathcal{O}_q = \lambda_q \bar{q} \Gamma q$  (where  $\Gamma$  indicates a generic Lorentz structure), this is obtained by the replacement  $\mathcal{O}_q \rightarrow \mathcal{O}_n + \mathcal{O}_p = f_n \bar{n} \Gamma n + f_p \bar{p} \Gamma p$ .

In order to map these operators to the ones describing the interaction with nucleus, it is convenient to distinguish between SI and SD interactions involving the quarks:

a) spin-independent interactions

In this case, the nucleus-level operator is obtained by the replacement:

$$\mathcal{O}_n + \mathcal{O}_p \rightarrow \mathcal{O}_T = [Z f_p + (A - Z) f_n] \bar{T} \Gamma T, \quad (2.4.9)$$

with  $T$  being the nucleus field,  $Z$  and  $A$  the atomic and mass number, respectively, and  $\Gamma = \{\mathbf{1}, \gamma^\mu\}$ . We can further consider two possible cases:

i) scalar interaction

If we parametrize the effective Lagrangian as  $\mathcal{L}_{\text{eff}}^{(\text{DD})} = \sum_q \lambda_q \bar{\chi} \chi \bar{q} q \equiv \bar{\chi} \chi \mathcal{O}_q$ , we have:

$$f_{n,p} = \sum_{q=u,d,s} f_{T_q}^{(n,p)} \lambda_q \frac{m_{n,p}}{m_q} + \frac{2}{27} f_{T_G} \sum_{q=c,b,t} \lambda_q \frac{m_{n,p}}{m_q}, \quad (2.4.10)$$

where  $f_{T_q}^{(n,p)}$  are numerical coefficients determined experimentally and  $f_{T_G} = 1 - f_{T_u}^{(n,p)} - f_{T_d}^{(n,p)} - f_{T_s}^{(n,p)}$ , together with  $f_{T_u}^{(n)} = f_{T_d}^{(p)}$  (and the same for  $u \leftrightarrow d$ ) and  $f_{T_s}^{(n)} = f_{T_s}^{(p)}$ .



The DM-nucleus cross section can be finally computed with the standard techniques, taking into account the non-relativistic limit and eq. (2.4.7a), yielding to:

$$\sigma_{\text{SI},T} = \frac{\langle |\mathcal{M}| \rangle^2}{16\pi s} \approx \frac{\mu_{\chi T}^2}{\pi} [Z f_p + (A - Z) f_n]^2. \quad (2.4.11)$$

ii) vector interaction

If we parametrize the effective Lagrangian as  $\mathcal{L}_{\text{eff}}^{(\text{DD})} = \sum_q \lambda_q \bar{\chi} \gamma^\mu \chi \bar{q} \gamma_\mu q \equiv \bar{\chi} \gamma^\mu \chi \mathcal{O}_{q,\mu}$ , we have:

$$f_n = \lambda_u + 2\lambda_d, \quad (2.4.12)$$

and the same with  $u \leftrightarrow d$  for the proton; this basically follows from eq. (2.4.7b), taking into account that  $q^\dagger q$  is the number of quarks and is conserved.

Similarly to the previous case, the DM-nucleus cross section is:

$$\sigma_{\text{SI},T} = \frac{\langle |\mathcal{M}| \rangle^2}{16\pi s} \approx \frac{\mu_{\chi T}^2}{\pi} [Z f_p + (A - Z) f_n]^2. \quad (2.4.13)$$

Given that in general different experiments use different nuclei, DD limits are usually recast in terms of the cross section between the DM and the nucleons, which is defined as:

$$\sigma_{\text{SI}} \equiv \sigma_{\text{SI},T} \Big|_{\mathbf{q}=0} \frac{\mu_{\chi N}^2}{\mu_{\chi T}^2} \frac{1}{A^2}, \quad (2.4.14)$$

where  $\mathbf{q}$  is the momentum transfer and  $\mu_{\chi N}$  the DM-nucleon reduced mass, with the nucleon mass defined as  $m_N \equiv (m_n + m_p)/2$ .

b) spin-dependent interactions

In this case, the nucleus-level operator is obtained by the replacement:

$$\mathcal{O}_n + \mathcal{O}_p \rightarrow \mathcal{O}_T = \left( \frac{\langle S_p \rangle}{J_T} f_p + \frac{\langle S_n \rangle}{J_T} f_n \right) \bar{T} \Gamma T, \quad (2.4.15)$$

where  $J_T$  is the spin of the nucleus and  $\Gamma = \{\gamma^5, \gamma^\mu \gamma^5\}$ .

We can further consider two possible cases:

i) pseudo-scalar interaction

If we parametrize the effective Lagrangian as  $\mathcal{L}_{\text{eff}}^{(\text{DD})} = \sum_q \lambda_q \bar{\chi} \gamma^5 \chi \bar{q} \gamma^5 q \equiv \bar{\chi} \gamma^5 \chi \mathcal{O}_q$ , we have:

$$f_{n,p} = \sum_{q=u,d,s} f_{T_q}^{(5n,5p)} \lambda_q \frac{m_{n,p}}{m_q}, \quad (2.4.16)$$

where, as for the scalar interactions,  $f_{T_q}^{(5n,5p)}$  are numerical coefficients determined experimentally.

The DM-nucleus cross section can be computed as for the previous cases, by making the replacement  $|\bar{T} \gamma^5 T|^2 \rightarrow 4m_T^2 J_T (J_T + 1) \mathbf{q}^2$ ; taking into account that  $\theta$  explicitly enters in the expression of  $|\mathbf{q}|$  (cf. eq. (2.4.1)), we obtain:

$$\sigma_{\text{SI},T} = \int d\Omega \frac{\langle |\mathcal{M}| \rangle^2}{64\pi^2 s} \approx \frac{4}{3\pi} \frac{\mu_{\chi T}^6 v^4}{m_\chi^2 m_T^2} J_T (J_T + 1) \left( \frac{\langle S_p \rangle}{J_T} f_p + \frac{\langle S_n \rangle}{J_T} f_n \right)^2, \quad (2.4.17)$$

from which it is clear the strong velocity suppression.

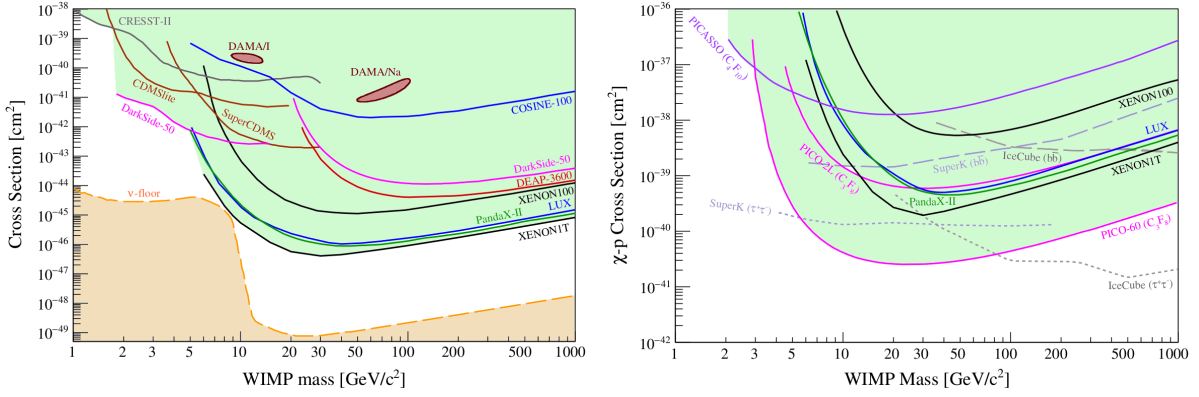


Figure 2.6: Current bounds from DD experiments. The space above each line is excluded at 90%. Left: limits for SD interactions between DM and nucleon. The orange, dashed line represent the irreducible background represented by neutrinos. Right panel: limits for SD interactions between DM and proton. Figure taken from ref. [78].

ii) axial-vector interaction

If we parametrize the effective Lagrangian as  $\mathcal{L}_{\text{eff}}^{(\text{DD})} = \sum_q \lambda_q \bar{\chi} \gamma^\mu \gamma^5 \chi \bar{q} \gamma^\mu \gamma^5 q \equiv \bar{\chi} \gamma^\mu \gamma^5 \chi \mathcal{O}_{q,\mu}$ , we have:

$$f_{n,p} = \sum_{q=u,d,s} \Delta_q^{(n,p)} \lambda_q, \quad (2.4.18)$$

where, once again,  $\Delta_q^{(n,p)}$  are numerical coefficients determined experimentally, and  $\Delta_u^{(n)} = \Delta_d^{(p)}$  (and the same for  $u \leftrightarrow d$ ) and  $\Delta_s^{(n)} = \Delta_s^{(p)}$ .

The DM-nucleus is:

$$\sigma_{\text{SI,T}} = \int d\Omega \frac{\langle |\mathcal{M}| \rangle^2}{64\pi^2 s} \approx \frac{4\mu_{\chi T}^2}{\pi} J_T (J_T + 1) \left( \frac{\langle S_p \rangle}{J_T} f_p + \frac{\langle S_n \rangle}{J_T} f_n \right)^2. \quad (2.4.19)$$

Also for SD interactions, it is convenient to introduce a cross section for DM-nucleon interactions; it is defined as:

$$\sigma_{\text{SI}} \equiv \sigma_{\text{SI,T}} \Big|_{\mathbf{q}=0} \frac{\mu_{\chi N}^2}{\mu_{\chi T}^2} \frac{1}{(\langle S_p \rangle + \langle S_n \rangle)^2} \frac{J_T}{(J_T + 1)}. \quad (2.4.20)$$

Current bounds from DD are shown in fig. 2.6, for both SI and SD DM-nucleon cross section. The characteristic shape can be understood as follows: from eq. (2.4.3), it is easy to show that there is a minimum value of  $m_\chi$  the experiments are sensitive to, and this corresponds to the weaker and weaker bound in fig. 2.6 for  $m_\chi \lesssim \mathcal{O}(10 \text{ GeV})$ ; on the other hand, we see from eq. (2.4.4) that the DM number density scales as  $m_\chi^{-1}$ , and this explains why the limits also get weaker at large masses.

Another important effect is given by annual modulation: since the Earth is moving around the Sun, while the DM is not expected to have a preferred direction of motion in the galaxy, there is a net effect on the DM flux reaching the earth: in particular, the latter is expected to be maximum in June, when the Earth moves in the opposite direction of this net “DM wind”, while it is minimum in December. This is the effect claimed to be observed by the DAMA/LIBRA experiment (see, e.g., ref. [79]).

## 2.4.2 Indirect detection

A second strategy to look for DM is to seek for products of DM annihilation: even if, as we stated before, dark matter annihilation is strongly suppressed, there is a non-vanishing possibility for it to happen, especially in regions where the DM density is very high (such as in dwarf galaxies, galactic centers etc.).

In general, only stable particles can reach the detectors: for this reason, electrons, positrons, (anti-)protons, photons and neutrinos are sought for; annihilations of DM into other SM particles reduce to these final products after decays.

Since ID is not a primary focus of this work, we will now simply recall some basic facts, and consider the case in which photons are the final particles which reach the detector. If we assume them to be produced within a volume  $dV$  located in the sky at the point  $(r, \theta, \phi)$ , where  $r$  is the distance from the detector, the expected flux of photons per unit of energy and time is [80]:

$$\frac{dN_\gamma}{dE dt dV} = \left( \frac{dN_\gamma}{dE} \right)_0 \frac{A}{4\pi r^2} \frac{1}{2} \langle \sigma v \rangle_{\text{eff}} n(\mathbf{r}), \quad (2.4.21)$$

where  $A$  is the area of the detector,  $\langle \sigma v \rangle_{\text{eff}}$  the thermally-averaged DM annihilation cross section and  $n(\mathbf{r})$  the DM number density; the factor of  $1/2$  comes from the fact that the final state is made of indistinguishable particles. In writing this expression, we assumed that the energy of photons does not change between the emission and the reception.

If we integrate along the line of sight and over the solid angle, we obtain:

$$\frac{1}{A} \frac{dN_\gamma}{dE dt} = \frac{\langle \sigma v \rangle_{\text{eff}}}{m_\chi^2} \left( \frac{dN_\gamma}{dE} \right)_0 J, \quad (2.4.22)$$

where

$$J \equiv \frac{1}{8\pi} \int dr d\Omega \rho_\chi(\mathbf{r}) \quad (2.4.23)$$

is the famous *J-factor* for annihilations. If we assume a Navarro-Frenk-White (NFW) profile for the DM density, which goes as  $\rho(r) \propto r^{-1}$  for small  $r$ , the dwarf satellite galaxies of the Milky Way have  $J \sim 10^{17 \div 20} \text{ GeV}^2 \text{ cm}^{-5}$ , while for the center of the Milky Way  $J \sim 10^{22} \text{ GeV}^2 \text{ cm}^{-5}$ . Despite the higher J-factor, the center of the galaxies are much richer in astrophysical backgrounds than dwarf galaxies; for this reason, the latter are usually good targets for ID experiments.

In addition, one should also consider the effect of redshift and absorption, which make the energy of the final states not be constant from the emission to the reception.

Similarly to what happens with DD, experimental bounds are usually expressed in terms on bounds on the cross section between DM and SM particles; we show in fig. 2.7 the upper bounds on the thermally-averaged DM annihilation cross section into  $b\bar{b}$  and  $\tau^+\tau^-$  from the Fermi-LAT experiment.

## 2.4.3 LHC searches

In general, DM can also be produced at colliders, and its presence can be inferred by an unbalance between initial and final energy in the detected tracks. An important quantity in LHC searches for DM is the *transverse momentum*,  $p_T$ ; if we take  $\hat{z}$  to be the longitudinal beam direction, the transverse momentum for a particle of total momentum  $p$  is defined as [82]:

$$p_T \equiv \sqrt{p_x^2 + p_y^2} = p \cos \theta, \quad (2.4.24)$$

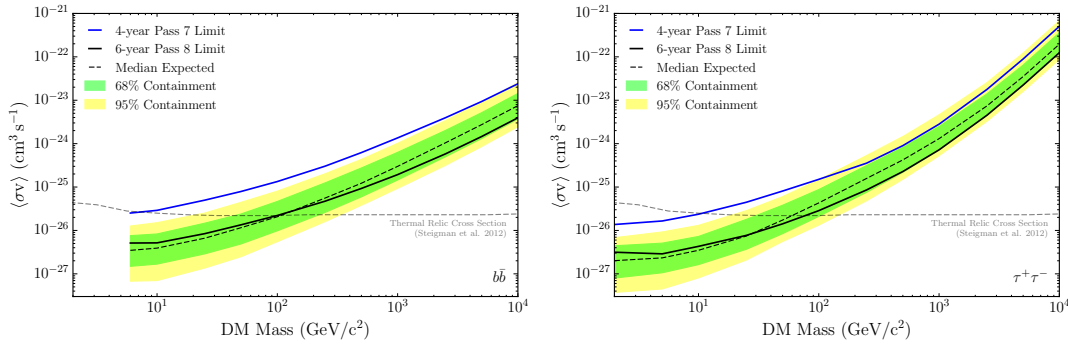


Figure 2.7: Upper bounds on the DM annihilation cross section into  $b\bar{b}$  (left) and  $\tau^+\tau^-$  (right) from the Fermi-LAT experiment. Figure taken from ref. [81].

where  $\theta$  is the polar angle. Given that, by definition,  $p_T = 0$  for incoming particles, the presence of particles which escape the detector (DM is a possibility, but also neutrinos behave similarly) can be inferred by summing over the transverse momenta of all outgoing states; to this purpose, one defines the *missing transverse momentum* as:

$$\boldsymbol{p}_T \equiv - \sum_i \boldsymbol{p}_{T,i}, \quad (2.4.25)$$

where the index  $i$  runs over all the detected tracks; the absolute value of this vector is called *missing transverse energy*, and indicated with  $\cancel{E}_T$  or  $MET$ , and is of great importance for DM searches.

LHC searches usually put some cuts in order to reduce the huge background; as an example, constraints on the rapidity  $y$  or the pseudo-rapidity  $\eta$ , defined for a particle respectively as

$$y \equiv \frac{1}{2} \ln \frac{E + p_z}{E - p_z} \quad (2.4.26a)$$

$$\eta \equiv \ln \cot \frac{\theta}{2}, \quad (2.4.26b)$$

are used; notice that these two quantities coincide for massless particles.

Other cuts are related to the separation between two jets; if we denote by  $\phi$  the azimuthal angle, and by  $\Delta$  the difference in a given quantity, the jet separation is usually defined:

$$\Delta R \equiv \sqrt{\Delta\eta^2 + \Delta\phi^2}. \quad (2.4.27)$$

Although different LHC searches can be the most relevant ones for different DM models, “mono- $X$ ” signatures are almost always present; these can be, for instance, monojet (MJ) (where “jet” stands for both quarks and gluons), mono-Higgs, mono-photon, and are schematically represented in fig. 2.8.

Two different approaches have been widely used in the literature to study LHC signatures of DM:

- effective models: in this case, non-renormalizable interactions between DM and SM particles are included. This approach has the virtue to be very general, leading to

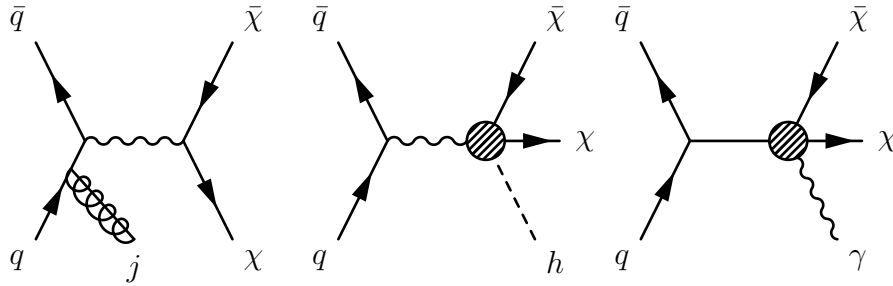


Figure 2.8: Schematic representation of some of the main signatures for DM physics at LHC: monojet, mono-Higgs and mono-photon, respectively.

bounds which are in principle applicable to a variety of different UV completion; on the other hand, it has the drawback that the effective approach is not always reliable, given the high energies reachable at LHC. Discussions about the EFT validity for DM can be found, e.g., in refs. [83–92];

- simplified models: in this second approach, only renormalizable operators usually appear, and new particles are introduced to mediate interactions between DM and SM fields (see, e.g., refs. [90,92,93]). These models are “simplified” because, for example, a bare mass term for the new gauge bosons is usually explicitly introduced. While they do not suffer of the problems of effective approaches related to the energies reached at LHC, it is not guaranteed that simplified models can be easily embedded in concrete UV theories.

In the following, we will discuss in detail two concrete realizations of these approaches, one for each of them.



# Chapter 3

## LHC interplay between dark matter and long-lived particles

*Since a particle cannot be sent into the infinitely distant past, our definition (of the scattering amplitude) in terms of the  $S$ -matrix makes no sense.*

Michael Peskin - about unstable particles

The majority of dark matter models predict LHC signatures in the form of monojet, where the events are characterized by a highly energetic jet and a large amount of missing transverse energy; great attention has been dedicated to this kind of searches, by both the ATLAS and CMS experiments (see, e.g., refs. [94–97]).

Another scenario which has been receiving more and more attention is represented by the possibility that unstable particles are produced at the LHC and travel a macroscopic (on collider scales) distances before decaying; these particles are called *long-lived particles*. This is not a feature which is absent in the Standard Model: massive SM particles, in fact, have lifetime which span about 66 orders of magnitude (from  $\tau \sim 10^{-25}$  s for the  $Z$  boson to  $\tau \gtrsim 10^{41}$  s for the proton), as schematically shown in fig. 3.1, taken from ref. [98]. However, LLPs in the SM have masses  $\lesssim 5$  GeV, so that particles with mass of  $\mathcal{O}(100$  GeV) which can travel a macroscopic distances ( $c\tau \gtrsim 10^{-5}$  m) can be a smoking gun for NP; in addition, SM particles which can be considered long-lived have a well-understood background.

Long-lived particles in association of BSM physics have been studied in different contexts, such as supersymmetry or composite-Higgs models (see, e.g., refs. [99–105]); in the context of DM model, this possibility has been considered in refs. [1, 2, 106–111].

Although LLPs offer excellent prospects for the discovery of NP, they also provide experimental physicists with a serious challenge: standard reconstruction techniques may reject events containing LLPs, precisely because of their unusual signatures, which can look like noise or misidentified objects; for this reason, dedicated searches are needed, in order to investigate the possible existence of LLPs. The awareness of both the potentiality and the difficulty related to the searches for long-lived particles led to the creation of the LHC LLP Community, whose aim is to fully exploit them for the study of NP at the LHC; many more details about LLPs can be found in the recent white paper [98].

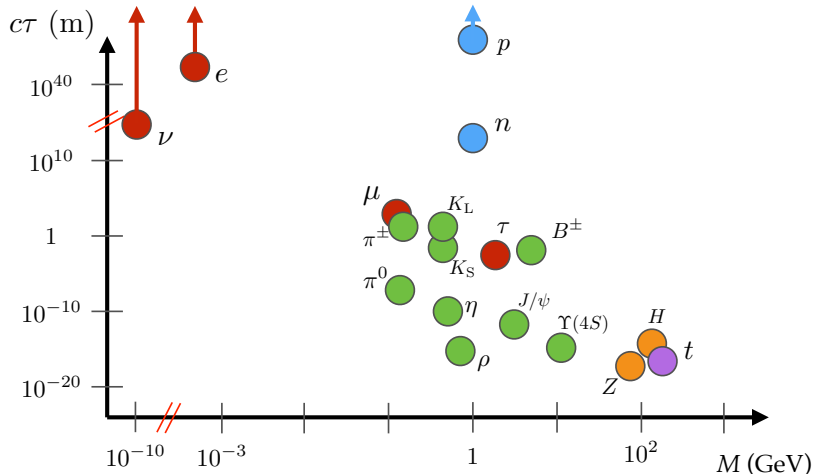


Figure 3.1: Particle lifetime  $c\tau$  as a function of the mass  $M$ , for several SM particles. Figure taken from ref. [98].

In this chapter, we discuss two DM models which are characterized by the presence of LLPs: the first one, based on ref. [1], is a simplified model which delivers displaced vertices (DVs); the second one, instead, is an effective theory where the LLP gives rise to bound states similar to the  $R$ -hadrons which emerge in supersymmetry, and is based on ref. [2]. The two models are presented in sections 3.1 and 3.2, respectively. We show that in both cases bounds from experimental searches looking for LLPs are crucial in order to constrain the parameter space; in particular, these turn out to be complementary (and sometimes even competitive) with more traditional searches based on MJ signatures. Extra details about the two models are given in appendices 3.A and 3.B, respectively.

### 3.1 Pseudo-Dirac dark matter

Current DD experiments put strong constraints on the DM scattering cross section, especially in the SI case (see fig. 2.6); in particular, these bounds usually rule out naïve relic density couplings in many models. A possible way out is represented by the breaking of the crossing symmetry between different contributions: in particular, if the scattering rate is suppressed, while the annihilation one is not, one could be able to evade current DD bounds without an overproduction of DM.

In this section, we study the pseudo-Dirac dark matter (pDDM) model, first considered in ref. [112] as an EFT; this is a simple extension of the SM where two dark Majorana fermions are introduced, and are characterized by small mass splitting (similar situations, realized also in a supersymmetric framework, were studied in refs. [113–117]). We extend the analysis of ref. [112] by considering a simplified model version of it, allowing then the interaction scale to be of  $\mathcal{O}(\text{TeV})$ , by introducing a new gauge boson, denoted by  $Z'$ : if it is integrated out, the model reduces to the effective one studied previously

The remarkable aspect of the model is that the heavier state,  $\chi_2$ , can be produced with an energy and a decay length which can lead to DVs at LHC, representing a promising direction in the search for NP [103, 104, 118–147].

We introduce the model in section 3.1.1, we discuss current constraints on the param-



eter space in section 3.1.2 and we show the results in section 3.1.3

### 3.1.1 Model Lagrangian

As a first case for the study of long-lived particles associated to DM, we consider the so-called pDDM model; it is a simplified model which includes a Dirac fermion  $\Psi$  described by a free Lagrangian which contains both a Dirac and a Majorana mass term, of the form:

$$\mathcal{L}_0 = \bar{\Psi}(i\not{\partial} - M_D)\Psi - \frac{m_L}{2}(\bar{\Psi}^c P_L \Psi + \text{h.c.}) - \frac{m_R}{2}(\bar{\Psi}^c P_R \Psi + \text{h.c.}), \quad (3.1.1)$$

where  $P_{L,R} = (1 \mp \gamma^5)/2$  are the chiral projectors and the superscript  $c$  denotes the charge conjugated. The ‘‘pseudo-Dirac’’ assumption consists in the fact that we take  $M_D \gg m_{L,R}$ .

Such a state interacts with the SM via a dark gauge boson  $Z'$  with mass  $m_{Z'}$  whose interactions are:

$$\mathcal{L}_{\text{int}} = \bar{\Psi}\gamma^\mu(c_L P_L + c_R P_R)\Psi Z'_\mu + \sum_f \bar{f}\gamma^\mu(c_L^{(f)} P_L + c_R^{(f)} P_R)f Z'_\mu, \quad (3.1.2)$$

where  $f$  is a SM fermion and we take the coefficients  $c$ 's to be real.

As already discussed in section 2.4.3, when dealing with simplified models, one usually does not commit to studying a particular UV completion; the simplest scenario, however, could be realized if we assume  $\Psi$  to be embedded in a fermion  $\Theta$  which is a doublet under a dark  $SU(2)'$  symmetry, spontaneously broken through a Higgs-like mechanism by a scalar field  $\Phi'$ . Let us assume that  $v'$  is the VEV of  $\Phi'$ ; the Dirac mass term is then reproduced like in the SM. As far as the Majorana mass term is concerned, instead, we can assume that new physics takes place at an even higher scale, and that it is responsible for the appearance of a Weinberg operator  $1/\Lambda \bar{\Theta}(i\sigma_2\Phi')(i\sigma_2\Phi')^\dagger \Theta^c$ ; such an interaction leads to a Majorana mass term for  $\Psi$  after  $\Phi'$  acquires a VEV. The hierarchy between  $M_D$  and  $m_{L,R}$  can then be easily understood by taking into account that  $M_D \propto v'$ , while  $m_L = m_R \propto v'^2/\Lambda \sim M_D v'/\Lambda$ . This simple UV completion is also anomaly-free; possible anomalies, in fact, may arise from triangular diagrams involving  $U(1)$ - $SU(2)$ - $SU(2)'$  and  $U(1)$ - $SU(2)'$ - $SU(2)'$  currents, but it is simple to show that if  $Z'$  couples to all the SM fermions, they are not present.

Another example of a possible UV completion as a pseudo-bino model was discussed in ref. [112]. In general,  $Z'$  cannot be associated to an abelian gauge symmetry, since the latter would be explicitly broken by the Majorana mass terms.

Given that our goal is to study the interplay of DM and LLPs, we assume that the  $Z'$  gauge boson only couples to SM quarks, given that these are responsible for the interesting phenomenology.

The two (Majorana) mass eigenstates of the free Lagrangian in eq. (3.1.1), denoted by  $\chi_{1,2}$ , are:

$$\chi_1 = \frac{i}{\sqrt{2}}(\Psi - \Psi^c) \quad (3.1.3a)$$

$$\chi_2 = \frac{1}{\sqrt{2}}(\Psi + \Psi^c), \quad (3.1.3b)$$

with masses  $m_{1,2} = M_D \mp (m_L + m_R)/2$ . Their derivation is explicitly discussed in appendix 3.A.1. The spectrum of the dark sector therefore consists of the DM,  $\chi_1$ , a

heavier companion  $\chi_2$  and a gauge boson,  $Z'$ , which we assume to be heavy ( $m_{Z'} \sim \mathcal{O}(1 \text{ TeV})$ ); in the pseudo-Dirac limit, the two fermions are close in mass, i.e.  $\Delta m \equiv m_2 - m_1 \ll m_1$ .

In terms of these fields, the interaction Lagrangian in eq. (3.1.2) becomes:

$$\mathcal{L}_{\text{int}} = \mathcal{L}_{\text{int}}^{(\chi_1\chi_2)} + \mathcal{L}_{\text{int}}^{(\chi_1\chi_1)} + \mathcal{L}_{\text{int}}^{(\chi_2\chi_2)} + \mathcal{L}_{\text{int}}^{(\bar{f}f)}, \quad (3.1.4)$$

where:

$$\mathcal{L}_{\text{int}}^{(\bar{f}f)} = \sum_f \bar{f} \gamma^\mu \left[ \frac{c_L^{(f)} + c_R^{(f)}}{2} - \frac{c_L^{(f)} - c_R^{(f)}}{2} \gamma^5 \right] f Z'_\mu \quad (3.1.5a)$$

$$\mathcal{L}_{\text{int}}^{(\chi_1\chi_2)} = i \frac{c_R + c_L}{2} \bar{\chi}_1 \gamma^\mu \chi_2 Z'_\mu \quad (3.1.5b)$$

$$\mathcal{L}_{\text{int}}^{(\chi_i\chi_i)} = \frac{c_R - c_L}{4} \bar{\chi}_i \gamma^\mu \gamma^5 \chi_i Z'_\mu \quad , \quad i = 1, 2. \quad (3.1.5c)$$

Remarkably, while the interactions between  $\chi_1$  and  $\chi_2$  occur via a vector coupling, those of  $\chi_1$  with itself (and the same for  $\chi_2$ ) are characterized by axial-vector couplings; this is indeed a consequence of the Majorana nature for the  $\chi$ 's. These two structure lead to different phenomenology for scatterings and annihilations [90, 93, 148, 149]; in particular, given that scattering processes between  $\chi_1$  and a nucleus are not energetic enough to produce a  $\chi_2$ , interactions relevant for DD proceed via the axial-vector coupling only. According to the discussion of section 2.4.1, then, we expect them to be SD; following the classification of ref. [90], the relevant non-relativistic operators are:

$$\mathcal{O}_4^{\text{NR}} = \mathbf{s}_\chi \cdot \mathbf{s}_N \quad (3.1.6)$$

$$\mathcal{O}_8^{\text{NR}} = \mathbf{s}_\chi \cdot \mathbf{v}_\perp \quad (3.1.7)$$

$$\mathcal{O}_9^{\text{NR}} = i \mathbf{s}_\chi \cdot (\mathbf{s}_N \times \mathbf{q}), \quad (3.1.8)$$

where  $\mathbf{s}_{\chi,N}$  is the spin of the DM and the nucleon, respectively,  $\mathbf{q}$  is the momentum transfer and  $\mathbf{v}_\perp = \mathbf{v} - \mathbf{q}/2\mu_{\chi N}$ , with  $\mathbf{v}$  being the DM-nucleon relative velocity and  $\mu_{\chi N}$  the reduced mass of the system. Each of these operators is strongly suppressed with respect to SI interactions [76, 150–152], allowing the model to evade DD constraints [75, 153, 154].

The suppression of the axial-vector interaction could make it hard to reproduce the correct relic density; as we will discuss, however, the presence of a slightly heavier partner,  $\chi_2$ , leads to coannihilations, solving this potential issue.

## Decay length

The interactions in eqs. (3.1.5a) and (3.1.5b) are responsible for the decay  $\chi_2 \rightarrow \chi_1 f \bar{f}$ , whose leading order width is:

$$\Gamma_{\chi_2 \rightarrow \chi_1 f \bar{f}} \approx \sum_f \frac{N_c^{(f)}}{480\pi^3} (c_L + c_R)^2 \left( c_L^{(f)2} + c_R^{(f)2} \right) \frac{\Delta m^5}{m_{Z'}^4}, \quad (3.1.9)$$

where higher-order terms in  $\Delta m/m_1$  and  $m_f/m_1$  have been neglected; a more complete expression for the decay width can be found in appendix 3.A.2. In the following, we focus our attention on SM quarks, but the analysis can be easily extended to include leptons.

The corresponding decay length in the  $\chi_2$ -rest frame is (at leading order in  $\Delta m/m_1$  and  $m_f/m_1$ ):

$$L_0 \approx 2.94 \text{ m} \left[ \sum_f N_c^{(f)} (c_L + c_R)^2 (c_L^{(f)2} + c_R^{(f)2}) \right]^{-1} \left( \frac{m_{Z'}}{1 \text{ TeV}} \right)^4 \left( \frac{1 \text{ GeV}}{\Delta m} \right)^5. \quad (3.1.10)$$

The neglected contributions can give corrections of the order of 30%, but this estimate correctly reproduces the order of magnitude of the decay length; in particular, for  $\Delta m \sim \mathcal{O}(\text{GeV})$  and  $m_{Z'} \sim \mathcal{O}(\text{TeV})$ ,  $L_0$  is of the order of the radius of the ATLAS and CMS detectors, allowing the observation of a signal in the form of DVs.

The mean decay length in the laboratory frame is then simply:

$$L_0^{\text{lab}} = \beta\gamma L_0, \quad (3.1.11)$$

where  $\beta\gamma \equiv p_2/m_2$  is the boost factor for  $\chi_2$ . The decay length  $L_{\text{lab}}$  of a particle in the detector then follows the probability distribution:

$$P(L^{\text{lab}}) = \frac{1}{L_0^{\text{lab}}} e^{-L^{\text{lab}}/L_0^{\text{lab}}}. \quad (3.1.12)$$

If we denote by  $p_2^T$  the momentum of  $\chi_2$  in the transverse direction, we can then define a transverse decay length as  $L_{T,0}^{\text{lab}} \equiv L_0 p_2^T/m_2$ . Following ref. [155], the total probability that the particle travels a transverse distance larger than some threshold  $L$  can then be approximated by simulating and averaging over a large number  $N$  of events,

$$P(L_T^{\text{lab}} > L) = \frac{1}{N} \sum_{i=1}^N \exp\left(-\frac{L}{L_{T,0}^{\text{lab}}(p_2^T = p_{2,i}^T)}\right). \quad (3.1.13)$$

## Relic density

Given that this model predicts the existence of two states which are very close in mass, coannihilations can be important in the determination of the DM relic density. The effective cross section is given by eq. (2.3.26), and in this case it simplifies to:

$$\langle\sigma v\rangle_{\text{eff}} = \frac{1}{(1 + \alpha)^2} (\langle\sigma v\rangle_{11} + 2\alpha\langle\sigma v\rangle_{12} + \alpha^2\langle\sigma v\rangle_{22}), \quad (3.1.14)$$

where  $\alpha \equiv (1 + \Delta m/m_1)^{3/2} e^{-x\Delta m/m_1}$ ,  $x \equiv m_1/T$  and  $\langle\sigma v\rangle_{ij} \equiv \langle\sigma v\rangle_{\chi_i\chi_j \rightarrow f\bar{f}}$ .

The complete expressions for the thermally-averaged cross sections are reported in eqs. (3.A.6a) and (3.A.6b); however, the leading-order effective cross section is:

$$\begin{aligned} \langle\sigma v\rangle_{\text{eff}} &\approx \sum_f \frac{N_c^{(f)}}{16\pi} (c_L + c_R)^2 (c_L^{(f)2} + c_R^{(f)2}) \frac{m_1^2}{m_{Z'}^4} \\ &\approx 0.08 \sum_f N_c^{(f)} (c_L + c_R)^2 (c_L^{(f)2} + c_R^{(f)2}) \left(\frac{m_1}{100 \text{ GeV}}\right)^2 \left(\frac{1 \text{ TeV}}{m_{Z'}}\right)^4 \langle\sigma v\rangle_{\text{WIMP}}, \end{aligned} \quad (3.1.15)$$

with  $\langle\sigma v\rangle_{\text{WIMP}} \equiv 3 \times 10^{-26} \text{ cm}^3 \text{ s}^{-1}$  being the typical WIMP annihilation cross section. From eqs. (3.A.6a) and (3.A.6b), we see that the self-annihilations are velocity suppressed, making the coannihilation contribution be the most important one in the determination of the effective cross section.

The relic density can be then computed by resorting to eqs. (2.3.17) and (2.3.19); in this case,  $g_\chi$  is actually given by  $g_\chi = g_{\chi_1}(1 + \alpha)$ , where  $g_{\chi_1} = 2$ .

## Link between decay length and relic abundance

By comparing eqs. (3.1.9) and (3.1.15), we see that the decay width of  $\chi_2$  and the effective cross section depend the same way on the coefficients  $c$ 's; this is simply because the main contribution to  $\langle\sigma v\rangle_{\text{eff}}$  comes from the same vertex which controls the decay, i.e.  $\chi_1\chi_2-f\bar{f}$ .

This fact only holds for the leading contribution to  $\langle\sigma v\rangle_{\text{eff}}$ , but it turns out to be a good approximation in the limit of small quark masses,  $m_f \approx 0$ , where the self-annihilations are velocity suppressed (see eq. (3.A.6b)). As already noticed in ref. [112], this allows for a link between two observables which are in principle completely unrelated: the  $\chi_2$  decay length (collider property) and the DM relic density (cosmological property).

In particular, the DM abundance can be expressed as a function of  $L_0$  and the other parameters of the model as:

$$\frac{\Omega h^2}{0.1194} \approx 1.26 \frac{x_F}{\sqrt{g_*}} \frac{1}{1 + \frac{1}{2x_F} \left(\frac{1-k}{1+k}\right)^2} \left(\frac{L_0}{1\text{ m}}\right) \left(\frac{100\text{ GeV}}{m_1}\right)^2 \left(\frac{\Delta m}{1\text{ GeV}}\right)^5, \quad (3.1.16)$$

where  $k \equiv c_R/c_L$ .

Thus, we can estimate the value of  $L_0$  for given  $(m_1, \Delta m, k)$  by imposing the observed value for  $\Omega h^2$ . In addition, we see that for given  $L_0$ , eq. (3.1.16) does not depend on  $m_{Z'}$ , and since  $x_F \sim \mathcal{O}(20)$ , then if  $k \gtrsim 0$ , it depends only very mildly on  $k$ .

If one is able to infer  $L_0$  (from DVs) and  $\Delta m$  (from the edge of di-jet distributions) by collider measurements, then it would be possible to make a prediction for the DM mass  $m_1$ .

### 3.1.2 Constraints on the parameter space

The parameter space of the model is spanned by the set:

$$\{m_1, \Delta m, m_{Z'}, c_L, c_R, c_L^{(f)}, c_R^{(f)}\}. \quad (3.1.17)$$

In order to avoid a full scan over the entire seven-dimensional parameter space, we can motivate benchmark points and apply a number of constraints before performing the main analysis; we will leave  $\{m_1, \Delta m\}$  free. Our signals of interest are not sensitive to the chirality of the quarks, so that we can set  $c_R^{(f)} = -c_L^{(f)}$  without loss of generality; this leads to a pure axial-vector coupling between the  $Z'$  and SM quarks. We have checked that perturbative unitarity is not violated for the values of masses and couplings considered in our analysis [148].

A first restriction on the parameter space could be represented by DD; in ref. [156] a general estimate for the SD cross section is presented and, adapted to our model, reads:

$$\sigma_{\text{SD}} \approx 2.4 \times 10^{-42} \text{ cm}^2 (c_R - c_L)^2 c_L^{(f)2} \left(\frac{1\text{ TeV}}{m_{Z'}}\right)^4 \left(\frac{\mu_{\chi N}}{1\text{ GeV}}\right)^2. \quad (3.1.18)$$

Such an estimate can be obtained by combining eqs. (2.4.19) and (2.4.20) and assuming that  $\lambda_q$  in eq. (2.4.18) is the same for all quarks. It turns out that current DD limits, such as those from LUX [157], are weaker than other constraints; for this reason, we do not consider DD in the following.

The relative magnitude of the axial-vector ( $\chi_i\chi_i$ ) and vector ( $\chi_1\chi_2$ ) couplings is controlled by the ratio  $k = c_R/c_L$ ; they are proportional to  $|c_R - c_L|$  and  $|c_R + c_L|$ , respectively,

so that the first one vanishes in the limit  $k \rightarrow 1$ , while the second one for  $k \rightarrow -1$ . The interplay between these two contributions is important for the potential observability of displaced vertices, and so we choose two benchmarks for  $k$ :  $k = -0.8$  and  $k = 0$ .

Note that a degeneracy arises because in all relevant observables,  $c_{L,R}$  always appear as either  $|c_L + c_R|^2$  or  $|c_L - c_R|^2$ ; as a consequence, the  $(c_L, c_R)$  plane is divided into four equivalent wedges separated by the straight lines  $k = -1$ ,  $k = 1$ . Any point in one of the four wedges can be mapped onto a point in any of the other three with no change in the phenomenology; concretely, choosing  $k = -0.8$  ( $0$ ) is equivalent to choosing  $k^{-1} = -0.8$  ( $0$ ) (by appropriately rescaling the coefficients); similarly, the transformation  $(c_L, c_R) \rightarrow -(c_L, c_R)$  has no effect.

## Dijets searches

Dijet searches put upper bounds on the couplings between the Standard Model and the dark mediator. We refer to the results of ref. [158]: in particular, in its figure 4, limits on the coupling between  $Z'$  and SM quarks in an axial-vector simplified model are shown. These constraints derive from a limit on  $Z'$  production rate, weighted by its branching ratio into quarks: for this reason, the bounds are sensitive to the ratio between  $Z'$  couplings with DM and quarks. In particular, the analysis of ref. [158] assumes a negligible coupling to DM, which provides the strongest limit on the coupling with quarks. In order to be conservative, we directly apply those constraints, although the presence of  $Z'$ -DM coupling would weaken the bounds.

In our notation, the coupling which is constrained is  $c_L^{(f)}$ , given that we are considering the case  $c_L^{(f)} = -c_R^{(f)}$ . We consider three benchmark values:  $c_L^{(f)} = 0.07$ ,  $c_L^{(f)} = 0.13$  and  $c_L^{(f)} = 0.25$  for  $m_{Z'} = 1.5$  TeV,  $m_{Z'} = 2.5$  TeV,  $m_{Z'} = 3.5$  TeV, respectively; these are arbitrarily large values compatible with dijets constraints. We assume these couplings to be universal, i.e. to be the same for all quarks and to be independent of  $m_1$  and  $\Delta m$ .

## Relic Density

For given  $m_1$ ,  $\Delta m$  and  $m_{Z'}$  (and then also  $c_L^{(f)}$ ), we can determine the contour corresponding to the observed DM relic density in the  $(c_L, c_R)$  plane; we take, for the observed value,  $\Omega h^2 = 0.1194$  [159]. This value is shown as a red line (with orange  $3\sigma$ -contour) in fig. 3.2, for three different values of  $m_1$ . The benchmark for  $k$  is a straight line in this plane, and is shown in blue. This line intercepts the relic density contour in two points; given that the phenomenology is invariant under the replacements  $(c_L, c_R) \rightarrow -(c_L, c_R)$  and  $k \rightarrow k^{-1}$ , a unique pair of coefficients is effectively determined. We choose the point for which  $c_L < 0$  and  $c_R > 0$ .

## $Z'$ width

A second restriction on  $c_L$  and  $c_R$  comes from a kinematic argument: given that we treat  $Z'$  as a physical intermediate state which is exchanged in the  $s$ -channel, it is necessary for its decay width to be small, i.e.  $\Gamma_{Z'} \ll m_{Z'}$ .

In eqs. (3.A.7a) to (3.A.7c), we provide the expressions for the partial decay widths of  $Z'$ : in general,  $\Gamma_{Z'}/m_{Z'} \propto (c_L \pm c_R)^2$ . Requiring this ratio to be less than some critical value identifies an elliptic region in the  $(c_L, c_R)$  plane (with the other parameters being fixed); we choose this ratio to be  $\Gamma_{Z'}/m_{Z'} \leq 0.2$ , which ensures that the Breit-Wigner

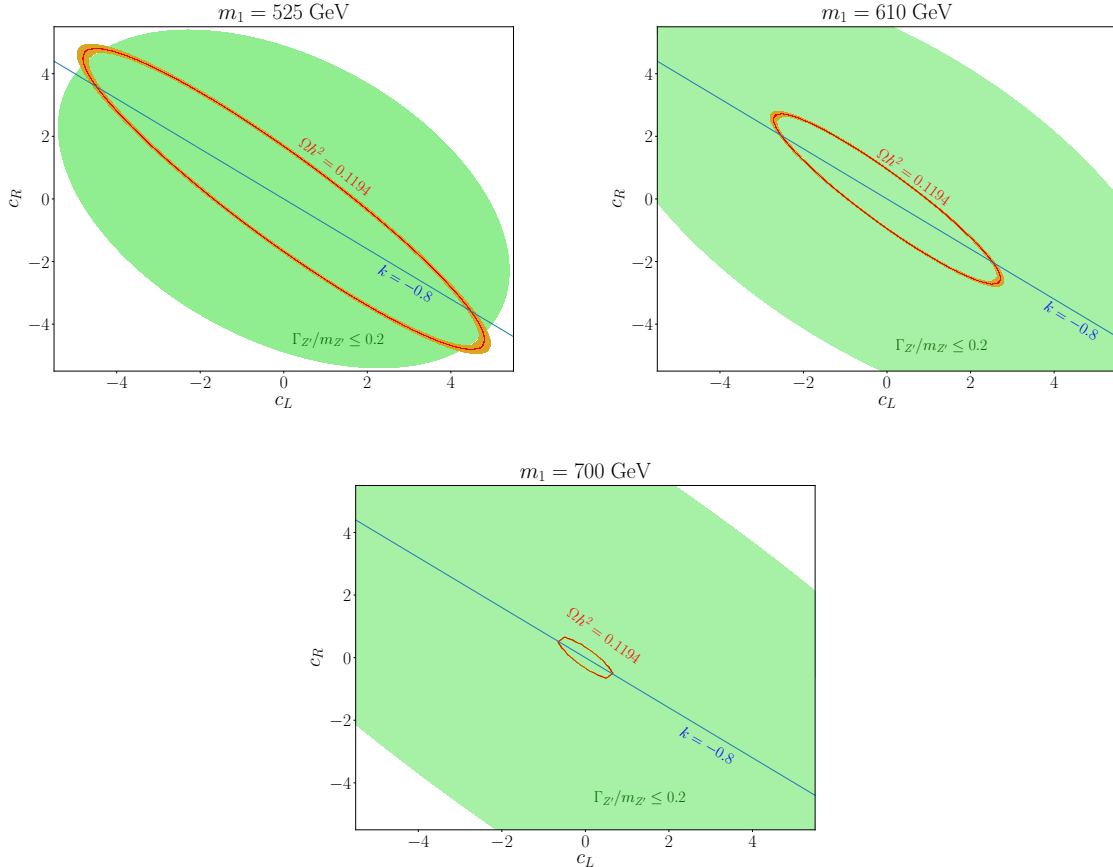


Figure 3.2: Interplay between the DM relic abundance (red line with orange  $3\sigma$ -contour) and the requirement  $\Gamma_{Z'}/m_{Z'} \leq 0.2$  (green region) in the  $(c_L, c_R)$  plane for  $m_{Z'} = 1.5$  TeV,  $\Delta m = 5$  GeV,  $k = -0.8$  (blue line) and different values of  $m_1$ .

approximation is sufficiently accurate [160, 161]. The corresponding allowed region is shown in green in fig. 3.2.

As we can see from fig. 3.2, too small values of  $m_1$  make the intercept between the relic density contour and the straight line corresponding to a fix  $k$  fall outside the allowed green region; on the other hand, too large masses tend to pick small values of  $c_L$  and  $c_R$ , which represent a problematic situation from a numerical point of view which we decide to avoid. Overall, then, this procedure also selects an allowed range of values for  $m_1$ , which we summarize in table 3.1. We choose the same range of  $\Delta m$  for all the values of  $m_{Z'}$ , namely  $1.5 \text{ GeV} \leq \Delta m \leq 8.0 \text{ GeV}$ .

### 3.1.3 Results

After discussing the model and the restrictions on the parameter space, we can move to the analysis and the results. As most of the DM models, also the pDDM is sensible to MJ searches; in addition, however, it can also leave a trace at LHC in the form of DVs, as anticipated. We discuss in the following how these two different strategies are complementary for exploring the parameter space of the model, and we show that DVs can be even competitive with MJ searches in the future.

	$m_{Z'} = 1.5 \text{ TeV}$	$m_{Z'} = 2.5 \text{ TeV}$	$m_{Z'} = 3.5 \text{ TeV}$
$c_L^{(f)}$	0.07	0.13	0.25
$m_1 \geq$	525 GeV	850 GeV	1100 GeV
$m_1 \leq$	700 GeV	1200 GeV	1600 GeV

	$m_{Z'} = 1.5 \text{ TeV}$	$m_{Z'} = 2.5 \text{ TeV}$	$m_{Z'} = 3.5 \text{ TeV}$
$c_L^{(f)}$	0.07	0.13	0.25
$m_1 \geq$	375 GeV	550 GeV	650 GeV
$m_1 \leq$	700 GeV	1200 GeV	1600 GeV

Table 3.1: Allowed range of  $m_1$  and choice for  $c_L^{(f)}$ , for different values of  $m_{Z'}$ , and  $k = -0.8$  (top) and  $k = 0$  (bottom).

### Monojet analysis

Monojet searches look at signatures characterized by an energetic jet and a large amount of  $\cancel{E}_T$ , and are performed by both the ATLAS and CMS experiments; we use the results from ref. [94], corresponding to an ATLAS analysis at 13 TeV with  $3.2 \text{ fb}^{-1}$  of integrated luminosity.

In signatures relevant for MJ, the production of DM can be explored using events where the jet is emitted in the form of initial state radiation (ISR); in addition, also the joint production  $\chi_1\text{-}\chi_2$ , followed by a decay of  $\chi_2$ , would lead to MJ signatures.

We simulated the processes

$$pp \rightarrow \chi_{1,2}\chi_{1,2}j \quad , \quad \text{with } \chi_2 \rightarrow \chi_1jj \quad (3.1.19)$$

with the choice of couplings and mass ranges discussed in table 3.1; we then applied the selection cuts performed by the ATLAS search to determine the current regions of the parameter space which are excluded. As described in ref. [94], the search is divided in seven signal regions, denoted by IM1-IM7, which differ from the cuts on the  $\cancel{E}_T$ , which go from 250 GeV to 750 GeV; they also provide upper limits on the cross section at 95% CL, denoted by  $\langle\sigma\rangle_{\text{obs}}^{95}$ , ranging from 553 fb to 19 fb.

The results strongly depend on the value of  $k$ : in particular, if  $k = -0.8$ , only the mass  $m_1 = 525 \text{ GeV}$  for  $m_{Z'} = 1.5 \text{ TeV}$  is currently excluded among the ones simulated; on the other hand, for  $k = 0$  all the DM masses below  $m_1 = \{550 \text{ GeV}, 800 \text{ GeV}, 850 \text{ GeV}\}$  for  $m_{Z'} = \{1.5 \text{ TeV}, 2.5 \text{ TeV}, 3.5 \text{ TeV}\}$  are already ruled out. The fact that larger values of  $m_{Z'}$  correspond to larger currently excluded DM masses follows from the selection procedure for the couplings we discussed in section 3.1.2: in particular, we showed that larger couplings are typically selected for heavier  $Z'$ .

In order to project the current bounds to high luminosity (HL), we have to estimate the corresponding uncertainties on the SM backgrounds; the latter are dominantly represented by  $Zj \rightarrow \nu\bar{\nu}j$  and  $Wj \rightarrow \ell\nu_\ell j$ . Exclusions at high luminosities could be carried out by simulating the background (see, e.g., ref. [162]); another possibility, however, is to rescale the current constraints, and we decide to follow this second approach. In particular, it is important to consider statistical and systematic uncertainties separately: in ref. [94], the systematic errors on the background are reported, ranging from 2% for IM1 to 4% for IM7 (section 7.1); in addition, also the total number of expected number of events at  $3.2 \text{ fb}^{-1}$  is given, together with the associated uncertainty (table 7). As an example, we

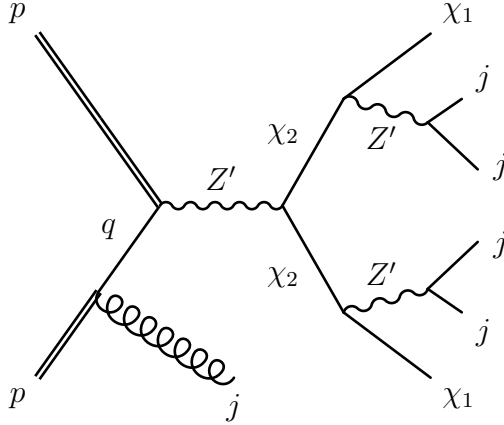


Figure 3.3: Schematic representation of the process leading to 2 DVs.

can consider the signal region IM7, where the expected number of event is  $N = 167 \pm 20$  at 95% CL; by taking into account that the statistical uncertainty is  $\delta N^{\text{st}} = \sqrt{N}$ , we have  $\delta N^{\text{st}} = 13$  and then  $\delta N^{\text{sys}} = 15$ , corresponding to 7.8% and 9.0%, respectively. The relative statistical error scales with the inverse square root of the number of events (and then of the luminosity),  $\delta^{\text{(stat)}} \propto \sqrt{\mathcal{L}^{-1}}$ ; on the other hand, it is not easy to predict how the systematic uncertainty changes with the luminosity: for this reason, we decide to parametrize it as  $\delta^{\text{(sys)}}(\mathcal{L}_2) = r \delta^{\text{(sys)}}(\mathcal{L}_1)$ , where  $\mathcal{L}_{1,2}$  denote two different integrated luminosities. If we take, for example,  $r = 0.4$ , we determine the expected number of SM events at  $100 \text{ fb}^{-1}$  to be  $N = 5219 \pm 201$  at 95% CL, corresponding to a bound on the NP cross section of  $\langle \sigma \rangle^{95} \approx 4 \text{ fb}$ ; in getting this bound, we assumed the number of observed events to be compatible with the background expectation.

At high luminosities, it is possible that at a better control on systematics is achieved or, on the other hand, that the high-luminosity environment leads to a degradation of the understanding of the SM backgrounds, and then to larger relative systematic uncertainties; for this reason, we take as a benchmark bound on the cross section  $\langle \sigma \rangle^{95} = 5 \text{ fb}$ , corresponding to a total uncertainty on the SM background of about 10%; we use this reference value also for projections at even higher luminosities, up to  $\mathcal{L} = 1000 \text{ fb}^{-1}$ , simply neglecting the statistical contribution. The bounds from current and projected MJ can be found in fig. 3.5, together with the limits from DVs; as can be seen, they are rather independent of  $\Delta m$ , given that MJ cuts mostly select events where the jet comes as ISR.

### Displaced vertices analysis

Displaced vertices are a smoking gun for BSM physics, with the expected background coming from vertex misidentification only. As anticipated, pDDM model delivers DVs if  $\chi_2$  is produced and travels an appreciable distance before decaying. The strongest signal is expected from the process  $pp \rightarrow \chi_2 \chi_2 j \rightarrow \chi_1 \chi_1 jjjjj$ , which is schematically shown in fig. 3.3: the presence of two  $\chi_2$ 's can lead to two DVs, for which the expected background is extremely small. The presence of ISR is responsible for the two  $\chi_2$ 's not to be in the back-to-back configuration; as a consequence,  $\cancel{E}_T$  increases, and allows us to trigger on events with high- $p_T + \cancel{E}_T$ . In addition, we are interested in the region of the parameter space for which  $\Delta m \lesssim 10 \text{ GeV}$ , so that the jets emitted from the decay of  $\chi_2$  have  $p_T \sim \mathcal{O}(1 \text{ GeV})$ : these are too soft to be triggered on, but can be of help for the offline analysis and for DVs identification. We simulate the events at parton level as outlined in appendix 3.A.3.



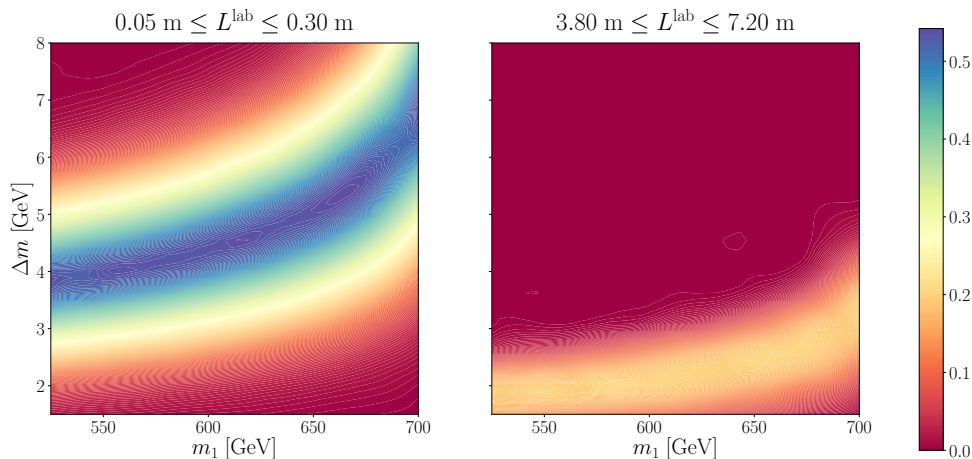


Figure 3.4: Probability that  $\chi_2$  decays in either the ATLAS inner detector (left panel) or muon solenoid (right panel) for  $m_{Z'} = 1.5$  TeV and with the couplings determined as discussed in section 3.1.2.

In order to deliver DVs, our model must at least admit a region of the parameter space in which  $\chi_2$  is enough long-lived to reach the inner detector of the experiment under consideration. We refer to ATLAS, and in particular to ref. [163], for the analysis; the decay must then occur in either the inner detector, with size  $0.05 \text{ m} < r < 0.3 \text{ m}$  or in the muon solenoid, where  $3.8 \text{ m} < r < 7.2 \text{ m}$ . We can compute the probability for  $\chi_2$  to decay in these two ranges of lengths by resorting to eq. (3.1.13), and the result is shown in fig. 3.4 for  $m_{Z'} = 1.5$  TeV; notice that with the couplings fixed as described in section 3.1.2, the decay length is only function of  $\{m_1, \Delta m, m_{Z'}\}$ . In particular, it is possible to notice that this probability can be significantly different from zero, especially in the inner detector.

In ref. [163], bounds on the number of events with two DVs at a CM energy  $\sqrt{s} = 8$  TeV are given; given that our process has high- $p_T$  and large  $\cancel{E}_T$ , the best limits come from the jets +  $\cancel{E}_T$  trigger. As already stated, the expected background is extremely small (of the order of  $10^{-4}$  events, cf. table IX), at  $20.3 \text{ fb}^{-1}$  of integrated luminosity and with the cuts  $p_T > 120$  GeV and  $MET > 200$  GeV. In order to make sure that the expected background remains approximately zero even at  $\sqrt{s} = 13$  TeV, we rescale the cuts to  $p_T > 200$  GeV and  $MET > 300$  GeV. These cuts make the pseudo-rapidity  $\eta$  small, so that no events are found in the barrel endcap.

The jets + MET trigger requires at least 7 tracks per vertex; whilst a full detector simulation is beyond the scope of our work, we have performed a Delphes-level [164] analysis of the process for several benchmark points in parameter space and found that approximately 25% to 50% of vertices passed this track requirement. In addition, we do not make a precise evaluation of the efficiency for the vertex reconstruction, but consider a benchmark value of 20%; such a choice may be viewed as an optimistic scenario for near-future displaced-vertex experimental analyses, and further emphasises the need for an increased focus on this signal by ATLAS and CMS.

We show the results in fig. 3.5, where we project current bounds to higher luminosities:  $\{100 \text{ fb}^{-1}, 300 \text{ fb}^{-1}, 1000 \text{ fb}^{-1}\}$ , respectively. As anticipated, we rescale the number of events by an efficiency coefficient which we take to be 20% (for each vertex); given that the expected background is approximately zero, we can exclude a point of the parameter

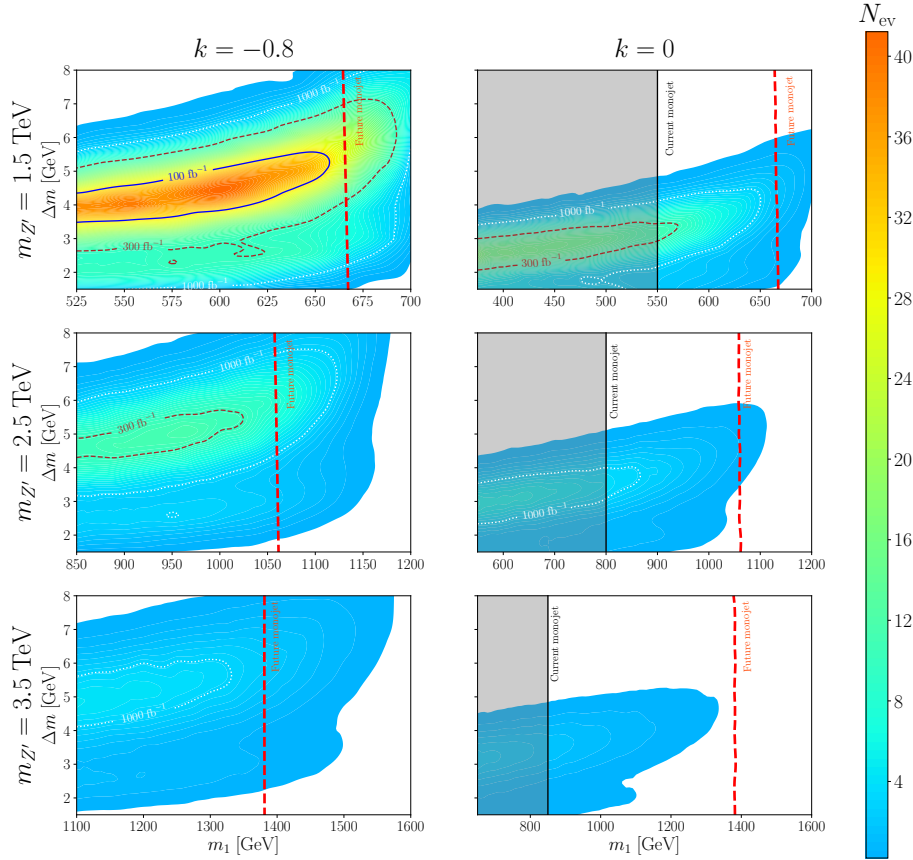


Figure 3.5: Current and future bounds coming from MJ and DVs. The colourbar refers to the number of events which pass the cuts at an integrated luminosity of  $1000 \text{ fb}^{-1}$ , and the region inside the white, dashed line is excluded at 95%CL; we show the same region also for  $100 \text{ fb}^{-1}$  and  $300 \text{ fb}^{-1}$  (in blue and orange, respectively). The grey portion of the parameter space is instead currently ruled out by MJ searches, while the red line corresponds to the future projection at  $1000 \text{ fb}^{-1}$ .

space at 95% CL if at least three events pass the cut (this simply comes from a Poisson distribution with 0 events). In the same plot, also limits from MJ are shown: in particular, future prospects are shown with the red, dashed line, and correspond to a total SM uncertainty of 10%, as described above. We show the the results for the two benchmark choices of  $k$  and different values of  $m_{Z'}$ . As can be seen, for  $k = 0$  a significant region of the parameter space is already excluded by MJ.

As expected, the result strongly depends on the value of  $k$ ; as  $k \rightarrow -1$ , the decay length of  $\chi_2$  increases (cf. eq. (3.1.9)), and a larger number of decays takes place within the detector volume; at the same time, the coupling  $\chi_2 \chi_2 Z'$  increases, maximising the production cross section. Therefore, the strongest constraints come when  $k$  is close to  $-1$ , but not so much that  $\chi_2$  decays outside the detector.

Finally, it is interesting to see that while the signal is maximum for small  $m_{Z'}$ , larger mediator masses allow us to probe larger  $m_1$ .

## 3.2 Chromo-electric dark matter

As discussed in section 2.1, DM must have (if any) extremely small electric and colour charge, and must be stable on cosmological timescales. It is however possible that the dark matter is just the lightest state of a full dark sector, in which some states can carry charges; in particular, the case in which some dark particles are coloured have recently attracted interest [155, 165–167]. Such a scenario can be particularly interesting for LHC, where the production cross section can be significantly enhanced by QCD effects.

A great deal of phenomenological properties of coloured dark sectors are rather general, i.e. they only depend on the representation of the coloured states under  $SU(3)_c$  [165]; on the other hand, however, specific features do depend on the particular model and the interactions between the dark sector and the SM.

A simple implementation of this idea could be obtained by considering an effective theory in which the dark states are fermions and communicate with the SM via a  $d = 5$  operator coupling the gluons and the heavier dark particle. Such a scenario is particularly interesting for LHC phenomenology because the coloured state could hadronize in bound states; in the supersymmetric context, this is a well-known possibility, and such bound states are called  $R$ -hadrons [168] (for more recent papers on the topic see, e.g., refs. [140, 141, 169–171]). In the following, we maintain the same terminology, although we do not refer to any supersymmetry; in addition, given that the heavier particle interacts with the DM through the  $d = 5$  operator, it is possible for it to travel macroscopic distances before decaying.

In section 3.2.1, we discuss the theoretical aspects of the models, while in section 3.2.2 we show the relevant experimental analyses.

### 3.2.1 Model Lagrangian

A possibility to couple DM to coloured SM particles is by considering a dark sector with more than one state, with some of the heavy ones being coloured [167, 172–179]. We consider a simple extension of the SM, where we add on top of it two Majorana fermions, denoted by  $\chi_1$  and  $\chi_2$ , with masses  $m_1$  and  $m_2 \equiv m_1 + \Delta m$ , and we assume that the heavier one is charged under  $SU(3)_c$ .

Couplings to quarks can be obtained at the renormalizable level by assuming the heavier state to be in the fundamental representation [167, 180, 181]; a coupling to gluons, instead, can be achieved through effective operators, starting at  $d = 5$ , with  $\chi_2$  being in the adjoint representation. We consider the latter possibility, and introduce the following free Lagrangian:

$$\mathcal{L}_0 = \frac{1}{2} \bar{\chi}_1 (i\not{\partial} - m_1) \chi_1 + \frac{1}{2} \bar{\chi}_2^a (i\not{D} - m_2) \chi_2^a, \quad (3.2.1)$$

with  $a$  being the colour index in the adjoint representation.

The interaction with the gluons mimics the (chromo-)electric and (chromo-)magnetic dipole moments, and we parametrize it as (see, e.g., refs. [182, 183]):

$$\mathcal{L}_{\text{int}} = \frac{i}{2m_1} \bar{\chi}_2^a \sigma^{\mu\nu} (\mu_\chi - id_\chi \gamma^5) \chi_1 G_{\mu\nu}^a, \quad (3.2.2)$$

where  $\sigma^{\mu\nu} \equiv i/2[\gamma^\mu, \gamma^\nu]$  and  $G_{\mu\nu}^a$  is the canonically normalized gluon field strength.

The two operators in the equation above lead to similar phenomenological results, and do not interfere with each others in the determination of the observables which are of interest for us; for this reason, we limit our attention to the operator proportional to  $d_\chi$ .

$ij \backslash SMSM$	$q \bar{q}$	$g g$
11		$\frac{2 d_\chi^4}{\pi} \frac{1}{m_1^2}$
12	$\frac{d_\chi^2}{24} \frac{\alpha_S}{m_1^2} v^2$	$\frac{3 d_\chi^2}{4} \frac{\alpha_S}{m_1^2}$
22	$\frac{3\pi}{16} \frac{\alpha_S^2}{m_2^2} \frac{1}{m_2^2}$	$\frac{27\pi}{32} \frac{\alpha_S^2}{m_2^2} \frac{1}{m_2^2}$

Table 3.2: Leading order contributions to the cross sections  $\langle \sigma v \rangle_{\chi_i \chi_j \rightarrow SMSM}$ .  $\alpha_s$  denotes the strong coupling, while  $v$  is the relative velocity in the  $\chi_i$ - $\chi_j$  CM frame.

The interactions between the dark sector and the SM are therefore completely described in terms of the parameters  $\{m_1, \Delta m, d_\chi\}$ ; a first requirement is  $d_\chi \ll 1$ : this is because it can be formally identified as  $d_\chi \sim m_1/\Lambda$ , with  $\Lambda$  identifying the scale of some underlying NP. We will come back to this point later, when we will briefly make a connection between the parametrization of eq. (3.2.2) and the general language of EFTs discussed in appendix B.

Being heavier than the DM,  $\chi_2$  decays into it: the leading process is  $\chi_2 \rightarrow \chi_1 g$ , whose decay length can be simply computed to be:

$$\Gamma_{\chi_2} = \frac{d_\chi^2}{\pi} \frac{\Delta m^3}{m_1^2} \frac{\left(1 + \frac{\Delta m}{2m_1}\right)^3}{\left(1 + \frac{\Delta m}{m_1}\right)^3} \approx \frac{d_\chi^2}{\pi} \frac{\Delta m^3}{m_1^2}. \quad (3.2.3)$$

Given that  $d_\chi$  is assumed to be small, it is possible that  $\chi_2$  travels macroscopic distances before decaying, being in fact a LLP.

## Relic density

The first requirement on the model is the correct reproduction of the DM relic abundance; this is determined by the processes  $\chi_i \chi_j \rightarrow SMSM$ , and the leading order expressions for the corresponding cross sections are reported in table 3.2. More complete expressions, used for the simulations, can be found in appendix 3.B.1.

A first modification to the standard paradigm is represented by coannihilations, which become relevant if  $\Delta m \ll m_1$ ; similarly to the pDDM model, the effective cross section defined in eq. (2.3.26) is:

$$\langle \sigma v \rangle_{\text{eff}} = \frac{1}{(1 + \alpha)^2} \left( \langle \sigma v \rangle_{11} + 2\alpha \langle \sigma v \rangle_{12} + \alpha^2 \langle \sigma v \rangle_{22} \right), \quad (3.2.4)$$

with  $\alpha \equiv g_{\chi_2}/g_{\chi_1} (1 + \Delta m/m_1)^{3/2} e^{-x\Delta m/m_1}$ ,  $x \equiv m_1/T$  and  $\langle \sigma v \rangle_{ij} \equiv \langle \sigma v \rangle_{\chi_i \chi_j \rightarrow SMSM}$ ; the numbers of degrees of freedom of  $\chi_1$  and  $\chi_2$  are  $g_{\chi_1} = 2$  and  $g_{\chi_2} = 16$ , respectively. The relic abundance is then computed in the standard way through eqs. (2.3.17) and (2.3.19), where  $g_\chi$  is now  $g_\chi = g_{\chi_1}(1 + \alpha)$ .

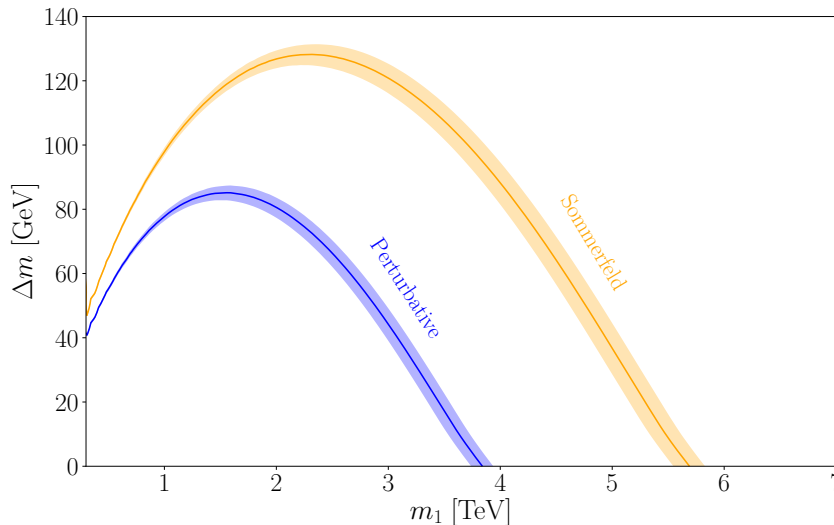


Figure 3.6: Profile of the observed DM relic density,  $\Omega h^2 = 0.1194$  [159], in the  $(m_1, \Delta m)$  plane, together with the corresponding  $3\sigma$ -contours; both the perturbative (blue) and Sommerfeld-enhanced (orange) result are shown.

A second important effect is due to the Sommerfeld enhancement, a non-perturbative effect which is due to the exchange of soft gluons between coloured particles in the initial state [184–186]. Model-independent treatments of this effect can be found in refs. [155, 165]; in these analyses, the relic density is assumed to be dominated by QCD effects (the case in which the DM contributes negligibly to coannihilations has also been considered in the general context of *sterile coannihilations* in ref. [187]).

We refer to the general analysis of ref. [165] for the treatment of the Sommerfeld enhancement, since also for our model it is reasonable to assume that coannihilations are dominated by QCD effect because of the smallness of  $d_\chi$  (cf. table 3.2); we review some relevant aspects of Sommerfeld enhancement in appendix 3.B.2.

The relic density profile  $\Omega h^2 = 0.1194$  [159] can be found in fig. 3.6; there, we show both the perturbative result obtained from eq. (3.2.4) and the one which takes the Sommerfeld enhancement into account. As can be seen, the correction significantly affects the result, and cannot be neglected.

Given that the relic abundance does not depend on  $d_\chi$  (up to small corrections), the number of free parameters can be reduced by imposing the correct value of  $\Omega h^2$ , and using it to fix, for instance,  $\Delta m$ ; this way, the decay width of  $\chi_2$  in eq. (3.2.3) only depends on the DM mass and  $d_\chi$ . As anticipated, the smallness of  $d_\chi$  can lead to macroscopic decay lengths; we show in fig. 3.7 the value of the decay length  $1/\Gamma_{\chi_2}$ , as functions of  $m_1$  and  $d_\chi$ . We see that in order for  $\chi_2$  to travel a distance of at least  $\mathcal{O}(10^{-3} \text{ m})$ , values of  $d_\chi$  as small as  $10^{-7} \div 10^{-6}$  are in general needed.

### Departure from chemical equilibrium

As discussed in detail in section 2.3.2, the general formula for the effective thermal cross section in presence of coannihilations, eq. (2.3.26), is obtained under the assumptions that conversion processes and decays are much faster than annihilations; in other words, it is

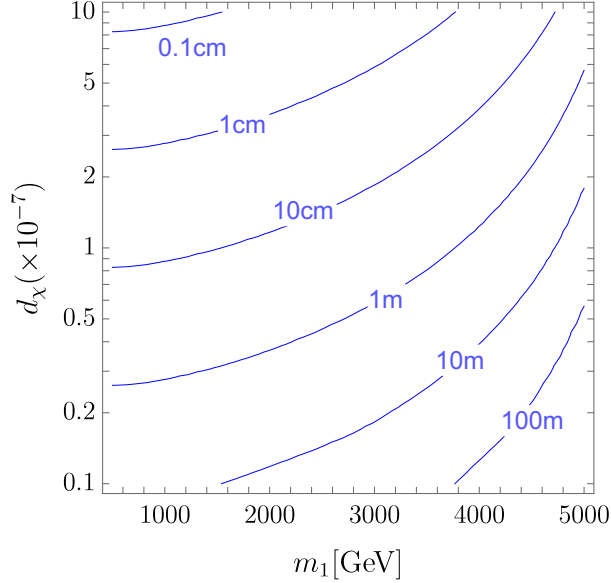


Figure 3.7: Decay lengths in the rest frame of  $\chi_2$  for the process  $\chi_2 \rightarrow \chi_1 g$ ; in all the  $(m_1, d_\chi)$  plane, the observed DM relic density is reproduced.

assumed that CE holds. While this is true in most of the situations, especially when the requirement of reproducing the correct DM abundance is imposed, in some special circumstances it can cease to be true.

In the model we are considering, as we showed, the relic density is independent of the coefficient which couples the dark sector and the SM ( $d_\chi$ ), leaving it a basically free parameter; since we are interested in small values of  $d_\chi$  (in such a way that  $\chi_2$  is a LLP), it is in principle possible that CE breaks down, given that the same parameter also controls conversion processes. In order to verify this condition, we have to evaluate the ratios  $\Gamma_{\chi_i \chi_j}/H$ , where  $\Gamma_{\chi_i \chi_j}$  generically represents the rate of a process involving  $\chi_i$  and  $\chi_j$ : it can be the scattering  $\chi_2 \chi_2 \rightarrow \chi_1 \chi_1$ , the decay  $\chi_2 \rightarrow \chi_1 g$ , the conversions  $\chi_2 g \rightarrow \chi_1 g$  and  $\chi_2 q \rightarrow \chi_1 q$ , as well as all the inverse reactions.

Since the rates of (inverse) decay and conversions are proportional to  $d_\chi^2$ , whereas that of scattering scales as  $d_\chi^4$ , the latter is expected to be the smallest one, and therefore negligible for determining CE. When the largest of all these rates, denoted by  $\Gamma_{\chi_i \chi_j}^{(\max)}$  becomes smaller than the Hubble parameter, we can consider CE to break down; if this is the case, we should resort to the full set of Boltzmann differential equations, as described in section 2.3.2.

It is reasonable to assume that scattering with gluons is the ultimate responsible for maintaining chemical equilibrium, since the corresponding cross section scales as  $\langle \sigma v \rangle_{\chi_2 g \leftrightarrow \chi_1 g} \propto \alpha_S d_\chi^2$  (cf. eq. (3.B.2)). We show the ratios  $\Gamma_{\chi_i \chi_j}/H$  as functions of temperature in fig. 3.8, for  $m_1 = 1$  TeV and  $d_\chi = 10^{-6}$  (in the direction  $\chi_2 \rightarrow \chi_1$ ): as can be seen, the scattering processes actually have the largest rates; in addition, we verified that also for different DM masses the scattering with gluons is always the main contribution. Since the CE has to be maintained until the DM freeze-out, and since the rate is monotonically decreasing with the temperature, we can simply evaluate it at freeze-out,  $20 \lesssim x_F \lesssim 30$ ; from fig. 3.8, we see that for  $d_\chi = 10^{-6}$ , the ratio  $\Gamma/H$  is roughly  $10^4$ . By rescaling it with  $d_\chi$ , we finally find that CE ceases to be valid for  $d_\chi \lesssim 10^{-8}$ .

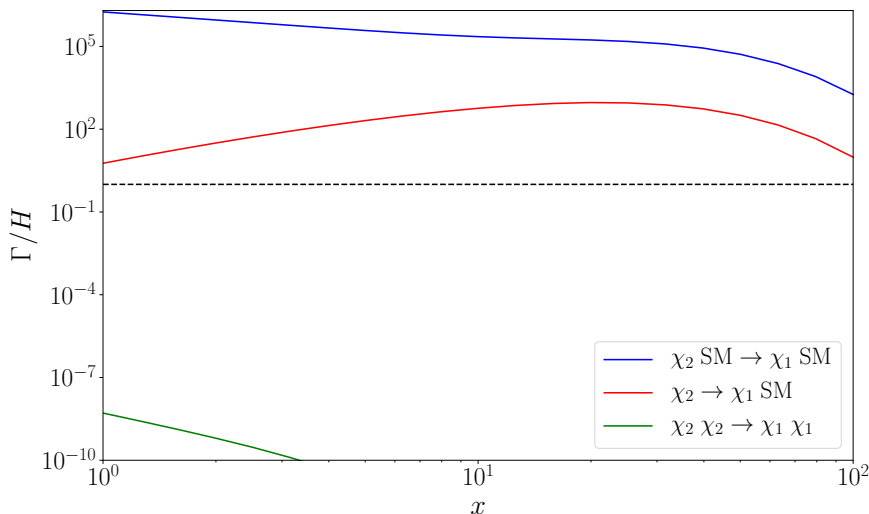


Figure 3.8: Ratios  $\Gamma_{\chi_i \chi_j}/H$  for different processes as functions of the temperature, for  $m_1 = 1$  TeV and  $d_\chi = 10^{-6}$ : in particular, scattering, decay and conversion are shown in blue, red and green, respectively.

Given that the resolution of the full set of Boltzmann equation is not the main goal of the model, we consider in the following values  $d_\chi \gtrsim 10^{-8}$ , in order to be in the regime of chemical equilibrium.

### 3.2.2 LHC analysis

Like most of the DM models, also this one predicts monojet signatures at LHC; in addition, however, also bounds from  $R$ -hadrons searches apply, given that  $\chi_2$  can travel a macroscopic distance and then hadronize; finally, also dijets signatures could arise, from the production and fragmentation of a bound state of two  $\chi_2$ 's. We are going to review these different searches in this subsection.

#### Bounds from monojet

The main channel of production of dark particles which is relevant for MJ is  $pp \rightarrow \chi_2 \chi_2 j$ , the other ones being suppressed by powers of  $d_\chi$ ; we apply recent bounds from the ATLAS experiment presented in ref. [96], which select events with large  $\cancel{E}_T$  and at least one high-energy jet, with CM energy  $\sqrt{s} = 13$  TeV and an integrated luminosity of  $36.1 \text{ fb}^{-1}$ .

Events are required to satisfy the conditions:  $\cancel{E}_T > 250$  GeV, leading- $p_T > 250$  GeV,  $|\eta|_{\text{leading jet}} < 2.4$ ; in addition, at most four jets with  $p_T > 30$  GeV and  $|\eta| < 2.8$  are allowed; finally, the condition  $\Delta\phi(\text{jet}, \cancel{p}_T) > 0.4$  must be satisfied for each selected jet. As usual for this kind of analyses, different signal regions are used, differing from each others by the cut on  $\cancel{E}_T$ ; in particular, the latter is  $\cancel{E}_T > 250$  GeV for IM1, and goes up to  $\cancel{E}_T > 1000$  GeV for IM10. We simulate parton-level events using MADGRAPH5\_AMC@NLO [188], then apply these cuts.

Constraints from MJ searches only apply if  $\chi_2$  decays promptly, i.e. within the beam-line radius,  $\ell_{\text{beam}} = 2.5$  cm; otherwise, if it enters the detector material, it will form an

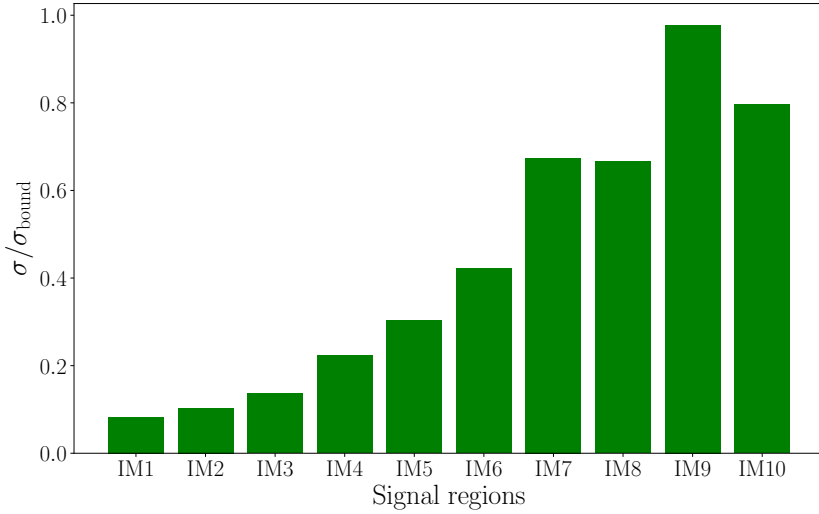


Figure 3.9: Ratio between the simulated cross section and the bounds coming from ref. [96] as functions of the different signal regions; the DM mass is  $m_1 = 860$  GeV.

$R$ -hadron within a very short timescale, of roughly  $\Lambda_{\text{QCD}}^{-1} \sim 10^{-24}$  s. We take this into account by considering the probability for each  $\chi_2$  to decay with transverse decay length  $\ell_T$  less than  $\ell_{\text{beam}}$  [155]:

$$\mathcal{P}(\ell_T < \ell_{\text{beam}}) = 1 - \exp\left(-\frac{\ell_{\text{beam}}}{\ell_T}\right), \quad (3.2.5)$$

where  $\ell_T = p_2^T/(m_2 \Gamma_{\chi_2})$  is the transverse distance travelled by  $\chi_2$ . Each event is weighted by this probability in order to find the effective cross-section where  $\chi_2$  decays promptly. We assume that all the coloured particles reaching the detecting stage hadronize.

In order to obtain a limit on the number of new physics events  $N_{\text{NP}}$ , we apply for both current and future luminosities a  $\chi^2$  analysis with 95% CL with unit efficiency and acceptance, according to ref. [165]:

$$\chi^2 = \frac{[N_{\text{obs}} - (N_{\text{SM}} + N_{\text{NP}})]^2}{N_{\text{NP}} + N_{\text{SM}} + \sigma_{\text{SM}}^2}, \quad (3.2.6)$$

where the error on the SM background is assumed to be normally distributed.

In order to determine which of the then signal regions of ref. [96] gives the strongest constraint on our model, we consider (for a given value of  $m_1$ ) the ratio between the cross section we simulated and the bound coming from the experimental search; the result is shown in fig. 3.9 for  $m_1 = 860$  GeV, leading to the strongest bound coming from IM9 (identified by the cut  $\cancel{E}_T > 900$  GeV). Given that different values of  $m_1$  change both the value of the simulated cross section and the kinematic distribution of the particles, it is not trivial to recast the bound of fig. 3.9 into limits on the DM mass.

For the signal region IM9, the number of events is (see table 5 of ref. [96]):

$$N_{\text{SM}} = 464 \pm 34 \quad , \quad N_{\text{obs}} = 468. \quad (3.2.7)$$

If we then apply eq. (3.2.6), we find that, at 95% CL, the number of NP events is  $N_{\text{NP}} < 85$ , leading to the bound  $\sigma_{\text{NP}} < 2.4$  fb at  $36.1 \text{ fb}^{-1}$  of integrated luminosity. By using this



value, we set a lower bound on the DM mass of  $m_1 > 860 \text{ GeV}$  for  $d_\chi \gtrsim 2 \times 10^{-7}$ . The full exclusion on the parameter space from current MJ searches is shown in fig. 3.11 with the blue region. For a given value of  $m_1$ , a lower limit on  $d_\chi$  is set by the requirement that  $\chi_2$  decays promptly in order not to reach the detector and form  $R$ -hadrons.

Next, we project the bounds from MJ to higher luminosity by following the strategy already adopted for the pDDM model; in particular, if we assume that the relative systematic error scales as  $\delta^{\text{sys}}(\mathcal{L}_2) \equiv r \delta^{\text{sys}}(\mathcal{L}_1)$  with the luminosity, we can translate an upper bound  $\sigma_{\text{NP}}^{(\text{max})}(\mathcal{L}_1)$  on the NP cross section at the luminosity  $\mathcal{L}_1$  into a bound on the same quantity at the luminosity  $\mathcal{L}_2$  as:

$$\sigma_{\text{NP}}^{(\text{max})}(\mathcal{L}_2) = \sigma_{\text{NP}}^{(\text{max})}(\mathcal{L}_1) \sqrt{r^2 + \left(\frac{\mathcal{L}_1}{\mathcal{L}_2} - r^2\right) \frac{N_1}{\delta N_1^2}}, \quad (3.2.8)$$

where  $N_1$  and  $\delta N_1$  refer to the luminosity  $\mathcal{L}_1$ .

We extrapolate the current bounds to  $\mathcal{L}_2 = 3000 \text{ fb}^{-1}$ , in an optimistic scenario where the systematic uncertainties reduce by a factor of 2 with respect to the current ones; in this case, the lower limit on the DM mass becomes  $m_1 > 1020 \text{ GeV}$ , and is shown with the light, blue region in fig. 3.11. Finally, in the extreme case in which the systematics remain unchanged (become negligible) with respect to the current value, the limit is  $m_1 > 900 \text{ GeV}$  ( $m_1 > 1250 \text{ GeV}$ ) (the square root in eq. (3.2.8) is a monotonically increasing function of  $r$ , as long as  $\sqrt{N_1} < \delta N_1$ ).

## Bounds from $R$ -hadrons

The colour charge of  $\chi_2$  allows it to hadronize with SM particles, forming particles analogous to the supersymmetric  $R$ -hadrons. If stable on detector timescales, these colourless states can be detected via ionization signatures as they travel through the detector (with a non-relativistic speed).

We use ATLAS bounds on  $R$ -hadrons [141], relative to a CM energy  $\sqrt{s} = 13 \text{ TeV}$  and integrated luminosity  $\mathcal{L} = 3.2 \text{ fb}^{-1}$ ; the relevant ones are those on gluinos, being  $\chi_2$  a colour octet.

To project current bounds to HL, we follow the procedure outlined in ref. [105], where it is assumed that the number of background events simply scales with the luminosity and that the signal acceptance-times-efficiency remains constant. The relevant results are the background counts of ref. [141] (see table 3). Notice that in the HL projection, results are limited by systematic uncertainties, rather than by statistics.

We simulated the pair production of  $\chi_2$ 's at parton level with MADGRAPH, where the model has been implemented using FEYNRULES [189]; we then applied the  $R$ -hadronization routine from PYTHIA 8.230 [190].

The probability for  $\chi_2$  to be stable at least up to the edge of the ATLAS calorimeter is:

$$\mathcal{P}(\ell > \ell_{\text{calo}}) = \exp\left(-\frac{\ell_{\text{calo}}}{\ell_T}\right), \quad (3.2.9)$$

where  $\ell_{\text{calo}} = 3.6 \text{ m}$  is the transverse distance to the edge of the calorimeter and  $\ell_T = p_2^T / (m_2 \Gamma_{\chi_2})$ , as before. This probability is applied on an event-by-event basis in order to find the effective cross-section of events yielding at least one  $R$ -hadron. This relies on the assumption that the lifetime of the resulting  $R$ -hadron is at least as long as the one of  $\chi_2$ . Following ref. [141], we assume that 90% of the  $\chi_2$ 's form charged  $R$ -hadrons.

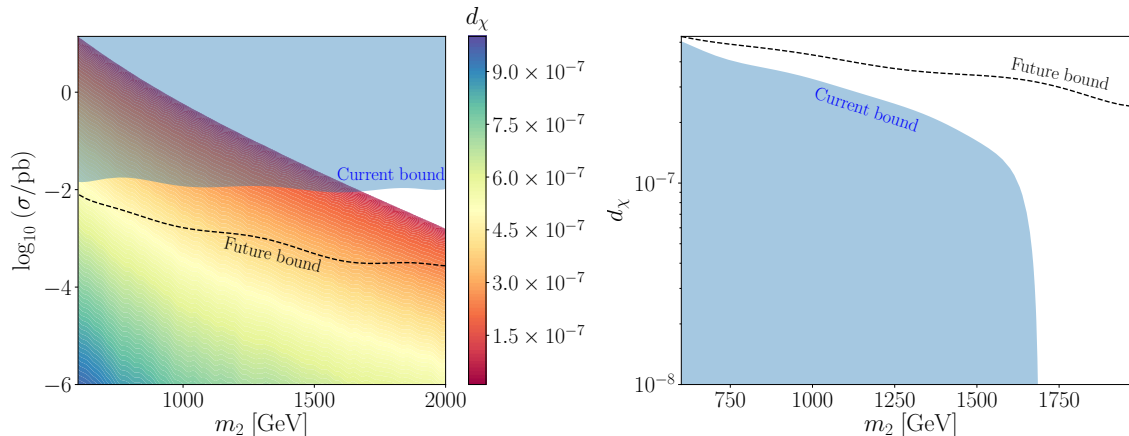


Figure 3.10: Results from  $R$ -hadrons searches. Left: contours showing the value of  $d_\chi$  yielding a given production cross section for calorimeter-stable  $\chi_2$ ; we also show with the blue, shaded region (dashed, black line) the region of the parameter space excluded by current (projected)  $R$ -hadron searches performed by ATLAS. Right: corresponding lower limit on  $d_\chi$ , shown with the same colour convention.

The contours showing the interplay between the production cross section (rescaled by the effective probability) and the mass of  $\chi_2$  is shown in fig. 3.10, together with the bounds from the ATLAS search; in addition, we also show a lower limit on  $d_\chi$ , which comes from the fact that if the latter is too small, the weight given by eq. (3.2.9) makes the simulated cross section exceed the experimental bound.

We can then combine these bounds with those coming from MJ searches. We already noticed that monojet ceases to be effective for small values of  $d_\chi$ , since the latter make  $\chi_2$  long-lived enough to form  $R$ -hadrons rather than decay into the DM; when this is the case, the relevant search is represented by  $R$ -hadrons, and the result is shown in fig. 3.11. In general, every bound can be shown in terms of  $m_1$  rather than  $m_2$ , since the mass splitting  $\Delta m$  is fixed by imposing the observed relic density (as discussed in section 3.2.1).

It is evident the complementarity of these two different searches, probing different regions of the parameter space, both with the current and future luminosity.

## Bounds from direct and indirect detection

Although a bit outside the main motivations for this model, we also checked if DD and ID results can exclude part of the parameter space. As far as ID is concerned, we focus on limits from antiproton fluxes [191]; it turns out that an upper bound on  $d_\chi$ , as a function of  $m_1$ , can be inferred from the upper limit on the annihilation cross section  $\sigma(\chi_1\chi_1 \rightarrow gg)$ . The result is that these bounds are much weaker than those coming from DD; in addition, they are even weaker than the requirement  $d_\chi \ll 1$ , in order for the EFT description to be valid. In particular, we found  $d_\chi \leq 0.2$  for  $m_1 = 1$  TeV and  $d_\chi \leq 1$  for  $m_1 = 5$  TeV.

On the other hand, the relevant processes for DD are of the form  $\chi_1 q \rightarrow \chi_1 q$ , and two different diagrams contribute to the cross sections; since we are only interested in a rough estimate, we consider the strongest bound coming from the constructive interference

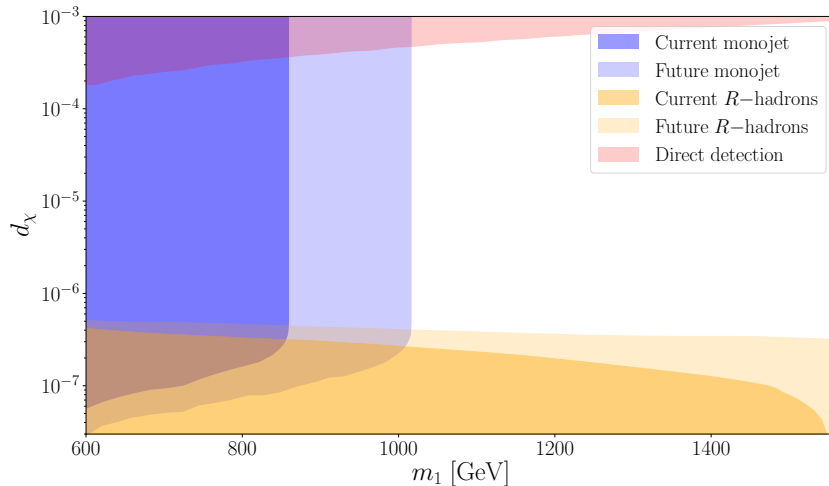


Figure 3.11: Combined bounds from MJ (blue) and  $R$ -hadrons (orange) searches; in both cases, the darker region corresponds to the current limits, while the lighter one refers to projections at high luminosity. Also the upper bound on  $d_\chi$  coming from DD is shown (red). In all the plane, the correct relic density is reproduced.

between the two contributions, and estimate the parton-level cross section as:

$$\sigma_{\text{DD}} \lesssim 4 \times 4\pi\alpha_s d_\chi^2 \frac{m_p^2}{m_1^4}, \quad (3.2.10)$$

where we used the proton mass  $m_p$  as an estimate of the parton energy; this becomes:

$$\sigma_{\text{DD}} \lesssim 1.55 \times 10^{-43} \left( \frac{d_\chi}{10^{-2}} \right)^2 \left( \frac{1 \text{ TeV}}{m_1} \right)^2 \text{ cm}^2. \quad (3.2.11)$$

We refer to the bounds from XENON1T [192], and we obtain an upper limit on  $d_\chi$ , as a function of the mass: such a bound is rather conservative, for the reasons explained above, but it still leaves a large portion of the parameter space available. The result is shown in fig. 3.11, together with the bounds coming from LHC searches.

#### Aside comment: about the EFT parametrization

As a final remark, we come back to the parametrization of the interaction Lagrangian given in eq. (3.2.2); if we had used the general recipe for EFTs discussed in appendix B, we should have written:

$$\mathcal{L}_{\text{int}} = c \frac{g_*^2}{16\pi^2} \frac{g_*}{m_*} \bar{\chi}_2^a \sigma^{\mu\nu} \gamma^5 \chi_1 G_{\mu\nu}^a, \quad (3.2.12)$$

where  $c$  is an  $\mathcal{O}(1)$  real coefficient, and  $m_*$  and  $g_*$  are the parameters of the UV theory; the factor of  $g_*^2/16\pi^2$  comes from the fact that dipole moment operators are usually generated at loop level<sup>1</sup>.

The bounds on  $d_\chi$ , shown in fig. 3.11, would then be translated into limits on the effective scale  $\Lambda \equiv m_*/g_*$ ; the result is shown in fig. 3.12 for two different values of  $g_*$  and  $c = 1$ . In particular, it turns out that the relevant experimental limits coming from LHC

<sup>1</sup>We thank Riccardo Rattazzi for pointing out this aspect.

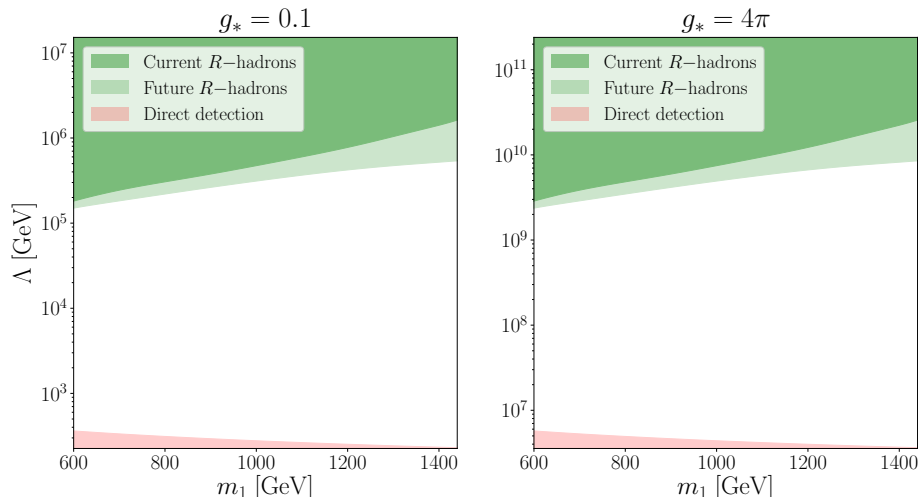


Figure 3.12: Current and future upper bounds on the effective scale  $\Lambda \equiv m_*/g_*$  coming from  $R$ -hadrons searches (green), together with lower limits coming from DD (red), for  $g_* = 0.1$  (left panel) and  $g_* = 4\pi$  (right panel). In both cases, we took  $c = 1$ .

are those from  $R$ -hadrons searches, those from MJ being less restrictive; as can be seen, the result strongly depends on the value of  $g_*$ . In the same plot, we also recast the upper limits on  $d_\chi$  coming from DD experiments in terms of lower bounds on  $\Lambda$ .

### Bounds from dijets

A last search strategy which could apply to our model is represented by dijets; if a pair of  $\chi_2$ 's is reproduced near rest, they could combine to form a QCD bound state analogous to gluonium, rather than decaying or forming  $R$ -hadrons. In particular, since the rate of production is completely controlled by QCD, we can use the results of ref. [193] relative to gluonium to estimate the production of bound states made of two  $\chi_2$ 's.

The strongest constraints on this channel come from limits on the dijets resonance production; we use the model-independent analysis from ATLAS discussed in ref. [194], making the conservative assumption of a narrow Gaussian width. We also assume that the fitting function for the mass distribution used there also applies to high luminosity, allowing us to project current bounds; to this purpose, we take the systematics to be unchanged in going from low to high luminosity.

The results are shown in the left panel of fig. 3.13, together with the theoretical production from ref. [193]; these limits assume that both the  $BR$  into dijets and the acceptance ( $A$ ) are equal to 1: this corresponds to the strongest limit possible, and the real case  $BR \times A < 1$  is characterized by weaker bounds. The bound can also be recast into an upper limit on the product  $BR \times A$ , and is shown in the right panel of fig. 3.13. Our model is not affected by values of  $BR \times A$  larger than the theoretical bound of 1; as can be seen, dijets constraints rule out the model for  $m_2 \lesssim 650$  GeV if  $BR \times A \gtrsim 0.1$ .

Overall, these bounds are rather conservative, for two reasons: on the one hand, the production rate is computed at 14 TeV, whereas the constraints are reported at 13 TeV, so that the corresponding production cross section would be smaller; on the other hand, we assumed a narrow Gaussian width, while a broader one would have weakened the bounds,

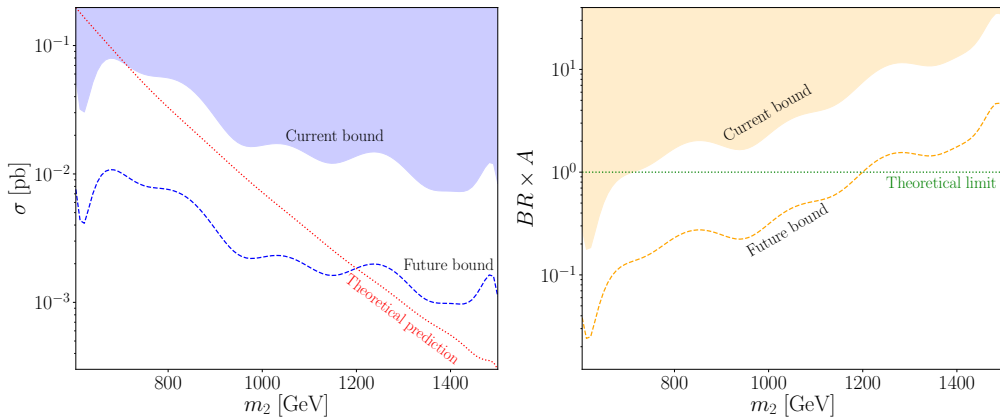


Figure 3.13: Current and projected limits from dijets searches. Left: currently (projected) bounds on the dijet production cross section from the ATLAS experiment are shown with the blue region (dashed line), together with the theoretical prediction (dotted, red line). Right: corresponding bound on the product  $BR \times A$ ; the maximum possible value  $BR \times A = 1$  is shown as a dotted horizontal line.

as can be seen in fig. 5 of ref. [194].

### 3.A Appendices for the pDDM model

In the following, we present the appendices relative to the pDDM model; in particular, we discuss the determination of the mass eigenstates, we provide more complete expressions for the decay widths and effective cross sections, and we explain how we simulated the events at LHC.

#### 3.A.1 Mass eigenstates

The mass term of eq. (3.1.1) can be written as:

$$\mathcal{L}_0 \supset -\frac{1}{2} \bar{n}_L M n_R^c + \text{h.c.}, \quad (3.A.1)$$

where  $n_{L,R} \equiv (\Psi_{L,R} \ \Psi_{L,R}^c)^T$  and  $M$  is a  $2 \times 2$  symmetric matrix; the latter can be diagonalized via a unitary rotation matrix  $U$  as  $M = U^T m U$ , and if we denote by  $\theta$  the corresponding angle, the requirements that off-diagonal entries of  $m$  vanish is:

$$2M_D \cos 2\theta + (m_L - m_R) \sin 2\theta = 0 \quad \Rightarrow \quad \theta \approx \frac{\theta}{4}, \quad (3.A.2)$$

where in the last step we took into account that  $M_D \gg m_{L,R}$ . The mass eigenvalues are  $m_{1,2} = (m_L + m_R)/2 \mp M_D$ ; in terms of the mass eigenstates  $n'_{L,R} \equiv U n_{L,R}$ , the mass term can be written as  $\mathcal{L}_0 \supset -1/2 \bar{\xi} m \xi$ , where  $\xi \equiv n_R^c + n'_L \equiv (\xi_1 \ \xi_2)^T$ . By taking into account that  $\Psi = (\xi_2 - \gamma^5 \xi_1)/\sqrt{2}$ , it is easy to show that the kinetic term is not canonically normalized; the correct normalization can be easily obtained by defining two

new fields  $\chi_{1,2}$  such that:

$$\begin{cases} \xi_1 \equiv a\gamma^5\chi_1 \\ \xi_2 \equiv \chi_2 \end{cases} \quad \text{where } a = ki, \quad k \in \mathbb{Z}. \quad (3.A.3)$$

For simplicity, we take  $k = 1$ , so that the mass eigenstates are:

$$\chi_1 = \frac{i}{\sqrt{2}} (\Psi - \Psi^c) \quad (3.A.4a)$$

$$\chi_2 = \frac{1}{\sqrt{2}} (\Psi + \Psi^c), \quad (3.A.4b)$$

with eigenvalues  $m_{1,2} = M_D \mp (m_L + m_R)/2$ . It is straightforward to show that  $\chi_{1,2}$  are Majorana fields.

### 3.A.2 Full expressions for decay widths and thermally-averaged cross sections

In this appendix, we provide the formulas for the cross sections and the decay widths which have been employed in the analysis.

In the limit  $m_f, \Delta m \ll m_1$ , we can approximate the decay width for the process  $\chi_2 \rightarrow \chi_1 f \bar{f}$  as:

$$\begin{aligned} \Gamma_{\chi_2 \rightarrow \chi_1 f \bar{f}} = & \sum_f \frac{N_c^{(f)}}{480\pi^3} (c_L + c_R)^2 \frac{\Delta m^5}{m_{Z'}^4} \left\{ \left( 1 - \frac{3}{2} \frac{\Delta m}{m_1} \right) (c_L^{(f)^2} + c_R^{(f)^2}) \right. \\ & - \frac{m_f^2}{2m_1^2} \left[ (36c_L^{(f)^2} + 33c_L^{(f)}c_R^{(f)} + 36c_R^{(f)^2}) + \frac{16m_1^2}{m_{Z'}^2} (2c_L^{(f)^2} + c_L^{(f)}c_R^{(f)} + 2c_R^{(f)^2}) \right. \\ & + \frac{10m_1^2}{\Delta m^2} \left( 1 - \frac{3}{2} \frac{\Delta m}{m_1} \right) (c_L^{(f)} + c_R^{(f)})^2 - \frac{65}{2} \frac{\Delta m}{m_1} (2c_L^{(f)^2} + c_L^{(f)}c_R^{(f)} + 2c_R^{(f)^2}) \\ & \left. \left. - \frac{24m_1\Delta m}{m_{Z'}^2} (2c_L^{(f)^2} + c_L^{(f)}c_R^{(f)} + 2c_R^{(f)^2}) \right] \right\} + \mathcal{O} \left[ \left( \frac{\Delta m}{m_1} \right)^7 \right] + \mathcal{O} \left[ \left( \frac{m_f}{m_1} \right)^4 \right]. \end{aligned} \quad (3.A.5)$$

The thermally averaged cross sections for the processes  $\chi_i \chi_i \rightarrow f \bar{f}$  and  $\chi_1 \chi_2 \rightarrow f \bar{f}$  are, respectively:

$$\begin{aligned} \langle \sigma v \rangle_{12} = & \sum_f \frac{N_c^{(f)}}{32\pi} \frac{(c_L + c_R)^2}{\left( 1 - \frac{(m_1 + m_2)^2}{m_{Z'}^2} \right)^2} \frac{(m_1 + m_2)^2}{m_{Z'}^4} \sqrt{1 - \frac{4m_f^2}{(m_1 + m_2)^2}} \\ & \left[ (c_L^{(f)^2} + c_R^{(f)^2}) - \frac{m_f^2}{(m_1 + m_2)^2} (c_L^{(f)^2} - 6c_L^{(f)}c_R^{(f)} + c_R^{(f)^2}) \right] + \mathcal{O} \left( \frac{1}{x} \right) \end{aligned} \quad (3.A.6a)$$

$$\langle \sigma v \rangle_{ii} = \sum_f \frac{N_c^{(f)}}{8\pi} \frac{(c_L - c_R)^2}{\left(1 - \frac{2m_i^2}{m_{Z'}^2} \frac{2x_i + 3}{x_i}\right)^2} \frac{m_i^2}{m_{Z'}^4} \sqrt{1 - \frac{2m_f^2}{m_1^2} \frac{x_i}{2x_i + 3}} \left[ \frac{c_L^{(f)^2} + c_R^{(f)^2}}{x_i} + \frac{m_f^2}{2m_1^2} \left(c_L^{(f)} - c_R^{(f)}\right)^2 \frac{x_i}{2x_i + 3} \right], \quad (3.A.6b)$$

where  $x_1 \equiv x = m_1/T$  and  $x_2 \equiv x(1 + \Delta m/m_1)$ .

The partial decay widths which have been used to determined the region of the parameter space where  $\Gamma_{Z'}/m_{Z'} \leq 0.2$  (see section 3.1.2) are:

$$\Gamma_{Z' \rightarrow \chi_1 \chi_2} = \frac{(c_L + c_R)^2}{48\pi} K m_{Z'} \left[ 1 + \frac{(m_1 + m_2)^2}{2m_{Z'}^2} \right] \left( 1 - \frac{\Delta m^2}{m_{Z'}^2} \right) \quad (3.A.7a)$$

$$\Gamma_{Z' \rightarrow \chi_i \chi_i} = \frac{(c_R - c_L)^2}{96\pi} m_{Z'} \left( 1 - \frac{4m_i^2}{m_{Z'}^2} \right)^{\frac{3}{2}} \quad (3.A.7b)$$

$$\Gamma_{Z' \rightarrow \bar{f} f} = \sum_f \frac{N_c^{(f)}}{24\pi} m_{Z'} \sqrt{1 - \frac{4m_f^2}{m_{Z'}^2}} \left[ \left( c_L^{(f)^2} + c_R^{(f)^2} \right) - \frac{m_f^2}{m_{Z'}^2} \left( c_L^{(f)^2} - 6c_L^{(f)} c_R^{(f)} + c_R^{(f)^2} \right) \right], \quad (3.A.7c)$$

where:

$$K \equiv \sqrt{1 - 2 \frac{m_1^2 + m_2^2}{m_{Z'}^2} + \left( \frac{m_2^2 - m_1^2}{m_{Z'}^2} \right)^2} \quad (3.A.8)$$

### 3.A.3 Details about the analysis

The simulations for the DV and MJ analyses are made by means of MG5\_aMC@NLOv2.4.2; we limit ourselves to a parton level analysis. For the DV searches, we consider the process  $pp \rightarrow \chi_2 \chi_2 j \rightarrow \chi_1 \chi_1 jjjjj$ . As described in main text, because of the two DVs, the high- $p_T$  and the large  $\cancel{E}_T$ , the background is extremely low. We handle the decay of  $\chi_2$  with the following steps:

1. we first generate 20k  $pp \rightarrow \chi_2 \chi_2 j$  events, at the CM energy  $\sqrt{s} = 13$  TeV. Here,  $j$  stands for the default multiparticle state containing quarks and the gluon;
2. we then generate 40k  $\chi_2 \rightarrow \chi_1 jj$  events; only quarks from the first two families can be produced, since we consider  $1.5 \text{ GeV} \leq \Delta m \leq 8.0 \text{ GeV}$ ;
3. we then merge these two sets of events, replacing the  $\chi_2$  in the  $2 \rightarrow 3$  process with its decay products, which we boost from the  $\chi_2$  rest frame into the lab frame by scaling the momenta and energy by  $\beta\gamma = \mathbf{p}_{\chi_2}/m_{\chi_2}$  and  $\gamma = E_{\chi_2}/m_{\chi_2}$  respectively. The system of 7 particles in the final state obtained this way is, for our purposes, physically equivalent to the one we would have obtained if we had run the full process at the MadGraph level. We have tested this procedure against direct decay of the  $\chi_2$  within the full  $2 \rightarrow 7$ -body process, and with decay of the  $\chi_2$  particle by interfacing the output  $2 \rightarrow 3$ -body .lhe file with BRIDGE [195], finding the equivalent final

kinematic distributions in all cases, with our procedure substantially faster than direct  $2 \rightarrow 7$  production in MadGraph<sup>2</sup>.

The vertex and jet identification efficiency is model-dependent and depends on the details of the detector [163], which we approximate by applying a relatively conservative flat efficiency of 20%.

## 3.B Appendices for the chromo-electric DM model

In the following, we present the appendices relative to the chromo-electric DM model; in particular, we provide the expressions for the effective cross sections, and we discuss the Sommerfeld enhancement.

### 3.B.1 Full expressions for the thermally-averaged cross sections

In this appendix, we provide analytical expressions for the differential cross sections of various (co)annihilation processes in the CM frame; we express them in terms of the energies  $E_{1,2} = \sqrt{m_{1,2}^2 + p^2}$  of  $\chi_{1,2}$ , and work in the CM frame, so that  $\theta$  is the angle between incoming and outgoing momenta. In the processes involving a quark  $q$ ,  $m_q$  denotes its mass.

#### $\chi_1\chi_1 \rightarrow gg$

This channel proceeds via the exchange of  $\chi_2$  in  $t$ - and  $u$ -channel, with thermally-averaged differential cross section:

$$\begin{aligned} \frac{d\sigma v}{d\Omega} = & \frac{d_\chi^4 E_1^2}{2\pi^2 m_1^4 (-2E_1 p \cos\theta + E_1^2 + m_2^2 + p^2)^2 (2E_1 p \cos\theta + E_1^2 + m_2^2 + p^2)^2} \\ & \left[ 4E_1^6 (m_2^2 + 2p^2 \sin^2\theta) \right. \\ & + 2E_1^4 (2m_2^2 p^2 (3 - 4\cos 2\theta) + 4m_2^4 + p^4 \sin^2\theta (-7\cos 2\theta + 1)) \\ & + E_1^2 (m_2^2 p^4 (7\cos 4\theta - 12\cos 2\theta + 1)) \\ & + E_1^2 (4m_2^4 p^2 (1 - 5\cos 2\theta) + 4m_2^6 + p^6 \sin 2\theta \sin 4\theta) \\ & \left. - 4p^2 (m_2^2 + p^2)^2 (p^2 \sin^4\theta - m_2^2) \right] \end{aligned} \quad (3.B.1)$$

#### $\chi_1\chi_2 \rightarrow gg$

This channel proceeds via the exchange of  $\chi_2$  in  $t$ - and  $u$ -channel, the exchange of a gluon in  $s$ -channel, and via the quartic vertex  $\chi_1\chi_2 gg$ , with thermally-averaged differential cross

---

<sup>2</sup>In the case of direct  $2 \rightarrow 7$  production in MadGraph, the extremely small width of the  $\chi_2$  leads to an error in the final kinematic distributions. This is corrected by upscaling the width in the parameter card by some factor, and rescaling the final cross-section by the same factor [196].



section:

$$\begin{aligned}
\frac{d\sigma v}{d\Omega} = & \frac{3g_s^2 d_\chi^2}{512\pi^2 E_1 E_2 m_1^2 (E_2^2 - p^2 \cos^2 \theta)^2} \\
& \left[ -8E_1^2 p^2 (E_2^2 (1 - 2 \cos 2\theta) + p^2 \cos^2 \theta) \right. \\
& + 8E_1 E_2 p^2 (E_2^2 (4 - 5 \cos^2 \theta) + p^2 \cos^2 \theta (4 - 3 \cos^2 \theta)) \\
& + 8E_1^3 E_2 (E_2^2 - p^2 \cos^2 \theta) \\
& + E_2^2 p^2 (4m_1 m_2 (1 - \cos 2\theta) + p^2 (3 \cos 4\theta - 11)) \\
& \left. + p^4 m_1 m_2 (\cos 4\theta - 1) + p^6 (\cos 4\theta + 7) \cos^2 \theta \right] \quad (3.B.2)
\end{aligned}$$

### $\chi_1 \chi_1 \rightarrow q \bar{q}$

This channel proceeds via the exchange of a gluon in  $s$ -channel, with thermally-averaged differential cross section:

$$\begin{aligned}
\frac{d\sigma v}{d\Omega} = & \frac{g_s^2 d_\chi^2 \sqrt{(E_1 + E_2)^2 - 4m_q^2}}{64\pi^2 E_1 E_2 (E_1 + E_2)^3 m_1^2} \\
& \left[ p^2 (2m_q^2 \cos 2\theta - (E_1 + E_2)^2 \cos^2 \theta) (E_1 E_2 - m_1 m_2) ((E_1 + E_2)^2 + 2m_q^2) \right] \quad (3.B.3)
\end{aligned}$$

### $\chi_2 \chi_2 \rightarrow g g$

This channel proceeds via the exchange of  $\chi_1$  in  $t$ - and  $u$ -channel, the exchange of a gluon in  $s$ -channel and the exchange of  $\chi_2$  in  $t$ - and  $u$ -channel; the first two channels have an amplitude proportional to  $d_\chi^2$ , while the others occur via QCD interactions, proportional to  $\alpha_s$ . The thermally-averaged differential cross section reads:

$$\begin{aligned}
\frac{d\sigma v}{d\Omega} = & - \frac{9g_s^4}{16384\pi^2 E_2^4 (E_2^2 - p^2 \cos^2 \theta)^2} \\
& \left[ E_2^2 p^4 (5 \cos 4\theta - 12 \cos 2\theta + 31) + 4E_2^4 p^2 (5 \cos 2\theta - 7) \right. \\
& \left. - 24E_2^6 + p^6 (\cos 4\theta - 4 \cos 2\theta + 11) \cos^2 \theta \right] \\
& + \frac{3g_s^2 d_\chi^2}{512\pi^2 m_1^2 (E_2^2 - p^2 \cos^2 \theta) (-2E_2 p \cos \theta + E_2^2 + m_1^2 + p^2) (2E_2 p \cos \theta + E_2^2 + m_1^2 + p^2)} \\
& \left[ 4E_2^4 (m_1 m_2 + 2p^2 \sin^2 \theta) + 2m_1 p^2 (-2m_1^2 m_2 \cos 2\theta + p^2 m_2 (\cos 4\theta + 1)) \right. \\
& + m_1 p^2 \sin^2 \theta (3 \cos 2\theta + 1) - 2E_2^2 (4m_1 p^2 m_2 \cos 2\theta - 2m_1^3 m_2 - 4m_1^2 p^2 \sin^2 \theta \\
& \left. + p^4 \sin^2 \theta (5 \cos 2\theta + 3)) + p^6 \sin^2 \theta (6 \cos 2\theta - \cos 4\theta + 3) \right] \\
& + \frac{d_\chi^4 E_2^2}{64\pi^2 m_1^4 (-2E_2 p \cos \theta + E_2^2 + m_1^2 + p^2)^2 (2E_2 p \cos \theta + E_2^2 + m_1^2 + p^2)^2} \\
& \left[ 2E_2^6 (8m_1^2 + 9p^2 \sin^2 \theta) + E_2^4 (m_1^2 p^2 (27 - 43 \cos 2\theta) + 32m_1^4 + 2p^4 \sin^2 \theta (3 - 14 \cos 2\theta)) \right. \\
& + E_2^2 (m_1^2 p^4 (21 \cos 4\theta - 34 \cos 2\theta - 3) \\
& - m_1^4 p^2 (59 \cos 2\theta + 5) + 16m_1^6 + 2p^6 \sin^2 \theta (4 \cos 4\theta - 6(\cos 2\theta) - 3)) \\
& \left. + p^2 (m_1^2 + p^2)^2 (m_1^2 (7 \cos 2\theta + 9) + 2p^2 \sin^2 \theta (4 \cos 2\theta + 3)) \right] \quad (3.B.4)
\end{aligned}$$

$\chi_2\chi_2 \rightarrow q\bar{q}$

This channel proceeds via the exchange of a gluon in  $s$ -channel, with thermally-averaged cross section:

$$\frac{d\sigma_v}{d\Omega} = \frac{3g_s^4 \sqrt{E_2^2 - m_q^2} (E_2^2 (m_q^2 + p^2 \cos^2 \theta - p^2) + 2E_2^4 - m_q^2 p^2 \cos^2 \theta)}{2048\pi^2 E_2^7} \quad (3.B.5)$$

### 3.B.2 Sommerfeld enhancement

The modifications to the standard paradigm for the computation of the relic abundance in presence of coloured particles can be studied by resorting to group theory considerations [165]. If we consider a generic representation  $R$  of  $SU(N)$ , the interactions can be expressed in terms quadratic and quartic invariants; in particular, the Casimir invariant  $C(R)$  and the Dynkin index  $T(R)$ , defined such that

$$(T^a T^a)_{ij} \equiv \delta_{ij} C(R) \quad , \quad \text{Tr}\{T^a T^b\} \equiv \delta^{ab} T(R) \quad , \quad (3.B.6)$$

where  $T$  denotes a generator of the representation  $R$ , can be used to construct the quartic invariants:

$$\text{Tr}\{T^a T^a T^b T^b\} \equiv K_1(R) = d(R) C^2(R) \quad (3.B.7a)$$

$$\text{Tr}\{T^a T^b T^a T^b\} \equiv K_2(R) = d(R) C^2(R) - \frac{d(A) C(A) T(R)}{2} \quad , \quad (3.B.7b)$$

where  $d(R)$  is the dimension of  $R$  and  $A$  stands for the adjoint representation.

When a coloured particle participates to the determination of the relic abundance, then non-perturbative effects due to Sommerfeld enhancement can dramatically change the result; in particular, for a single abelian massless vector, with potential  $V = \alpha_S/r$ , the cross section is modified as:

$$\sigma_{\text{non-pert.}} = S \left( \frac{\alpha_S}{\beta} \right) \sigma_{\text{pert}} \quad , \quad (3.B.8)$$

where  $\beta$  is the velocity of the incoming particle,  $\sigma_{\text{pert}}$  is computed with the standard techniques, and  $S$  is defined as:

$$S(x) = -\frac{\pi x}{1 - e^{\pi x}} \quad . \quad (3.B.9)$$

In the non-abelian case, the potential between two particles in the representations  $R$  and  $R'$  can be obtained by considering the decomposition of the the tensor product of the two representations [197]:

$$V = \frac{\alpha_S}{r} \sum_a T_R^a \otimes T_{R'}^a \quad . \quad (3.B.10)$$

The group theory decomposition into a sum of irreducible representations allows us to write the potential as:

$$V = \frac{\alpha_S}{2r} \left( \sum_Q C_Q \mathbf{1}_Q - C_R \mathbf{1} - C_{R'} \mathbf{1} \right) \quad . \quad (3.B.11)$$

In the case of interest for us, where  $R = \mathbf{8} = R'$ , it can be finally shown that the corrections from Sommerfeld enhancement to the annihilations into gluons and quarks are, respectively [165]:

$$\frac{\sigma_{\text{non-pert.}}}{\sigma_{\text{pert.}}} \Big|_{\chi_2 \chi_2 \rightarrow gg} = \frac{1}{6} S \left( -\frac{3\alpha_S}{\beta} \right) + \frac{1}{3} S \left( -\frac{3\alpha_S}{2\beta} \right) + \frac{1}{2} S \left( \frac{\alpha_S}{\beta} \right) \quad (3.B.12a)$$

$$\frac{\sigma_{\text{non-pert.}}}{\sigma_{\text{pert.}}} \Big|_{\chi_2 \chi_2 \rightarrow q\bar{q}} = S \left( -\frac{3\alpha_S}{2\beta} \right). \quad (3.B.12b)$$



# Chapter 4

## Dark matter within a composite 2HDM with extra singlets

*Non-renormalizable theories are  
just as renormalizable as  
renormalizable theories.*

Steven Weinberg

We discussed in detail the naturalness problem related to the SM Higgs, namely the fact that one should expect  $m_h$  to be of the order of the cutoff under which the UV theory reduces to the SM. As anticipated, a possible solution is to suppose that the Higgs is not an elementary particle, but rather a composite object; if this is the case, we have to distinguish two regimes: at low energies, the prediction for the Higgs mass given by eq. (1.4.4) is like in the SM, i.e. it develops a quadratic divergence [27]; at higher energies, however, quanta have a short enough wavelength to resolve the internal structure of the Higgs, leading to a decreasing behaviour for  $dm_h^2/dE$ . We can imagine this to happen at a confinement scale  $m_* \sim 1/l_*$ , where  $l_*$  represents the physical size of the Higgs. Overall, then, the integrand of eq. (1.4.4) is expected to grow linearly at small energies, reach a peak at  $m_* \sim \mathcal{O}(1 \text{ TeV})$  and then decay quickly.

This picture requires the existence of a new strongly-coupled sector, emerging from an even more fundamental theory at a UV scale  $\Lambda_{\text{UV}} \gg m_*$ , at which the theory is close to a fixed point of the renormalization group (RG). The assumption is that no operators with a scaling dimension considerably lower than 4 exist in the UV theory, so that no parameters with positive dimension appear (contrarily to what happens, for example, in the SM with the parameter  $\mu$  of eq. (1.1.8)); if this is the case, then no unprotected scales are present in the fundamental theory. This aspect is crucial because it allows the RG flow towards the IR to be sufficiently slow, requiring a “time”  $t = \log(\Lambda_{\text{UV}}/m_*)$  to depart from the fixed point and confine. This “time” can be arbitrarily long, resulting in a strong suppression of  $m_*$  with respect to  $\Lambda_{\text{UV}}$ ; this mechanism, by which a scale  $m_*$  is generated starting from a theory without dimensionful parameters, is called *dimensional transmutation* [198].

In CH models, we usually distinguish between *composite* and *elementary* sectors, the latter containing all the SM states we know cannot be composite objects at the TeV scale; since also the weak gauge bosons belong to this category, the composite sector must be characterized by a global symmetry group  $\mathcal{G}$  which contains the electroweak (EW) one,  $\mathcal{G} \supset \mathcal{G}_{\text{EW}} = \text{SU}(2)_L \times \text{U}(1)_Y$ . Similarly to what happens in QCD, the group  $\mathcal{G}$  is expected

to be spontaneously broken (roughly) at the confinement scale  $m_*$  to a subgroup  $\mathcal{H}$ , delivering a number of NGBs; the Higgs is assumed to be one of them. The Higgs mass and the potential, responsible for EWSB, are obtained by explicitly breaking  $\mathcal{G}$ , making the Goldstones become pseudo-Nambu-Goldstone bosons (pNGBs); such an explicit breaking is obtained via the interactions between the composite and the elementary sectors. The fact that the Higgs results as a pNGB is a key point: if this were not the case, in fact, we should expect  $m_h \sim m_*$ ; but then, analogously to what happens in QCD, also a series of other resonances with masses of the order of  $m_*$  would be present. The fact that such states have not been observed forces us to consider  $m_h \ll m_* \sim \mathcal{O}(1 \text{ TeV})$ . The interaction Lagrangian, responsible for the explicit breaking of  $\mathcal{G}$ , must not contain strongly relevant operators, in order to ensure the global symmetry to be approximate.

The minimal composite Higgs model (MCHM) is based on the breaking pattern  $\text{SO}(5) \rightarrow \text{SO}(4)$  [199], thus delivering 4 NGBs which constitute the Higgs doublet. By slightly enlarging the groups, i.e. by considering the pattern  $\text{SO}(6) \rightarrow \text{SO}(5)$ , one has the minimal CH model which also includes DM [200–204]. Other possibilities considered in the literature are  $\text{SO}(6) \rightarrow \text{SO}(4) \times \text{SO}(2)$  [202, 205–207],  $\text{SO}(7) \rightarrow G_2$  [208],  $\text{SO}(7) \rightarrow \text{SO}(6)$  [209–211],  $\text{SO}(7) \rightarrow \text{SO}(5)$  [212],  $\text{SU}(4) \times \text{SU}(4) \rightarrow \text{SU}(4)$  [213, 214],  $\text{SU}(5) \rightarrow \text{SO}(5)$  [215], and  $\text{SU}(6) \rightarrow \text{SO}(6)$  [216–218].

In this chapter, which is based on ref. [3], we study in detail the breaking pattern  $\text{SO}(7) \rightarrow \text{SO}(5) \times \text{SO}(2)$ , which turns out to be a composite two-Higgs doublet model (2HDM) with two extra singlet, the lightest of which will be a WIMP dark matter candidate. After the general discussion of section 4.1 about how EWSB can be addressed in CH models, we discuss the theoretical aspects of the model in section 4.2; section 4.3 is dedicated to the spectrum and the interactions of the pNGBs, while in sections 4.4 and 4.5 we show how this model predicts thermal and non-thermal productions of DM, respectively. Finally, the appendices are organized as follows: we discuss in appendix 4.A the identification of the NGBs, we show how EWPTs and Higgs couplings fit constrain the parameter space in appendix 4.B and we present a list of effective couplings in appendix 4.C.

## 4.1 Vacuum misalignment

The last ingredient which is needed in order for a CH model to be realistic is a way to correctly account for EWSB; this is achieved through a mechanism known as *vacuum misalignment*, which we now review. As a starting point, we introduce a reference vacuum  $\mathbf{F}$ , and assume that the NGBs are encoded in the field:

$$\phi(x) = e^{i\frac{\sqrt{2}}{f}\Pi_i(x)\hat{T}^i} \mathbf{F} \equiv U(\Pi)\mathbf{F}, \quad (4.1.1)$$

where  $U(\Pi)$  is the Goldstone matrix. Here,  $f$  is related to the energy scale  $m_*$  by  $f \equiv m_*/g_*$ .

This construction, which is based on the CCWZ formalism, is reviewed in appendix A. We then divide the generators in two subsets, according to their effect on the vacuum, i.e.:

$$\{T^a, \hat{T}^i\} \quad : \quad T^a \mathbf{F} = 0 \quad , \quad \hat{T}^i \mathbf{F} \neq 0, \quad (4.1.2)$$

This choice is purely a convention, and other possibilities may exist.

Given that the new sector is endowed with a global symmetry group  $\mathcal{G}$ , it must contain the EW group  $\mathcal{G}_{\text{EW}}$ , which is gauged by introducing the appropriate covariant derivatives. Since  $\mathcal{G}$  is spontaneously broken at a scale which is assumed to be much higher than the

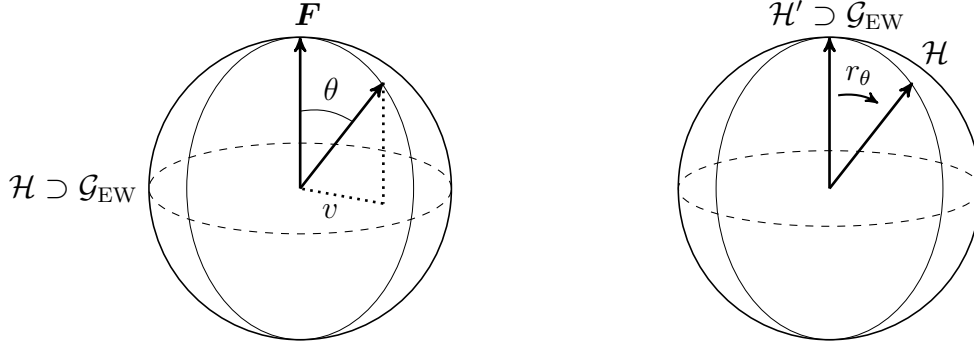


Figure 4.1: Schematic representation of vacuum misalignment. Left: in the first parametrization, the reference vacuum  $\mathbf{F}$  is displaced by the VEV of the pNGBs; the *physical* vacuum is not left invariant by the action of  $\mathcal{G}_{\text{EW}} \subset \mathcal{H}$ , leading to EWSB. Right: in the second parametrization, the electroweak group  $\mathcal{G}_{\text{EW}}$  is not orthogonal to the *physical* vacuum (which is orthogonal to  $\mathcal{H}$ , by definition); after the explicit breaking of  $\mathcal{G}$ , this leads to EWSB. In this parametrization, no VEV for the pNGBs is allowed.

weak one, two different choices regarding the embedding of  $\mathcal{G}_{\text{EW}}$  are possible, as we now review:

- i) a first possibility is to assume  $\mathcal{G}_{\text{EW}}$  to be entirely embedded in  $\mathcal{H}$ ,  $\mathcal{G}_{\text{EW}} \subset \mathcal{H} \subset \mathcal{G}$ ; with this particular choice for the embedding, once the group is gauged, the gauge bosons  $W_\mu^a$  and  $B_\mu$  only couple to the currents associated to the unbroken generators  $T^a$ .

Given that only a subgroup of  $\mathcal{G}$  is gauged, the latter is explicitly broken (analogously to the breaking of  $\text{SU}(2)_L \times \text{SU}(2)_R$  in the SM due to the presence of  $g'$ ). In addition, as we will see in a concrete example, also the interactions between the NGBs and the fermions explicitly break  $\mathcal{G}$ .

As discussed in appendix A, a VEV for the NGBs  $\Pi_i$ 's is not physical, since it can be eliminated via transformations belonging to  $\mathcal{G}/\mathcal{H}$ ; this implies that if  $\mathcal{G}$  is unbroken,  $\langle \phi \rangle$  is parallel to  $\mathbf{F}$ , and then invariant under  $\mathcal{G}_{\text{EW}}$ : EWSB does not occur. However, the explicit breaking of  $\mathcal{G}$  due to the NGBs interactions with gauge bosons and fermions generates a potential for the Goldstones, making them become pNGBs which in turn leads to a VEV for the  $\Pi_i$ 's. This VEV now cannot now be eliminated by symmetry transformations, since  $\mathcal{G}$  is explicitly broken. The effect is that the vacuum of the theory is not parallel to  $\mathbf{F}$  anymore, and therefore it is not invariant under  $\mathcal{G}_{\text{EW}}$ : the EW symmetry is spontaneously broken; this is schematically shown in the left sketch of fig. 4.1.

The amount of EWSB depends on the projection of the physical vacuum  $\langle \phi \rangle$  on the plane identified by  $\mathcal{H}$  (since it contains  $\mathcal{G}_{\text{EW}}$ ); if we define  $f \equiv |\mathbf{F}|$  and  $\theta \equiv \|\langle \Pi \rangle\|/f$ , the EWSB scale is:

$$v = f \sin \theta. \quad (4.1.3)$$

Being a dimensionless parameter, we expect in general  $\theta \sim \mathcal{O}(1)$ , so that  $v \sim f$ : if this is the case, this construction reduces to the case of technicolour; in CH models, instead, we demand  $\theta \ll 1$ , and we usually express this condition by requiring:

$$\xi \equiv \frac{v^2}{f^2} \ll 1; \quad (4.1.4)$$

ii) a second possibility is to assume that the EW group is embedded in a group  $\mathcal{H}'$  which does not coincide with  $\mathcal{H}$ ; as long as the global symmetry is unbroken, such a distinction is not physical, since one group can be always mapped into the other. Similarly to the other case, however, the gauging of  $\mathcal{H}'$  explicitly breaks  $\mathcal{G}$ , and a potential for the NGBs is generated, making them become pNGBs. After this explicit breaking is not possible to align the two vacua (relative to  $\mathcal{H}$  and  $\mathcal{H}'$ ) anymore: in particular, the *physical* vacuum of the theory, orthogonal to  $\mathcal{H}$ , is not left invariant by the action of  $\mathcal{H}'$ , leading to EWSB. This is represented in the right sketch of fig. 4.1. In this parametrization, therefore, two sets of generators must be considered: a first one,  $\{T_\theta\}$ , related to the breaking  $\mathcal{G} \rightarrow \mathcal{H}$ , and a second one,  $\{T\}$ , related to  $\mathcal{G} \rightarrow \mathcal{H}'$ ; the mapping between the two is obtained via a rotation matrix  $r_\theta$ , and if we assume the generators to be normalized as  $\text{Tr}\{T^A T^B\} = \delta^{AB}$ , we have:

$$T_\theta = r_\theta T r_\theta^{-1}. \quad (4.1.5)$$

As a consequence, two Goldstone matrices can be introduced:

$$U \equiv U(\Pi) = e^{i\frac{\sqrt{2}}{f}\Pi} \quad , \quad U_\theta \equiv U(\Pi_\theta) = e^{i\frac{\sqrt{2}}{f}\Pi_\theta}, \quad (4.1.6)$$

with  $\Pi \equiv \Pi^i \hat{T}^i$  and  $\Pi_\theta \equiv \Pi^i \hat{T}_\theta^i$ . In this parametrization, the pNGBs are defined around the *physical* vacuum, and are not allowed to take any VEV.

The rotation matrix  $r_\theta$  can be obtained by considering the Goldstone matrix in the *gauge* basis  $\{T\}$  with the NGBs set to the corresponding VEVs, i.e.:

$$r_\theta \equiv U(\langle \Pi \rangle). \quad (4.1.7)$$

Such an approach is used, for example, in refs. [219, 220], and we will also exploit it in our discussion.

These two parametrization are different, but equivalent; nevertheless, the second one has the virtue that for breaking patterns different from  $\text{SO}(N) \rightarrow \text{SO}(N-1)$  (for which a parametrization for the pNGBs analogous to the minimal scenario is always possible [27]), one can expand the Goldstone matrix  $U_\theta$  in the fields but keep the exact expressions for the parameters related to the vacuum.

## 4.2 Construction of the model

In this section, we discuss in detail the aspects of model building for the CH model based on the breaking pattern  $\text{SO}(7) \rightarrow \text{SO}(5) \times \text{SO}(2)$ ; we adopt the second one of the two parametrizations outlined above for vacuum misalignment, i.e. we assume the EW group to be embedded in a subgroup  $\mathcal{H}'$  which does not coincide with  $\mathcal{H}$ .

As we will see, this breaking pattern delivers two  $\text{SU}(2)_L$  doublets, being effectively a composite 2HDM, and two singlets.

We discuss in section 4.2.1 the embedding of the NGBs, while we show how they are coupled to SM fermions and how the scalar potential is generated in sections 4.2.2 and 4.2.3, respectively.



## 4.2.1 Goldstone embedding

It is convenient to introduce the generators in the *gauge* basis,  $\text{SO}(7) \rightarrow \text{SO}(5)' \times \text{SO}(2)'$ , which is then related to the *physical* one by eq. (4.1.5):

$$(T_L^\alpha)_{ab} = -\frac{i}{2} [\epsilon_{\alpha\beta\gamma} \delta_{\beta a} \delta_{\gamma b} + (\delta_{\alpha a} \delta_{4b} - \delta_{ab} \delta_{4a})] \quad (4.2.1a)$$

$$(T_R^\alpha)_{ab} = -\frac{i}{2} [\epsilon_{\alpha\beta\gamma} \delta_{\beta a} \delta_{\gamma b} - (\delta_{\alpha a} \delta_{4b} - \delta_{ab} \delta_{4a})] \quad (4.2.1b)$$

$$(T_5^\omega)_{ab} = -\frac{i}{\sqrt{2}} [\delta_{\omega a} \delta_{5b} - \delta_{5a} \delta_{\omega b}] \quad (4.2.1c)$$

$$(T_2)_{ab} = -\frac{i}{\sqrt{2}} [\delta_{6a} \delta_{7b} - \delta_{7a} \delta_{6b}] \quad (4.2.1d)$$

$$(\hat{T}_1^i)_{ab} = -\frac{i}{\sqrt{2}} [\delta_{ia} \delta_{6b} - \delta_{6a} \delta_{ib}] \quad (4.2.1e)$$

$$(\hat{T}_2^i)_{ab} = -\frac{i}{\sqrt{2}} [\delta_{ia} \delta_{7b} - \delta_{7a} \delta_{ib}] \quad (4.2.1f)$$

where  $\alpha, \beta, \gamma = 1, 2, 3$ ,  $a, b = 1, \dots, 7$ ,  $\omega = 1, \dots, 4$  and  $i = 1, \dots, 5$ . We indicate by  $T_{L,R}$  the generators of  $\text{SO}(4)' \subset \text{SO}(5)'$ , by  $T_5$  the remaining ones of  $\text{SO}(5)'$ , and by  $T_2$  that of  $\text{SO}(2)'$ ; finally,  $\hat{T}_{1,2}$  are the broken generators.

If we define  $T^A \equiv \{T_L, T_R, T_5\}$ , we have the following commutation relations:

$$\begin{aligned} [\hat{T}_1^i, \hat{T}_1^j] &= (t^A)_{ij} T^A = [\hat{T}_2^i, \hat{T}_2^j] \quad , \quad [\hat{T}_1^i, \hat{T}_2^j] = -\frac{i}{\sqrt{2}} \delta_{ij} T_2 \quad , \quad [T^A, T_2] = 0 \quad , \\ [\hat{T}_{1,2}^i, T^A] &= (t^A)_{ij} \hat{T}_{1,2}^j \quad , \quad [\hat{T}_1^i, T_2] = \frac{i}{\sqrt{2}} \hat{T}_2^i \quad , \quad [\hat{T}_2^i, T_2] = -\frac{i}{\sqrt{2}} \hat{T}_1^i \end{aligned} \quad (4.2.2)$$

where  $t^A$  is the upper  $5 \times 5$  block of  $T^A$ , together with:

$$\begin{aligned} [T_{L,R}^\alpha, T_{L,R}^\beta] &= i \epsilon_{\alpha\beta\gamma} T_{L,R}^\gamma \quad , \quad [T_L^\alpha, T_5^4] = -\frac{i}{2} T_5^\alpha \quad , \quad [T_R^\alpha, T_5^4] = \frac{i}{2} T_5^\alpha \quad , \\ [T_L^\alpha, T_5^\beta] &= \frac{i}{2} (\delta_{\alpha\beta} T_5^4 + \epsilon_{\alpha\beta\gamma} T_5^\gamma) \quad , \quad [T_R^\alpha, T_5^\beta] = \frac{i}{2} (-\delta_{\alpha\beta} T_5^4 + \epsilon_{\alpha\beta\gamma} T_5^\gamma) \quad , \quad (4.2.3) \\ [T_5^{\omega_1}, T_5^{\omega_2}] &= \frac{i}{2} \epsilon_{\omega_1 \omega_2 \omega_3} (T_L^{\omega_3} + T_R^{\omega_3}) \quad , \quad [T_L^\alpha, T_R^\beta] = 0. \end{aligned}$$

It is evident from eqs. (4.2.1a) to (4.2.1f) that with this choice for the generators, a generic  $\mathcal{G}$  transformation is in the form:

$$\{T_L, T_R, T_5, T_2, \hat{T}_1, \hat{T}_2\} \sim \left( \begin{array}{cc|cc} & & & \\ & T_{L,R} & & T_5 \\ & & & \\ & & & \\ \hline & & & \\ & T_5 & & 0 \\ & & & \\ \hline & & \hat{T}_1 & \hat{T}_2 \\ & & \hat{T}_2 & T_2 \end{array} \right) , \quad (4.2.4)$$

so that  $\mathcal{H}'$  transformations are block-diagonal.

We use the first letters of the alphabet for the indices of a generic  $\text{SO}(7)$  transformation,  $a, b, c, \dots = 1, \dots, 7$ ; because of its block-diagonal form, instead, an  $\text{SO}(5)' \times \text{SO}(2)'$  transformation will have  $\bar{a}, \bar{b}, \dots$  indices, where  $\bar{a} = \{i, \mu\}$ , with  $i$  and  $\mu$  being  $\text{SO}(5)'$  fiveplet and  $\text{SO}(2)'$  doublet indices, respectively. In the following, we do not make a distinction between upper or lower indices; on the other hand, instead, their position is important: the first index refers to the row, while the second one to the column.

In order to identify the transformations properties and the quantum numbers of the NGBs, as well as the symmetries of the theory, it is convenient to consider the limit of no misalignment, where  $r_\theta = \mathbf{1}$ ; in this case, the pNGB matrix takes the form:

$$\Pi = \hat{T}^I \Pi^I \equiv -\frac{i}{\sqrt{2}} \begin{pmatrix} \mathbb{0}_{5 \times 5} & \Phi_1 & \Phi_2 \\ -\Phi_1^T & 0 & 0 \\ -\Phi_2^T & 0 & 0 \end{pmatrix}, \quad \begin{aligned} \Phi_1 &= (\Pi_1 \dots \Pi_5)^T \\ \Phi_2 &= (\Pi_6 \dots \Pi_{10})^T \end{aligned}, \quad (4.2.5)$$

and  $I = 1, \dots, 10$ . The NGBs transform as a  $(\mathbf{5}, \mathbf{2})$  of  $\text{SO}(5)' \times \text{SO}(2)'$ , and as  $(\mathbf{5}, \mathbf{2}) = 2 \times \mathbf{4} + 2 \times \mathbf{1}$  under  $\text{SO}(4) \subset \text{SO}(5)'$ . It is then convenient to parametrize the two fiveplets of NGBs as:

$$\Phi_1 = (\phi_1, \eta)^T, \quad \Phi_2 = (\phi_2, \kappa)^T. \quad (4.2.6)$$

It is sometimes useful to consider the bidoublet notation for  $\phi_{1,2}$ , which is defined as usual as:

$$\phi_\alpha = \frac{1}{\sqrt{2}} (i\sigma^k \phi_\alpha^k + \mathbb{1} \phi_\alpha^4), \quad \alpha = 1, 2, \quad k = 1, 2, 3. \quad (4.2.7)$$

We will use the symbol  $\phi$  for both the fourplet and the bidoublet notations, the correct one being clear from the context.

From the discussion of appendix A, we see that the Goldstone matrix has  $a\bar{a}$  indices and transforms as:

$$U_{a\bar{a}} \rightarrow g_{ab} U_{b\bar{b}} h_{\bar{b}\bar{a}}^{-1}. \quad (4.2.8)$$

As already stated in ref. [205], a VEV for the second doublet can lead to dramatic violations of EWPTs, in particular because of contributions to the  $\hat{T}$  parameter. A possible way out is given by discrete symmetries, which can prevent the appearance of the second VEV. To this purpose, we introduce the discrete symmetry

$$C_2 = \text{diag}(1, 1, 1, 1, 1, 1, -1), \quad (4.2.9)$$

acting on the NGBs matrix as  $U \rightarrow C_2 U C_2$ , and on the NGBs as  $(\Phi_1, \Phi_2) \rightarrow (\Phi_1, -\Phi_2)$ . We will come back to this symmetry later, when we will show that it is explicitly broken by the interactions of the strong sector with SM fermions.

Another discrete symmetry which is useful to our purposes is the parity

$$P_7 = \text{diag}(1, 1, 1, 1, -1, 1, 1), \quad (4.2.10)$$

which can help in stabilizing the singlets, since  $(\eta, \kappa) \rightarrow -(\eta, \kappa)$  under it.

Another symmetry we assume to be respected by the theory is  $CP$ ; in order to determine the  $CP$ -parities of the NGBs we must study the interactions between the strong sector and SM fermions (see section 4.2.2). We will show that  $CP$  remains unbroken in this model.

The CCWZ construction does not take account of a contribution which arises at 0th order in the perturbative expansion: the Wess-Zumino-Witten (WZW) term [221, 222], which could in principle affect the stability of the pNGBs. In general, the parameter

Field	SO(4)'	$C_2$	$P_7$
$\phi_1$	<b>4</b>	+	+
$\phi_2$	<b>4</b>	-	+
$\eta$	<b>1</b>	+	-
$\kappa$	<b>1</b>	-	-

Table 4.1: Representations under SO(4)' and parities under the discrete symmetries for the NGBs.

controlling the anomalies is given by  $d_{abc} \equiv \frac{1}{2}\text{Tr}(T_a \{T_b, T_c\})$ , where the  $T$ 's generically denote the generators. In the model we study, no WZW anomaly emerges at the order we consider; in addition, it is possible to prove that such a term does not emerge in general, since the fifth de Rham cohomology group of  $\text{SO}(7)/\text{SO}(5) \times \text{SO}(2)$  vanishes [223, 224]<sup>1</sup>. This implies that the singlets remain stable, and therefore the discrete symmetry  $P_7$  is unbroken to all orders in the perturbative expansion.

We show in table 4.1 the representations of the NGBs under SO(4)' and the corresponding parities under the discrete symmetries.

This discussion is valid in the case of no misalignment,  $r_\theta = \mathbf{1}$ ; in general, the generators which enter in eq. (4.2.5) are related to the ones in the *gauge* basis of eqs. (4.2.1a) to (4.2.1f) by eq. (4.1.5). As already stated, we will show that  $C_2$  is explicitly broken, whereas  $P_7$  and  $CP$  are not; compatibly with these symmetries, the most general misalignment between the *physical* and *gauge* basis is:

$$r_\theta = \begin{pmatrix} 1 & 0 & 0 & 0 & 0 & 0 & 0 \\ 0 & 1 & 0 & 0 & 0 & 0 & 0 \\ 0 & 0 & c_2 & 0 & 0 & 0 & s_2 \\ 0 & 0 & 0 & c_1 & 0 & s_1 & 0 \\ 0 & 0 & 0 & 0 & 1 & 0 & 0 \\ 0 & 0 & 0 & -s_1 & 0 & c_1 & 0 \\ 0 & 0 & -s_2 & 0 & 0 & 0 & c_2 \end{pmatrix}, \quad (4.2.11)$$

where we defined  $s_{1,2} (c_{1,2}) \equiv \sin \theta_{1,2} (\cos \theta_{1,2})$ , with  $\theta_{1,2} \equiv \langle \Pi_{4,8} \rangle / f$ ; the form of  $r_\theta$  comes from the fact that the  $CP$ -even NGBs are  $\Pi_4$  and  $\Pi_8$ , as we will show.

It is then convenient to define:

$$\begin{aligned} \sin \theta_1 &\equiv \sqrt{\xi} \cos \beta \\ \sin \theta_2 &\equiv \sqrt{\xi} \sin \beta \end{aligned}. \quad (4.2.12)$$

The previous discussion about a vanishing VEV for  $\phi_2$  would translate into the requirement  $\beta = 0$ . As we will discuss, although  $C_2$  is effectively broken, bounds from EWPTs require  $\theta_2 \ll \theta_1$ , and then  $\beta \ll 1$ .

According to the CCWZ prescription, the low-energy effective Lagrangian containing the kinetic terms for the NGBs plus derivative interactions is (see eq. (A.2.31)):

$$\mathcal{L}_\Pi^{(2)} \equiv \frac{f^2}{4} \text{Tr} [d_\mu^{(\theta)} d^{(\theta)\mu}], \quad (4.2.13)$$

where  $d_\mu^{(\theta)} \equiv i \text{Tr}[U_\theta^{-1} D_\mu U_\theta \hat{T}_\theta^I] \hat{T}_\theta^I$  is the  $d$  symbol in the *physical* basis, and the covariant derivative is defined, in terms of the (non-canonically normalized) gauge fields  $A_\mu =$

<sup>1</sup>We thank Joe Davighi for pointing out this mathematical aspect.

$gW_\mu^\alpha T_L^\alpha + g'B_\mu T_R^3$ , as  $D_\mu U \equiv \partial_\mu U - iA_\mu U$ . The masses for the  $W$  and  $Z$  bosons can be obtained from eq. (4.2.13) by setting the NGBs to zero, and read:

$$m_W^2 = \frac{g^2 f^2}{4} (\sin^2 \theta_1 + \sin^2 \theta_2) \quad (4.2.14a)$$

$$m_Z^2 = \frac{f^2 (g^2 + g'^2)}{4} (\sin^2 \theta_1 + \sin^2 \theta_2) \left[ 1 - \frac{\xi}{4} (1 - \cos 4\beta) \right]. \quad (4.2.14b)$$

The SM prediction for  $m_W$  is then correctly reproduced if we identify the Higgs VEV  $v$  by the equation:

$$\xi \equiv \frac{v^2}{f^2}, \quad (4.2.15)$$

which is the usual definition of the  $\xi$  parameter in CH models (cf. eq. (4.1.4)); on the other hand, we see that  $m_Z$  differs from the SM prediction by the factor

$$m_Z = m_Z^{(\text{SM})} \left[ 1 - \frac{\xi}{4} (1 - \cos 4\beta) \right]^{\frac{1}{2}}, \quad (4.2.16)$$

leading to a tree-level contribution to the  $\rho$  parameter defined in eq. (1.1.13) (or, equivalently, to  $\hat{T}$ ). We will come back later to this aspect when discussing restrictions on the parameter space from EWPTs, but we can notice that this contribution is due to the fact that the VEV  $\langle \Pi_8 \rangle$  breaks the custodial symmetry down to  $\text{SO}(2)$ .

From eq. (4.2.13), it is also possible to find out the expressions for the Goldstone bosons  $G_i$  which are eaten to give mass to  $W$  and  $Z$ ; in general, they can be identified by looking for interactions like  $-g/(2\sqrt{2})v \partial^\mu G_+ W_\mu^-$  (see, e.g., ref. [225]). While the general case can be found in appendix 4.A, we report here the expressions for  $\phi_{1,2}$  in the case of no misalignment,  $\beta = 0$ , in which:

$$\phi_1 = \begin{pmatrix} \frac{G_+ + G_-}{\sqrt{2}} \\ \frac{i(G_+ - G_-)}{\sqrt{2}} \\ G_0 \\ h \end{pmatrix}, \quad \phi_2 = \begin{pmatrix} \frac{-i(H_+ - H_-)}{\sqrt{2}} \\ \frac{H_+ + H_-}{\sqrt{2}} \\ H_0 \\ A_0 \end{pmatrix}. \quad (4.2.17)$$

Here,  $h$  is the physical Higgs, while  $H_0$  ( $A_0$ ) represents the  $CP$ -even (odd) component of the second doublet.

## 4.2.2 Partial compositeness

In CH models, the interactions between the strong sector and SM fermions are usually studied by resorting to the paradigm of *partial compositeness* [226]: the idea is that SM quarks are linearly coupled to fermionic operators of the strong sector  $\mathcal{O}_{L,R}$ ; in principle, the composite operators can be in any representation of the group  $\mathcal{G}$ , but we consider here the simplest case in which they are in the fundamental,  $\mathcal{O}_{L,R} \in \mathbf{7}$  of  $\text{SO}(7)$  (for other representations, see, e.g., ref. [210]). In the following, we mainly focus on the top quark, since the corresponding Yukawa is the largest one, and it represents the main contribution to the potential.

The composite operators must be such to contain the SM quarks representations when decomposed under  $\mathcal{G}_{\text{EW}}$ , i.e.  $\mathbf{2}_{\frac{1}{6}}, \mathbf{1}_{\frac{2}{3}}, \mathbf{1}_{-\frac{1}{3}}$ . In CH models, in general, one has to enlarge the symmetry group in order to reproduce these representations; this is easily obtained by considering an extra  $U(1)_X$ , with  $X$  properly chosen (typically,  $X = 2/3$ ). The hypercharge is then defined as  $Y = T_R^3 + X$ . To determine which operators the left- and right-handed quarks can couple to, we have to consider the decomposition of the  $\mathbf{7}_{\frac{2}{3}}$  of  $SO(7)$  under the EW group; this is:

$$\mathbf{7}_{\frac{2}{3}} = (\mathbf{5}, \mathbf{1})_{\frac{2}{3}} \oplus (\mathbf{1}, \mathbf{2})_{\frac{2}{3}} = \mathbf{2}_{\frac{7}{6}} \oplus \mathbf{2}_{\frac{1}{6}} \oplus \mathbf{1}_{\frac{2}{3}} \oplus \mathbf{1}_{\frac{2}{3}} \oplus \mathbf{1}_{\frac{2}{3}}, \quad (4.2.18)$$

under  $SO(5)' \times SO(2)'$  and  $\mathcal{G}_{\text{EW}}$ , respectively. According to table 1.1, we then see that the right-handed quark  $t_R$  can couple to both the singlet of  $SO(5)'$  and the  $\mathbf{1}_{\frac{2}{3}}$  coming from the  $\mathbf{5}$ ; the left-handed quark  $q_L$ , instead, can only couple with the  $\mathbf{2}_{\frac{1}{6}}$  coming from the  $\mathbf{5}$ .

In partial compositeness, two equivalent approaches are possible: on the one hand, one can assume the quarks to be part of  $\mathcal{G}$ -incomplete multiplets; on the other hand, one can consider the case where the couplings are promoted to fields (called *spurions*) which belong to some representation of  $\mathcal{G}$ . We take the latter approach, being it suitable also for the generation of the scalar potential. We then introduce the Lagrangian:

$$\mathcal{L}_{\text{int}}^f = \bar{q}_L^\alpha \mathcal{Y}_L^{\alpha T} \mathcal{O}_L + \bar{t}_R \mathcal{Y}_R^T \mathcal{O}_R + \text{h.c.}, \quad (4.2.19)$$

where  $\mathcal{Y}_{L,R}$  denote the spurions,  $a = 1, \dots, 7$  is an  $SO(7)$  index and  $\alpha = 1, 2$  is the flavour index of the quark doublet.

The SM fermions are assumed to be even under both  $C_2$  and  $P_7$ , implying for the spurions the transformation properties:

$$\mathcal{Y}_{L,R} \rightarrow C_2 \mathcal{Y}_{L,R} \quad , \quad \mathcal{Y}_{L,R} \rightarrow P_7 \mathcal{Y}_{L,R}. \quad (4.2.20)$$

Equation (4.2.19) exhibits two ‘‘elementary’’ symmetries: a  $U(2)_L^{\text{el}}$ , under which the components of  $q_L^\alpha$  and  $\mathcal{Y}_L^\alpha$  are rotated, and a  $U(1)_R^{\text{el}}$ , under which  $t_R$  and  $\mathcal{Y}_R$  are charged. Compatibly with these symmetries, and with  $P_7$ , the most general VEVs for the spurions are:

$$\mathcal{Y}_L = \frac{y_L}{\sqrt{2}} \begin{pmatrix} 0 & 0 & i & 1 & 0 & 0 & 0 \\ i & -1 & 0 & 0 & 0 & 0 & 0 \end{pmatrix}^T \quad (4.2.21a)$$

$$\mathcal{Y}_R = y_R \begin{pmatrix} 0 & 0 & 0 & 0 & 0 & \cos \theta_t & i \sin \theta_t \end{pmatrix}^T, \quad (4.2.21b)$$

with  $y_L$  and  $y_R$  real.

It is evident that  $C_2$  is explicitly broken by the VEV of  $\mathcal{Y}_R$  unless  $\theta_t = 0$ .

In the following, it will be important to distinguish between two concepts of symmetries: we define *spurionic* the symmetries of the strong sector which are respected by the Lagrangian before the spurions acquire a VEV; on the other hand, we define *residual* the symmetries which are respected also once the spurions have acquired a VEV. In the following, we assume that spurionic symmetries remain unbroken.

Similarly to what is done with the gauge fields, it is convenient to ‘‘dress’’ the spurions and define:

$$\bar{\mathcal{Y}}_L^\alpha \equiv \left( r_\theta^{-1} U_\theta^\dagger \mathcal{Y}_L \right)^\alpha \quad (4.2.22a)$$

$$\bar{\mathcal{Y}}_R \equiv r_\theta^{-1} U_\theta^\dagger \mathcal{Y}_R. \quad (4.2.22b)$$

This definition is consistent with the standard one, i.e.  $\bar{\mathcal{Y}} = U^\dagger \mathcal{Y}$ : this can be easily checked by going to the basis of the VEV, where  $\langle U_\theta \rangle = \mathbf{1}$  and  $\langle U \rangle = r_\theta$ .

In general, the dressing procedure has the effect of starting from an object transforming with an index  $a$  of  $\mathcal{G}$ , and obtaining a new object which transforms with an index  $\bar{a}$  of  $\mathcal{H}$ ; it is then understood that whenever a barred quantity appears, barred indices are implicit. The idea is now simple: we use the dressed spurions to write invariants under  $\mathcal{H}$ , and they will also be automatically invariant under the full  $\mathcal{G}$ ; in particular, we can consider a low-energy effective Lagrangian coming from integrating out the composite operators (notice that the pNGBs are included in the dressed spurions).

In the aligned limit,  $r_\theta = \mathbf{1}$ , the dressed spurions transform as a  $(\mathbf{5}, \mathbf{1}) \oplus (\mathbf{1}, \mathbf{2})$  under  $\text{SO}(5) \times \text{SO}(2)$ , with components given by:

$$(\bar{\mathcal{Y}}_5)^i, (\bar{\mathcal{Y}}_2)^\mu, \quad (4.2.23)$$

where  $i = 1, \dots, 5$ , while  $\mu = 1, 2$  being the index associated to  $\text{SO}(2)$ . The effective Lagrangian can then be constructed by combining the components above with  $\delta_{ij}$ ,  $\delta_{\mu\nu}$  and  $\epsilon_{\mu\nu}$ ; the latter possibility, however, violates the  $C_2$ -spurionic and will not be considered. In addition, only left-right combinations have to be included because of chirality. Finally, the two invariants which can be constructed with  $\delta$  symbols are not independent, due to the singlet one can obtain by combining two  $\mathbf{7}$ . The interaction Lagrangian for the top quark is then:

$$\mathcal{L}_t = c_t \frac{m_*}{g_*^2} \bar{q}_L^\alpha (\bar{\mathcal{Y}}_{L,2}^\alpha)^\dagger (\bar{\mathcal{Y}}_{R,2})^\mu t_R, \quad (4.2.24)$$

where the factor  $m_*/g_*^2$  comes from dimensional analysis (see appendix B), and  $c_t$  is expected to be an  $\mathcal{O}(1)$  coefficient.

From eq. (4.2.24), we can read both the top mass and the top-NGBs interactions; by expanding around  $\beta = 0$ , the top Yukawa coupling is easily obtained:

$$Y_t \approx c_t \frac{y_L y_R}{g_*} (\sqrt{1 - \xi} \cos \theta_t + \beta \sin \theta_t). \quad (4.2.25)$$

Note that the parenthesis approaches  $\beta$  for  $\theta_t \rightarrow \pi/2$ , leading to a potential suppression of the Yukawa coupling; this can be compensated by considering slightly larger values of either  $c_t$  or  $y_L y_R/g_*$ .

The same analysis could also be repeated for other quarks; however, since  $Y_{q \neq t} \ll Y_t$ , their role is less relevant, the only exception being possibly represented by the  $b$  quark; in particular, since this choice does not have a major impact in what follows, we take  $\theta_b = 0$ . One potential issue of the model is due to FCNCs: as outlined in section 1.2.1, in fact, a special feature of the SM is that Yukawa interactions are flavour diagonal because the Yukawa and mass matrices can be simultaneously diagonalized. This is in general not the case for a model with more than one Higgs doublet; however, as discussed in detail in ref. [205], flavour problems can be avoided if the Yukawa matrices are aligned, i.e. if we take  $\theta_u = \theta_c = \theta_t$  and  $\theta_d = \theta_s = \theta_b$ . If this is the case, MFV is actually enforced, leading to the so-called tipe-III composite Higgs model; in this case, if we generically denote by  $Y_1^q$  and  $Y_2^q$  the couplings of the quark  $q$  with the two doublets, we have  $Y_1^q \propto Y_2^q$ . In the following, we make this assumptions about the embedding of the quarks.

A crucial point is that eq. (4.2.24) leads to the interaction  $ihA_0 \bar{t} \gamma^5 t$  after the spurions are set to the corresponding VEVs; such an interaction has two consequences: first, it implies that  $A_0$  (i.e. the fourth component of  $\phi_2$ ) is  $CP$ -odd, as anticipated; in addition,

this term explicitly breaks  $C_2$  (the residual one, in the language introduced before), leading in general to a non-vanishing VEV for the second doublet.

It also turns out that the two singlets  $\eta$  and  $\kappa$  have opposite  $CP$ -parities: we choose  $\eta$  to be even, and  $\kappa$  to be odd.

### 4.2.3 Potential for the pNGBs

The scalar potential is generated by the explicit breaking of the Goldstone symmetry; since the composite sector is  $\mathcal{G}$ -invariant, such a breaking can only come from interactions between the composite and elementary sectors. Furthermore, given that elementary fields do not couple with the Goldstone bosons directly, the potential cannot be generated by loop diagrams with only elementary fields internal lines. As a consequence, an even number of insertions of elementary couplings (denoted generically as  $g_{\text{SM}}$ ) is needed.

Following the discussion of appendix B, the potential can be schematically written as (see, e.g., ref. [227]):

$$V(\Pi) \sim \frac{m_*^4}{g_*^2} \left( \frac{g_*^2}{16\pi^2} \right)^L \left( \frac{g_{\text{SM}}}{g_*} \right)^{\mu_G} \left( \frac{y}{g_*} \right)^{\mu_F} \hat{V} \left( \frac{\Pi}{f} \right), \quad (4.2.26)$$

where  $L$  is the number of loops at which the potential is generated,  $\mu_G$  and  $\mu_F$  count the number of insertions of gauge and fermionic spurions, and  $\hat{V}$  is a dimensionless function of its argument.

#### Fermionic contribution

The main source of explicit breaking of the Goldstone symmetry can be found in the coupling of the composite sector with elementary quarks, and in particular with the top. As anticipated, the generation potential is best studied with the method of spurions: for the quark contribution, the Lagrangian is the same one which generates the top Yukawa coupling, i.e. eq. (4.2.24).

We can then use the dressed spurions in eqs. (4.2.22a) and (4.2.22b) to construct invariants under  $\text{SO}(5) \times \text{SO}(2)$  which in the end will be responsible for the breaking of the symmetry, leading to the generation of the potential; given the two elementary symmetries of eq. (4.2.19), all the invariants built from the Yukawa spurions have to be combinations of the matrices:

$$\bar{\Delta}_L^{\bar{a}\bar{b}} \equiv \bar{\mathcal{Y}}_L^{*\alpha,\bar{a}} \bar{\mathcal{Y}}_L^{\alpha,\bar{b}} \quad (4.2.27a)$$

$$\bar{\Delta}_R^{\bar{a}\bar{b}} \equiv \bar{\mathcal{Y}}_R^{*\bar{a}} \bar{\mathcal{Y}}_R^{\bar{b}}, \quad (4.2.27b)$$

At lowest order, i.e.  $\mathcal{O}(y^2)$ , in principle two invariants can be formed for each chirality; however, they are not independent, as it can be seen by considering the trace of  $\bar{\Delta}$ . From eqs. (4.2.22a) and (4.2.22b), we have:

$$\text{Tr } \bar{\Delta} = \bar{\Delta}^{\bar{a}\bar{a}} = \mathcal{Y}^{*a} \mathcal{Y}^a = \Delta^{aa}, \quad (4.2.28)$$

which is independent of the NGBs, and therefore only contributes to the vacuum energy. As a consequence, at lowest order, we are left with:

$$\mathcal{I}_{(1,0)}^{(1)} = \bar{\Delta}_L^{ii} \quad , \quad \mathcal{I}_{(0,1)}^{(1)} = \bar{\Delta}_R^{ii}. \quad (4.2.29)$$

We can proceed in a similar way for the order  $\mathcal{O}(y^4)$ : the invariants will be combinations of  $\Delta_{L,R}$ ,  $\delta_{ab}$ ,  $\delta_{ij}$  and  $\delta_{\mu\nu}$ . With the VEVs given in eqs. (4.2.21a) and (4.2.21b), the non-vanishing invariants are:

$$\begin{aligned}\mathcal{I}_{(2,0)}^{(1)} &\equiv \bar{\Delta}_L^{ij} \bar{\Delta}_L^{ji}, & \mathcal{I}_{(1,1)}^{(1)} &\equiv \bar{\Delta}_L^{ij} \bar{\Delta}_R^{ji}, & \mathcal{I}_{(0,2)}^{(1)} &\equiv \bar{\Delta}_R^{ij} \bar{\Delta}_R^{ji}, \\ \mathcal{I}_{(2,0)}^{(2)} &\equiv \bar{\Delta}_L^{ii} \bar{\Delta}_L^{jj}, & \mathcal{I}_{(1,1)}^{(2)} &\equiv \bar{\Delta}_L^{ii} \bar{\Delta}_R^{jj}, & \mathcal{I}_{(0,2)}^{(2)} &\equiv \bar{\Delta}_R^{ij} \bar{\Delta}_R^{ij}, \\ \mathcal{I}_{(0,2)}^{(3)} &\equiv \Im [\bar{\Delta}_R^{\bar{a}i} \bar{\Delta}_R^{\bar{a}i}],\end{aligned}\tag{4.2.30}$$

where the indices have to be interpreted as already indicated. While the operators in the first line are generated at one loop, all the other ones are generated at two loops [205], and are then suppressed by a further factor of  $g_*^2/(4\pi)^2$ , which can however be  $\mathcal{O}(1)$ . The last invariant deserves one final comment: we consider only the imaginary part because the “full” invariant  $\bar{\Delta}_R^{\bar{a}i} \bar{\Delta}_R^{\bar{a}i}$  only contributes to the vacuum energy (for a reason similar to the previous one about  $\Delta^{\bar{a}a}$ ): therefore, the real and imaginary parts are not independent.

The general form of the scalar potential in eq. (4.2.26) can be specialized for this case as:

$$V_{\text{fermion}} = N_c \frac{m_*^4}{16\pi^2} \sum_{n_L, n_R, i} \frac{1}{g_*^{2(n_L+n_R)}} c_{(n_L, n_R)}^{(i)} \mathcal{I}_{(n_L, n_R)}^{(i)},\tag{4.2.31}$$

where  $\mathcal{I}_{(n_L, n_R)}^{(i)}$  is an invariant formed with  $n_{L,R}$  powers of  $\bar{\Delta}_{L,R}$ , and  $c_{(n_L, n_R)}^{(i)}$  are  $\mathcal{O}(1)$  coefficients. Since the fermions in the loop generating the potential are coloured, there is a factor  $N_c = 3$  accounting for the number of colours. Notice that  $\mathcal{I}_{(n_L, n_R)}^{(i)} \propto y_L^{2n_L} y_R^{2n_R}$ , which is the reason for the denominator in eq. (4.2.31).

Since we assume  $CP$ -invariance, we take  $c_{(0,2)}^{(3)} = 0$ , given that the associated invariant contains  $CP$ -breaking terms.

It turns out that  $c_{(1,0)}^{(1)}$ ,  $c_{(0,1)}^{(1)}$ ,  $c_{(2,0)}^{(1)}$ ,  $c_{(1,1)}^{(1)}$ ,  $c_{(0,2)}^{(1)}$ ,  $c_{(1,1)}^{(2)}$  and  $c_{(0,2)}^{(2)}$  are the most relevant coefficients for numerical estimates. We fix instead  $c_{(2,0)}^{(2)}$  to 1.

## Gauge contribution

Another source of explicit breaking of the symmetry comes from gauge interactions, encoded in the Lagrangian:

$$\mathcal{L}_{\text{int}}^{\text{gauge}} = g W_\mu^\alpha J_L^{\mu, \alpha} + g' B_\mu (J_R^{\mu, 3} + J_X^\mu),\tag{4.2.32}$$

where  $J_L^{\mu, \alpha}$ ,  $J_R^{\mu, \alpha}$  and  $J_X^\mu$  are the  $SU(2)_L$ ,  $U(1)_R$  and  $U(1)_X$  currents, respectively.

Even in this case, it is convenient to resort to the method of spurions to identify the operators that actually drive this breaking. Let us first focus on the term associated to  $J_R^{\mu, 3}$ ; we promote the coupling  $g'$  to a field and define:

$$\mathcal{G}' \equiv \sum_{A=1}^{21} \mathcal{G}'_A T^A = g' T_3^R.\tag{4.2.33}$$

We can then write a formally invariant contribution to eq. (4.2.32) as:

$$\mathcal{L}_{\text{int}}^{\text{gauge}} \supset \sum_{A=1}^{21} B_\mu \mathcal{G}'_A J_A^\mu = B_\mu \text{Tr}(\mathcal{G}' J^\mu),\tag{4.2.34}$$



where  $\mathcal{G}'$  transforms as  $\mathcal{G}' \rightarrow g \mathcal{G}' g^\dagger$  under an element  $g \in G$ .

It is then convenient to consider the dressed spurion

$$\bar{\mathcal{G}}' \equiv r_\theta^{-1} U_\theta^\dagger \mathcal{G}' U_\theta r_\theta, \quad (4.2.35)$$

whose components  $\bar{\mathcal{G}}'_A = \text{Tr} [\bar{\mathcal{G}}' T^A]$  organize in multiplets of  $\text{SO}(5) \times \text{SO}(2)$  as:

$$\mathbf{21} = (\mathbf{10}, \mathbf{1}) \oplus (\mathbf{5}, \mathbf{2}) \oplus (\mathbf{1}, \mathbf{1}), \quad (4.2.36)$$

associated to  $\{T_L, T_R, T_5\}$ ,  $\{\hat{T}_1, \hat{T}_2\}$  and  $T_2$ , respectively.

The first observation is that a generic invariant must contain at least two powers of  $\mathcal{G}'$ , because of the symmetry  $\mathcal{G}' \rightarrow -\mathcal{G}'$ ,  $B_\mu \rightarrow -B_\mu$ . In addition, to count and classify the invariants, we can work at the leading order of  $\bar{\mathcal{G}}'$ , which actually coincides with  $\mathcal{G}'$ . We can thus organize the components of  $\bar{\mathcal{G}}'$  as:

$$(\bar{\mathcal{G}}'_{10})^I, (\bar{\mathcal{G}}'_{\hat{T}})_\mu^i, \bar{\mathcal{G}}'_2, \quad (4.2.37)$$

with  $I = 1, \dots, 10$  being an index in the adjoint, while  $i = 1, \dots, 5$  and  $\mu = 1, 2$  being the indices associated to  $\text{SO}(5)$  and  $\text{SO}(2)$ , respectively. The invariant symbols we can use to form invariants are  $\delta_{IJ}$ ,  $\delta_{ij}$ ,  $\delta_{\mu\nu}$  and  $\epsilon_{\mu\nu}$ : in principle, then, we would have 4 invariants; however, the one which comes from the combination of  $\delta_{ij}$  and  $\epsilon_{\mu\nu}$  vanishes because of symmetry considerations. In addition, it is easy to check that:

$$\sum_{A=1}^{21} \text{Tr}^2 (\mathcal{G}' T^A) = \sum_{A=1}^{21} \text{Tr}^2 (\bar{\mathcal{G}}' T^A) = \sum_{A=1}^{21} \bar{\mathcal{G}}'_A \bar{\mathcal{G}}'_A. \quad (4.2.38)$$

Since the l.h.s. is independent of the Goldstone bosons, the r.h.s. only contributes to the vacuum energy. By taking this into account, we see that there are only two independent invariants, which we take to be:

$$(\bar{\mathcal{G}}'_{10})^I (\bar{\mathcal{G}}'_{10})_I, \quad \bar{\mathcal{G}}'_2 \bar{\mathcal{G}}'_2. \quad (4.2.39)$$

Similarly to what we did for the fermionic contribution, it is convenient to express these invariants in terms of matrix elements; we then introduce the notation:

$$\Gamma_{g'}^{abcd} \equiv (\mathcal{G}')^{ab} (\mathcal{G}')^{cd}, \quad (4.2.40)$$

and define the invariants:

$$\begin{aligned} \mathcal{I}_{g'}^{(1)} &\equiv -(\bar{\mathcal{G}}'_{10})^I (\bar{\mathcal{G}}'_{10})_I = \bar{\Gamma}_{g'}^{ijij} \\ \mathcal{I}_{g'}^{(2)} &\equiv -\bar{\mathcal{G}}'_2 \bar{\mathcal{G}}'_2 = \bar{\Gamma}_{g'}^{\mu\nu\mu\nu} \end{aligned} \quad (4.2.41)$$

The analysis proceeds exactly the same way for the other two terms in eq. (4.2.32). For the coupling  $g$  we can introduce the spurion  $\mathcal{G}^\alpha \equiv \mathcal{G}_A^\alpha T^A = g T_L^\alpha$  and define:

$$\Gamma_g^{abcd} \equiv (\mathcal{G}^\alpha)^{ab} (\mathcal{G}_\alpha)^{cd}. \quad (4.2.42)$$

The corresponding invariants are:

$$\begin{aligned} \mathcal{I}_g^{(1)} &\equiv \bar{\Gamma}_g^{ijij} \\ \mathcal{I}_g^{(2)} &\equiv \bar{\Gamma}_g^{\mu\nu\mu\nu} \end{aligned} \quad (4.2.43)$$

Finally, also the term proportional to  $J_X^\mu$  has to be considered: we denote the corresponding spurion by  $\mathcal{G}'_X = g'$ . Since a term of order  $(\mathcal{G}'_X)^2$  is a singlet under  $\mathcal{G}$  and contributes to the vacuum energy only, we are left with:

$$\tilde{\Gamma}_{g'}^{ab} \equiv (\mathcal{G}')^{ab} \mathcal{G}'_X. \quad (4.2.44)$$

The only invariant we can build out of this object is:

$$\mathcal{I}_{g'}^{(3)} \equiv \epsilon_{\mu\nu} \tilde{\Gamma}_{g'}^{\mu\nu}, \quad (4.2.45)$$

which however violates the  $C_2$ -spurionic and therefore will not be considered in the following.

The potential given in eq. (4.2.26) can be specialized for the gauge contributions as:

$$V_{\text{gauge}} = \frac{m_*^4}{16\pi^2} \sum_{i=1}^2 \sum_{\tilde{g}=g,g'} \frac{1}{g_*^2} c_{\tilde{g}}^{(i)} \mathcal{I}_{\tilde{g}}^{(i)}, \quad (4.2.46)$$

where  $c_{g,g'}^{(i)}$  are  $\mathcal{O}(1)$  coefficients.

Since the gauge contribution to the potential is subleading with respect to the fermionic one, we fix all the  $c_{g,g'}^{(i)}$  to 1.

If we generically denote by  $c_i$  the  $\mathcal{O}(1)$  coefficients, we introduce three different ranges of variations for them:

- *strictly* natural coefficients:  $0.2 \leq |c_i| \leq 5$ ;
- *loosely* natural coefficients:  $0.1 \leq |c_i| \leq 10$ ;
- unnatural coefficients:  $|c_i| < 0.1$  or  $|c_i| > 10$ .

### 4.3 pNGBs dynamics

In this section, we discuss the dynamics of the pNGBs; in particular, section 4.3.1 is dedicated to the structure of the vacuum of the theory, while we discuss the spectrum and the interactions of the pNGBs in sections 4.3.2 and 4.3.3, respectively.

#### 4.3.1 Structure of the vacuum

The pNGBs potential  $V$  is given by the sum of the contributions in eqs. (4.2.31) and (4.2.46); its minimum can be found in terms of the misalignment angles  $\theta_1$  and  $\theta_2$  (or, equivalently from eq. (4.2.12),  $\xi$  and  $\beta$ ) by solving for two of the free  $\mathcal{O}(1)$  coefficients. We choose to solve for  $c_{(1,0)}^{(1)}$  and  $c_{(1,1)}^{(1)}$ , checking a posteriori that the solution lies within the desired naturalness range. At leading order in  $y_{L,R}/g_* < 1$ , we have:

$$\xi = \sin^2 \theta_1 + \sin^2 \theta_2 \approx \frac{2N_c y_L^4 c_{(2,0)}^{(1)} + g_*^2 \left( N_c y_L^2 c_{(1,0)}^{(1)} - 3g^2 c_g^{(1)} - g'^2 c_{g'}^{(1)} \right)}{N_c y_L^4 c_{(2,0)}^{(1)}}. \quad (4.3.1)$$

A tuning among the coefficients in the numerator must be imposed in order to reproduce the desired fine tuning, the amount of which is of order  $\Delta \sim \xi^{-1}$ . As already discussed in ref. [205], a hierarchy  $\theta_2 \ll \theta_1$ , i.e.  $\beta \ll 1$ , can be naturally obtained; in fact, we have:

$$\tan \beta = \frac{\sin \theta_2}{\sin \theta_1} \approx \frac{N_c c_{(1,1)}^{(1)} y_L^2 y_R^2 \sin 2\theta_t}{2g_*^2 (g'^2 c_{g'}^{(1)} + 2N_c y_R^2 c_{(0,1)}^{(1)} \cos 2\theta_t)}. \quad (4.3.2)$$

In the following, we will be mainly interested in two regions of the parameter space:  $\theta_t \approx \pi/2$  and  $\theta_t \approx \pi/4$ . For  $\theta_t \approx \pi/2$ , a strong suppression is naturally obtained; furthermore, for  $g' \ll y_R \cos 2\theta_t$ , we have  $\tan \beta \approx y_L^2/g_*^2 \tan 2\theta_t$  which is small for  $y_L < g_*$ . For  $\theta_t \approx \pi/4$ , instead, the term proportional to  $g'^2$  cannot be neglected, but values of  $\beta \sim 0.1$  are still naturally obtained.

### 4.3.2 Spectrum of the pNGBs

Since  $\beta$  is always naturally small in the regions of parameter space we consider, we can perform a power expansion in the masses of the pNGBs obtained from the potential. Because of the symmetries of the model, a non-diagonal mass matrix between  $\Pi_4$  and  $\Pi_8$  in general arises, and it can be diagonalized via an  $\text{SO}(2)$  transformation; it turns out that the diagonalization angle  $\alpha$  is  $\alpha \approx \beta$ .

Once the VEV of the theory is determined, i.e. the conditions on  $\xi$  and  $\beta$  have been imposed, we can find the expression for the Higgs mass; at leading order in  $\xi$  and  $\beta$ , and neglecting contributions from two loops and gauge invariants, we find:

$$\begin{aligned} m_h^2 &\approx \frac{N_c f^2 \xi}{16\pi^2} \left( 2y_L^4 c_{(2,0)}^{(1)} + y_R^4 c_{(0,2)}^{(1)} (3 + 4 \cos 2\theta_t + \cos 4\theta_t) \right) \\ &\approx \frac{N_c g_*^2}{8\pi^2} m_t^2 \left( 2 \frac{y_L^2}{y_R^2} c_{(2,0)}^{(1)} + \frac{y_R^2}{y_L^2} c_{(0,2)}^{(1)} (3 + 4 \cos 2\theta_t + \cos 4\theta_t) \right), \end{aligned} \quad (4.3.3)$$

where in the second line we substituted the expression for the top-Yukawa (cf. eq. (4.2.25)); we then solve for the coefficient  $c_{(2,0)}^{(1)}$ , by using the experimental value  $m_h \approx 125$  GeV.

A small value of  $g_*$ , i.e. light top partners, helps to avoid a further tuning in order to obtain the correct Higgs mass; for this reason, in the numerical analysis, we fix  $g_* = 3$

Given that the mass matrix is diagonal, the masses of other pNGBs,  $H_0$ ,  $A_0$ ,  $H_\pm$ ,  $\eta$  and  $\kappa$  can be easily determined as functions of the remaining coefficients; to leading order in  $\xi$ , these read:

$$m_{H_0}^2 \approx -N_c \frac{y_R^2}{8\pi^2} \left( c_{(0,1)}^{(1)} + \frac{y_L^2}{8\pi^2} c_{(1,1)}^{(2)} \right) m_*^2 \cos(2\theta_t), \quad (4.3.4a)$$

$$m_{A_0}^2 \approx m_{H_0}^2, \quad (4.3.4b)$$

$$m_{H_\pm}^2 \approx m_{H_0}^2 - \frac{m_h^2}{2}, \quad (4.3.4c)$$

$$m_\eta^2 \approx N_c \frac{y_R^2}{8\pi^2} \left( c_{(0,1)}^{(1)} + \frac{y_L^2}{8\pi^2} c_{(1,1)}^{(2)} \right) m_*^2 \cos^2 \theta_t, \quad (4.3.4d)$$

$$m_\kappa^2 \approx N_c \frac{y_R^2}{8\pi^2} \left( c_{(0,1)}^{(1)} + \frac{y_L^2}{8\pi^2} c_{(1,1)}^{(2)} \right) m_*^2 \sin^2 \theta_t. \quad (4.3.4e)$$

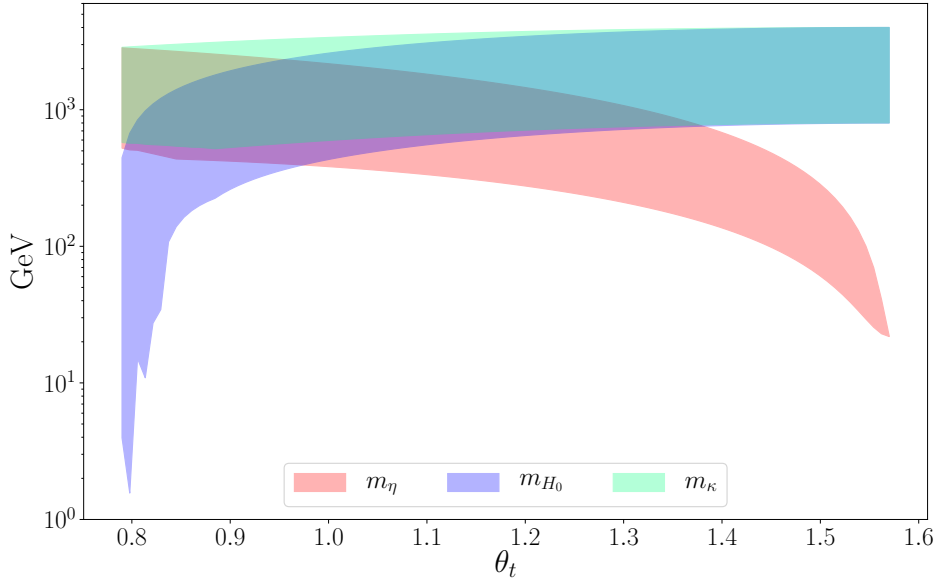


Figure 4.2: Mass spectrum for  $\xi = 0.061$ ,  $\beta = 0.1$  and  $g_* = 3$ . The bands are obtained by varying  $c_{(0,1)}^{(1)}$ ,  $c_{(0,2)}^{(1)}$ ,  $c_{(0,2)}^{(2)}$  and  $c_{(1,1)}^{(2)}$  in the strictly natural range,  $|c_i| \in [0.2, 5]$ .

As we can see,  $H_0$ ,  $A_0$  and  $H_{\pm}$  are almost degenerate in mass. We assume in the following that  $\pi/4 < \theta_t < \pi/2$  and  $c_{(0,1)}^{(1)}, c_{(1,1)}^{(2)} > 0$ . When  $\theta_t \approx \pi/2$ , also the first order in  $\xi$  has to be included in the estimate for  $m_{\eta}$ ; it turns out that:

$$m_{\eta}^2 \approx N_c c_{(0,1)}^{(1)} \frac{y_R^2}{8\pi^2} m_*^2 \cos^2 \theta_t + \xi \frac{m_h^2}{2}. \quad (4.3.5)$$

The spectrum is shown in fig. 4.2 for  $\xi = 0.061$  and  $\beta = 0.1$ , as well as different values of  $c_{(0,1)}^{(1)}$ ,  $c_{(0,2)}^{(1)}$ ,  $c_{(0,2)}^{(2)}$  and  $c_{(1,1)}^{(2)}$ . The two most promising regions are for  $\theta_t \approx \pi/2$ , where  $\eta$  is by far the lightest pNGB (other than the SM Higgs), with a mass  $m_{\eta} \sim \mathcal{O}(100 \text{ GeV})$ , while all other pNGBs have  $\mathcal{O}(1 \text{ TeV})$  masses and do not participate directly to the phenomenology; a second potentially interesting region is for  $\theta_t \gtrsim \pi/4$ , where  $\eta$  and  $\kappa$  are very close in mass (but  $\eta$  is always lighter), both of  $\mathcal{O}(1 \text{ TeV})$ ; such a region could be interesting for two reasons: on the one hand, there could be coannihilations between  $\eta$  and  $\kappa$ , while on the other hand there could be non-thermal effect due to the decay of  $\kappa$  after its freeze-out.

### 4.3.3 Interactions among the pNGBs

In order to study the pNGBs interactions, it is convenient to consider separately those coming from CCWZ and the ones coming from partial compositeness and the potential.

#### Interactions from CCWZ

The CCWZ Lagrangian in eq. (4.2.13) contains pNGB interactions with the SM gauge bosons, as well as derivative interactions among the pNGBs. These can be effectively

described as:

$$\begin{aligned}
\mathcal{L}_\Pi^{(2)} \supset & \mathcal{L}_{\text{kin}} + \left( m_W^2 W_\mu^+ W_\mu^- + \frac{m_Z^2}{2} Z_\mu Z^\mu \right) \left( 1 + \frac{2g_V}{v} h + \frac{b_h}{v^2} h^2 + \frac{\lambda_\eta^{(V)}}{2v^2} \eta^2 + \frac{\lambda_\kappa^{(V)}}{2v^2} \kappa^2 + \dots \right) \\
& - \frac{2}{v} \left( g_{H_0 W} m_W^2 W_\mu^+ W_\mu^- + \frac{g_{H_0 Z} m_Z^2}{2} Z_\mu Z^\mu \right) H_0 \\
& - \frac{k_{\text{der}}}{4v^2} \left[ [\Phi_1^2 (\partial_\mu \Phi_1)^2 - (\Phi_1 \partial_\mu \Phi_1)^2] + [\Phi_2^2 (\partial_\mu \Phi_2)^2 - (\Phi_2 \partial_\mu \Phi_2)^2] + \right. \\
& \quad \left. 2 [\Phi_1 \Phi_2 (\partial_\mu \Phi_1 \partial^\mu \Phi_2) - (\Phi_1 \partial_\mu \Phi_2) (\Phi_2 \partial_\mu \Phi_1)] + \left( \Phi_1 \overset{\leftrightarrow}{\partial}_\mu \Phi_2 \right)^2 \right] \\
& - \frac{m_W m_Z}{2v} g_{H_+ V} W_\mu^- Z^\mu H_+ + \text{h.c.} + \dots
\end{aligned} \tag{4.3.6}$$

where  $\mathcal{L}_{\text{kin}}$  contains the pNGB kinetic terms,  $k_{\text{der}} = 2\xi/3$ , and  $\Phi_{1,2}$  are the two pNGB fiveplets of *physical* fields introduced in eq. (4.2.6); the expressions for the effective couplings can be found in appendix 4.C. In writing the equation above, we neglected all the couplings which break the custodial symmetry and which become negligible once the limits from EWPTs are taken into account; we also omitted interactions with two gauge bosons and two pNGBs, being less relevant for the phenomenology discussed in the following.

It is worth noticing that interactions with three pNGBs and two derivatives, such as  $\partial_\mu \eta \partial^\mu \eta h$ , are absent from the Lagrangian above; this might seem surprising, since such interactions have been long known to be present in similar scenarios, and their relevance has been often stressed (see, e.g., refs. [200–202, 210]). These usually arise from  $\mathcal{O}(\Pi^4)$  terms, once the Higgs(es) takes a VEV; however, since we employ a parametrization in which pNGBs do not take a VEV, these terms are not generated. Another way to easily understand their absence is to set to zero the gauge and Yukawa couplings: in this case, the global symmetry is exact and all vacua are degenerate, so that the SO(5) and SO(5)' subgroups are physically equivalent. In this limit, the two-derivative NGBs interactions start at  $\mathcal{O}(\Pi^4)$  in both vacua (and are of the form specified in eq. (4.3.6)). Now, switching on the gauge and Yukawa couplings selects SO(5)' as the true vacuum; however, since derivative interactions do not depend on these couplings, and since in our descriptions fields do not take a VEV, the derivative interactions are not affected and therefore cubic ones are not generated.

The connection with the description most commonly employed in the literature (where NGBs are excitations around the *gauge* vacuum SO(5), with the Higgs taking a VEV) can be easily obtained via a non-linear field redefinition (see, e.g., refs. [202, 205]); for example, in the limit of  $\theta_2 = 0$  this is given by:

$$h \rightarrow \tilde{h} + \theta_1 \frac{\tilde{\eta}^2}{3f} + \mathcal{O}(\theta_1^2), \tag{4.3.7}$$

$$\eta \rightarrow \tilde{\eta} - \theta_1 \frac{\tilde{\eta} \tilde{h}}{3f} + \mathcal{O}(\theta_1^2), \tag{4.3.8}$$

where  $\tilde{h}$  and  $\tilde{\eta}$  are the physical fields in the *gauge* description.

Such a transformation generates cubic derivative interactions from the kinetic terms, as well as non-derivative interactions from the pNGBs mass terms; the net effect of this is to keep physical observables invariant under such transformations.

## Interactions with fermions and from the potential

The relevant interactions between pNGBs and SM quarks are:

$$\mathcal{L}_q \supset -\frac{m_q}{v} \bar{q} q \left( k_q h + k_{H_0 q} H_0 - \frac{g_q}{2v^2} \eta^2 + \frac{g_{\kappa q}}{2v^2} \kappa^2 \right) - \frac{g_{\eta \kappa q}}{v^2} m_q \eta \kappa \bar{q} \gamma^5 q. \quad (4.3.9)$$

As far as the potential is concerned, instead, we have:

$$\begin{aligned} V \supset & -\frac{g_{\eta h}}{2} v \eta^2 h - \frac{g_{\eta H_0}}{2} v \eta^2 H_0 - \frac{g_{\kappa h}}{2} v \kappa^2 h - \frac{g_{\kappa H_0}}{2} v \kappa^2 H_0 \\ & - \frac{\lambda_{\eta h}}{4} \eta^2 h^2 - \frac{\lambda_{\eta H_0}}{4} \eta^2 H_0^2 + \frac{\lambda_{\eta A_0}}{4} \eta^2 A_0^2 + \frac{\lambda_{\eta H_+}}{2} \eta^2 H_+ H_- \\ & - \frac{g_{A_0 h}}{2} v h A_0^2 - \frac{g_{A_0 H_0}}{2} v H_0 A_0^2 - g_{H_+ h} v h H_+ H_- - g_{H_+ H_0} v H_0 H_+ H_- \\ & + \frac{m_h^2}{2v^2} \lambda v h^3 - \frac{\lambda_{H_0}}{6} v H_0^3 + \frac{g_{H_0}}{2} v h H_0^2 - \frac{g_{H_0 h h}}{2} v h^2 H_0 \\ & - \frac{\lambda_{\kappa h}}{4} \kappa^2 h^2 - \frac{\lambda_{\kappa H_0}}{4} \kappa^2 H_0^2 + \frac{\lambda_{\kappa A_0}}{4} \kappa^2 A_0^2 + \frac{\lambda_{\kappa H_+}}{2} \kappa^2 H_+ H_-. \end{aligned} \quad (4.3.10)$$

Finally, we can consider effective interactions between the pNGBs and the gluon, obtained by integrating out the top at 1 loop; these read:

$$\mathcal{L}_g^{t\text{-loop}} \supset \frac{g_{gh}}{v} h G_{\mu\nu}^a G_a^{\mu\nu} + \frac{g_{gH_0}}{v} H_0 G_{\mu\nu}^a G_a^{\mu\nu} + \frac{g_{g\eta}}{v^2} \eta^2 G_{\mu\nu}^a G_a^{\mu\nu} \quad (4.3.11)$$

Even in this case, the expressions for the effective couplings can be found in appendix 4.C. We require them to be always less than  $4\pi$  for perturbative reasons: this usually forces  $c_{(0,1)}^{(1)}$  to be smaller than 1.

## 4.4 Thermal dark matter scenario

From fig. 4.2, we see that a first region of interest is for  $\theta_t \lesssim \pi/2$ : in this case,  $\eta$  is much lighter than all other pNGBs (with the exception of the Higgs) and is the DM candidate; the abundance is generated through standard freeze-out. As already pointed out, in addition,  $\beta$  is naturally small, and no further tuning is necessary. Finally, we can see from eq. (4.2.25) that the top mass is suppressed, requiring either a large  $c_t$  or  $y_{LYR} \gtrsim g_*$ : for naturalness reasons, we choose the second option, and take  $y_L = 2$ ,  $y_R = 3 = g_*$ ; other choices are possible, but we do not expect them to lead to a significant change in the results.

In principle, also the region around  $\theta_t = \pi/4$  could be interesting, because coannihilations between  $\eta$  and  $\kappa$  could lead to a thermal relic abundance; we checked, however, that this is not the case, and the correct relic density cannot be reproduced.

In section 4.4.1, we determine the relic abundance of DM predicted by the model; in sections 4.4.2 to 4.4.4, we consider the limits from LHC searches, DD and ID, respectively, while we summarize the results in section 4.4.5.

### 4.4.1 Relic Density

In the region  $\theta_t \lesssim \pi/4$ , the main contribution to the DM relic density come from annihilations of  $\eta$  into SM gauge bosons, Higgs and top quark; other contributions, such as

$\eta\eta \rightarrow VV^*$ , with  $V = W, Z$ , can be important at low masses, before the threshold for on-shell production.

The thermally-averaged cross sections for the main annihilation channels are:

$$\langle\sigma v_{\text{rel}}\rangle_{\eta\eta\rightarrow VV} = \frac{\alpha_V}{32\pi m_\eta^2} \frac{m_V^4}{v^4} \left| \lambda_\eta^{(V)} + \frac{2g_{\eta h}g_V v^2}{4m_\eta^2 - m_h^2 + im_h\Gamma_h} - \frac{2g_{\eta H_0}g_{H_0V} v^2}{4m_\eta^2 - m_{H_0}^2} \right|^2 \left[ 2 + \left( \frac{2m_\eta^2 - m_V^2}{m_V^2} \right)^2 \right] \sqrt{1 - \frac{m_V^2}{m_\eta^2}} \quad (4.4.1a)$$

$$\langle\sigma v_{\text{rel}}\rangle_{\eta\eta\rightarrow hh} = \frac{1}{64\pi m_\eta^2} \left| \lambda_{\eta h} + \frac{3g_{\eta h}\lambda m_h^2}{4m_\eta^2 - m_h^2 + im_h\Gamma_h} - \frac{4g_{\eta H_0}g_{H_0hh} v^2}{4m_\eta^2 - m_{H_0}^2 + im_{H_0}\Gamma_{H_0}} - \frac{2g_{\eta h}^2 v^2}{m_h^2 - 2m_\eta^2} + \frac{k_{\text{der}}(5m_\eta^2 - m_h^2)}{v^2} \right|^2 \sqrt{1 - \frac{m_h^2}{m_\eta^2}} \quad (4.4.1b)$$

$$\langle\sigma v_{\text{rel}}\rangle_{\eta\eta\rightarrow q\bar{q}} = \frac{3}{4\pi} \frac{m_q^2}{v^4} \left| g_q + \frac{g_{\eta h}k_q v^2}{4m_\eta^2 - m_h^2 + im_h\Gamma_h} - \frac{g_{\eta H_0}k_{H_0q} v^2}{4m_\eta^2 - m_{H_0}^2} \right|^2 \left( 1 - \frac{m_q^2}{m_\eta^2} \right)^{\frac{3}{2}}, \quad (4.4.1c)$$

with  $\alpha_V = 1$  ( $1/2$ ) for  $W$  ( $Z$ ).

The thermally-averaged cross section for the process  $\eta\eta \rightarrow VV^*$  is instead:

$$\langle\sigma v_{\text{rel}}\rangle_{\eta\eta\rightarrow VV^*} = \sum_f \frac{k_{(V)}^2 N_c^{(f)}}{1536\pi^3 m_\eta^2} \frac{m_V^4}{v^4} \left( \lambda_\eta^{(V)} + \frac{2g_{\eta h}g_V v^2}{4m_\eta^2 - m_h^2} \right)^2 F(\varepsilon_V, \zeta_f), \quad (4.4.2)$$

where we neglected the exchange of  $H_0$  in the  $s$ -channel,  $N_c^{(f)}$  is the number of colours of the final state  $f$ , and:

$$F(\varepsilon_V, \zeta_f) = \int_{\varepsilon_V}^{1 + \frac{\varepsilon_V^2}{4} - \zeta_f^2} dy \frac{\sqrt{y^2 - \varepsilon_V^2}}{(1-y)^2} \frac{1}{\varepsilon_V^2} \sqrt{1 - \frac{4\zeta_f^2}{4 - 4y + \varepsilon_V^2}} \left\{ (\tau_{(V)}^2 + \chi_{(V)}^2) [4y^2 - 12\varepsilon_V^2 y + 8\varepsilon_V^4 + 3\varepsilon_V^4] + \frac{2\zeta_f^2}{4 - 4y + \varepsilon_V^2} \left[ \tau_{(V)}^2 (4y^2 - 12\varepsilon_V^2 y + 8\varepsilon_V^4 + 3\varepsilon_V^4) + 2\chi_{(V)}^2 (2y^2 + 12\varepsilon_V^2 y - 14\varepsilon_V^4 - 3\varepsilon_V^4) \right] \right\} \quad (4.4.3)$$

with:

$$k_{(V)} = \begin{cases} \frac{g}{2\sqrt{2}} \\ \frac{\sqrt{g^2 + g'^2}}{2} \end{cases}, \quad \tau_{(V)} = \begin{cases} 1 \\ c_V \end{cases}, \quad \chi_{(V)} = \begin{cases} 1 & , \quad V = W \\ c_A & , \quad V = Z \end{cases}, \quad (4.4.4)$$

$\varepsilon_V \equiv \frac{m_V}{m_\eta}$  and  $\zeta_f \equiv (m_{f_1} + m_{f_2})/(2m_\eta)$ ,  $f_1$  and  $f_2$  being the final states of  $V^*$  decay. Obviously, also the coefficients  $\tau_{(V)}$  and  $\chi_{(V)}$  depend on the final states.

The relic abundance can then be computed using eq. (2.3.19), and the result is shown in fig. 4.3. The darker (lighter) region is obtained by letting the coefficients vary inside

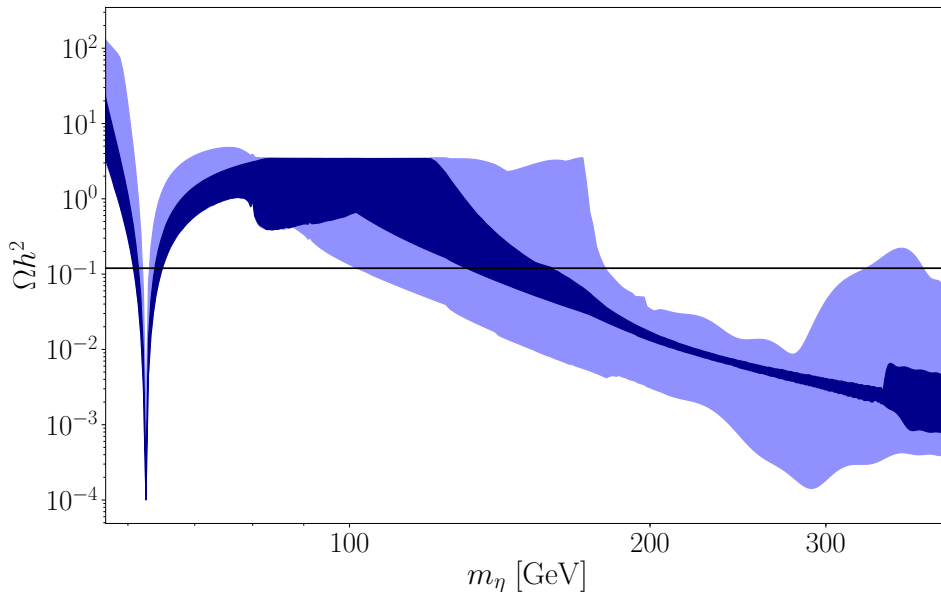


Figure 4.3: Relic density as a function of the DM mass  $m_\eta$ , for  $\xi = 0.061$  (corresponding to  $f = 1$  TeV) and  $\beta = 0.1$ ; the black line corresponds to the measured value  $\Omega h^2 = 0.1198$  [46]. The dark (light) blue region is obtained by letting the coefficients in the potential vary within the strictly (loosely) natural range (see section 4.2.3).

the strictly (loosely) natural range, with the nomenclature introduced in section 4.2.3.

The reason why a plateau appears for  $m_\eta \lesssim m_h$  is because the cross section is dominated by annihilations into SM gauge bosons: since the latter do not depend on the  $c_i$ 's, the annihilation cross section is always bounded from below and, since  $\Omega h^2 \sim 1/\langle\sigma v\rangle$ , this corresponds to a maximum in the relic density. The situation changes at larger masses, when new annihilation channels open up, where it is possible that a cancellation in the main contributions to the effective cross section occurs: this is precisely the case in the region  $m_\eta \approx 400$  GeV of fig. 4.3, where  $\eta$  is sufficiently heavy so that the exchange of  $H_0$  compensates the exchange of  $h$  in  $s$ -channel, the two contributions having opposite signs. The consequence is an enhancement in the relic density, even if one could naively expect it to decrease for large masses.

The most important effective coupling is  $g_{\eta h}$ , describing the interactions between two  $h$ 's and one  $\eta$ . It contributes to different processes with different signs, so it is non-trivial to describe its role analytically; the results highly depend on the parameters  $\xi$  and  $\beta$  and, guided by EWPTs, we decide to focus our attention on  $\xi = 0.061$  (corresponding to  $f = 1$  TeV) and  $\beta = 0.1$ . From fig. 4.3, we see that there are two good mass regimes which give the correct relic density,  $\Omega h^2 = 0.1198$  [46], for strictly natural coefficients:  $m_\eta \approx m_h/2$  and  $m_\eta \approx 150$  GeV; a third one, at  $m_\eta \approx 400$  GeV, also reproduces the correct relic density if the coefficients are allowed to vary inside the loosely natural range. However, as we will show, this high mass range is already excluded by DD experiments.



## 4.4.2 LHC searches

In the region of parameter space where  $m_\eta \leq 62.5$  GeV, the Higgs can decay into two DM particles,  $h \rightarrow \eta\eta$ . Experimental constraints on invisible Higgs decays have been obtained by ATLAS and CMS [228, 229] for various possible assumptions on the Higgs couplings to SM particles. Since the couplings of the Higgs to quarks and gauge bosons in our model are different from the SM ones, the widths of the decays into SM particles have to be appropriately rescaled. The invisible branching ratio is defined as:

$$BR_{\text{inv}} \equiv \frac{\Gamma_{h \rightarrow \eta\eta}}{\Gamma_{h \rightarrow \eta\eta} + \Gamma_{SM}^{(\xi, \beta)}}, \quad (4.4.5)$$

where  $\Gamma_{SM}^{(\xi, \beta)}$  is the correction to the SM decay widths due to the composite sector, and for our model is

$$\Gamma_{SM}^{(\xi, \beta)} \simeq g_V^2 \Gamma_{h \rightarrow WW} + g_V^2 \Gamma_{h \rightarrow ZZ} + k_t^2 \Gamma_{h \rightarrow gg} + k_b^2 \Gamma_{h \rightarrow b\bar{b}} + \Gamma_{h \rightarrow \tau\tau}. \quad (4.4.6)$$

Anyway, we do not expect a significant departure from the SM prediction, given the small values of  $\xi$  and  $\beta$  allowed by EWPTs. We take as an experimental bound  $BR_{\text{inv}} < 19\%$  at 95% CL [228]; at HL, LHC will reach a 95% CL exclusion sensitivity of 1.9%, while future electron-positron colliders could be able to reach sub-percent precision (see, e.g., ref. [230] for a recent review of Higgs boson measurements at future colliders).

In our model, the invisible Higgs decay width is given by:

$$\Gamma_{h \rightarrow \eta\eta} = \frac{g_{\eta h}^2}{32\pi m_h} v^2 \sqrt{1 - \frac{4m_\eta^2}{m_h^2}}, \quad (4.4.7)$$

which depends on the coefficients  $c_i$ 's via the effective coupling  $g_{\eta h}$ . The corresponding prediction for the invisible branching ratio of the Higgs, obtained by letting the  $c_i$ 's vary inside the strictly (loosely) natural range are shown as dark (light) yellow regions in fig. 4.4; the predictions of the model are always below the current bound, while HL-LHC will be able to test most of this region of the parameter space with this kind of searches. On the same plot, we show in blue the narrow region where the correct relic density is reproduced.

The production of  $\eta$ 's (either direct, or through the decay of some heavier scalars such as  $H_0$ ) could lead to missing energy traces; in this case, we should look at specific tags: in our model, the most relevant ones will be one energetic jet, MJ, or two well-separated jets, resulting in VBF signature. In both cases, it is important to include the effective coupling of gluons to the massive scalars, given by eq. (4.3.11), since this gives the main contribution to the production cross section. We implemented the model in FEYNRULES [189, 231] and generated simulated events with MADGRAPH5 [188]; contributions from diagrams involving  $H_0$  can be relevant, and were therefore included. For masses above 50 GeV, neither monojet nor VBF put any constraints on the model, being the signal always at least an order of magnitude below the experimental limits (see, e.g., refs. [96, 232]) for any value of  $\xi$ ,  $\beta$  allowed by EWPTs.

Overall, DM searches at LHC do not put important constraints on the parameter space of our model.

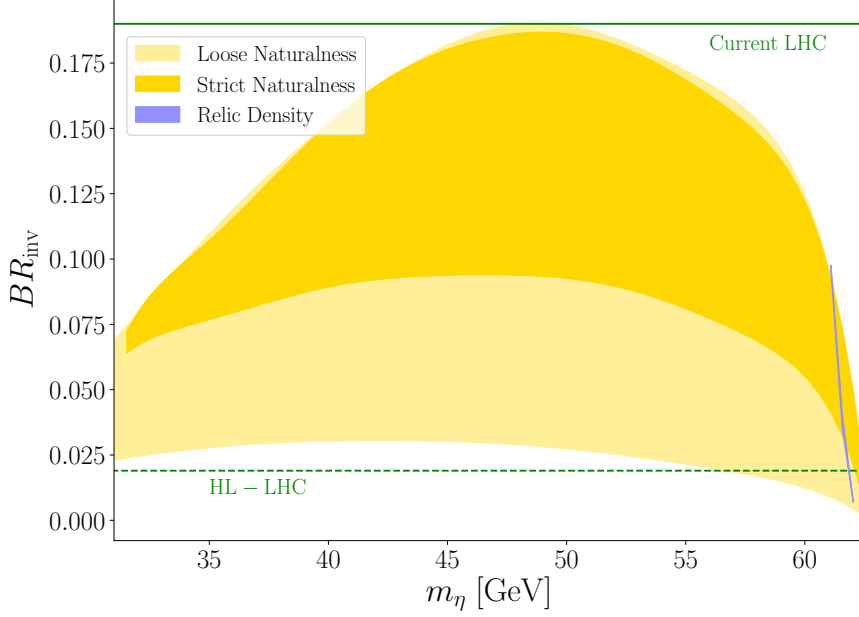


Figure 4.4: Branching ratio of invisible Higgs decays as a function of the DM mass. The dark (light) yellow region corresponds to strictly (loosely) natural  $\mathcal{O}(1)$  coefficients. The current bound,  $BR_{\text{inv}} < 0.19$ , is shown as a green solid line, while the HL-LHC prospect is shown with the dashed line. Finally, the region of the parameter space where the observed relic density is reproduced is shown in blue.

### 4.4.3 Direct detection

The DM candidate  $\eta$  can interact with quarks with both a contact interaction (cf. (4.3.9)) and an  $s$ -channel exchange of  $h$  and  $H_0$ . According to the general discussion of section 2.4.1, we can parametrize the interaction Lagrangian as:

$$\mathcal{L}_{\text{DD}}^{(\text{eff})} = \sum_q a_q m_q \eta^2 \bar{q} q. \quad (4.4.8)$$

The coefficient  $a_q$  is computed to:

$$a_q = \frac{1}{2} \left[ \frac{g_q}{v^2} - \left( k_q \frac{g_{\eta h}}{m_h^2} - k_{H_0 q} \frac{g_{\eta H_0}}{m_{H_0}^2} \right) \right]. \quad (4.4.9)$$

The choice of aligning the Yukawa matrices in order to avoid FCNCs, discussed in section 4.2.2, leads to  $a_u = a_c = a_t$  and  $a_d = a_s = a_b$ .

By repeating the steps that led to eqs. (2.4.11) and (2.4.14), the spin-independent nucleon cross section turns out to be:

$$\sigma_{\text{SI}} = \frac{\mu_{\chi N}^2}{\pi m_\chi^2} \left( \frac{Z f_p + (A - Z) f_n}{A} \right)^2, \quad (4.4.10)$$

with:

$$f_{n,p} = \sum_{q=u,d,s} f_{T_q}^{(n,p)} a_q m_{n,p} + \frac{2}{27} f_{T_G} \sum_{q=c,b,t} a_q m_{n,p}. \quad (4.4.11)$$

We take  $f_{T_u}^{(n)} = 0.026$ ,  $f_{T_d}^{(n)} = 0.020$  (and the opposite for  $p$ ),  $f_{T_s}^{(n)} = 0.043 = f_{T_s}^{(p)}$  [77] and  $f_{T_G} = 0.911$  [233].

Given that the value of  $a_q$  in eq. (4.4.9) depends on the coefficients  $c_i$ , a cancellation in the scattering amplitude can occur, allowing to evade bounds from DD; currently, the strongest constrain comes from the XENON1T experiment [234].

As can be seen in fig. 4.5, the strongest restrictions on the parameter space of our model come from DD; for this reason, we also show projections for the future XENONnT experiment [235]; the majority of the parameter space, for the benchmark values of  $\xi$  and  $\beta$  we consider, will be tested.

#### 4.4.4 Indirect detection

We briefly discuss bounds from ID, although somewhat beyond our main interests. In particular, we focus on limits from dwarf spheroidal galaxies (dSphs) given by Fermi-LAT, and reported in ref. [81]; the relevant one for our model is given by DM-annihilation into  $b\bar{b}$ , and shown in fig. 2.7.

In the region  $m_\eta \approx m_h/2$ , only the direct process  $\eta\eta \rightarrow b\bar{b}$  has to be considered; for larger  $m_\eta$ , instead, also the intermediate productions of  $W$ ,  $Z$ ,  $h$  (and possibly other NGBs) are important: as a conservative estimate, we assume that these intermediate states completely decay into  $b\bar{b}$ ; we checked that the inclusion of the corresponding branching ratios does not alter the general results.

Similarly to what was done in ref. [210], we decide not to consider anti-protons bounds from AMS-02, due to the still unclear size of the systematic uncertainties, and limit ourselves to dSphs.

#### 4.4.5 Discussion

As anticipated, there are three regions in which the correct relic density is reproduced, at least with loosely natural  $\mathcal{O}(1)$  coefficients:  $m_\eta \approx m_h/2$ ,  $m_\eta \approx 150$  GeV and  $m_\eta \approx 400$  GeV.

We choose as benchmark values  $\xi = 0.061$  (corresponding to  $f = 1$  TeV) and  $\beta = 0.1$ , and we show the main results in the  $m_\eta$ - $g_{\eta h}$  plane in fig. 4.5 for loosely natural coefficients. The orange (purple) hatched area is excluded by DD (ID), while in the blue one the correct relic density is reproduced. The grey region finally corresponds to unnatural coefficients.

##### Low mass range ( $m_\eta \approx m_h/2$ )

In the first region, the correct relic density is reproduced for masses just below and just above the on-shell Higgs production threshold of 62.5 GeV. The corresponding mass range is clearly very narrow, being the correct relic abundance obtained thanks to the Higgs resonance (this feature is the second of the exceptions described in section 2.3.2); since there is no any dynamical argument for which the DM mass should be in such a narrow range, this first region may be viewed as a rather *ad hoc* one.

Bounds from the Higgs invisible BR and ID do not exclude any parts of the region where the correct relic density is obtained, while DD sets an upper bound on  $g_{\eta h}$ . Anyway, the relevant cross section for ID is below the current bound by just an  $\mathcal{O}(1)$  factor, so that we expect future ID experiments to be able to test this region. In addition, also HL-LHC will probe a large portion of the parameter space (see fig. 4.4).

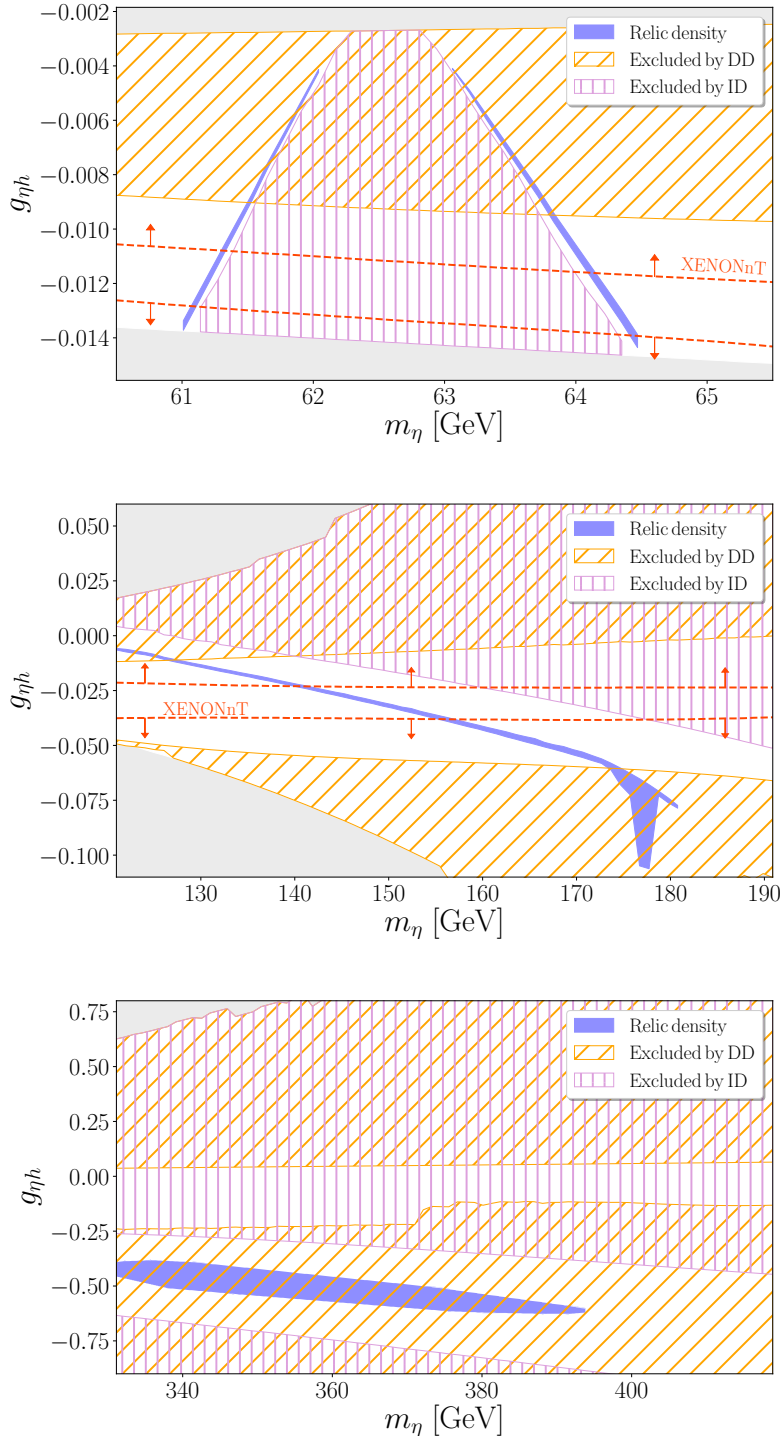


Figure 4.5: Main results for  $\xi = 0.061$ ,  $\beta = 0.1$  and loosely natural  $\mathcal{O}(1)$  coefficients. The blue region corresponds to the  $3\sigma$ -relic density contour; the orange and purple hatched regions are excluded by DD and ID, respectively; the dashed, red lines correspond to prospects of DD bounds from XENONnT; finally, the grey region corresponds to unnatural  $\mathcal{O}(1)$  coefficients.

### Intermediate mass range ( $m_\eta \approx 150$ GeV)

In the second region,  $m_\eta \gtrsim 100$  GeV, the most stringent bounds on the parameter space come from DD and from the requirement of natural  $\mathcal{O}(1)$  coefficient; LHC experiments

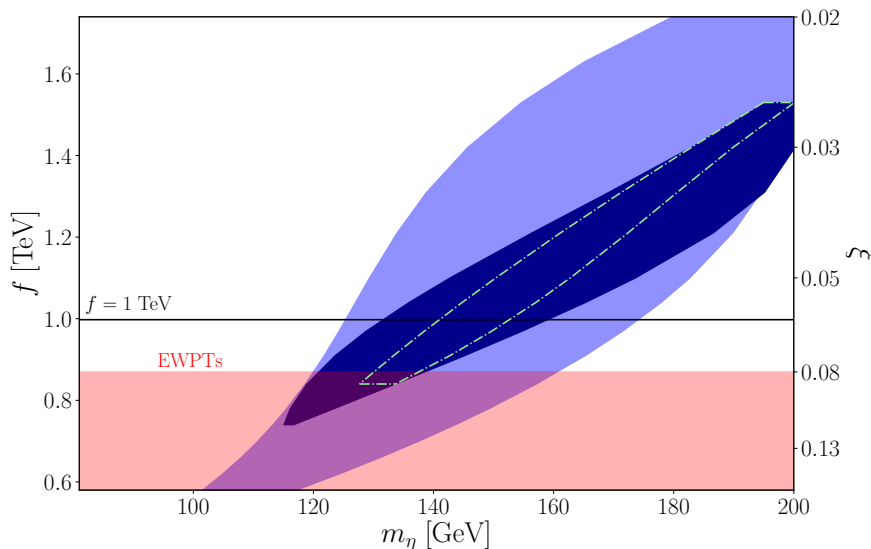


Figure 4.6: The dark (light) blue region represents values of  $m_\eta$  and  $f$  for which it is possible to reproduce the correct relic density at  $3\sigma$ , evade DD constraints, all while having strictly (loosely) natural coefficients  $c_i$ . The red region is excluded by our combined fit of EWPTs and Higgs couplings (see appendix 4.B), while the black horizontal line corresponds to the benchmark value of  $f = 1$  TeV ( $\xi = 0.061$ ) we consider. The green, dashed region corresponds to the projection with DD limits from XENONnT and strictly natural coefficients.

are instead not relevant, and are not expected to significantly improve in the near future; also bounds from ID, although consciously overestimated, do not exclude portions of the parameter space where the correct relic density is reproduced.

Upper and lower bounds on  $m_\eta$  are set by DD results (cf. fig. 4.5); if we considered strictly natural coefficients, then masses below 135 GeV would be excluded.

The feature at  $m_\eta \approx 180$  GeV is because of a cancellation in the cross section for  $\eta\eta \rightarrow t\bar{t}$ , due to the different sign between the effective couplings  $g_{\eta h}$  and  $g_{\eta H_0}$ , as can be seen by looking at eq. (4.4.1c).

Among the three regions in which the correct relic density can be reproduced, this one seems to be the most promising one: on the one hand, bounds from ID are pretty weak and those from DD leave a significant portion of the parameter space available; on the other hand, the relic abundance can be obtained with natural  $\mathcal{O}(1)$  coefficients, without the need of extra fine tuning.

On the one hand, by decreasing the value of  $\xi$  we enlarge the good mass range; on the other hand, this comes at the price of a higher level of fine tuning. For this reason, it is interesting to investigate how the correct DM mass range varies with varying fine tuning; we show the result in fig. 4.6. We see that this models allows for small values of  $f$ , up to  $f \approx 750$  GeV for strictly natural coefficients, and even below 600 GeV for loosely natural ones. The upper bound on  $\xi$  comes from a combination of bounds from EWPTs and Higgs couplings fit: we discuss these constraints in appendix 4.B.

This result should be compared to other similar non-minimal composite DM models in the literature, for which significantly larger values of  $f$  were found to be necessary (see, e.g., refs. [202, 209]).

What happens by varying  $\beta$  is less trivial: in principle, an increase of  $\beta$  would result in a larger dependence on the subleading terms and on the  $c_i$ 's; however, we verified that this is not the case for the values of  $\beta$  allowed by EWPTs.

### Large mass range ( $m_\eta \approx 400$ GeV)

The third region of interest is for  $m_\eta \approx 400$  GeV; as already stated, it turns out that a cancellation between the exchanges of  $h$  and  $H_0$  in  $s$ -channel takes place in the main contributions to the annihilation cross section. Despite this enhancement, the correct relic density can only be reproduced with loosely natural  $\mathcal{O}(1)$  coefficients.

As can be seen from fig. 4.5, the benchmark point we consider is already excluded by current DD constraints; in order to evade this bounds, we should take  $\xi \lesssim 0.01$ ; since this would spoil the virtue of the model, i.e. delivering a viable DM candidate with a relatively low fine tuning, we do not study this region of the mass range any further.

## 4.5 Non-thermal dark matter scenario

The greater complexity of the  $\text{SO}(7) \rightarrow \text{SO}(5) \times \text{SO}(2)$  breaking pattern with respect to the minimal case can lead to a richer DM phenomenology; in particular, the larger number of pNGBs can lead to DM production mechanisms others than standard freeze-out. This can naturally happen in the region around  $\theta_t = \pi/4$ , where the DM candidate,  $\eta$ , is almost degenerate in mass with the other singlet,  $\kappa$  (cf. fig. 4.2).

If  $\eta$  and  $\kappa$  are sufficiently close in mass, it is possible that  $\kappa$  also undergoes thermal freeze-out, and later decays; because of  $P_7$ , which remains unbroken, the final state must include one  $\eta$ : in this scenario, then, it is possible to have a non-thermal production of DM, as opposed to standard thermal freeze-out.

Because of  $CP$ , which is also unbroken, the main decay channels are  $\kappa \rightarrow \eta A_0$  and  $\kappa \rightarrow \eta q \bar{q}$ ; it turns out that only the latter is kinematically allowed, resulting in a further suppression for the decay width due to phase-space.

The decay width for the process  $\kappa \rightarrow \eta q \bar{q}$  is:

$$\Gamma_{\kappa \rightarrow \eta q \bar{q}} = \frac{3}{32\pi^3 m_\kappa} \frac{m_q^2}{v^4} |g_{\eta\kappa q}|^2 \int_{m_\eta}^{\frac{m_\kappa + m_\eta^2 - 4m_q^2}{2m_\kappa}} dq_0 \sqrt{q_0^2 - m_\eta^2} (m_\kappa^2 + m_\eta^2 - 2m_\kappa q_0) \sqrt{1 - \frac{4m_q^2}{m_\kappa^2 + m_\eta^2 - 2m_\kappa q_0}}, \quad (4.5.1)$$

where the expression for the effective coupling  $g_{\eta\kappa q}$  is reported in appendix 4.C.

The lifetime of  $\kappa$  has to be compared to the age of the universe when  $\eta$  freezes-out (which roughly corresponds to the one of the freeze-out of  $\kappa$ , because of the small mass splitting), which is given by:

$$\frac{t_F}{1 \text{ s}} \approx \frac{1.5^2}{\sqrt{g_{*,EU}}} \left( \frac{1 \text{ MeV}}{m_\eta} \right)^2 x_F^2, \quad (4.5.2)$$

with  $g_{*,EU} \approx 100$  being the effective number of relativistic species in the early universe at freeze-out and  $x_F \approx 25$ . Given that  $\Gamma_{\kappa \rightarrow \eta q \bar{q}} \propto m_q^2$ , if  $\Delta m_{\kappa,\eta} \equiv m_\kappa - m_\eta > 2m_t$ , the decay is completely dominated by the  $t\bar{t}$  final state, and it always takes place before  $\kappa$  freezes-out.

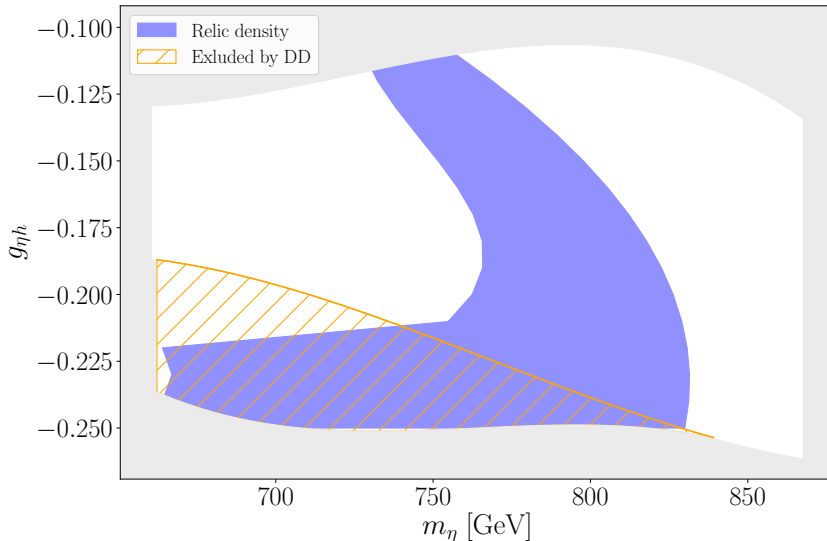


Figure 4.7: Relic density from non-thermal DM production for  $\xi = 0.01$ ,  $\beta = 0.2$ ,  $y_L = 1 = y_R$ ,  $g_* = 3$  and loosely natural  $\mathcal{O}(1)$  coefficients. The blue region corresponds to the  $3\sigma$ -relic density contour; the orange hatched region is excluded by DD; in the grey region the  $\mathcal{O}(1)$  coefficients lie outside the range  $[0.1, 10]$ .

If the decay is sufficiently slow, then, two independent contributions participate to the determination of the relic density: on the one hand,  $\eta$  undergoes standard freeze-out; on the other hand, the temporary abundance of  $\kappa$  is completely converted in DM, given that one  $\eta$  is produced per decay. The total abundance of  $\eta$ , at the end of  $\kappa$ -decays, is given by (see, e.g., ref. [236]):

$$\Omega_{\text{DM}} h^2 = \Omega_{\eta} h^2 + \frac{m_{\eta}}{m_{\kappa}} \Omega_{\kappa} h^2. \quad (4.5.3)$$

Given that  $H_0$ ,  $A_0$ ,  $H_{\pm}$  are all lighter than  $\eta$ , they also have to be included as final states of  $\eta$ - and  $\kappa$ -annihilations; on the contrary, as in standard coannihilations, conversion processes between  $\eta$  and  $\kappa$  are not relevant for the final relic density determination.

We do not report the formulas of the annihilation cross sections, but these can be easily determined from the interactions in eqs. (4.3.6) and (4.3.9) to (4.3.11).

When non-thermal effects take place, it turns out that the two contributions to the relic density are of the same order, i.e.  $\Omega_{\eta} \approx \Omega_{\kappa}$ . Compared to the thermal case, however, a higher level fine tuning on  $\xi$  is needed in order to evade DD constraints.

Similarly to fig. 4.5, we show in fig. 4.7 the results in the  $m_{\eta}$ - $g_{\eta h}$  plane, for  $\xi = 0.01$ ,  $\beta = 0.2$ ,  $y_L = 1 = y_R$ ,  $g_* = 3$ ; in the whole plane,  $\mathcal{O}(1)$  coefficients are allowed to vary within the loosely natural range. Even for non-thermal effects, DD sets the strongest bounds on the model, while ID is completely ineffective. In this plot, the mass splitting is always in the range  $20 \text{ GeV} \lesssim \Delta m_{\kappa, \eta} \lesssim 50 \text{ GeV}$ .

As one can see from eq. (4.3.4d), this range of masses for  $m_{\eta}$  roughly corresponds to  $\theta_t \approx \pi/4$ , as anticipated. While large mass splittings tend to favour a fast decay for  $\kappa$ , non-thermal effects are always possible for small mass differences, although a larger and larger unnaturalness of the coefficients is required, (corresponding to a larger and larger fine tuning for  $\Delta m_{\kappa, \eta}/m_{\eta}$ ).

Despite the higher fine tuning which is needed, the non-thermal production mechanism

for DM represents an intriguing feature; we think this is one of the most peculiar and interesting aspects of the model. The greater level of complexity with respect to the minimal case has been traded for a richer spectrum of NGBs which can play an active role in DM phenomenology.

## 4.A Identification of the physical fields

In this appendix, we provide the general expressions for the embedding of NGBs, and the identification of physical particles.

We parametrize the two fourplets as:

$$\phi_1 = \begin{pmatrix} -\frac{i(h^+ - h^-)}{\sqrt{2}} \\ \frac{h^+ + h^-}{\sqrt{2}} \\ \frac{i(h_0 - h_0^*)}{\sqrt{2}} \\ \frac{h_0 + h_0^*}{\sqrt{2}} \end{pmatrix}, \quad \phi_2 = \begin{pmatrix} -\frac{\xi^+ + \xi^-}{\sqrt{2}} \\ \frac{i(\xi^+ - \xi^-)}{\sqrt{2}} \\ -\frac{\xi_0 + \xi_0^*}{\sqrt{2}} \\ \frac{i(\xi_0 - \xi_0^*)}{\sqrt{2}} \end{pmatrix}. \quad (4.A.1)$$

From eq. (4.2.13) we then obtain the expressions for the eaten Goldstones  $G^\pm$  and  $G^0$ , which read:

$$G^\pm = \mp i(h^\pm \cos \beta + \xi^\pm \sin \beta) \quad (4.A.2a)$$

$$G^0 = \frac{i}{\sqrt{1 - \frac{\xi}{4}(1 - \cos 4\beta)}} \left[ \frac{h_0 - h_0^*}{\sqrt{2}} \cos \beta \sqrt{1 - \xi \sin^2 \beta} + \frac{\xi_0 - \xi_0^*}{\sqrt{2}} \sin \beta \sqrt{1 - \xi \cos^2 \beta} \right] \quad (4.A.2b)$$

The orthogonal fields  $H_\pm$  and  $A_0$  can then be easily found:

$$H_\pm = \mp i(-h^\pm \sin \beta + \xi^\pm \cos \beta) \quad (4.A.3a)$$

$$A_0 = \frac{i}{\sqrt{1 - \frac{\xi}{4}(1 - \cos 4\beta)}} \left[ -\frac{h_0 - h_0^*}{\sqrt{2}} \sin \beta \sqrt{1 - \xi \cos^2 \beta} + \frac{\xi_0 - \xi_0^*}{\sqrt{2}} \cos \beta \sqrt{1 - \xi \sin^2 \beta} \right] \quad (4.A.3b)$$

These formulas are easily inverted to give:

$$\Pi_1 = \frac{1}{\sqrt{2}} [(G^+ + G^-) \cos \beta - (H^+ + H^-) \sin \beta] \quad (4.A.4a)$$

$$\Pi_2 = \frac{i}{\sqrt{2}} [(G^+ - G^-) \cos \beta - (H^+ - H^-) \sin \beta] \quad (4.A.4b)$$

$$\Pi_3 = \frac{1}{\sqrt{1 - \frac{\xi}{4}(1 - \cos 4\beta)}} \left[ G^0 \cos \beta \sqrt{1 - \xi \sin^2 \beta} - A^0 \sin \beta \sqrt{1 - \xi \cos^2 \beta} \right] \quad (4.A.4c)$$

$$\Pi_6 = \Pi_2|_{\beta \rightarrow \beta + \pi/2}, \quad \Pi_7 = -\Pi_1|_{\beta \rightarrow \beta + \pi/2}, \quad \Pi_9 = -\Pi_3|_{\beta \rightarrow \beta + \pi/2}, \quad (4.A.4d)$$



which reduce to eq. (4.2.17) for  $\beta = 0$ .

We define the two remaining degrees of freedom as:

$$\tilde{h} \equiv \frac{h_0 + h_0^*}{\sqrt{2}}, \quad \tilde{H}_0 \equiv -\frac{\xi_0 + \xi_0^*}{\sqrt{2}}. \quad (4.A.5)$$

These states cannot be identified with the SM Higgs  $h$  and the  $CP$ -even component of the second doublet  $H_0$ , since in general the latter are related to  $\tilde{h}$  and  $\tilde{H}_0$  by the rotation:

$$\begin{pmatrix} h \\ H_0 \end{pmatrix} = \begin{pmatrix} \cos \alpha & -\sin \alpha \\ \sin \alpha & \cos \alpha \end{pmatrix} \begin{pmatrix} \tilde{h} \\ \tilde{H}_0 \end{pmatrix}. \quad (4.A.6)$$

As we discuss in text, it turns out that, at leading order,  $\alpha \approx \beta$ .

## 4.B Bounds from EWPTs and Higgs couplings fit

In this appendix, we discuss the restrictions on the parameter space coming from Higgs couplings fit and EWPTs.

In general, given a set  $\{x_i\}$  of values for some variable  $X$ , we can compute the  $\chi^2$  as:

$$\chi^2 = \sum_{i,j} (x_i - \mu_i)(\sigma^2)_{ij}^{-1}(x_j - \mu_j), \quad (4.B.1)$$

where  $\mu_i$  is the expected value of  $x_i$  and  $\sigma^2$  is the covariance matrix. In this parametrization,  $X$  should be thought as a vector, possibly encoding different physical variables.

The covariance matrix  $\sigma^2$  can be obtained from the correlation matrix  $\rho$  as:

$$\sigma_{ij}^2 = \sigma_i \rho_{ij} \sigma_j \quad (\text{no sum over } i, j), \quad (4.B.2)$$

where  $\sigma_i \equiv \sqrt{\sigma_{ii}^2}$  is the uncertainty on  $x_i$ .

Let us suppose that the  $\chi^2$  in eq. (4.B.1) is minimized for the set  $\{\bar{x}_i\}$ ; if the  $x_i$ 's are in turn functions of other variables  $\{y_i\}$ , and we denote by  $\{\bar{y}_i\}$  the values of  $y_i$  corresponding to the minimum chi squared, we can approximate  $\chi^2$  for  $y_i \approx \bar{y}_i$  as:

$$\chi^2 \approx \chi^2(\bar{y}) + \sum_{i,j} \frac{\partial^2 \chi^2}{\partial y_i \partial y_j} (y_i - \bar{y}_i)(y_j - \bar{y}_j) \equiv \chi^2(\bar{y}) + \sum_{i,j} (y_i - \bar{y}_i)(\sigma_y^2)_{ij}^{-1}(y_j - \bar{y}_j). \quad (4.B.3)$$

Therefore, the minimum of the  $\chi^2$  has been shifted from zero to  $\chi^2(\bar{y})$ , which in general does not vanish. However, what matters in order to determine if a given set of values  $\{y_i\}$  is excluded or not, is not  $\chi^2$ , but the difference  $\Delta\chi^2 \equiv \chi^2 - \chi^2(\bar{y})$ .

From  $\sigma_y^2$ , it is possible to compute the uncertainties on  $y_i$ , and then to obtain the new correlation matrix by inverting eq. (4.B.2).

### 4.B.1 Higgs couplings fit

For the fit on Higgs couplings, we refer to [237]; in fig. 22, the correlation matrix in terms of the modifiers  $\{\kappa_{gZ}, \lambda_{Zg}, \lambda_{tg}, \lambda_{WZ}, \lambda_{\gamma Z}, \lambda_{\tau Z}, \lambda_{bZ}\}$  is reported:

$$\rho = \begin{pmatrix} 1 & -0.07 & -0.17 & -0.50 & -0.57 & -0.26 & -0.26 \\ -0.07 & 1 & 0.38 & -0.57 & -0.33 & -0.33 & -0.48 \\ -0.17 & 0.38 & 1 & -0.19 & -0.13 & -0.19 & 0.30 \\ -0.50 & -0.57 & -0.19 & 1 & 0.48 & 0.26 & 0.41 \\ -0.57 & -0.33 & -0.13 & 0.48 & 1 & 0.34 & 0.35 \\ -0.26 & -0.33 & -0.19 & 0.26 & 0.34 & 1 & 0.27 \\ -0.26 & -0.48 & 0.30 & 0.41 & 0.35 & 0.27 & 1 \end{pmatrix} \quad (4.B.4)$$

The definitions of the modifiers, together with the corresponding best-fits and uncertainties, is reported in table 10 of the same paper; in general, a modifier is defined as the ratio between some process and the corresponding one predicted by SM, i.e.  $\kappa_i \equiv \sigma_i/\sigma_i^{\text{SM}}$  or  $\kappa_i \equiv \Gamma_i/\Gamma_i^{\text{SM}}$ .

For simplicity, we consider the mean uncertainty for each modifier, so that:

$$\begin{aligned}
\kappa_{gZ} &\equiv \frac{\kappa_g g_Z}{\kappa_h} = 1.06 \pm 0.07 \\
\lambda_{Zg} &\equiv \frac{g_Z}{\kappa_g} = 1.06 \pm 0.14 \\
\lambda_{tg} &\equiv \frac{k_t}{\kappa_g} = 1.09 \pm 0.14 \\
\lambda_{WZ} &\equiv \frac{g_W}{g_Z} = 0.99 \pm 0.09 \quad , \\
\lambda_{\gamma Z} &\equiv \frac{\kappa_\gamma}{g_Z} = 0.95 \pm 0.08 \\
\lambda_{\tau Z} &\equiv \frac{\kappa_\tau}{g_Z} = 0.95 \pm 0.13 \\
\lambda_{bZ} &\equiv \frac{k_b}{g_Z} = 0.91 \pm 0.17
\end{aligned} \tag{4.B.5}$$

where for  $\{g_W, g_Z, k_b, k_t\}$  we used a different notation with respect to ref. [237], since these are effective couplings which can be directly computed for our model (see appendix 4.C). From table 7 of ref. [237], we read the expressions of  $\{\kappa_g, \kappa_\gamma, \kappa_h\}$  in terms of these effective couplings:

$$\kappa_g^2 = 1.04k_t^2 + 0.002k_b^2 - 0.04k_t k_b \tag{4.B.6a}$$

$$\kappa_\gamma^2 = 1.59g_W^2 + 0.07k_t^2 - 0.67g_W k_t \tag{4.B.6b}$$

$$\begin{aligned}
\kappa_h^2 &= (0.22g_W^2 + 0.03g_Z^2 + 0.58k_b^2 + 0.08\kappa_g^2 + 0.0023\kappa_\gamma^2 + 0.06\kappa_\tau^2 + 0.03\kappa_c^2 \\
&\quad + 0.0015\kappa_{(Z\gamma)}^2 + 0.0004\kappa_s^2 + 0.00022\kappa_\mu^2)/(1 - BR_{\text{BSM}}) \quad ,
\end{aligned} \tag{4.B.6c}$$

where  $BR_{\text{BSM}}$  included BSM effects to the Higgs branching ratio. We take for simplicity  $\kappa_\tau = \kappa_\mu = \kappa_s = k_b$ ,  $\kappa_c = k_t$ ,  $\kappa_{(Z\gamma)} = 1$  and  $BR_{\text{BSM}} = 0$ .

By using these relations, and following the discussion around eq. (4.B.3), we can determine mean values, uncertainties and correlation matrix for the set of effective couplings  $\{g_W, g_Z, k_b, k_t\}$ ; the result is:

$$\begin{pmatrix} g_W \\ g_Z \\ k_b \\ k_t \end{pmatrix} = \begin{pmatrix} 1.041 \pm 0.076 \\ 1.066 \pm 0.096 \\ 1.038 \pm 0.087 \\ 1.025 \pm 0.153 \end{pmatrix} \quad , \quad \rho_{k-g} = \begin{pmatrix} 1 & 0.66 & 0.31 & 0.83 \\ 0.66 & 1 & 0.02 & 0.65 \\ 0.31 & 0.02 & 1 & 0.57 \\ 0.83 & 0.65 & 0.57 & 1 \end{pmatrix} \tag{4.B.7}$$

We can now substitute the expressions of the effective couplings reported in appendix 4.C and obtain the bounds on  $(\xi, \beta, \theta_t, \theta_b)$  coming from the fit of the Higgs couplings. The result is shown in fig. 4.8 for  $\theta_b = 0$  and the maximum and minimum values of  $\theta_t$  we considered in the analysis: for each of them, the region of the parameter space on the right of the corresponding line is excluded at 95% CL.

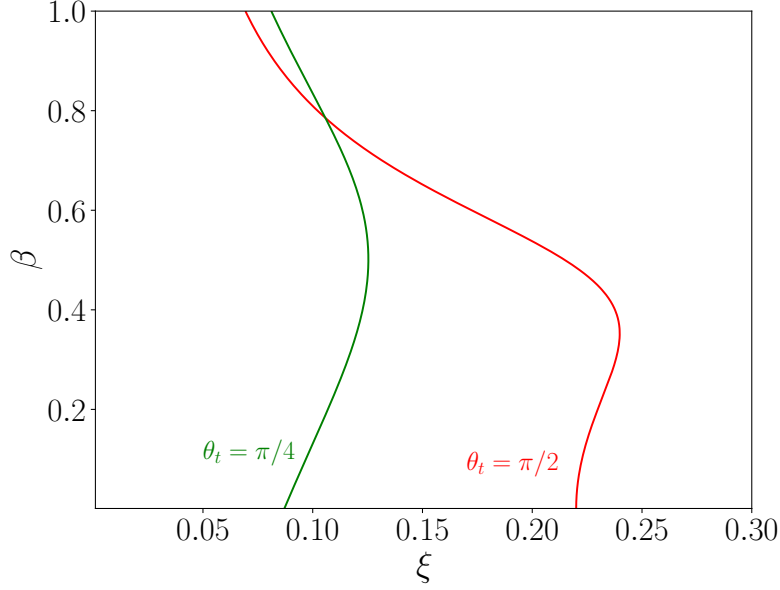


Figure 4.8: Bounds on the parameter space coming from the fit of Higgs couplings for  $\theta_b = 0$ . The region on the right of each line is excluded at 95% CL.

## 4.B.2 EWPTs

EWPTs put strong bounds on CH models, since oblique parameters usually receive contributions for three main reasons: corrections to gauge bosons propagators due to the NGBs which run in the loop, the appearance of vector resonances and the presence of fermionic states (see, e.g., [27]); we call these three contributions to the oblique parameters IR, UV and fermionic, respectively. An additional one comes from the fact that the custodial symmetry is broken, as discussed in section 4.2.1. We denote this last contribution 2HDM.

In order to determine the corrections to the oblique parameters  $\hat{S}$  and  $\hat{T}$  due to these effects, we make some simplifying assumptions: we use naive dimensional analysis (NDA) to estimate the UV contribution, we neglect the fermionic one from the top partners because it is generated at 1-loop, and we consider the leading order due to the IR and 2HDM effects. The 2HDM is easily read from eq. (4.2.16) by taking into account that  $\hat{T} = \rho - 1$ . The various corrections are:

$$\Delta\hat{S}_{\text{IR}} \approx \frac{g^2}{192\pi^2} \xi \log\left(\frac{v^2 g_*^2}{m_h^2 \xi}\right) \quad \Delta\hat{T}_{\text{IR}} \approx -\frac{3g'^2}{64\pi^2} \xi \log\left(\frac{v^2 g_*^2}{m_h^2 \xi}\right) \quad (4.B.8a)$$

$$\Delta\hat{S}_{\text{UV}} \approx \frac{m_W^2 \xi}{g_*^2 v^2} \quad \Delta\hat{T}_{\text{UV}} \approx 0 \quad (4.B.8b)$$

$$\Delta\hat{S}_{\text{fermion}} \approx 0 \quad \Delta\hat{T}_{\text{fermion}} \approx 0 \quad (4.B.8c)$$

$$\Delta\hat{S}_{\text{2HDM}} \approx 0 \quad \Delta\hat{T}_{\text{2HDM}} \approx \frac{\xi}{4} [1 - \cos 4\beta] \quad (4.B.8d)$$

Notice that the IR and UV contributions are the same as in the MCHM, at least at leading order.

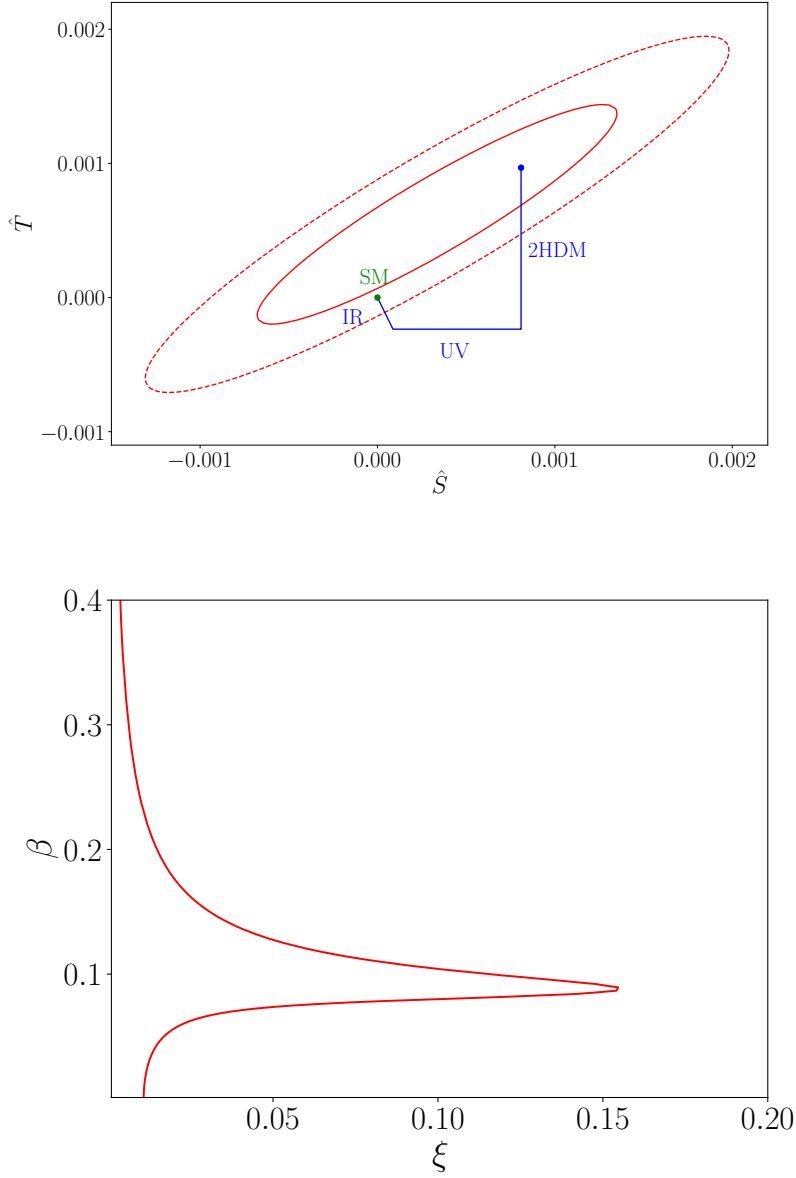


Figure 4.9: Top: contributions to the oblique parameters  $\hat{S}$  and  $\hat{T}$  for our model. Bottom: 95% CL bounds on  $\xi$  and  $\beta$  for  $g_* = 3$ .

Due to the smallness of  $\beta$ , the last contribution contributes positively to the  $\hat{T}$  parameter, and this is a fundamental result for our model, as we can see from the top panel of fig. 4.9: the continuous and dashed contour represent the 68% and 95% CL from EWPTs; we show in blue the different contributions to  $\hat{S}$  and  $\hat{T}$ . In the bottom panel, instead, we show the 95% CL in the  $(\xi, \beta)$  plane; in this case, the result is not affected by  $\theta_t$  and  $\theta_b$ , but only depends on  $g_*$ , which we take equal to 3. The exclusion is computed in a similar way to what we did for the fit on the Higgs couplings, with mean value and uncertainty on  $S$  and  $T$  reported in eq. (1.3.10),

$$S = 0.04 \pm 0.08 \quad , \quad T = 0.08 \pm 0.07, \quad (4.B.9)$$

and taking into account that  $\hat{S} \approx S/119$  and  $\hat{T} \approx T/129$  [29]

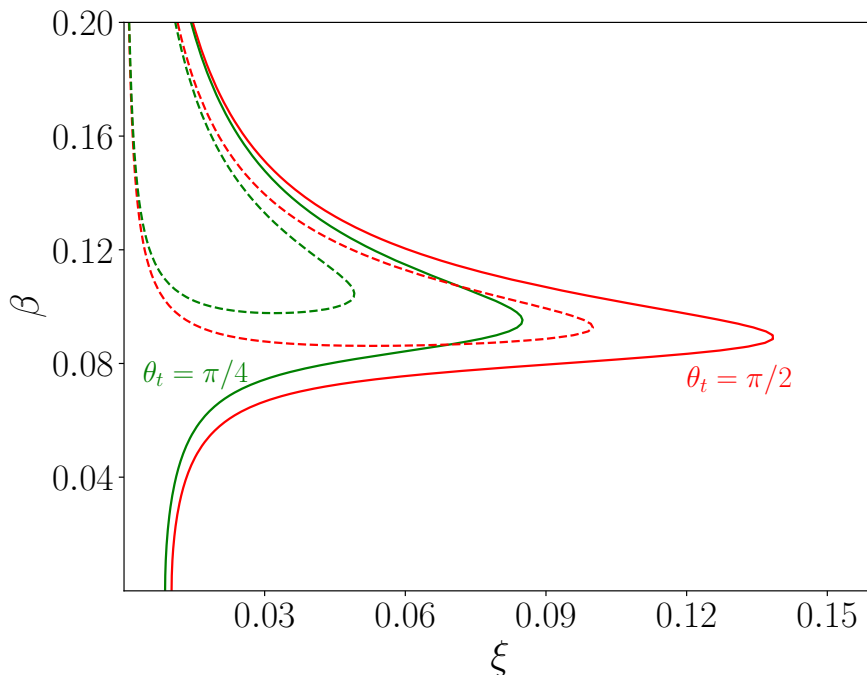


Figure 4.10: Combined results from Higgs fit and EWPTs bounds in the  $(\xi, \beta)$  plane for  $\theta_b = 0, g_* = 3$  and two different values of  $\theta_t$ . The region which is not enclosed in the solid (dashed) contour is excluded at 95% (68%) CL.

### 4.B.3 Combined results

We can combine the two types of bounds discussed above and obtain the overall restriction on the parameter space (mainly  $\xi$  and  $\beta$ ): to this purpose, we consider the ratio between the two likelihoods:

$$\lambda \equiv \frac{\mathcal{L}_0}{\mathcal{L}_1}, \quad (4.B.10)$$

where  $\mathcal{L}_0$  and  $\mathcal{L}_1$  are related to the null and alternative hypothesis, respectively. By taking into account that  $\chi^2 \sim -2 \log \lambda$  (Wilks' theorem), we can simply sum the  $\chi^2$ 's from the Higgs fit and EWPTs; the result is shown in fig. 4.10 for the two reference values of  $\theta_t$  we considered in the analysis,  $\theta_b = 0$  and  $g_* = 3$ . In order to be conservative, we take  $\xi \lesssim 0.08$  as the benchmark bound from combined Higgs and EWPTs limits, as shown in fig. 4.6.

## 4.C Expressions of the effective couplings

In this appendix, we provide the expressions of the effective couplings which appear in eqs. (4.3.6) and (4.3.9) to (4.3.11); to this purpose, it is convenient to introduce the

following set of rescaled coefficients:

$$\begin{aligned}
\tilde{c}_y^{(1)} &\equiv N_c c_{(1,0)}^{(1)} y_L^2 & \tilde{c}_y^{(2)} &\equiv N_c c_{(0,1)}^{(1)} y_R^2 & \tilde{c}_y^{(3)} &\equiv N_c c_{(2,0)}^{(1)} y_L^4/g_*^2 \\
\tilde{c}_y^{(4)} &\equiv N_c c_{(1,1)}^{(1)} y_L^2 y_R^2/g_*^2 & \tilde{c}_y^{(5)} &\equiv N_c c_{(0,2)}^{(1)} y_R^4/g_*^2 & \tilde{c}_y^{(6)} &\equiv N_c c_{(2,0)}^{(2)} y_L^4/(4\pi)^2 \\
\tilde{c}_y^{(7)} &\equiv N_c c_{(1,1)}^{(2)} y_L^2 y_R^2/(4\pi)^2 & \tilde{c}_y^{(8)} &\equiv N_c c_{(0,2)}^{(2)} y_R^4/(4\pi)^2 & \tilde{c}_y^{(9)} &\equiv N_c c_{(0,2)}^{(3)} y_R^4/(4\pi)^2
\end{aligned}$$

$$\begin{aligned}
\tilde{c}_g^{(1)} &\equiv c_{g'}^{(1)} g'^2 & \tilde{c}_g^{(2)} &\equiv c_{g'}^{(2)} g'^2 \\
\tilde{c}_g^{(3)} &\equiv c_g^{(1)} g^2 & \tilde{c}_g^{(4)} &\equiv c_{g'}^{(2)} g^2
\end{aligned}$$

In the following, we provide the list of all the effective couplings used in the computations. The couplings have been listed separately depending on the particles involved in the interaction.

#### 4.C.1 Interactions between NGBs and gauge bosons

As far as the couplings between the NGBs and the  $W$  and  $Z$  bosons, reported in eq. (4.3.6), are concerned, we have:

$$g_V \approx \sqrt{1 - \xi} \quad , \quad b_h \approx 1 - 2\xi \quad , \quad (4.C.1a)$$

$$\lambda_\eta^{(V)} \approx 2\xi \quad , \quad \lambda_\kappa^{(V)} \approx -\xi\beta^2 \quad , \quad (4.C.1b)$$

$$g_{H_0W} \approx -\frac{\beta\xi}{2} \quad , \quad g_{H_0Z} \approx \frac{3\beta\xi}{2} \quad , \quad g_{H_0V} \approx \xi\beta \quad (4.C.1c)$$

The 1-loop couplings with the gluons (cf. eq. (4.3.11)), instead, we have:

$$g_{gh} = -i \frac{\alpha_S}{8\pi} \tau_h [1 + (1 - \tau_h)f(\tau_h)] \quad , \quad \tau_h = \frac{4m_t^2}{m_h^2} \quad , \quad (4.C.1d)$$

$$g_{gH_0} = -i k_{H_0t} \frac{\alpha_S}{8\pi} \tau_{H_0} [1 + (1 - \tau_{H_0})f(\tau_{H_0})] \quad , \quad \tau_{H_0} = \frac{4m_t^2}{m_{H_0}^2} \quad , \quad (4.C.1e)$$

$$g_{g\eta} = -i g_t \frac{\alpha_S}{8\pi} \tau_\eta [1 + (1 - \tau_\eta)f(\tau_\eta)] \quad , \quad \tau_\eta = \frac{m_t^2}{m_\eta^2} \quad . \quad (4.C.1f)$$

where  $f(\tau_X)$  is the usual function appearing for gluon effective couplings (see for instance eq. (1.198) of [238]).

Notice that since this vertex is generated by a quark-loop the resulting coupling for  $H_0$  and  $\eta$  will be suppressed by a factor  $\xi$  with respect to the one to the SM Higgs and so it is not expected to play a relevant role, although it has been included in our simulations.

## 4.C.2 Interactions between NGBs and fermions

Interactions with SM quarks, given by eq. (4.3.9), have effective couplings:

$$k_q \approx 1 - \frac{7}{6}\xi - \frac{\xi \cos(3\beta + \alpha_q \theta_q)}{3 \cos(\beta - \alpha_q \theta_q)}, \quad (4.C.2a)$$

$$g_q \approx -2\xi \frac{\cos \beta \cos \theta_q}{\cos(\beta - \alpha_q \theta_q)}, \quad (4.C.2b)$$

$$k_{H_0q} \approx \frac{2\xi \sin(4\beta) + (-6 + \xi) \sin(2\beta - 2\alpha_q \theta_q) + 4\xi \sin(2\beta + 2\alpha_q \theta_q)}{12 \cos^2(\beta - \alpha_q \theta_q)}, \quad (4.C.2c)$$

$$g_{\kappa q} \approx -2\alpha_q \xi \frac{\sin \beta \sin \theta_q}{\cos(\beta - \alpha_q \theta_q)}, \quad (4.C.2d)$$

$$g_{\eta \kappa q} \approx -i\alpha_q \xi \tan(\beta - \alpha_q \theta_q). \quad (4.C.2e)$$

with  $\alpha_q = 1$  ( $-1$ ) for quarks with charge  $2/3$  ( $-1/3$ ).

## 4.C.3 Interactions among pNGBs

Finally, the effective couplings between the pNGBs, responsible for the interactions in eq. (4.3.10), are expanded in  $\xi$  and  $\beta$ ; the first orders are:

$$\begin{aligned} g_{\eta h} \approx & -\frac{g_*^2}{8\pi^2} \cos^2 \theta_t [2\tilde{c}_y^{(5)} - \tilde{c}_y^{(7)} + 2\tilde{c}_y^{(8)} + 2 \cos(2\theta_t)(\tilde{c}_y^{(5)} + \tilde{c}_y^{(8)})] \\ & + \frac{g_*^2 \beta}{4\pi^2} \cot \theta_t \cos(2\theta_t)(\tilde{c}_y^{(2)} + 2\tilde{c}_y^{(7)}) \\ & - \frac{g_*^2 \beta^2}{8\pi^2} \cot^2 \theta_t [\tilde{c}_y^{(5)} - 2\tilde{c}_y^{(8)} - 2 \cos(2\theta_t)(\tilde{c}_y^{(2)} + \tilde{c}_y^{(5)} + 2\tilde{c}_y^{(7)} - \tilde{c}_y^{(8)}) \\ & + \tilde{c}_y^{(5)} \cos(4\theta_t)] \end{aligned} \quad (4.C.3a)$$

$$\begin{aligned} \lambda_{\eta h} \approx & \frac{g_*^2}{24\pi^2} \cos^2 \theta_t [2\tilde{c}_y^{(2)} - 6\tilde{c}_y^{(5)} + 7\tilde{c}_y^{(7)} - 6\tilde{c}_y^{(8)} - 6 \cos(2\theta_t)(\tilde{c}_y^{(5)} + \tilde{c}_y^{(8)})] \\ & + \frac{g_*^2 \beta}{4\pi^2} \cot \theta_t \cos(2\theta_t)(\tilde{c}_y^{(2)} + 2\tilde{c}_y^{(7)}) \\ & - \frac{g_*^2 \beta^2}{24\pi^2} \cot^2 \theta_t [\tilde{c}_y^{(2)} + 3\tilde{c}_y^{(5)} + 2\tilde{c}_y^{(7)} - 6\tilde{c}_y^{(8)} \\ & - \cos(2\theta_t)(7\tilde{c}_y^{(2)} + 6\tilde{c}_y^{(5)} + 14\tilde{c}_y^{(7)} - 6\tilde{c}_y^{(8)}) + 3\tilde{c}_y^{(5)} \cos(4\theta_t)] \end{aligned} \quad (4.C.3b)$$

$$\begin{aligned}
\lambda &\approx 1 - \beta^2 \\
&- \frac{g_*^2 \beta^2}{16\pi^2} \frac{v^2}{m_h^2} \left[ \tilde{c}_g^{(1)} + \tilde{c}_g^{(2)} + \tilde{c}_g^{(3)} + \tilde{c}_g^{(4)} - 16\tilde{c}_y^{(2)} + \tilde{c}_y^{(5)} - 32\tilde{c}_y^{(7)} + 2\tilde{c}_y^{(8)} \right. \\
&\quad - \cos(2\theta_t)(14\tilde{c}_y^{(2)} - 2\tilde{c}_y^{(5)} + 29\tilde{c}_y^{(7)} - 2\tilde{c}_y^{(8)}) \\
&\quad \left. + 8 \csc^2 \theta_t (\tilde{c}_y^{(2)} + 2\tilde{c}_y^{(7)}) + \tilde{c}_y^{(5)} \cos(4\theta_t) \right] \tag{4.C.3c}
\end{aligned}$$

$$\begin{aligned}
g_{H_0} &\approx \frac{m_h^2}{v^2} (1 - \beta^2) \\
&- \frac{g_*^2}{8\pi^2} \left[ \tilde{c}_g^{(1)} + \tilde{c}_g^{(2)} + \tilde{c}_g^{(3)} + \tilde{c}_g^{(4)} + \tilde{c}_y^{(5)} + 2\tilde{c}_y^{(8)} + \cos(2\theta_t)(2\tilde{c}_y^{(5)} - \tilde{c}_y^{(7)} + 2\tilde{c}_y^{(8)}) \right. \\
&\quad \left. + \tilde{c}_y^{(5)} \cos(4\theta_t) \right] \\
&+ \frac{g_*^2 \beta}{4\pi^2} \csc \theta_t [\cos \theta_t + \cos(3\theta_t)] (\tilde{c}_y^{(2)} + 2\tilde{c}_y^{(7)}) \\
&+ \frac{g_*^2 \beta^2}{16\pi^2} \left[ 15(\tilde{c}_g^{(1)} + \tilde{c}_g^{(2)} + \tilde{c}_g^{(3)} + \tilde{c}_g^{(4)} + \tilde{c}_y^{(5)} + 2\tilde{c}_y^{(8)}) \right. \\
&\quad \left. + \cos(2\theta_t)(14\tilde{c}_y^{(2)} + 6\tilde{c}_y^{(5)} + 25\tilde{c}_y^{(6)}\tilde{c}_y^{(8)} + 15\tilde{c}_y^{(5)} \cos(4\theta_t)) \right] \tag{4.C.3d}
\end{aligned}$$

$$\begin{aligned}
g_{H_0 hh} &\approx \frac{g_*^2 \beta}{8\pi^2} \left[ 3 \left[ \tilde{c}_g^{(1)} + \tilde{c}_g^{(2)} + \tilde{c}_g^{(3)} + \tilde{c}_g^{(4)} + \tilde{c}_y^{(5)} + 2\tilde{c}_y^{(8)} \right] + \cos(2\theta_t)(4\tilde{c}_y^{(2)} + 6\tilde{c}_y^{(5)} + 5\tilde{c}_y^{(7)} + 6\tilde{c}_y^{(8)}) \right. \\
&\quad \left. + 3\tilde{c}_y^{(5)} \cos(4\theta_t) \right] \\
&- \frac{g_*^2 \beta^2}{2\pi^2} \cot(2\theta_t) [\cos \theta_t + \cos(3\theta_t)] (\tilde{c}_y^{(2)} + 2\tilde{c}_y^{(7)}) \tag{4.C.3e}
\end{aligned}$$

$$\begin{aligned}
\lambda_{\eta H_0} &\approx - \frac{g_*^2}{8\pi^2} \cos^2 \theta_t \left[ 2\tilde{c}_y^{(5)} - \tilde{c}_y^{(7)} - 2\tilde{c}_y^{(8)} - 2 \cos(2\theta_t) (\tilde{c}_y^{(5)} - \tilde{c}_y^{(8)}) \right] \\
&+ \frac{g_*^2 \beta^2}{24\pi^2} \left[ \tilde{c}_y^{(2)} - 3\tilde{c}_y^{(5)} + 2\tilde{c}_y^{(7)} - 6\tilde{c}_y^{(8)} - \cos(2\theta_t) (7\tilde{c}_y^{(2)} + 6\tilde{c}_y^{(5)} + 14\tilde{c}_y^{(7)} + 6\tilde{c}_y^{(8)}) \right. \\
&\quad \left. - 3\tilde{c}_y^{(5)} \cos(4\theta_t) \right] \tag{4.C.3f}
\end{aligned}$$

$$\begin{aligned}
\lambda_{H_0} &\approx - \frac{3g_*^2 \beta}{8\pi^2} \left[ \tilde{c}_g^{(1)} + \tilde{c}_g^{(2)} + \tilde{c}_g^{(3)} + \tilde{c}_g^{(4)} + \tilde{c}_y^{(5)} + 2\tilde{c}_y^{(8)} - \cos(2\theta_t)(2\tilde{c}_y^{(5)} - \tilde{c}_y^{(7)} + 2\tilde{c}_y^{(8)}) \right. \\
&\quad \left. + \tilde{c}_y^{(5)} \cos(4\theta_t) \right] + \frac{3g_*^2 \beta^2}{2\pi^2} \tan \theta_t \cos(2\theta_t) (\tilde{c}_y^{(2)} + 2\tilde{c}_y^{(7)}) \tag{4.C.3g}
\end{aligned}$$



$$g_{\eta H_0} \approx \frac{g_*^2 \beta}{8\pi^2} \left[ \tilde{c}_y^{(5)} + 2\tilde{c}_y^{(8)} + 2\cos(2\theta_t)(\tilde{c}_y^{(2)} + \tilde{c}_y^{(5)} + 2\tilde{c}_y^{(7)} + \tilde{c}_y^{(8)}) + \tilde{c}_y^{(5)} \cos(4\theta_t) \right] \\ - \frac{g_*^2 \beta^2}{4\pi^2} \tan \theta_t \cos(2\theta_t)(\tilde{c}_y^{(2)} + 2\tilde{c}_y^{(7)}) \quad (4.C.3h)$$

$$g_{A_0 h} \approx \frac{g_*^2}{8\pi^2} \left[ -\frac{8\pi^2 m_h^2}{g_*^2 v^2} + \tilde{c}_y^{(5)} + \tilde{c}_y^{(8)} + \cos(2\theta_t)(2\tilde{c}_y^{(5)} - \tilde{c}_y^{(7)} + 2\tilde{c}_y^{(8)}) + \cos(4\theta_t)(\tilde{c}_y^{(5)} + \tilde{c}_y^{(8)}) \right] \\ - \frac{g_*^2 \beta}{4\pi^2} \csc \theta_t \sec \theta_t (\tilde{c}_y^{(2)} + 2\tilde{c}_y^{(7)}) \cos^2(2\theta_t) \\ - \frac{g_*^2 \beta^2}{16\pi^2} \left[ -\frac{16\pi^2 m_h^2}{g_*^2 v^2} + 7\tilde{c}_g^{(1)} + 7\tilde{c}_g^{(2)} + 7\tilde{c}_g^{(3)} + 7\tilde{c}_g^{(4)} + 16\tilde{c}_y^{(2)} + 7\tilde{c}_y^{(5)} + 32\tilde{c}_y^{(7)} + 14\tilde{c}_y^{(8)} \right. \\ \left. + \cos(2\theta_t)(14\tilde{c}_y^{(2)} + 6\tilde{c}_y^{(5)} + 25\tilde{c}_y^{(7)} + 6\tilde{c}_y^{(8)}) \right. \\ \left. - 16 \csc^2(2\theta_t)(\tilde{c}_y^{(2)} + 2\tilde{c}_y^{(7)}) + 7\tilde{c}_y^{(5)} \cos(4\theta_t) \right] \quad (4.C.3i)$$

$$g_{A_0 H_0} \approx -\frac{g_*^2 \beta}{8\pi^2} \left[ \tilde{c}_g^{(1)} + \tilde{c}_g^{(2)} + \tilde{c}_g^{(3)} + \tilde{c}_g^{(4)} + \tilde{c}_y^{(5)} + 2\tilde{c}_y^{(8)} - \cos(2\theta_t)(2\tilde{c}_y^{(5)} - \tilde{c}_y^{(7)} + 2\tilde{c}_y^{(8)}) \right. \\ \left. + \tilde{c}_y^{(5)} \cos(4\theta_t) \right] + \frac{g_*^2 \beta^2}{2\pi^2} \tan \theta_t \cos(2\theta_t)(\tilde{c}_y^{(2)} + 2\tilde{c}_y^{(7)}) \quad (4.C.3j)$$

$$g_{\kappa h} \approx \frac{g_*^2}{8\pi^2} \sin^2 \theta_t [\tilde{c}_y^{(7)} - 4(\tilde{c}_y^{(5)} - \tilde{c}_y^{(8)}) \cos^2 \theta_t] \\ - \frac{g_*^2 \beta^2}{8\pi^2} [\tilde{c}_y^{(5)} + 2\tilde{c}_y^{(8)} - 2\cos(2\theta_t)(\tilde{c}_y^{(2)} + \tilde{c}_y^{(5)} + 2\tilde{c}_y^{(7)} + \tilde{c}_y^{(8)}) + \tilde{c}_y^{(5)} \cos(4\theta_t)] \quad (4.C.3k)$$

$$g_{\kappa H_0} \approx -\frac{g_*^2 \beta}{2\pi^2} \sin^2 \theta_t (\tilde{c}_y^{(8)} - \tilde{c}_y^{(5)} \cos(2\theta_t)) + \frac{g_*^2 \beta^2}{4\pi^2} \tan \theta_t \cos(2\theta_t)(\tilde{c}_y^{(2)} + 2\tilde{c}_y^{(7)}) \quad (4.C.3l)$$

$$\lambda_{\kappa h} \approx \frac{g_*^2}{8\pi^2} \sin^2 \theta_t (\tilde{c}_y^{(7)} - 4\cos^2 \theta_t (\tilde{c}_y^{(5)} - \tilde{c}_y^{(8)})) \\ + \frac{g_*^2 \beta^2}{24\pi^2} \left[ \tilde{c}_y^{(2)} - 3\tilde{c}_y^{(5)} + 2\tilde{c}_y^{(7)} - 6\tilde{c}_y^{(8)} + \cos(2\theta_t)(5\tilde{c}_y^{(2)} + 6\tilde{c}_y^{(5)} + 10\tilde{c}_y^{(7)} + 6\tilde{c}_y^{(8)}) \right. \\ \left. - 3\tilde{c}_y^{(5)} \cos(4\theta_t) \right] \quad (4.C.3m)$$

$$\lambda_{\kappa H_0} \approx -\frac{g_*^2}{24\pi^2} \left[ 2(2\tilde{c}_y^{(7)} + \tilde{c}_y^{(2)}) \cos^2 \theta_t - \sin^2 \theta_t (4\tilde{c}_y^{(2)} + 11\tilde{c}_y^{(7)}) + 12 \sin^4 \theta_t (\tilde{c}_y^{(5)} + \tilde{c}_y^{(8)}) \right] \\ + \frac{g_*^2 \beta}{24\pi^2} [3 - 5 \cos(2\theta_t)] \csc \theta_t \sec \theta_t \cos(2\theta_t)(\tilde{c}_y^{(2)} + 2\tilde{c}_y^{(7)}) \\ - \frac{g_*^2 \beta^2}{24\pi^2} \left[ 13\tilde{c}_y^{(2)} - 3\tilde{c}_y^{(5)} + 26\tilde{c}_y^{(7)} - 6\tilde{c}_y^{(8)} - \cos(2\theta_t)(13\tilde{c}_y^{(2)} - 3\tilde{c}_y^{(5)} + 26\tilde{c}_y^{(7)} - 6\tilde{c}_y^{(8)}) \right. \\ \left. + 2(\csc^2 \theta_t - 4 \sec^2 \theta_t)(\tilde{c}_y^{(2)} + 2\tilde{c}_y^{(7)}) \right] \quad (4.C.3n)$$

$$\begin{aligned}
\lambda_{\eta A_0} &\approx \frac{g_*^2}{8\pi^2} \cos^2 \theta_t [2\tilde{c}_y^{(5)} - \tilde{c}_y^{(7)} - 2\tilde{c}_y^{(8)} - 2 \cos(2\theta_t)(\tilde{c}_y^{(5)} - \tilde{c}_y^{(8)})] \\
&\quad - \frac{\beta^2 g_*^2}{24\pi^2} [\tilde{c}_y^{(2)} - 3\tilde{c}_y^{(5)} + 2\tilde{c}_y^{(7)} - 6\tilde{c}_y^{(8)} - \cos(2\theta_t)(7\tilde{c}_y^{(2)} + 6\tilde{c}_y^{(5)} + 14\tilde{c}_y^{(7)} + 6\tilde{c}_y^{(8)}) \\
&\quad \quad - 3\tilde{c}_y^{(5)} \cos(4\theta_t)] \tag{4.C.3o}
\end{aligned}$$

$$\begin{aligned}
\lambda_{\eta H_+} &\approx \frac{g_*^2}{8\pi^2} \cos^2 \theta_t [2\tilde{c}_y^{(5)} - \tilde{c}_y^{(7)} - 2\tilde{c}_y^{(8)} - 2 \cos(2\theta_t)(\tilde{c}_y^{(5)} - \tilde{c}_y^{(8)})] \\
&\quad - \frac{\beta^2 g_*^2}{24\pi^2} [\tilde{c}_y^{(2)} - 3\tilde{c}_y^{(5)} + 2\tilde{c}_y^{(7)} - 6\tilde{c}_y^{(8)} - \cos(2\theta_t)(7\tilde{c}_y^{(2)} + 6\tilde{c}_y^{(5)} + 14\tilde{c}_y^{(7)} + 6\tilde{c}_y^{(8)}) \\
&\quad \quad - 3\tilde{c}_y^{(5)} \cos(4\theta_t)] \tag{4.C.3p}
\end{aligned}$$

$$\begin{aligned}
g_{H+h} &\approx -\frac{g_*^2}{16\pi^2} [\tilde{c}_y^{(5)} + 2\tilde{c}_y^{(6)} - 2\tilde{c}_y^{(7)} - \tilde{c}_y^{(8)} - \cos(4\theta_t)(\tilde{c}_y^{(5)} - \tilde{c}_y^{(8)}) - 2\tilde{c}_g^{(3)} - 2\tilde{c}_g^{(4)}] \\
&\quad - \frac{\beta^2 g_*^2}{4\pi^2} [\tilde{c}_y^{(5)} + 2\tilde{c}_y^{(8)} + \tilde{c}_y^{(5)} \cos(4\theta_t) + \tilde{c}_g^{(1)} + \tilde{c}_g^{(2)} + \tilde{c}_g^{(3)} + \tilde{c}_g^{(4)}] \tag{4.C.3q}
\end{aligned}$$

$$\begin{aligned}
g_{H+H_0} &\approx -\frac{\beta g_*^2}{8\pi^2} \cos^2 \theta_t \left[ \tilde{c}_y^{(5)} + 2\tilde{c}_y^{(8)} - \cos(2\theta_t)(2\tilde{c}_y^{(5)} - \tilde{c}_y^{(7)} + 2\tilde{c}_y^{(8)}) + \tilde{c}_y^{(5)} \cos(4\theta_t) \right. \\
&\quad \quad \left. + \tilde{c}_g^{(1)} + \tilde{c}_g^{(2)} + \tilde{c}_g^{(3)} + \tilde{c}_g^{(4)} \right] \\
&\quad + \frac{\beta^2 g_*^2}{2\pi^2} (\tilde{c}_y^{(2)} + 2\tilde{c}_y^{(7)}) \cos(2\theta_t) \tan \theta_t \tag{4.C.3r}
\end{aligned}$$

$$\begin{aligned}
\lambda_{\kappa A_0} &\approx \frac{g_*^2}{24\pi^2} [2(\tilde{c}_y^{(2)} + 2\tilde{c}_y^{(7)}) \cos^2 \theta_t - \sin^2 \theta_t [4\tilde{c}_y^{(2)} + 11\tilde{c}_y^{(7)} - 12 \sin^2 \theta_t (\tilde{c}_y^{(5)} + \tilde{c}_y^{(8)})]] \\
&\quad + \frac{\beta g_*^2}{24\pi^2} (\tilde{c}_y^{(2)} + 2\tilde{c}_y^{(7)}) \cos(2\theta_t) [5 \cos(2\theta_t) - 3] \csc \theta_t \sec \theta_t \\
&\quad + \frac{\beta^2 g_*^2}{24\pi^2} \left[ 13\tilde{c}_y^{(2)} - 3\tilde{c}_y^{(5)} + 26\tilde{c}_y^{(7)} - 6\tilde{c}_y^{(8)} - \cos(2\theta_t)(13\tilde{c}_y^{(2)} - 6\tilde{c}_y^{(5)} + 26\tilde{c}_y^{(7)} - 6\tilde{c}_y^{(8)}) \right. \\
&\quad \quad \left. - 3\tilde{c}_y^{(5)} \cos(4\theta_t) + 2(\tilde{c}_y^{(2)} + 2\tilde{c}_y^{(7)})(\csc^2 \theta_t - 4 \sec^2 \theta_t) \right] \tag{4.C.3s}
\end{aligned}$$

$$\begin{aligned}
\lambda_{\kappa H_+} &\approx \frac{g_*^2}{24\pi^2} [2(\tilde{c}_y^{(2)} + 2\tilde{c}_y^{(7)}) \cos^2 \theta_t - \sin^2 \theta_t [4\tilde{c}_y^{(2)} + 11\tilde{c}_y^{(7)} - 12 \sin^2 \theta_t (\tilde{c}_y^{(5)} + \tilde{c}_y^{(8)})]] \\
&\quad + \frac{\beta g_*^2}{24\pi^2} (\tilde{c}_y^{(2)} + 2\tilde{c}_y^{(7)}) \cos(2\theta_t) [5 \cos(2\theta_t) - 3] \csc \theta_t \sec \theta_t \\
&\quad + \frac{\beta^2 g_*^2}{24\pi^2} \left[ 13\tilde{c}_y^{(2)} - 3\tilde{c}_y^{(5)} + 26\tilde{c}_y^{(7)} - 6\tilde{c}_y^{(8)} - \cos(2\theta_t)(13\tilde{c}_y^{(2)} - 6\tilde{c}_y^{(5)} + 26\tilde{c}_y^{(7)} - 6\tilde{c}_y^{(8)}) \right. \\
&\quad \quad \left. - 3\tilde{c}_y^{(5)} \cos(4\theta_t) + 2(\tilde{c}_y^{(2)} + 2\tilde{c}_y^{(7)})(\csc^2 \theta_t - 4 \sec^2 \theta_t) \right] \tag{4.C.3t}
\end{aligned}$$

$$k_{\text{der}} = \frac{2\xi}{3} \tag{4.C.3u}$$

# Chapter 5

## Summary and conclusions

The existence of dark matter is a clear signal that the Standard Model cannot be the definitive theory to describe particle physics. While many experimental evidences show unequivocally that DM exists, it not clear what its real nature is; an appealing possibility is that it is in the form of WIMPs, characterized by an annihilation cross section of the order of the weak scale and mass in the GeV-TeV range. In order to test this possibility, many experiments have been built, and also LHC provides a unique opportunity in this perspective.

In this work, we first focused on this aspect, i.e. we investigated the potential of LHC in exploring the parameter space of DM models. Our interest pointed towards signatures others than the standard monojet and, in particular, we considered the possibility in which LLPs are produced; such a scenario has been receiving an increasing attention, especially because the expected background in the SM can be extremely small.

In chapter 3, we first studied the pDDM model, characterized by two Majorana fermions  $\chi_{1,2}$  almost degenerate in mass; this simple extension of the SM predicts the existence of DVs, whose potential lies in the fact that the expected SM background is very low. We studied the sensitivity of MJ and DVs to the parameter space and projected the current limits to high luminosity, showing that searches for displaced vertices are essential in order to properly constrain the model. We then considered the chromo-electric DM model, where a coloured particle can lead to bound states similarly to what happens in SUSY; we then applied experimental bounds from  $R$ -hadrons searches, comparing them with those from MJ, and projected the current limits to high luminosity, showing that also in this case a complementarity between the searches exists; in particular, while MJ ones can exclude all values of  $d_\chi$  up to a maximum DM mass,  $R$ -hadrons searches can explore regions of the parameter space with smaller couplings but larger masses.

Overall, we showed that, if present, LLPs signatures can represent a smoking gun for new physics. Given that these kind of searches are particularly challenging from an experimental point of view, and that dedicated methods are also required in order to correctly reconstruct the background, it is essential to pursue in this direction to fully exploit the potential of LHC.

In chapter 4, we studied a non-minimal CH model characterized by two doublets and two singlet, the lightest of which is the DM candidate. We showed that it is possible to evade current experimental constraints (mainly direct detection) with the minimum fine tuning allowed by EWPTs, whereas a higher compositeness scale is usually required by other CH models which aim to address for DM. In addition, we also studied the possibility of reproducing the relic abundance of dark matter via non-thermal effects; although a

higher fine tuning is required in this framework, this possibility is only possible thanks to the greater complexity of the model, and we think it represents one of its most interesting features.

While the existence of dark matter is incontrovertible in the light of observations, we are far from knowing its real nature; the WIMP paradigm is just one possibility, but we are not guaranteed at all it is the correct one. For this reason, it is essential to keep on studying this fascinating problem if we aim to properly understand nature.

# Appendix A

## CCWZ formalism

### A.1 Geometrical interpretation

Before considering the full CCWZ construction, it is useful to first have a geometrical interpretation of the results we are going to obtain.

Let us suppose we have a theory of scalar fields  $\phi = (\varphi_1, \varphi_2, \dots)$ ; the set  $\phi$  can be thought as a set of coordinates on some manifold  $M$ . Let  $\phi_0$  be the field configuration which minimizes the scalar potential, and  $\mathcal{G}$  a symmetry group which acts on the fields as  $\phi \rightarrow T_g(\phi)$ , where  $g \in \mathcal{G}$ ; let  $\mathfrak{g}$  be the algebra of  $\mathcal{G}$ .

We assume that  $\phi_0$  is not invariant under the full group  $\mathcal{G}$ , but only under a subgroup  $\mathcal{H} = \{h \in \mathcal{G} : T_h(\phi_0) = \phi_0\}$ : this means that the symmetry is spontaneously broken. We denote by  $\{T^a\}$  the set of generators of  $\mathcal{H}$ , which span a subalgebra  $\mathfrak{h}$  of  $\mathfrak{g}$ . In general, then,  $\phi_0$  is left invariant only by the transformations  $T_h$ , with  $h \in \mathcal{H}$ ; let us denote by  $N$  the submanifold of  $M$  generated by  $T_g(\phi_0)$ , for each  $g \in \mathcal{G}$ . As we will see, the Goldstone bosons can be viewed as coordinates on  $N$ .

We choose a set  $\{\hat{T}^i\}$  which do not leave  $\phi_0$  invariant, i.e.  $T_{\{\hat{T}^i\}}(\phi_0) \neq \phi_0$ ; these generators belong to the coset  $\mathcal{G}/\mathcal{H}$  and are a basis of a vector space  $\mathfrak{b} \subset \mathfrak{g}$ . Given that the sets  $\{T^a\}$  and  $\{\hat{T}^i\}$  are linearly independent, the algebra  $\mathfrak{g}$  decomposes in the direct sum  $\mathfrak{g} = \mathfrak{h} \oplus \mathfrak{b}$  (the sum is at the level of vector spaces and not of algebras, since in general  $\mathfrak{b}$  is not a subalgebra). In addition,  $\mathfrak{b}$  is defined only modulo the action of unbroken generators.

The only assumption behind the CCWZ construction is that  $\mathfrak{b}$  is invariant under  $\mathcal{H}$ , meaning that for each  $\hat{T}^i \in \mathfrak{b}$  and  $h \in \mathcal{H}$ , then  $h\hat{T}^i h^{-1} \in \mathfrak{b}$  (this is called ‘invariance’ of  $\mathfrak{b}$  because  $\mathcal{H}$  acts on  $\hat{T}^i$  as if they were in the adjoint representation): this requirement is equivalent to say that  $[T^a, \hat{T}^i] \in \mathfrak{b}$ , which is always satisfied for compact  $\mathcal{H}$  [27].

Let us consider a particular  $\phi \in N$  sufficiently close to  $\phi_0$ ;  $\phi$  is said to correspond to a set of Goldstone coordinates  $G_i, i = 1, \dots, \dim \mathcal{G} - \dim \mathcal{H}$  if  $\phi = T_U(\phi_0)$ , with  $U = e^{iG^i \hat{T}^i}$ . If this is the case, the Goldstone coordinates are nothing but the transformation parameters that send from  $\phi_0$  to  $\phi$ , as shown in fig. A.1. In this sense, the Goldstone bosons also represent coordinates on the submanifold  $N$ , at least in a vicinity of  $\phi_0$ . In addition, since  $\mathcal{G}$  is only spontaneously broken (meaning that the potential is invariant under the action of  $\mathcal{G}$ ),  $\phi$  has the same energy as  $\phi_0$ , so that the Goldstone coordinates  $G_i$  parametrize a degenerate vacuum.

The next step is to understand how  $U$  transforms under a transformation  $g \in \mathcal{G}$ . Given a point  $\phi = T_U(\phi_0) \in N$ , we consider the transformation  $T_g(\phi)$ : the CCWZ construction ensures, as we will see, that there exists a  $U' = U'(g, G_i)$  such that  $T_g(\phi) = T_{U'}(\phi_0)$ ; in

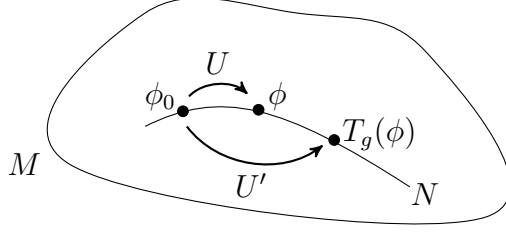


Figure A.1: Geometrical visualization of the CCWZ formalism.

particular, it always exists an  $h = h(g, G_i) \in \mathcal{H}$  such that  $U' = gUh^{-1}(g, G_i)$ .

## A.2 General construction

We now formalize the general idea outlined above. As already stated, we consider a symmetry group  $\mathcal{G}$  which is spontaneously broken to a subgroup  $\mathcal{H}$ , and divide its generators  $\{T^A\}$  (normalized in such a way that  $\text{Tr}(T^A T^B) = \delta_{AB}$ ) in two sets  $\{T^a, \hat{T}^i\}$  such that:

$$\exists \mathbf{F} \quad : \quad T^a \mathbf{F} = 0 \quad , \quad \hat{T}^i \mathbf{F} \neq 0, \quad (\text{A.2.1})$$

where  $\mathbf{F}$  is a reference vacuum (which in general does not coincide with the physical vacuum).

Starting from  $\mathbf{F}$ , we see that good candidates to be (modulo a normalization factor) Goldstone bosons are encoded in:

$$\mathbf{F}_\theta \equiv e^{i\theta_A(x)T^A} \mathbf{F}. \quad (\text{A.2.2})$$

The  $\theta_A(x)$ 's being good candidates to represent Goldstone bosons is because for constant  $\theta_A$  the one above is a symmetry transformation, leading to a configuration with the same energy as the vacuum; for spacetime-dependent  $\theta_A(x)$ , then, only derivative terms can arise: if this was not the case, i.e. if  $\theta_A(x)$  had a potential, the latter would not vanish in the limit  $\theta_A(x) \rightarrow \text{const.}$ , leading to an energy different from the one of  $\mathbf{F}$ . Not having a potential, and in particular not having a mass, the  $\theta_A(x)$ 's are then good candidates to be Goldstone bosons.

However, some of the  $\theta_A(x)$ 's are redundant and non physical; in general, in fact, an element group  $g \in \mathcal{G}$  can be decomposed as [27]:

$$g = e^{i\alpha_A T^A} = e^{i\alpha_i \hat{T}^i} e^{i\alpha_a T^a}, \quad (\text{A.2.3})$$

and the last term does not have effect when acting on  $\mathbf{F}$ . We then assume the Goldstone bosons  $\Pi_i(x)$  to be encoded in:

$$\phi(x) = U[\Pi] \mathbf{F} \quad , \quad U[\Pi] \equiv e^{i\frac{\sqrt{2}}{f}\Pi_i(x)\hat{T}^i} \equiv e^{i\frac{\sqrt{2}}{f}\Pi(x)}. \quad (\text{A.2.4})$$

In the following, we use the symbol  $\Pi(x)$  for both the Goldstone matrix,  $\Pi_i(x)\hat{T}^i$ , and the length of the Goldstone vector,  $\sqrt{\Pi_i^2(x)}$ , the correct one being clear from the context.

As already anticipated, we want to understand how  $U[\Pi]$  transforms under a generic group element  $g \in \mathcal{G}$ , i.e. to determine a transformation

$$\Pi_i(x) \rightarrow \Pi'_i(x) \quad (\text{A.2.5})$$

which is a symmetry transformation of  $\phi(x)$ . A naive answer would be  $U \rightarrow gU$ , but this is not valid because in general  $gU \in \mathcal{G}$ , and so  $\phi$  would not be made out of broken generators only anymore. However, we know from eq. (A.2.3) that  $gU$  can be expressed as the product of an element of  $\mathcal{G}/\mathcal{H}$  and one of  $\mathcal{H}$ ; we can then write:

$$gU[\Pi] = U[\Pi'] h(\Pi, g), \quad (\text{A.2.6})$$

where  $h(\Pi, g) \in \mathcal{H}$  depends on the particular  $g$  and on the Goldstone fields (and then also on spacetime coordinates  $x$ ). We then found that under a  $\mathcal{G}$  transformation the Goldstone matrix transforms to:

$$U[\Pi'] = gU[\Pi] h^{-1}(\Pi, g). \quad (\text{A.2.7})$$

From eq. (A.2.4), we also see that under this transformation:

$$\phi \rightarrow g\phi. \quad (\text{A.2.8})$$

Being the symmetry only spontaneously broken, the transformation above has to be respected also by the effective Lagrangian for the Goldstone bosons, and for this reason only peculiar terms are allowed.

Since all this treatment is independent of the representation of the generators, the Goldstone matrix  $U[\Pi]$  can be defined for any representation of the generators  $T^A$ . Furthermore, the important symmetry to classify allowed operators is given by  $\mathcal{G}$ : from this point of view, the symmetry is not really broken, in the sense it affects the allowed operators in the effective Lagrangian. Finally, given that  $\Pi'_i$  has some complicated dependence on  $\Pi_i$ , it is said to transform *non-linearly*.

In general, the commutation relations for the generators  $\{T^A\}$  can be classified as:

$$[T^a, T^b] = i f^{abc} T^c \quad (\text{A.2.9a})$$

$$[T^a, \hat{T}^i] = i f^{aij} \hat{T}^j \quad (\text{A.2.9b})$$

$$[\hat{T}^i, \hat{T}^j] = i f^{ijk} \hat{T}^k + i f^{ija} T^a, \quad (\text{A.2.9c})$$

where the absence of  $f^{abi}$  in the first equation is due to the fact that  $\mathfrak{h}$  is a subalgebra, while the absence of  $f^{aib}$  in the second one comes from the hypothesis that  $\mathcal{H}$  is a compact subgroup, as already stated. In addition, for *symmetric cosets*, also  $f^{ijk} = 0$ ; this is realized if there exists an automorphism  $\hat{T} \rightarrow -\hat{T}$ , which can be associated with a  $\mathbb{Z}_2$  symmetry on the Goldstone bosons.

It is then useful to define:

$$f^{abc} \equiv i (T_{\text{ad}}^a)_{bc} \quad (\text{A.2.10a})$$

$$f^{aij} \equiv i (T_{\Pi}^a)_{ij}, \quad (\text{A.2.10b})$$

where in the first line we defined the generators of the adjoint representation  $\mathbf{A}_{\mathcal{H}}$  of  $\mathfrak{h}$ , while in the second one we have a set of matrices  $\{T_{\Pi}^a\}$  which forms another representation  $\mathbf{R}_{\Pi}$  of  $\mathfrak{h}$ ; in general, the latter can be identified from:

$$\mathbf{A}_{\mathcal{G}} = \mathbf{A}_{\mathcal{H}} \oplus \mathbf{R}_{\Pi}. \quad (\text{A.2.11})$$

It is now interesting to see how the Goldstone bosons transform under symmetry transformations:

i) transformation under  $\mathcal{H}$ .

In this case  $g = h \in \mathcal{H}$ , and we have:

$$\begin{aligned}
hU[\Pi] &= h \left( \mathbf{1} + i \frac{\sqrt{2}}{f} \Pi_i \hat{T}^i + \dots \right) h^{-1} h \\
&= \left[ \mathbf{1} + i \frac{\sqrt{2}}{f} \Pi_i \left( \hat{T}^i - i \alpha_a (T_{\Pi}^a)_{ij} \hat{T}^j + \dots \right) + \dots \right] h \\
&= \left[ \mathbf{1} + i \frac{\sqrt{2}}{f} \Pi_i \hat{T}^j (e^{i \alpha_a T_{\Pi}^a})_{ji} + \dots \right] h = \\
&= e^{i \frac{\sqrt{2}}{f} \hat{T}^i (e^{i \alpha_a T_{\Pi}^a} \Pi)_i} h = U [e^{i \alpha_a T_{\Pi}^a} \Pi] h,
\end{aligned} \tag{A.2.12}$$

which is precisely in the form of eq. (A.2.7).

From eq. (A.2.4), we see that the Goldstone bosons transform as:

$$\Pi_i \rightarrow (e^{i \alpha_a T_{\Pi}^a})_{ij} \Pi_j, \tag{A.2.13}$$

which implies that  $\mathbf{R}_{\Pi}$  is nothing but the representation the Goldstone bosons transform with under the action of  $\mathcal{H}$ . In addition,  $\mathcal{H}$  acts linearly on the Goldstone bosons.

From eq. (A.2.13), it is also possible to determine how the Goldstone matrix changes under infinitesimal transformations; by taking into account eq. (A.2.10), in fact, we get:

$$\Pi \rightarrow \Pi + i \alpha_a f_{aji} \Pi_j \hat{T}^i = \Pi + \alpha_a [T_a, \Pi]; \tag{A.2.14}$$

ii) transformation under  $\mathcal{G}/\mathcal{H}$ .

In this case  $g \equiv g_{\mathcal{G}/\mathcal{H}} \in \mathcal{G}/\mathcal{H}$ , and there is no an easy way to study the transformation properties of the Goldstone bosons but considering infinitesimal transformations; however, it is not necessary to resort to eq. (A.2.7), but it suffices to consider  $g_{\mathcal{G}/\mathcal{H}} U[\Pi]$ , since it is automatically an element of the coset  $\mathcal{G}/\mathcal{H}$ . This is:

$$U[\Pi'] = g_{\mathcal{G}/\mathcal{H}} U[\Pi] = \mathbf{1} + i \alpha_i \hat{T}^i + i \frac{\sqrt{2}}{f} \Pi_i \hat{T}^i + \dots, \tag{A.2.15}$$

which implies that:

$$\Pi_i \rightarrow \Pi_i + \frac{f}{\sqrt{2}} \alpha_i + \mathcal{O} \left( \alpha \frac{\Pi^2}{f} + \dots \right), \tag{A.2.16}$$

which is the famous *shift symmetry* of the Goldstone bosons, which only allows for derivative terms involving them, preventing a potential.

A simple case which can be treated exactly is when we consider the VEV  $\langle \Pi_i \rangle$  of the Goldstones, and take  $g_{\mathcal{G}/\mathcal{H}} = U^{-1}$ ; in this case, we obtain:

$$\langle \Pi_i \rangle \rightarrow \mathbf{0}, \tag{A.2.17}$$

which implies that the VEV of the Goldstone bosons is not physical.



### A.2.1 $d$ and $e$ symbols

The two fundamental objects to construct the Goldstone Lagrangian are the  $d_\mu$  and  $e_\mu$  symbols, defined from the Goldstone matrix  $U[\Pi]$ . Since we saw that, schematically,  $[\hat{T}, \hat{T}] \sim \hat{T} + T$ , we can write:

$$i U^{-1}[\Pi] \partial_\mu U[\Pi] \equiv d_\mu^i \hat{T}^i + e_\mu^a T^a \equiv d_\mu + e_\mu, \quad (\text{A.2.18})$$

where  $d_\mu^i \in \mathbf{R}_\Pi$  and  $e_\mu^a \in \mathbf{A}_\mathcal{H}$ .

Taking into account that  $h \in \mathcal{H}$  is spacetime-dependent because it depends on the Goldstone fields  $\Pi$ 's, we have that under a group transformation:

$$i U^{-1}[\Pi] \partial_\mu U[\Pi] \rightarrow i h U^{-1}[\Pi] \partial_\mu U[\Pi] h^{-1} + i h \partial_\mu h^{-1}. \quad (\text{A.2.19})$$

Given that the last term is an element of  $\mathcal{H}$ , we identify the transformation properties of  $d_\mu$  and  $e_\mu$  as:

$$d_\mu \rightarrow h d_\mu h^{-1} \quad (\text{A.2.20a})$$

$$e_\mu \rightarrow h(e_\mu + i \partial_\mu) h^{-1}. \quad (\text{A.2.20b})$$

The first equation, once written in components, reads:

$$d_\mu^i \rightarrow (e^{i\alpha_a T_\Pi^a})_{ij} d_\mu^j, \quad (\text{A.2.21})$$

showing that  $d_\mu^i$  transforms like the Goldstone fields  $\Pi$ 's; this is natural, since it can be easily shown from eq. (A.2.18) that:

$$d_\mu^i = -\frac{\sqrt{2}}{f} \partial_\mu \Pi^i + \mathcal{O}\left(\frac{\partial \Pi}{f}, \frac{\Pi^2}{f^2}\right). \quad (\text{A.2.22})$$

However, differently from  $\Pi^i$ ,  $d_\mu^i$  transforms with  $\mathbf{R}_\Pi$  under the full group  $\mathcal{G}$ , and not only an  $\mathcal{H}$ -transformation. For this reason, it is more convenient to write down the effective Lagrangian starting from  $d_\mu$  rather than from the Goldstone fields. On the other hand, from eq. (A.2.20b) it also follows that  $e_\mu$  transforms like a (non-canonically normalized) gauge field, and as such it can be adopted to construct covariant derivatives and field strengths.

The general idea is to use  $d_\mu$  and  $e_\mu$  to write down the effective Lagrangian for the Goldstone fields; as we have just shown, if we write a Lagrangian which is invariant under  $\mathcal{H}$ , it is automatically invariant under the full group  $\mathcal{G}$  as well. The simplest operator we can consider is the one which only contains two derivatives, and it can be constructed from two  $d$  symbols (since  $\mathbf{R}_\Pi$  is real for compact  $\mathcal{H}$ ), leading to a kinetic term in the Lagrangian of the form:

$$\mathcal{L}_\Pi^{(2)} \equiv \frac{f^2}{4} \text{Tr}[d_\mu d^\mu] = \frac{1}{2} \partial_\mu \Pi^i \partial^\mu \Pi^i + \sum_n \mathcal{O}\left[(\partial \Pi)^2 \left(\frac{\Pi}{f}\right)^n\right], \quad (\text{A.2.23})$$

which provides the kinetic term for the Goldstones plus an infinite series of derivative interactions.

## A.2.2 Local invariance

The present formalism can be extended to include spacetime-dependent group transformations. To this purpose, we introduce a set of gauge fields:

$$A_\mu \equiv A_\mu^A T^A \quad : \quad A_\mu \xrightarrow{g \in \mathcal{G}} g(A_\mu + i\partial_\mu)g^{-1} \equiv A_\mu^{(g)}, \quad (\text{A.2.24})$$

with  $g = g(x) \in \mathcal{G}$  being a local transformation.

In this definition,  $A_\mu$  is non-canonically normalized; in fact, when restricted to the Standard Model, it reads:

$$A_\mu^{(\text{SM})} = g W_\mu^\alpha T_L^\alpha + g' B_\mu Y_W. \quad (\text{A.2.25})$$

The gauging procedure then consists, as usual, in modifying the Lagrangian by adding a coupling between the gauge field and an appropriate current to keep into account the spacetime-dependent nature of the group elements  $g$ , i.e.:

$$\mathcal{L} \rightarrow \mathcal{L} + J_\mu^A A_\mu^A. \quad (\text{A.2.26})$$

It can be convenient to consider the case in which the full group  $\mathcal{G}$  is gauged, and only at the end decouple the unwanted gauge fields by setting to zero the corresponding coupling constants; the advantage of this procedure lies in the fact that it allows for local invariance under the full  $\mathcal{G}$ , with the gauge fields transforming as in eq. (A.2.24).

It is also convenient to introduce a new object  $\bar{A}_\mu$ , called *dressed* gauge field, defined as:

$$\bar{A}_\mu \equiv A_\mu^{(U^{-1})} = U^{-1}[\Pi] (A_\mu + i\partial_\mu) U[\Pi]. \quad (\text{A.2.27})$$

The object  $\bar{A}_\mu$  is extremely useful because of its transformation property: in fact, under an element  $g(x) \in \mathcal{G}$ :

$$\bar{A}_\mu \rightarrow (A_\mu^{(g)})^{(hU^{-1}g^{-1})} = A_\mu^{(hU^{-1})} = (A_\mu^{(U^{-1})})^{(h)} = \bar{A}_\mu^{(h)} = h(\bar{A}_\mu + i\partial_\mu)h^{-1}. \quad (\text{A.2.28})$$

Therefore, the dressing procedure allows one, starting from an object transforming with the full group  $\mathcal{G}$ , to obtain a quantity which transforms under the subgroup  $\mathcal{H}$ . The same logic is used, e.g., in composite Higgs models to write the effective Lagrangian responsible for the interactions between the (pseudo-)Nambu-Goldstone bosons and the SM fermions.

In analogy with eq. (A.2.18), we can define the  $d$  and  $e$  symbols for the case of local invariance as:

$$\bar{A}_\mu = U^{-1}[\Pi] (A_\mu + i\partial_\mu) U[\Pi] \equiv d_\mu[A] + e_\mu[A]. \quad (\text{A.2.29})$$

This definition is consistent because it reduces to eq. (A.2.18) in the ungauged limit  $A_\mu = 0$ .

Analogously to the previous analysis, the transformation properties of these symbols are:

$$d_\mu[A] \rightarrow h d_\mu[A] h^{-1} \quad (\text{A.2.30a})$$

$$e_\mu[A] \rightarrow h(e_\mu[A] + i\partial_\mu)h^{-1}. \quad (\text{A.2.30b})$$

In addition, the two-derivatives Lagrangian simply generalizes to:

$$\mathcal{L}_\Pi^{(2)} \equiv \frac{f^2}{4} \text{Tr} (d_\mu[A] d^\mu[A]), \quad (\text{A.2.31})$$

which also provides the interactions between the Goldstone bosons and the gauge fields.

# Appendix B

## Effective field theories

In its simplest formulation, an EFT can be thought as characterized by two dimensionful quantities: a(n inverse) length scale  $m_*$ , identifiable with the scale at which the short-distance interactions take place, and a coupling  $0 \leq g_* \lesssim 4\pi$ . We sometimes call  $m_*$  a *mass*, with a slight abuse of notation, for a reason that will be clear in the following.<sup>1</sup>

At distances much larger than  $m_*^{-1}$ , we can describe the theory with an effective Lagrangian, where the heavy fields have been integrated out. We assume that the general form of the effective Lagrangian is:

$$\mathcal{L}_{\text{eff}} = \frac{m_*^4}{g_*^2} \hat{\mathcal{L}} \left( \frac{\partial}{m_*}, \frac{g_*\phi}{m_*}, \frac{g_*\psi}{m_*^{3/2}} \right), \quad (\text{B.1.1})$$

where  $\hat{\mathcal{L}}$  is a dimensionless function of its argument.

The equation above goes under the name of “SILH power-counting”, named after the model where it was first introduced [239]. The particular form of eq. (B.1.1) is an assumption, but it is well motivated by many phenomenological models: for example, in the maximally strongly coupled case,  $g_* \sim 4\pi$ , eq. (B.1.1) correctly reproduces the predictions from naive dimensional analysis [240, 241]. In addition, as we will see below, its applicability goes beyond the case of a strongly interacting sector.

It is then easy to derive the dimensions of  $m_*$  and  $g_*$  in terms of length ( $L$ ) and energy ( $E$ ) by restoring the physical units  $\hbar \neq 1$ : in particular, one easily finds from eq. (B.1.1) that  $[m_*] = L^{-1}$  and  $[g_*] = [\hbar]^{-1/2} = E^{-1/2}L^{-1/2}$  (we are still working with  $c = 1$ ). It is then evident that eq. (B.1.1) automatically provides canonically normalized fields without explicit factors of  $\hbar$  in the Lagrangian.

This simple power-counting rule has two important consequences: first of all, it shows that the “real” couplings in the SM are the Yukawa’s,  $y$ , and the square of the gauge couplings,  $\alpha_{SM} \propto g_{SM}^2$ . In addition, eq. (B.1.1) allows us to estimate the effective Lagrangian also in the case where some heavy fields are integrated out at loop level; given that a factor of  $\hbar/(16\pi^2)$  will appear for every loop, and that  $m_*$  and  $g_*$  are the only dimensionful parameters of the strong sector, the most general form of the effective Lagrangian is (restoring natural units) [27, 239]:

$$\mathcal{L}_{\text{eff}} = \frac{m_*^4}{g_*^2} \left[ \hat{\mathcal{L}}^{(0)} \left( \frac{\partial}{m_*}, \frac{g_*\phi}{m_*}, \frac{g_*\psi}{m_*^{3/2}} \right) + \frac{g_*^2}{16\pi^2} \hat{\mathcal{L}}^{(1)} \left( \frac{\partial}{m_*}, \frac{g_*\phi}{m_*}, \frac{g_*\psi}{m_*^{3/2}} \right) + \dots \right], \quad (\text{B.1.2})$$

where the dots stand for higher loops.

---

<sup>1</sup>Actually,  $m_*$  is a mass in units of  $\hbar$ , i.e.  $[m_*] = M/[\hbar]$ , if we work with  $c = 1$ .

Another parametrization, sometimes used in the literature (see, e.g., [83]), is equivalent to eq. (B.1.1) and somehow more transparent. If we imagine to have an effective Lagrangian  $\mathcal{L}_{\text{eff}}$ , we can imagine to decompose it in two contributions according to renormalizability, similarly to what we did in section 1.2:

$$\mathcal{L}_{\text{eff}} = \mathcal{L}_{\text{ren}} + \sum_{d>4,i} c_i^{(d)} \mathcal{O}_i^{(d)}, \quad (\text{B.1.3})$$

where  $\mathcal{O}_i^{(d)}$  is a gauge-invariant operator of energy dimension (in natural units)  $d$ . The coefficients  $c_i^{(d)}$  will be functions of  $m_*$  and  $g_*$ , the only dimensionful parameters of the underlying UV theory; in particular, if  $\mathcal{O}_i^{(d)}$  is made of  $n_i$  fields  $\phi_i$  of spin  $s_i$  and  $k_i$  derivatives, then  $[\mathcal{O}_i^{(d)}] = [\hbar]^{n_i/2} L^{-d}$  (remember that  $[\phi_i] = [\hbar]^{n_i/2} L^{-(s_i+1)}$ ), with  $d \equiv n_i(s_i + 1) + k_i$ . By restoring the physical units, we then obtain:

$$[c_i^{(d)}] = [\hbar] L^{-4} [\mathcal{O}_i^{(d)}]^{-1} = [\hbar]^{1-n_i/2} L^{d-4} \quad \Rightarrow \quad c_i^{(d)} \sim \frac{g_*^{n_i-2}}{m_*^{d-4}}. \quad (\text{B.1.4})$$

This power counting could also have been obtained directly from eq. (B.1.2) by expanding it in the arguments of  $\hat{\mathcal{L}}$ . Even in this case, a suppression of  $g_*^2/(16\pi^2)$  appears in the estimate of  $c_i^{(d)}$  if the operator is generated at 1-loop.

As a final remark, we want to stress that from the SILH power counting we can also appreciate the difference between the concepts of scales and masses [242]. If we consider an effective operator of the form:

$$c \mathcal{O} \sim \frac{1}{\Lambda^{d-4}} \partial^k \phi^n, \quad (\text{B.1.5})$$

where  $n$  and  $k$  were defined above, from eq. (B.1.4) we immediately obtain:

$$\Lambda \sim \frac{m_*}{g_*^{\frac{n-2}{d-4}}}. \quad (\text{B.1.6})$$

$\Lambda$  is what we refer to as a *scale*, and we see that it is the product of a mass by some power of the corresponding coupling. In the prototypical example of the weak theory, we can make the identification  $\Lambda \sim G_F^{-\frac{1}{2}} \sim m_W/g$ ; we then see that while the scale identifies where perturbative unitarity breaks down in the absence of new degrees of freedom, the mass is associated to the energy at which new states can be produced.

# Bibliography

- [1] A. Davoli, A. De Simone, T. Jacques and V. Sanz, *Displaced Vertices from Pseudo-Dirac Dark Matter*, *JHEP* **11** (2017) 025, [[1706.08985](#)].
- [2] A. Davoli, A. De Simone, T. Jacques and A. Morandini, *LHC Phenomenology of Dark Matter with a Color-Octet Partner*, *JHEP* **07** (2018) 054, [[1803.02861](#)].
- [3] A. Davoli, A. De Simone, D. Marzocca and A. Morandini, *Composite 2HDM with singlets: a viable dark matter scenario*, [1905.13244](#).
- [4] S. Weinberg, *A Model of Leptons*, *Phys. Rev. Lett.* **19** (1967) 1264–1266.
- [5] S. L. Glashow, *Partial Symmetries of Weak Interactions*, *Nucl. Phys.* **22** (1961) 579–588.
- [6] P. W. Higgs, *Broken Symmetries and the Masses of Gauge Bosons*, *Phys. Rev. Lett.* **13** (1964) 508–509.
- [7] ATLAS collaboration, G. Aad et al., *Observation of a new particle in the search for the Standard Model Higgs boson with the ATLAS detector at the LHC*, *Phys. Lett.* **B716** (2012) 1–29, [[1207.7214](#)].
- [8] CMS collaboration, S. Chatrchyan et al., *Observation of a new boson at a mass of 125 GeV with the CMS experiment at the LHC*, *Phys. Lett.* **B716** (2012) 30–61, [[1207.7235](#)].
- [9] A. Denner, S. Heinemeyer, I. Puljak, D. Rebuszi and M. Spira, *Standard Model Higgs-Boson Branching Ratios with Uncertainties*, *Eur. Phys. J.* **C71** (2011) 1753, [[1107.5909](#)].
- [10] S. R. Coleman, J. Wess and B. Zumino, *Structure of phenomenological Lagrangians. 1.*, *Phys. Rev.* **177** (1969) 2239–2247.
- [11] C. G. Callan, Jr., S. R. Coleman, J. Wess and B. Zumino, *Structure of phenomenological Lagrangians. 2.*, *Phys. Rev.* **177** (1969) 2247–2250.
- [12] R. Contino, *The Higgs as a Composite Nambu-Goldstone Boson*, in *Physics of the large and the small, TASI 09, proceedings of the Theoretical Advanced Study Institute in Elementary Particle Physics, Boulder, Colorado, USA, 1-26 June 2009*, pp. 235–306, 2011. [1005.4269](#). DOI.
- [13] R. Contino, C. Grojean, M. Moretti, F. Piccinini and R. Rattazzi, *Strong Double Higgs Production at the LHC*, *JHEP* **05** (2010) 089, [[1002.1011](#)].

- [14] E. Farhi and L. Susskind, *Technicolor*, *Phys. Rept.* **74** (1981) 277.
- [15] L. Susskind, *Dynamics of Spontaneous Symmetry Breaking in the Weinberg-Salam Theory*, *Phys. Rev.* **D20** (1979) 2619–2625.
- [16] G. 't Hooft, *Renormalizable Lagrangians for Massive Yang-Mills Fields*, *Nucl. Phys.* **B35** (1971) 167–188.
- [17] G. 't Hooft and M. J. G. Veltman, *Regularization and Renormalization of Gauge Fields*, *Nucl. Phys.* **B44** (1972) 189–213.
- [18] S. Weinberg, *The Quantum theory of fields. Vol. 1: Foundations*. Cambridge University Press, 2005.
- [19] L. Wolfenstein, *Parametrization of the Kobayashi-Maskawa Matrix*, *Phys. Rev. Lett.* **51** (1983) 1945.
- [20] PARTICLE DATA GROUP collaboration, M. Tanabashi et al., *Review of Particle Physics*, *Phys. Rev.* **D98** (2018) 030001.
- [21] S. L. Glashow, J. Iliopoulos and L. Maiani, *Weak Interactions with Lepton-Hadron Symmetry*, *Phys. Rev.* **D2** (1970) 1285–1292.
- [22] G. D'Ambrosio, G. F. Giudice, G. Isidori and A. Strumia, *Minimal flavor violation: An Effective field theory approach*, *Nucl. Phys.* **B645** (2002) 155–187, [[hep-ph/0207036](#)].
- [23] G. 't Hooft, *Naturalness, chiral symmetry, and spontaneous chiral symmetry breaking*, *NATO Sci. Ser. B* **59** (1980) 135–157.
- [24] M. J. G. Veltman, *Limit on Mass Differences in the Weinberg Model*, *Nucl. Phys.* **B123** (1977) 89–99.
- [25] M. S. Chanowitz, M. A. Furman and I. Hinchliffe, *Weak Interactions of Ultraheavy Fermions*, *Phys. Lett.* **78B** (1978) 285.
- [26] P. Sikivie, L. Susskind, M. B. Voloshin and V. I. Zakharov, *Isospin Breaking in Technicolor Models*, *Nucl. Phys.* **B173** (1980) 189–207.
- [27] G. Panico and A. Wulzer, *The Composite Nambu-Goldstone Higgs*, *Lect. Notes Phys.* **913** (2016) pp.1–316, [[1506.01961](#)].
- [28] M. E. Peskin and D. V. Schroeder, *An Introduction to quantum field theory*. Addison-Wesley, Reading, USA, 1995.
- [29] R. Barbieri, A. Pomarol, R. Rattazzi and A. Strumia, *Electroweak symmetry breaking after LEP-1 and LEP-2*, *Nucl. Phys.* **B703** (2004) 127–146, [[hep-ph/0405040](#)].
- [30] M. E. Peskin and T. Takeuchi, *Estimation of oblique electroweak corrections*, *Phys. Rev.* **D46** (1992) 381–409.
- [31] J. Haller, A. Hoecker, R. Kogler, K. Mönig, T. Peiffer and J. Stelzer, *Update of the global electroweak fit and constraints on two-Higgs-doublet models*, *Eur. Phys. J.* **C78** (2018) 675, [[1803.01853](#)].

- [32] G. F. Giudice, *Naturalness after LHC8*, *PoS EPS-HEP2013* (2013) 163, [[1307.7879](#)].
- [33] G. F. Giudice, *The Dawn of the Post-Naturalness Era*, in *From My Vast Repertoire ...: Guido Altarelli's Legacy* (A. Levy, S. Forte and G. Ridolfi, eds.), pp. 267–292. 2019. [1710.07663](#). DOI.
- [34] D. B. Kaplan, H. Georgi and S. Dimopoulos, *Composite Higgs Scalars*, *Phys. Lett.* **136B** (1984) 187–190.
- [35] D. B. Kaplan and H. Georgi,  *$SU(2) \times U(1)$  Breaking by Vacuum Misalignment*, *Phys. Lett.* **136B** (1984) 183–186.
- [36] H. Georgi and D. B. Kaplan, *Composite Higgs and Custodial  $SU(2)$* , *Phys. Lett.* **145B** (1984) 216–220.
- [37] M. J. Dugan, H. Georgi and D. B. Kaplan, *Anatomy of a Composite Higgs Model*, *Nucl. Phys.* **B254** (1985) 299–326.
- [38] J. Wess and B. Zumino, *Supergauge Transformations in Four-Dimensions*, *Nucl. Phys.* **B70** (1974) 39–50.
- [39] P. Fayet and S. Ferrara, *Supersymmetry*, *Phys. Rept.* **32** (1977) 249–334.
- [40] P. Fayet, *Supersymmetry, Particle Physics and Gravitation*, *Ettore Majorana Int. Sci. Ser. Phys. Sci.* **7** (1980) 587.
- [41] J. C. Kapteyn, *First Attempt at a Theory of the Arrangement and Motion of the Sidereal System*, *Astrophys. J.* **55** (1922) 302–328.
- [42] F. Zwicky, *Die Rotverschiebung von extragalaktischen Nebeln*, *Helv. Phys. Acta* **6** (1933) 110–127.
- [43] V. C. Rubin and W. K. Ford, Jr., *Rotation of the Andromeda Nebula from a Spectroscopic Survey of Emission Regions*, *Astrophys. J.* **159** (1970) 379–403.
- [44] K. G. Begeman, A. H. Broeils and R. H. Sanders, *Extended rotation curves of spiral galaxies: Dark haloes and modified dynamics*, *Mon. Not. Roy. Astron. Soc.* **249** (1991) 523.
- [45] D. Clowe, M. Bradac, A. H. Gonzalez, M. Markevitch, S. W. Randall, C. Jones et al., *A direct empirical proof of the existence of dark matter*, *Astrophys. J.* **648** (2006) L109–L113, [[astro-ph/0608407](#)].
- [46] PLANCK collaboration, N. Aghanim et al., *Planck 2018 results. VI. Cosmological parameters*, [1807.06209](#).
- [47] L. Wyrzykowski, J. Skowron, S. Kozłowski, A. Udalski, M. K. Szymański, M. Kubiak et al., *The OGLE view of microlensing towards the Magellanic Clouds – IV. OGLE-III SMC data and final conclusions on MACHOs\**, *Monthly Notices of the Royal Astronomical Society* **416** (2011) 2949–2961.

- [48] M. Lisanti, *Lectures on Dark Matter Physics*, in *Proceedings, Theoretical Advanced Study Institute in Elementary Particle Physics: New Frontiers in Fields and Strings (TASI 2015): Boulder, CO, USA, June 1-26, 2015*, pp. 399–446, 2017. [1603.03797](#). DOI.
- [49] E. W. Kolb and M. S. Turner, *The Early Universe*, *Front. Phys.* **69** (1990) 1–547.
- [50] A. A. Klypin, A. V. Kravtsov, O. Valenzuela and F. Prada, *Where are the missing Galactic satellites?*, *Astrophys. J.* **522** (1999) 82–92, [[astro-ph/9901240](#)].
- [51] M. Boylan-Kolchin, J. S. Bullock and M. Kaplinghat, *Too big to fail? The puzzling darkness of massive Milky Way subhaloes*, *Mon. Not. Roy. Astron. Soc.* **415** (2011) L40, [[1103.0007](#)].
- [52] B. Audren, J. Lesgourgues, G. Mangano, P. D. Serpico and T. Tram, *Strongest model-independent bound on the lifetime of Dark Matter*, *JCAP* **1412** (2014) 028, [[1407.2418](#)].
- [53] L. Roszkowski, E. M. Sessolo and S. Trojanowski, *WIMP dark matter candidates and searches—current status and future prospects*, *Rept. Prog. Phys.* **81** (2018) 066201, [[1707.06277](#)].
- [54] K. Griest and M. Kamionkowski, *Unitarity Limits on the Mass and Radius of Dark Matter Particles*, *Phys. Rev. Lett.* **64** (1990) 615.
- [55] N. Arkani-Hamed, S. Dimopoulos and G. R. Dvali, *The Hierarchy problem and new dimensions at a millimeter*, *Phys. Lett.* **B429** (1998) 263–272, [[hep-ph/9803315](#)].
- [56] I. Antoniadis, N. Arkani-Hamed, S. Dimopoulos and G. R. Dvali, *New dimensions at a millimeter to a Fermi and superstrings at a TeV*, *Phys. Lett.* **B436** (1998) 257–263, [[hep-ph/9804398](#)].
- [57] L. Randall and R. Sundrum, *A Large mass hierarchy from a small extra dimension*, *Phys. Rev. Lett.* **83** (1999) 3370–3373, [[hep-ph/9905221](#)].
- [58] H.-C. Cheng, J. L. Feng and K. T. Matchev, *Kaluza-Klein dark matter*, *Phys. Rev. Lett.* **89** (2002) 211301, [[hep-ph/0207125](#)].
- [59] R. D. Peccei and H. R. Quinn, *CP Conservation in the Presence of Instantons*, *Phys. Rev. Lett.* **38** (1977) 1440–1443.
- [60] F. Wilczek, *Problem of Strong P and T Invariance in the Presence of Instantons*, *Phys. Rev. Lett.* **40** (1978) 279–282.
- [61] V. B. Klaer and G. D. Moore, *The dark-matter axion mass*, *JCAP* **1711** (2017) 049, [[1708.07521](#)].
- [62] T. Yanagida, *Horizontal gauge symmetry and masses of neutrinos*, *Conf. Proc.* **C7902131** (1979) 95–99.
- [63] M. Gell-Mann, P. Ramond and R. Slansky, *Complex Spinors and Unified Theories*, *Conf. Proc.* **C790927** (1979) 315–321, [[1306.4669](#)].



- [64] A. Boyarsky, M. Drewes, T. Lasserre, S. Mertens and O. Ruchayskiy, *Sterile Neutrino Dark Matter*, *Prog. Part. Nucl. Phys.* **104** (2019) 1–45, [[1807.07938](#)].
- [65] S. Hawking, *Gravitationally collapsed objects of very low mass*, *Mon. Not. Roy. Astron. Soc.* **152** (1971) 75.
- [66] M. Khlopov, B. A. Malomed and I. B. Zeldovich, *Gravitational instability of scalar fields and formation of primordial black holes*, *Mon. Not. Roy. Astron. Soc.* **215** (1985) 575–589.
- [67] N. Bartolo, V. De Luca, G. Franciolini, M. Peloso, D. Racco and A. Riotto, *Testing primordial black holes as dark matter with LISA*, *Phys. Rev.* **D99** (2019) 103521, [[1810.12224](#)].
- [68] L. Hui, J. P. Ostriker, S. Tremaine and E. Witten, *Ultralight scalars as cosmological dark matter*, *Phys. Rev.* **D95** (2017) 043541, [[1610.08297](#)].
- [69] S. Dodelson, *Modern Cosmology*. Academic Press, Amsterdam, 2003.
- [70] K. Griest and D. Seckel, *Three exceptions in the calculation of relic abundances*, *Phys. Rev.* **D43** (1991) 3191–3203.
- [71] R. T. D’Agnolo, D. Pappadopulo and J. T. Ruderman, *Fourth Exception in the Calculation of Relic Abundances*, *Phys. Rev. Lett.* **119** (2017) 061102, [[1705.08450](#)].
- [72] M. W. Goodman and E. Witten, *Detectability of Certain Dark Matter Candidates*, *Phys. Rev.* **D31** (1985) 3059.
- [73] XENON collaboration, E. Aprile et al., *Dark Matter Search Results from a One Ton-Year Exposure of XENON1T*, *Phys. Rev. Lett.* **121** (2018) 111302, [[1805.12562](#)].
- [74] PANDAX-II collaboration, X. Cui et al., *Dark Matter Results From 54-Ton-Day Exposure of PandaX-II Experiment*, *Phys. Rev. Lett.* **119** (2017) 181302, [[1708.06917](#)].
- [75] LUX collaboration, D. S. Akerib et al., *Results from a search for dark matter in the complete LUX exposure*, *Phys. Rev. Lett.* **118** (2017) 021303, [[1608.07648](#)].
- [76] M. Cirelli, E. Del Nobile and P. Panci, *Tools for model-independent bounds in direct dark matter searches*, *JCAP* **1310** (2013) 019, [[1307.5955](#)].
- [77] A. Berlin, D. Hooper and S. D. McDermott, *Simplified Dark Matter Models for the Galactic Center Gamma-Ray Excess*, *Phys. Rev.* **D89** (2014) 115022, [[1404.0022](#)].
- [78] M. Schumann, *Direct Detection of WIMP Dark Matter: Concepts and Status*, [1903.03026](#).
- [79] R. Bernabei et al., *First Model Independent Results from DAMA/LIBRA-Phase2*, *Universe* **4** (2018) 116, [[1805.10486](#)].

- [80] T. R. Slatyer, *Indirect Detection of Dark Matter*, in *Proceedings, Theoretical Advanced Study Institute in Elementary Particle Physics : Anticipating the Next Discoveries in Particle Physics (TASI 2016): Boulder, CO, USA, June 6-July 1, 2016*, pp. 297–353, 2018. [1710.05137](#). DOI.
- [81] FERMI-LAT collaboration, M. Ackermann et al., *Searching for Dark Matter Annihilation from Milky Way Dwarf Spheroidal Galaxies with Six Years of Fermi Large Area Telescope Data*, *Phys. Rev. Lett.* **115** (2015) 231301, [[1503.02641](#)].
- [82] T. Han, *Collider phenomenology: Basic knowledge and techniques*, pp. 407–454, 2005. [hep-ph/0508097](#). DOI.
- [83] R. Contino, A. Falkowski, F. Goertz, C. Grojean and F. Riva, *On the Validity of the Effective Field Theory Approach to SM Precision Tests*, *JHEP* **07** (2016) 144, [[1604.06444](#)].
- [84] G. Busoni, A. De Simone, E. Morgante and A. Riotto, *On the Validity of the Effective Field Theory for Dark Matter Searches at the LHC*, *Phys. Lett.* **B728** (2014) 412–421, [[1307.2253](#)].
- [85] E. Morgante, *On the validity of the effective field theory for dark matter searches at the LHC*, *Nuovo Cim.* **C38** (2015) 32, [[1409.6668](#)].
- [86] G. Busoni, *Limitation of EFT for DM interactions at the LHC*, *PoS DIS2014* (2014) 134, [[1411.3600](#)].
- [87] G. Busoni, A. De Simone, T. Jacques, E. Morgante and A. Riotto, *On the Validity of the Effective Field Theory for Dark Matter Searches at the LHC Part III: Analysis for the t-channel*, *JCAP* **1409** (2014) 022, [[1405.3101](#)].
- [88] G. Busoni, A. De Simone, J. Gramling, E. Morgante and A. Riotto, *On the Validity of the Effective Field Theory for Dark Matter Searches at the LHC, Part II: Complete Analysis for the s-channel*, *JCAP* **1406** (2014) 060, [[1402.1275](#)].
- [89] N. F. Bell, Y. Cai, J. B. Dent, R. K. Leane and T. J. Weiler, *Dark matter at the LHC: Effective field theories and gauge invariance*, *Phys. Rev.* **D92** (2015) 053008, [[1503.07874](#)].
- [90] A. De Simone and T. Jacques, *Simplified models vs. effective field theory approaches in dark matter searches*, *Eur. Phys. J.* **C76** (2016) 367, [[1603.08002](#)].
- [91] S. Bruggisser, F. Riva and A. Urbano, *The Last Gasp of Dark Matter Effective Theory*, *JHEP* **11** (2016) 069, [[1607.02475](#)].
- [92] F. Kahlhoefer, *Review of LHC Dark Matter Searches*, *Int. J. Mod. Phys.* **A32** (2017) 1730006, [[1702.02430](#)].
- [93] J. Abdallah et al., *Simplified Models for Dark Matter Searches at the LHC*, *Phys. Dark Univ.* **9-10** (2015) 8–23, [[1506.03116](#)].
- [94] ATLAS collaboration, M. Aaboud et al., *Search for new phenomena in final states with an energetic jet and large missing transverse momentum in pp collisions at  $\sqrt{s} = 13$  TeV using the ATLAS detector*, *Phys. Rev.* **D94** (2016) 032005, [[1604.07773](#)].

- [95] CMS collaboration, D. Vannerom, *Search for dark matter with jets and missing transverse energy at 13 TeV*, *PoS LHCP2016* (2016) 218.
- [96] ATLAS collaboration, M. Aaboud et al., *Search for dark matter and other new phenomena in events with an energetic jet and large missing transverse momentum using the ATLAS detector*, [1711.03301](#).
- [97] CMS collaboration, A. M. Sirunyan et al., *Search for new phenomena in final states with two opposite-charge, same-flavor leptons, jets, and missing transverse momentum in pp collisions at  $\sqrt{s} = 13$  TeV*, [1709.08908](#).
- [98] J. Alimena et al., *Searching for Long-Lived Particles beyond the Standard Model at the Large Hadron Collider*, [1903.04497](#).
- [99] J. D. Wells, *Implications of supersymmetry breaking with a little hierarchy between gauginos and scalars*, in *11th International Conference on Supersymmetry and the Unification of Fundamental Interactions (SUSY 2003) Tucson, Arizona, June 5-10, 2003*, 2003. [hep-ph/0306127](#).
- [100] N. Arkani-Hamed and S. Dimopoulos, *Supersymmetric unification without low energy supersymmetry and signatures for fine-tuning at the LHC*, *JHEP* **06** (2005) 073, [[hep-th/0405159](#)].
- [101] A. Arvanitaki, N. Craig, S. Dimopoulos and G. Villadoro, *Mini-Split*, *JHEP* **02** (2013) 126, [[1210.0555](#)].
- [102] N. Arkani-Hamed, A. Gupta, D. E. Kaplan, N. Weiner and T. Zorawski, *Simply Unnatural Supersymmetry*, [1212.6971](#).
- [103] Y. Cui and B. Shuve, *Probing Baryogenesis with Displaced Vertices at the LHC*, *JHEP* **02** (2015) 049, [[1409.6729](#)].
- [104] C. Csaki, E. Kuflik, S. Lombardo, O. Slone and T. Volansky, *Phenomenology of a Long-Lived LSP with R-Parity Violation*, *JHEP* **08** (2015) 016, [[1505.00784](#)].
- [105] J. Barnard, P. Cox, T. Gherghetta and A. Spray, *Long-Lived, Colour-Triplet Scalars from Unnaturalness*, *JHEP* **03** (2016) 003, [[1510.06405](#)].
- [106] D. E. Kaplan, M. A. Luty and K. M. Zurek, *Asymmetric Dark Matter*, *Phys. Rev.* **D79** (2009) 115016, [[0901.4117](#)].
- [107] M. Baumgart, C. Cheung, J. T. Ruderman, L.-T. Wang and I. Yavin, *Non-Abelian Dark Sectors and Their Collider Signatures*, *JHEP* **04** (2009) 014, [[0901.0283](#)].
- [108] K. R. Dienes, S. Su and B. Thomas, *Distinguishing Dynamical Dark Matter at the LHC*, *Phys. Rev.* **D86** (2012) 054008, [[1204.4183](#)].
- [109] I.-W. Kim and K. M. Zurek, *Flavor and Collider Signatures of Asymmetric Dark Matter*, *Phys. Rev.* **D89** (2014) 035008, [[1310.2617](#)].
- [110] R. T. Co, F. D'Eramo, L. J. Hall and D. Pappadopulo, *Freeze-In Dark Matter with Displaced Signatures at Colliders*, *JCAP* **1512** (2015) 024, [[1506.07532](#)].

- [111] Y. Hochberg, E. Kuflik and H. Murayama, *SIMP Spectroscopy*, *JHEP* **05** (2016) 090, [[1512.07917](#)].
- [112] A. De Simone, V. Sanz and H. P. Sato, *Pseudo-Dirac Dark Matter Leaves a Trace*, *Phys. Rev. Lett.* **105** (2010) 121802, [[1004.1567](#)].
- [113] S. Abel and M. Goodsell, *Easy Dirac Gauginos*, *JHEP* **06** (2011) 064, [[1102.0014](#)].
- [114] G. F. Giudice, T. Han, K. Wang and L.-T. Wang, *Nearly Degenerate Gauginos and Dark Matter at the LHC*, *Phys. Rev.* **D81** (2010) 115011, [[1004.4902](#)].
- [115] P. J. Fox, A. E. Nelson and N. Weiner, *Dirac gaugino masses and supersoft supersymmetry breaking*, *JHEP* **08** (2002) 035, [[hep-ph/0206096](#)].
- [116] D. Tucker-Smith and N. Weiner, *Inelastic dark matter*, *Phys. Rev.* **D64** (2001) 043502, [[hep-ph/0101138](#)].
- [117] A. E. Nelson, N. Rius, V. Sanz and M. Unsal, *The Minimal supersymmetric model without a mu term*, *JHEP* **08** (2002) 039, [[hep-ph/0206102](#)].
- [118] M. J. Strassler and K. M. Zurek, *Echoes of a hidden valley at hadron colliders*, *Phys. Lett.* **B651** (2007) 374–379, [[hep-ph/0604261](#)].
- [119] M. J. Strassler and K. M. Zurek, *Discovering the Higgs through highly-displaced vertices*, *Phys. Lett.* **B661** (2008) 263–267, [[hep-ph/0605193](#)].
- [120] C. Cheung, J. T. Ruderman, L.-T. Wang and I. Yavin, *Lepton Jets in (Supersymmetric) Electroweak Processes*, *JHEP* **04** (2010) 116, [[0909.0290](#)].
- [121] P. Meade, S. Nussinov, M. Papucci and T. Volansky, *Searches for Long Lived Neutral Particles*, *JHEP* **06** (2010) 029, [[0910.4160](#)].
- [122] J. L. Feng, M. Kamionkowski and S. K. Lee, *Light Gravitinos at Colliders and Implications for Cosmology*, *Phys. Rev.* **D82** (2010) 015012, [[1004.4213](#)].
- [123] A. Falkowski, J. T. Ruderman, T. Volansky and J. Zupan, *Hidden Higgs Decaying to Lepton Jets*, *JHEP* **05** (2010) 077, [[1002.2952](#)].
- [124] P. Meade, M. Reece and D. Shih, *Long-Lived Neutralino NLSPs*, *JHEP* **10** (2010) 067, [[1006.4575](#)].
- [125] P. Meade, M. Papucci and T. Volansky, *Odd Tracks at Hadron Colliders*, *Phys. Rev. Lett.* **109** (2012) 031801, [[1103.3016](#)].
- [126] ATLAS collaboration, G. Aad et al., *Search for displaced muonic lepton jets from light Higgs boson decay in proton-proton collisions at  $\sqrt{s} = 7$  TeV with the ATLAS detector*, *Phys. Lett.* **B721** (2013) 32–50, [[1210.0435](#)].
- [127] ATLAS collaboration, G. Aad et al., *Search for long-lived stopped R-hadrons decaying out-of-time with pp collisions using the ATLAS detector*, *Phys. Rev.* **D88** (2013) 112003, [[1310.6584](#)].
- [128] J. C. Helo, M. Hirsch and S. Kovalenko, *Heavy neutrino searches at the LHC with displaced vertices*, *Phys. Rev.* **D89** (2014) 073005, [[1312.2900](#)].

- [129] P. Jaiswal, K. Kopp and T. Okui, *Higgs Production Amidst the LHC Detector*, *Phys. Rev.* **D87** (2013) 115017, [[1303.1181](#)].
- [130] ATLAS collaboration, G. Aad et al., *Search for long-lived neutral particles decaying into lepton jets in proton-proton collisions at  $\sqrt{s} = 8$  TeV with the ATLAS detector*, *JHEP* **11** (2014) 088, [[1409.0746](#)].
- [131] M. R. Buckley, V. Halyo and P. Lujan, *Don't Miss the Displaced Higgs at the LHC Again*, [1405.2082](#).
- [132] CMS collaboration, V. Khachatryan et al., *Search for Long-Lived Neutral Particles Decaying to Quark-Antiquark Pairs in Proton-Proton Collisions at  $\sqrt{s} = 8$  TeV*, *Phys. Rev.* **D91** (2015) 012007, [[1411.6530](#)].
- [133] ATLAS collaboration, G. Aad et al., *Search for massive, long-lived particles using multitrack displaced vertices or displaced lepton pairs in pp collisions at  $\sqrt{s} = 8$  TeV with the ATLAS detector*, *Phys. Rev.* **D92** (2015) 072004, [[1504.05162](#)].
- [134] J. D. Clarke, *Constraining portals with displaced Higgs decay searches at the LHC*, *JHEP* **10** (2015) 061, [[1505.00063](#)].
- [135] C. Csaki, E. Kuffik, S. Lombardo and O. Slone, *Searching for displaced Higgs boson decays*, *Phys. Rev.* **D92** (2015) 073008, [[1508.01522](#)].
- [136] D. Curtin and C. B. Verhaaren, *Discovering Uncolored Naturalness in Exotic Higgs Decays*, *JHEP* **12** (2015) 072, [[1506.06141](#)].
- [137] CMS collaboration, V. Khachatryan et al., *Search for Decays of Stopped Long-Lived Particles Produced in Proton-Proton Collisions at  $\sqrt{s} = 8$  TeV*, *Eur. Phys. J.* **C75** (2015) 151, [[1501.05603](#)].
- [138] Z. Liu and B. Tweedie, *The Fate of Long-Lived Superparticles with Hadronic Decays after LHC Run 1*, *JHEP* **06** (2015) 042, [[1503.05923](#)].
- [139] P. Schwaller, D. Stolarski and A. Weiler, *Emerging Jets*, *JHEP* **05** (2015) 059, [[1502.05409](#)].
- [140] ATLAS collaboration, M. Aaboud et al., *Search for metastable heavy charged particles with large ionization energy loss in pp collisions at  $\sqrt{s} = 13$  TeV using the ATLAS experiment*, *Phys. Rev.* **D93** (2016) 112015, [[1604.04520](#)].
- [141] ATLAS collaboration, M. Aaboud et al., *Search for heavy long-lived charged R-hadrons with the ATLAS detector in  $3.2 \text{ fb}^{-1}$  of proton-proton collision data at  $\sqrt{s} = 13$  TeV*, *Phys. Lett.* **B760** (2016) 647–665, [[1606.05129](#)].
- [142] B. C. Allanach, M. Badziak, G. Cottin, N. Desai, C. Hugonie and R. Ziegler, *Prompt Signals and Displaced Vertices in Sparticle Searches for Next-to-Minimal Gauge Mediated Supersymmetric Models*, *Eur. Phys. J.* **C76** (2016) 482, [[1606.03099](#)].
- [143] A. Coccaro, D. Curtin, H. J. Lubatti, H. Russell and J. Shelton, *Data-driven Model-independent Searches for Long-lived Particles at the LHC*, *Phys. Rev.* **D94** (2016) 113003, [[1605.02742](#)].

- [144] CMS collaboration, V. Khachatryan et al., *Search for long-lived charged particles in proton-proton collisions at  $\sqrt{s} = 13$  TeV*, *Phys. Rev.* **D94** (2016) 112004, [[1609.08382](#)].
- [145] R. Mahbubani, P. Schwaller and J. Zurita, *Closing the window for compressed Dark Sectors with disappearing charged tracks*, [1703.05327](#).
- [146] O. Buchmueller, A. De Roeck, M. McCullough, K. Hahn, K. Sung, P. Schwaller et al., *Simplified Models for Displaced Dark Matter Signatures*, [1704.06515](#).
- [147] S. Antusch, E. Cazzato and O. Fischer, *Sterile neutrino searches via displaced vertices at LHCb*, [1706.05990](#).
- [148] F. Kahlhoefer, K. Schmidt-Hoberg, T. Schwetz and S. Vogl, *Implications of unitarity and gauge invariance for simplified dark matter models*, *JHEP* **02** (2016) 016, [[1510.02110](#)].
- [149] M. Duerr, F. Kahlhoefer, K. Schmidt-Hoberg, T. Schwetz and S. Vogl, *How to save the WIMP: global analysis of a dark matter model with two s-channel mediators*, *JHEP* **09** (2016) 042, [[1606.07609](#)].
- [150] J. Fan, M. Reece and L.-T. Wang, *Non-relativistic effective theory of dark matter direct detection*, *JCAP* **1011** (2010) 042, [[1008.1591](#)].
- [151] A. L. Fitzpatrick, W. Haxton, E. Katz, N. Lubbers and Y. Xu, *The Effective Field Theory of Dark Matter Direct Detection*, *JCAP* **1302** (2013) 004, [[1203.3542](#)].
- [152] J. B. Dent, L. M. Krauss, J. L. Newstead and S. Sabharwal, *General analysis of direct dark matter detection: From microphysics to observational signatures*, *Phys. Rev.* **D92** (2015) 063515, [[1505.03117](#)].
- [153] PANDAX-II collaboration, A. Tan et al., *Dark Matter Results from First 98.7 Days of Data from the PandaX-II Experiment*, *Phys. Rev. Lett.* **117** (2016) 121303, [[1607.07400](#)].
- [154] XENON100 collaboration, E. Aprile et al., *XENON100 Dark Matter Results from a Combination of 477 Live Days*, *Phys. Rev.* **D94** (2016) 122001, [[1609.06154](#)].
- [155] S. El Hedri, A. Kaminska, M. de Vries and J. Zurita, *Simplified Phenomenology for Colored Dark Sectors*, *JHEP* **04** (2017) 118, [[1703.00452](#)].
- [156] G. Busoni et al., *Recommendations on presenting LHC searches for missing transverse energy signals using simplified s-channel models of dark matter*, [1603.04156](#).
- [157] LUX collaboration, D. S. Akerib et al., *Limits on spin-dependent WIMP-nucleon cross section obtained from the complete LUX exposure*, *Phys. Rev. Lett.* **118** (2017) 251302, [[1705.03380](#)].
- [158] ATLAS collaboration, T. A. collaboration, *Search for New Phenomena in Dijet Events with the ATLAS Detector at  $\sqrt{s}=13$  TeV with 2015 and 2016 data*, .
- [159] PLANCK collaboration, P. A. R. Ade et al., *Planck 2015 results. XIII. Cosmological parameters*, [1502.01589](#).

- [160] H. An, X. Ji and L.-T. Wang, *Light Dark Matter and  $Z'$  Dark Force at Colliders*, *JHEP* **07** (2012) 182, [[1202.2894](#)].
- [161] T. Jacques and K. Nordström, *Mapping monojet constraints onto Simplified Dark Matter Models*, *JHEP* **06** (2015) 142, [[1502.05721](#)].
- [162] D. Barducci, A. Belyaev, A. K. M. Bharucha, W. Porod and V. Sanz, *Uncovering Natural Supersymmetry via the interplay between the LHC and Direct Dark Matter Detection*, *JHEP* **07** (2015) 066, [[1504.02472](#)].
- [163] ATLAS collaboration, G. Aad et al., *Search for long-lived, weakly interacting particles that decay to displaced hadronic jets in proton-proton collisions at  $\sqrt{s} = 8$  TeV with the ATLAS detector*, *Phys. Rev.* **D92** (2015) 012010, [[1504.03634](#)].
- [164] DELPHES 3 collaboration, J. de Favereau, C. Delaere, P. Demin, A. Giammanco, V. Lemaître, A. Mertens et al., *DELPHES 3, A modular framework for fast simulation of a generic collider experiment*, *JHEP* **02** (2014) 057, [[1307.6346](#)].
- [165] A. De Simone, G. F. Giudice and A. Strumia, *Benchmarks for Dark Matter Searches at the LHC*, *JHEP* **06** (2014) 081, [[1402.6287](#)].
- [166] M. J. Baker et al., *The Coannihilation Codex*, *JHEP* **12** (2015) 120, [[1510.03434](#)].
- [167] M. Garny, J. Heisig, B. LülF and S. Vogl, *Coannihilation without chemical equilibrium*, *Phys. Rev.* **D96** (2017) 103521, [[1705.09292](#)].
- [168] G. R. Farrar and P. Fayet, *Phenomenology of the Production, Decay, and Detection of New Hadronic States Associated with Supersymmetry*, *Phys. Lett.* **76B** (1978) 575–579.
- [169] CMS collaboration, C. Collaboration, *Search for stopped long-lived particles produced in pp collisions at  $\sqrt{s} = 13$  TeV*, .
- [170] A. D. Bond, G. Hiller, K. Kowalska and D. F. Litim, *Directions for model building from asymptotic safety*, *JHEP* **08** (2017) 004, [[1702.01727](#)].
- [171] M. Garny, J. Heisig, M. Hufnagel and B. LülF, *Top-philic dark matter within and beyond the WIMP paradigm*, [1802.00814](#).
- [172] A. Pierce and J. Thaler, *Natural Dark Matter from an Unnatural Higgs Boson and New Colored Particles at the TeV Scale*, *JHEP* **08** (2007) 026, [[hep-ph/0703056](#)].
- [173] K. Hamaguchi, S. P. Liew, T. Moroi and Y. Yamamoto, *Isospin-Violating Dark Matter with Colored Mediators*, *JHEP* **05** (2014) 086, [[1403.0324](#)].
- [174] A. Ibarra, A. Pierce, N. R. Shah and S. Vogl, *Anatomy of Coannihilation with a Scalar Top Partner*, *Phys. Rev.* **D91** (2015) 095018, [[1501.03164](#)].
- [175] J. Ellis, F. Luo and K. A. Olive, *Gluino Coannihilation Revisited*, *JHEP* **09** (2015) 127, [[1503.07142](#)].
- [176] S. P. Liew and F. Luo, *Effects of QCD bound states on dark matter relic abundance*, *JHEP* **02** (2017) 091, [[1611.08133](#)].

- [177] A. Mitridate, M. Redi, J. Smirnov and A. Strumia, *Cosmological Implications of Dark Matter Bound States*, *JCAP* **1705** (2017) 006, [[1702.01141](#)].
- [178] V. De Luca, A. Mitridate, M. Redi, J. Smirnov and A. Strumia, *Colored Dark Matter*, [1801.01135](#).
- [179] S. Biondini and M. Laine, *Thermal dark matter co-annihilating with a strongly interacting scalar*, [1801.05821](#).
- [180] M. Garny, A. Ibarra, S. Rydbeck and S. Vogl, *Majorana Dark Matter with a Coloured Mediator: Collider vs Direct and Indirect Searches*, *JHEP* **06** (2014) 169, [[1403.4634](#)].
- [181] F. Giacchino, A. Ibarra, L. Lopez Honorez, M. H. G. Tytgat and S. Wild, *Signatures from Scalar Dark Matter with a Vector-like Quark Mediator*, *JCAP* **1602** (2016) 002, [[1511.04452](#)].
- [182] K. Sigurdson, M. Doran, A. Kurylov, R. R. Caldwell and M. Kamionkowski, *Dark-matter electric and magnetic dipole moments*, *Phys. Rev.* **D70** (2004) 083501, [[astro-ph/0406355](#)].
- [183] V. Barger, W.-Y. Keung, D. Marfatia and P.-Y. Tseng, *Dipole Moment Dark Matter at the LHC*, *Phys. Lett.* **B717** (2012) 219–223, [[1206.0640](#)].
- [184] A. Sommerfeld, *Über die beugung und bremsung der elektronen*, *Annalen der Physik* **403** (1931) 257–330.
- [185] J. L. Feng, M. Kaplinghat and H.-B. Yu, *Sommerfeld Enhancements for Thermal Relic Dark Matter*, *Phys. Rev.* **D82** (2010) 083525, [[1005.4678](#)].
- [186] S. El Hedri, A. Kaminska and M. de Vries, *A Sommerfeld Toolbox for Colored Dark Sectors*, *Eur. Phys. J.* **C77** (2017) 622, [[1612.02825](#)].
- [187] R. T. D’Agnolo, C. Mondino, J. T. Ruderman and P.-J. Wang, *Exponentially Light Dark Matter from Coannihilation*, [1803.02901](#).
- [188] J. Alwall, R. Frederix, S. Frixione, V. Hirschi, F. Maltoni, O. Mattelaer et al., *The automated computation of tree-level and next-to-leading order differential cross sections, and their matching to parton shower simulations*, *JHEP* **07** (2014) 079, [[1405.0301](#)].
- [189] A. Alloul, N. D. Christensen, C. Degrande, C. Duhr and B. Fuks, *FeynRules 2.0 - A complete toolbox for tree-level phenomenology*, *Comput. Phys. Commun.* **185** (2014) 2250–2300, [[1310.1921](#)].
- [190] T. Sjostrand, S. Mrenna and P. Z. Skands, *A Brief Introduction to PYTHIA 8.1*, *Comput. Phys. Commun.* **178** (2008) 852–867, [[0710.3820](#)].
- [191] A. Cuoco, J. Heisig, M. Korsmeier and M. Krämer, *Constraining heavy dark matter with cosmic-ray antiprotons*, [1711.05274](#).



- [192] Y. Kim, A. Lindner and Y. K. Semertzidis, eds., *Proceedings, 12th Patras Workshop on Axions, WIMPs and WISPs (PATRAS 2016)*, (Hamburg), Verlag Deutsches Elektronen-Synchrotron, Verlag Deutsches Elektronen-Synchrotron, 2017. 10.3204/PUBDB-2017-11637.
- [193] M. R. Kauth, J. H. Kuhn, P. Marquard and M. Steinhauser, *Gluinonia: Energy Levels, Production and Decay*, *Nucl. Phys.* **B831** (2010) 285–305, [[0910.2612](#)].
- [194] ATLAS collaboration, M. Aaboud et al., *Search for new phenomena in dijet events using  $37\text{ fb}^{-1}$  of  $pp$  collision data collected at  $\sqrt{s} = 13\text{ TeV}$  with the ATLAS detector*, *Phys. Rev.* **D96** (2017) 052004, [[1703.09127](#)].
- [195] P. Meade and M. Reece, *BRIDGE: Branching ratio inquiry / decay generated events*, [hep-ph/0703031](#).
- [196] “Madgraph launchpad: why production and decay cross-section didn’t agree.” <https://answers.launchpad.net/mg5amcnlo/+faq/2442>.
- [197] A. Strumia, *Sommerfeld corrections to type-II and III leptogenesis*, *Nucl. Phys.* **B809** (2009) 308–317, [[0806.1630](#)].
- [198] S. R. Coleman and E. J. Weinberg, *Radiative Corrections as the Origin of Spontaneous Symmetry Breaking*, *Phys. Rev.* **D7** (1973) 1888–1910.
- [199] K. Agashe, R. Contino and A. Pomarol, *The Minimal composite Higgs model*, *Nucl. Phys.* **B719** (2005) 165–187, [[hep-ph/0412089](#)].
- [200] M. Frigerio, A. Pomarol, F. Riva and A. Urbano, *Composite Scalar Dark Matter*, *JHEP* **07** (2012) 015, [[1204.2808](#)].
- [201] D. Marzocca and A. Urbano, *Composite Dark Matter and LHC Interplay*, *JHEP* **07** (2014) 107, [[1404.7419](#)].
- [202] N. Fonseca, R. Zukanovich Funchal, A. Lessa and L. Lopez-Honorez, *Dark Matter Constraints on Composite Higgs Models*, *JHEP* **06** (2015) 154, [[1501.05957](#)].
- [203] S. Bruggisser, F. Riva and A. Urbano, *Strongly Interacting Light Dark Matter*, *SciPost Phys.* **3** (2017) 017, [[1607.02474](#)].
- [204] B. Gripaios, A. Pomarol, F. Riva and J. Serra, *Beyond the Minimal Composite Higgs Model*, *JHEP* **04** (2009) 070, [[0902.1483](#)].
- [205] J. Mrazek, A. Pomarol, R. Rattazzi, M. Redi, J. Serra and A. Wulzer, *The Other Natural Two Higgs Doublet Model*, *Nucl. Phys.* **B853** (2011) 1–48, [[1105.5403](#)].
- [206] S. De Curtis, L. Delle Rose, S. Moretti and K. Yagyu, *Supersymmetry versus Compositeness: 2HDMs tell the story*, *Phys. Lett.* **B786** (2018) 189–194, [[1803.01865](#)].
- [207] S. De Curtis, L. Delle Rose, S. Moretti and K. Yagyu, *A Concrete Composite 2-Higgs Doublet Model*, *JHEP* **12** (2018) 051, [[1810.06465](#)].
- [208] G. Ballesteros, A. Carmona and M. Chala, *Exceptional Composite Dark Matter*, *Eur. Phys. J.* **C77** (2017) 468, [[1704.07388](#)].

- [209] R. Balkin, M. Ruhdorfer, E. Salvioni and A. Weiler, *Charged Composite Scalar Dark Matter*, *JHEP* **11** (2017) 094, [[1707.07685](#)].
- [210] R. Balkin, M. Ruhdorfer, E. Salvioni and A. Weiler, *Dark matter shifts away from direct detection*, *JCAP* **1811** (2018) 050, [[1809.09106](#)].
- [211] L. Da Rold and A. N. Rossia, *The Minimal Simple Composite Higgs Model*, [1904.02560](#).
- [212] M. Chala, R. Gröber and M. Spannowsky, *Searches for vector-like quarks at future colliders and implications for composite Higgs models with dark matter*, *JHEP* **03** (2018) 040, [[1801.06537](#)].
- [213] T. Ma and G. Cacciapaglia, *Fundamental Composite 2HDM:  $SU(N)$  with 4 flavours*, *JHEP* **03** (2016) 211, [[1508.07014](#)].
- [214] Y. Wu, T. Ma, B. Zhang and G. Cacciapaglia, *Composite Dark Matter and Higgs*, *JHEP* **11** (2017) 058, [[1703.06903](#)].
- [215] R. Balkin, G. Perez and A. Weiler, *Little composite dark matter*, *Eur. Phys. J.* **C78** (2018) 104, [[1707.09980](#)].
- [216] G. Cacciapaglia, H. Cai, A. Deandrea and A. Kushwaha, *Fundamental Composite Higgs model in  $SU(6)/SO(6)$* , [1904.09301](#).
- [217] T. Alanne, D. Buarque Franzosi, M. T. Frandsen and M. Rosenlyst, *Dark matter in (partially) composite Higgs models*, *JHEP* **12** (2018) 088, [[1808.07515](#)].
- [218] A. Carmona and M. Chala, *Composite Dark Sectors*, *JHEP* **06** (2015) 105, [[1504.00332](#)].
- [219] R. Contino, D. Marzocca, D. Pappadopulo and R. Rattazzi, *On the effect of resonances in composite Higgs phenomenology*, *JHEP* **10** (2011) 081, [[1109.1570](#)].
- [220] A. Agugliaro, G. Cacciapaglia, A. Deandrea and S. De Curtis, *Vacuum misalignment and pattern of scalar masses in the  $SU(5)/SO(5)$  composite Higgs model*, *JHEP* **02** (2019) 089, [[1808.10175](#)].
- [221] J. Wess and B. Zumino, *Consequences of anomalous Ward identities*, *Phys. Lett.* **37B** (1971) 95–97.
- [222] E. Witten, *Global Aspects of Current Algebra*, *Nucl. Phys.* **B223** (1983) 422–432.
- [223] J. Davighi and B. Gripaios, *Homological classification of topological terms in sigma models on homogeneous spaces*, *JHEP* **09** (2018) 155, [[1803.07585](#)].
- [224] J. Davighi and B. Gripaios, *Topological terms in Composite Higgs Models*, *JHEP* **11** (2018) 169, [[1808.04154](#)].
- [225] H. E. Logan, *TASI 2013 lectures on Higgs physics within and beyond the Standard Model*, [1406.1786](#).
- [226] D. B. Kaplan, *Flavor at SSC energies: A New mechanism for dynamically generated fermion masses*, *Nucl. Phys.* **B365** (1991) 259–278.

- [227] G. Panico and A. Wulzer, *The Discrete Composite Higgs Model*, *JHEP* **09** (2011) 135, [[1106.2719](#)].
- [228] CMS collaboration, A. M. Sirunyan et al., *Search for invisible decays of a Higgs boson produced through vector boson fusion in proton-proton collisions at  $\sqrt{s} = 13$  TeV*, [1809.05937](#).
- [229] ATLAS collaboration, M. Aaboud et al., *Combination of searches for invisible Higgs boson decays with the ATLAS experiment*, Submitted to: *Phys. Rev. Lett.*, [[1904.05105](#)].
- [230] J. de Blas et al., *Higgs Boson Studies at Future Particle Colliders*, [1905.03764](#).
- [231] N. D. Christensen and C. Duhr, *FeynRules - Feynman rules made easy*, *Comput. Phys. Commun.* **180** (2009) 1614–1641, [[0806.4194](#)].
- [232] ATLAS collaboration, M. Aaboud et al., *Search for invisible higgs boson decays in vector boson fusion at  $\sqrt{s} = 13$  tev with the atlas detector*, Submitted to: *Phys. Lett.* (2018), [[1809.06682](#)].
- [233] P. Junnarkar and A. Walker-Loud, *Scalar strange content of the nucleon from lattice QCD*, *Phys. Rev.* **D87** (2013) 114510, [[1301.1114](#)].
- [234] XENON collaboration, E. Aprile et al., *First Dark Matter Search Results from the XENON1T Experiment*, *Phys. Rev. Lett.* **119** (2017) 181301, [[1705.06655](#)].
- [235] XENON collaboration, E. Aprile et al., *Physics reach of the XENON1T dark matter experiment*, *JCAP* **1604** (2016) 027, [[1512.07501](#)].
- [236] M. Fairbairn and J. Zupan, *Dark matter with a late decaying dark partner*, *JCAP* **0907** (2009) 001, [[0810.4147](#)].
- [237] ATLAS COLLABORATION collaboration, *Combined measurements of Higgs boson production and decay using up to  $80 \text{ fb}^{-1}$  of proton–proton collision data at  $\sqrt{s} = 13$  TeV collected with the ATLAS experiment*, Tech. Rep. ATLAS-CONF-2018-031, CERN, Geneva, Jul, 2018.
- [238] T. Plehn, *Lectures on LHC Physics*, *Lect. Notes Phys.* **844** (2012) 1–193, [[0910.4182](#)].
- [239] G. F. Giudice, C. Grojean, A. Pomarol and R. Rattazzi, *The Strongly-Interacting Light Higgs*, *JHEP* **06** (2007) 045, [[hep-ph/0703164](#)].
- [240] A. Manohar and H. Georgi, *Chiral Quarks and the Nonrelativistic Quark Model*, *Nucl. Phys.* **B234** (1984) 189–212.
- [241] H. Georgi, *Generalized dimensional analysis*, *Phys. Lett.* **B298** (1993) 187–189, [[hep-ph/9207278](#)].
- [242] G. F. Giudice and M. McCullough, *A Clockwork Theory*, *JHEP* **02** (2017) 036, [[1610.07962](#)].